

NUMERICAL METHODS FOR MULTIPHYSICS FLOW PROBLEMS

A THESIS SUBMITTED TO  
THE GRADUATE SCHOOL OF NATURAL AND APPLIED SCIENCES  
OF  
MIDDLE EAST TECHNICAL UNIVERSITY

BY

MİNE AKBAŞ BELENLİ

IN PARTIAL FULFILLMENT OF THE REQUIREMENTS  
FOR  
THE DEGREE OF DOCTOR OF PHILOSOPHY  
IN  
MATHEMATICS

APRIL 2016



Approval of the thesis:

**NUMERICAL METHODS FOR MULTIPHYSICS FLOW PROBLEMS**

submitted by **MİNE AKBAŞ BELENLİ** in partial fulfillment of the requirements for the degree of **Doctor of Philosophy in Mathematics Department, Middle East Technical University** by,

Prof. Dr. Gülbin Dural Ünver  
Dean, Graduate School of **Natural and Applied Sciences** \_\_\_\_\_

Prof. Dr. Mustafa Korkmaz  
Head of Department, **Mathematics** \_\_\_\_\_

Prof. Dr. Songül Kaya Merdan  
Supervisor, **Mathematics Department, METU** \_\_\_\_\_

Prof. Dr. Leo G. Rebholz  
Co-supervisor, **Mathematical Sciences, Clemson University** \_\_\_\_\_

**Examining Committee Members:**

Prof. Dr. Münevver Tezer  
Mathematics Department, METU \_\_\_\_\_

Prof. Dr. Songül Kaya Merdan  
Mathematics Department, METU \_\_\_\_\_

Assoc. Prof. Dr. Selin Aradağ  
Mechanical Engineering Department, TOBB ETU \_\_\_\_\_

Assoc. Prof. Dr. Canan Bozkaya  
Mathematics Department, METU \_\_\_\_\_

Assoc. Prof. Dr. Niyazi Şahin  
Mathematics-Computer Department, YBU \_\_\_\_\_

**Date:** \_\_\_\_\_

**I hereby declare that all information in this document has been obtained and presented in accordance with academic rules and ethical conduct. I also declare that, as required by these rules and conduct, I have fully cited and referenced all material and results that are not original to this work.**

Name, Last Name: MİNE AKBAŞ BELENLİ

Signature :

# ABSTRACT

## NUMERICAL METHODS FOR MULTIPHYSICS FLOW PROBLEMS

Belenli, Mine Akbaş

Ph.D., Department of Mathematics

Supervisor : Prof. Dr. Songül Kaya Merdan

Co-Supervisor : Prof. Dr. Leo G. Rebholz

April 2016, 131 pages

In this dissertation, efficient and reliable numerical algorithms for approximating solutions of multiphysics flow problems are investigated by using numerical methods. The interaction of multiple physical processes makes the systems complex, and two fundamental difficulties arise when attempting to obtain numerical solutions of these problems: the need for algorithms that reduce the problems into smaller pieces in a stable and accurate way and for large (sometimes intractable) amount of computational resources to resolve all the physical scales. Although these two difficulties are often stated as separate issues, in practice they are quite related. The objective of this thesis is to advance state of the art in algorithms, and their better understanding through analysis, for two types of multiphysics problems: incompressible non-isothermal fluid flow, and magnetohydrodynamic flow.

The first component of this thesis is to develop numerical algorithms that decouple the multiphysics systems of equations into smaller, easier to solve sub-problems. However, splitting up problems into components is well known to (sometimes dramatically) reduce accuracy and cause numerical instabilities. It will be rigorously proven that the decoupling algorithms proposed and studied herein are stable and accurate. Numerical tests are used to verify the stability and accuracy.

The second component of the thesis is to construct the numerical scheme that use the Variational Multiscale (VMS) method to reduce the computational cost of these problems, by reducing the size of the smallest scale needing to be resolved. At the same

time, the algorithm will decouple the VMS modeling/stabilization equations from the multiphysics system, and decouple the multiphysics system into its components. This thesis proposes such an efficient algorithm and rigorously proves it is stable and accurate, as well as giving guidance into picking the stabilization parameters. Numerical experiments verify the theoretical results, and reveal that the algorithm gives accurate solutions on coarse discretizations, i.e. with significantly less computational cost than the requirement to be resolved of the original (unstabilized) physical systems. Lastly, this thesis considers the notion of long-time stability for decoupling algorithms for multiphysics problems. It is quite common for stable numerical methods to be stable only over finite time intervals, and to produce numerical solutions that non-physically grow linearly or even exponentially with time, even when the true solution does not grow. Hence, it is desirable to use algorithms that are stable at all times, so that stability and accuracy can be preserved as long as possible in a numerical simulation. This thesis proves unconditional long time stability results for a particular class of linearized, second order methods for multiphysics problems and also for the usual incompressible Navier-Stokes equations.

Keywords: MHD, MHD in Elsässer variables, Non-isothermal incompressible flows, Finite Element Method, VMS method, grad-div stabilization, projection method, long time stability.

# ÖZ

## ÇOKLU FİZİK PROBLEMLERİ İÇİN SAYISAL METOTLAR

Belenli, Mine Akbaş

Doktora, Matematik Bölümü

Tez Yöneticisi : Prof. Dr. Songül Kaya Merdan

Ortak Tez Yöneticisi : Prof. Dr. Leo G. Rebholz

Nisan 2016 , 131 sayfa

Bu tezde, sayısal yöntemler kullanılarak çoklu fizik problemlerinin yaklaşık çözümleri için etkili ve gerçekçi sayısal algoritmalar araştırılır. Birden çok fiziksel sürecin karşılıklı etkileşiminin sistem üzerindeki karmaşık etkisi nedeniyle, bu problemlerin sayısal çözümlerinin elde edilmesinde iki temel zorluk ortaya çıkar: problemi daha küçük alt parçalara indirgeyen, kararlı ve hassas algoritmalara ve tüm fiziksel ölçeklerin çözülmesi için çok geniş bilgisayar hafızasına olan gereksinim. Bu iki zorluk sıklıkla ayrı problemler olarak ifade edilmesine karşın, uygulamada birbirleriyle yakından ilgilidir. Bu tezin amacı iki çeşit çoklu fizik problemi; sıcaklığı sabit olmayan, sıkıştırılmaz akışkan akışı ve manyetohidrodinamik akışları için yeni algoritmalar geliştirmek ve analiz yoluyla onların daha iyi anlaşılmasına katkı sağlamaktır.

Bu tezin birinci unsuru çoklu fizik denklemlerini daha küçük, daha kolay çözülebilen alt problemlere ayırıştırıran nümerik algoritmaları geliştirmektir. Ancak, problemlerin bileşenlerine ayırıştırılmasının doğruluğu azalttığı ve sayısal kararsızlıklara yol açtığı iyi bilinmektedir. Burada önerilen ve çalışılan ayırıştırırmalı algoritmaların kararlı ve hassas oldukları titiz bir şekilde ispatlanacaktır. Sayısal testler algoritmaların kararlılığını ve hassaslığını doğrulamak için kullanılır.

Bu tezin ikinci unsuru çözülmesi gerekli olan en küçük ölçeğin boyutunu azaltarak bu problemlerin hesaplama maliyetini indirmek için Varyasyonel Çoklu Ölçek (VMS) metotunu kullanan sayısal algoritmaları oluşturmaktır. Aynı zamanda, algoritmalar VMS modelleme/kararlılık denklemlerini çoklu fizik sisteminden ayırıştırarak

ve çoklu fizik sistemini bileşenlerine ayrıştıracaktır. Bu tez, bu şekilde etkili algoritmalar önerir ve kararlılık parametrelerinin seçimine rehberlik etmesinin yanı sıra algoritmaların kararlı ve hassas olduğunu titiz bir şekilde ispatlar. Sayısal testler teorik sonuçları doğrular ve algoritmanın kaba ayrıştırma üzerinde, yani orjinal (kararsız) fizik sisteminin çözülebilmesi için gerekli olan hesaplama maliyetinden önemli ölçüde daha az hesaplama maliyeti ile doğru sonuçlar verdiğini ortaya çıkarır.

Son olarak, bu tez, çoklu fizik problemlerini ayrıştıran algoritmalar için uzun zamanlı kararlılık kavramını göz önüne alır. Kararlı sayısal metotların yalnızca sonlu zaman aralıkları üzerinde kararlı olması ve gerçek çözümün büyümediğinde bile doğrusal hatta üstel olarak fiziksel olmayan bir şekilde zamanla artan sayısal çözümler üretmesi oldukça yaygındır. Dolayısıyla, kararlılık ve hassaslığın sayısal simülasyonda mümkün olduğunca uzun korunacak şekilde tüm zamanlarda kararlı olan algoritmaların kullanılması arzu edilir. Bu tez genel, sıkıştırılmaz Navier-Stokes denklemleri ve çoklu fizik problemleri için doğrusal, ikinci mertebe özellikli metotların koşulsuz kararlılık sonuçlarını ispatlar.

Anahtar Kelimeler: MHD, Elsässer değişkenlerinde MHD, Sıcaklığı sabit olmayan sıkıştırılmaz akışkanlar, Sonlu elemanlar yöntemi, VMS metodu, grad-div stabilizasyon, izdüşüm yöntemi, uzun zamanlı kararlılık.



*To my mother and my father: Gülsim and Veli Akbaş.*

## ACKNOWLEDGMENTS

This thesis arose with the help of kind, precious people around me and especially my great family.

First of all, I would like to thank to my advisor Prof. Dr. Songül Merdan for her valuable advice, encouragement, continuous support during my thesis.

I am grateful for committee member Prof. Dr. Münevver Tezer for her valuable comments, immense response, and kindly approach during the thesis writing and my Ph. D. courses. I also would like to thank for committee member Assoc. Prof. Dr. Selin Aradağ for her kindly, gentle approach. My thanks also go to remaining committee members Assoc. Prof. Dr. Canan Bozkaya and Assoc. Prof. Dr. Niyazi Şahin for their valuable comments.

My sincere thanks go to Prof. Dr. Zafer Nurlu and Prof. Dr. Mahmut Kuzucuoğlu for their kindly and friendly approach during my Ph.D. courses.

I also want to thank the Mathematical Department of METU for pleasant, peaceful, calm atmosphere and colleagues at METU helping me during my Ph. D.

I especially would like to express my appreciation to The Scientific and Technological Research Council of Turkey (TUBITAK) since it gave me a chance to research in the U.S.A by supporting me financially.

Above all, my special thanks go to Prof. Dr. Leo G. Rebholz for his patient, kindly and friendly approach. I am also grateful to him for his valuable guidance, encouragement and continuous support. My thanks also go to Amy Rebholz for her nice friendship and gentle hospitality when I was in the U.S.A.

My final special and sincere thanks go to my great family for their continuous support, endless love and believing in my success: Veli, Gülsüm, Kadir, Kadriye, Metin, Ali, Aykut Akbaş, and my little son. I am grateful to owe them.

# TABLE OF CONTENTS

ABSTRACT . . . . .	v
ÖZ . . . . .	vii
ACKNOWLEDGMENTS . . . . .	x
TABLE OF CONTENTS . . . . .	xi
LIST OF TABLES . . . . .	xv
LIST OF FIGURES . . . . .	xvi
CHAPTERS	
1 INTRODUCTION . . . . .	1
1.1 Three Multiphysics Flow Problems . . . . .	3
1.1.1 Definition of Some Physical Notions . . . . .	4
1.1.2 The Navier Stokes Equations . . . . .	5
1.1.2.1 The Nondimensional Form of the NSE	10
1.1.3 Incompressible non-isothermal fluid flow driven by natural convection . . . . .	12
1.1.3.1 Heat Transfer Fundamentals . . . . .	12
1.1.3.2 Derivation of the Non-Isothermal Fluid Flows . . . . .	13

	1.1.3.3	Dimensionless Form of the Boussinesq System . . . . .	15
	1.1.4	Magnetohydrodynamic Equations . . . . .	17
	1.1.4.1	Derivation of MHD Equations in Primitive Variables . . . . .	17
	1.1.4.2	Dimensionless form of MHD equations in primitive variables . . . . .	20
	1.1.4.3	Derivation of MHD equations in Elsässer variables . . . . .	22
2		AN EXPLICITLY DECOUPLED VARIATIONAL MULTISCALE METHOD FOR INCOMPRESSIBLE NON ISOTHERMAL FLUID FLOWS . . . . .	25
	2.1	Mathematical Preliminaries . . . . .	29
	2.2	Numerical Scheme . . . . .	40
	2.3	Stability and Convergence Analysis . . . . .	41
	2.3.1	Convergence Analysis . . . . .	45
	2.4	Numerical Experiments . . . . .	56
	2.4.1	Convergence Rate Verification . . . . .	56
	2.4.2	Luigi Ferdinando Marsigli’s physical model of gravity driven, two-layer flow . . . . .	60
	2.4.2.1	Marsigli’s experiment set-up . . . . .	60
3		NUMERICAL ANALYSIS OF MHD IN ELSÄSSER VARIABLES . . . . .	67
	3.1	Mathematical Preliminaries . . . . .	69
	3.2	Numerical Scheme . . . . .	71
	3.3	Stability and Convergence Analysis . . . . .	72

	3.3.1	Convergence Analysis . . . . .	74
3.4		Numerical Experiments . . . . .	84
	3.4.1	Numerical Experiment 1: Convergence of grad-div stabilized penalty projection scheme to coupled scheme as $\gamma \rightarrow \infty$ . . . . .	85
	3.4.2	Numerical experiment 2: MHD Channel flow with full step . . . . .	85
	3.4.2.1	Experiment setup . . . . .	87
4		LONG TIME STABILITY ANALYSIS OF MULTIPHYSICS FLOW PROBLEMS . . . . .	91
	4.1	Mathematical Preliminaries . . . . .	93
	4.2	Long time stability of the NSE . . . . .	95
	4.2.1	Numerical Experiment . . . . .	96
	4.2.1.1	Numerical Experiment 1: Comparison of the stability of the solutions of BDF2LE and CNLE schemes for the NSE over long time interval . . . . .	98
	4.2.1.2	Numerical Experiment 2 : Comparison of the mass conservation in long-time simulation of the NSE with different finite elements . . . . .	99
	4.3	Long time stability analysis of the Boussinesq System . . . . .	101
	4.4	Long time stability of MHD in primitive variables . . . . .	105
	4.5	The long time stability of MHD in Elsässer variables . . . . .	108
	4.5.1	Numerical Experiment . . . . .	111
5		CONCLUSIONS AND FUTURE WORK . . . . .	117

5.1	Future Work . . . . .	118
	REFERENCES . . . . .	119
	CURRICULUM VITAE . . . . .	129

## LIST OF TABLES

### TABLES

Table 2.1	Velocity errors with fixed time step and small $T$ to isolate the spatial errors. . . . .	58
Table 2.2	Temperature errors with fixed time step and small $T$ to isolate the spatial errors. . . . .	58
Table 2.3	Velocity errors with fixed fine mesh and large $T = 1.0$ to isolate the temporal errors. . . . .	59
Table 2.4	Temperature errors with fixed fine mesh and large $T = 1.0$ to isolate the temporal errors. . . . .	59
Table 3.1	Shown above are differences between the penalty-projection and coupled schemes solutions for varying $\gamma$ , and the divergence of solutions for Algorithm 3.2.1. . . . .	85

## LIST OF FIGURES

### FIGURES

Figure 2.1 Spatial velocity and temperature errors with fixed time step and small $T$ . . . . .	58
Figure 2.2 Temporal velocity and temperature errors with fixed mesh size. . .	60
Figure 2.3 The Marsigli's Flow Setup . . . . .	61
Figure 2.4 Resolved temperature contours and velocity streamlines for the $Re=1,000$ , $Ri=4$ , $Pr = 1$ Marsigli flow test with $T = 2, 4$ , and $8$ . . . . .	63
Figure 2.5 Coarse mesh DNS (no model) solutions for temperature contours and velocity streamlines for the $Re=1,000$ , $Ri=4$ , $Pr = 1$ Marsigli flow test with $T = 2, 4$ , and $8$ . . . . .	64
Figure 2.6 Coarse mesh model solutions for temperature contours and velocity streamlines for the $Re=1,000$ , $Ri=4$ , $Pr = 1$ Marsigli flow test with $T = 2, 4$ , and $8$ . . . . .	65
Figure 3.1 Differences between the penalty-projection and coupled schemes solutions, and the divergence of solutions for Algorithm 3.2.1 for varying $\gamma$ . . . . .	86
Figure 3.2 Geometry of the problem for channel flow . . . . .	88
Figure 3.3 Velocity solutions (shown as streamlines over velocity) for MHD channel flow over full step with varying $s$ at $T = 40$ . . . . .	89
Figure 3.4 Magnetic field magnitudes for MHD channel flow over full step with varying $s$ at $T = 40$ . . . . .	89
Figure 3.5 Velocity solutions (shown as streamlines over velocity) for MHD channel flow over full step with varying $s$ at $T = 40$ . . . . .	90
Figure 4.1 Discrete velocity solutions of the BDF2LE and the CNLE schemes for the NSE with $\Delta t = 0.25$ varying $\nu$ . . . . .	98



Figure 4.2 Discrete velocity solutions of the BDF2LE and the CNLE schemes for the NSE with $\Delta t = 0.25$ varying $\nu$ . . . . .	99
Figure 4.3 Shown above plots of the $L^2$ -norm of the computed solution $\ u_h^n\ $ versus time, for viscosities $\nu = \frac{1}{100}, \frac{1}{500}$ . . . . .	100
Figure 4.4 Shown above plots of the $L^2$ -norm of the computed solution $\ u_h^n\ $ versus time, for viscosity $\nu = \frac{1}{1000}$ . . . . .	101
Figure 4.5 Energy vs. time for discrete velocity solutions of MHD in Elsässer variables with $\nu = 1.0, \nu_m = 1.0$ ( $1/2 < \nu/\nu_m < 2$ ). . . . .	113
Figure 4.6 Energy vs. time for discrete velocity solutions of MHD in Elsässer variables with $\nu = 0.0125, \nu_m = 0.01$ ( $1/2 < \nu/\nu_m < 2$ ). . . . .	113
Figure 4.7 Energy vs. time for discrete velocity solutions of MHD in Elsässer variables with $\nu = 0.01$ and $\nu_m = 1$ ( $\nu/\nu_m < 1/2$ ). . . . .	114
Figure 4.8 Energy vs. time for discrete velocity solutions of MHD in Elsässer variables with $\nu = 0.01$ and $\nu_m = 0.001$ ( $\nu/\nu_m > 2$ ). . . . .	114
Figure 4.9 Energy vs. time for discrete velocity solutions of MHD in Elsässer variables with $\nu = 1$ and $\nu_m = 0.5$ ( $\nu/\nu_m = 2$ ). . . . .	115
Figure 4.10 Energy vs. time for discrete velocity solutions of MHD in Elsässer variables with $\nu = 0.2$ and $\nu_m = .095$ ( $\nu/\nu_m = 2.105$ ). . . . .	115



# CHAPTER 1

## INTRODUCTION

Many important problems encountered in applied sciences combine several different physical phenomena, such as fluid flow, heat and mass transfer, and electromagnetism. Such problems are referred to as ‘multiphysics problems’, since the systems of equations that describe them must couple together physical equations for the individual physical laws. From a mathematical point of view, these multiphysics systems consist of systems of partial differential equations (PDE) comprised of the PDE for each physical process, all coupled together.

When the multiphysics system of PDE involve the fluid flow, finding the analytical solutions to the problems governed by the Navier Stokes equations (NSE) is not available. This is because of the mathematical gap in finding the analytic solutions to the NSE as well as the complexity of fluid flow at high *Reynolds* number, which leads to the requirement of the much more computer capacity in simulations. Therefore coupling additional equations to Navier Stokes only makes the situation worse. Hence, numerical methods are employed to solve multiphysics problems.

Two approaches are used in the literature for computing the approximate solutions of multiphysics problems: monolithic and partitioned. The monolithic approach solves the entire coupled system together, which leads to the need to solve massive, coupled, block linear systems at each time step of a simulation. This approach is preferred when there is a strong connection between distinct physics at play, since in this case partitioning the problem can be numerically unstable. Partitioned methods, on the other hand, decompose the systems of equations at each time step into smaller, easier to solve, subproblems. For example, the fluid part of a problem would be solved separately from the transport part. Here, it is much easier to get answers at each time step,

however, if the decoupling is not done carefully, numerical instabilities can quickly destroy solutions. Typically, the systems are decoupled through the time stepping scheme, by approximating physical variables based on their values at previous time steps. To give some examples, partitioned methods are commonly used in ocean-atmosphere simulations, and monolithic methods are sometimes preferable in some fluid structure problems in biomedical applications such as simulation of fluid being pumped by the heart.

One of the discretization tool is the finite element method. This is a widely used method, since it is built on a solid mathematical foundation, and can typically be more easily applied to problems posed on complex geometries, which is common in most modern engineering design problems.

It is a big challenge to develop numerical algorithms that captures the correct physical behavior of the flow, and produces the accurate approximate solutions over a finite time interval. The main difficulty arising regarding how to devise an efficient algorithm is the requirement of a very fine mesh to get the full resolution of the solutions, which exceeds today's computer capacity for most of the flow problems. Creating numerical algorithms possessing stability properties over a long time interval is another challenge. Therefore, to know to what extent a numerical algorithm possessing such a property, and if there is a time step restriction for it to hold, is of special interest, especially due to the importance of predicting weather and climate events.

The first goal in this thesis is to create efficient and reliable numerical algorithms over a finite time interval for two multiphysics flow problems: the incompressible, non-isothermal fluid flow driven by natural convection (the Boussinesq system), and magnetohydrodynamic flows (MHD). A key component of the proposed methods is that they decouple the systems in a stable way. In the study of the first problem, the proposed algorithm is created by using a variant of the projection based Variational Multiscale method, due to the success of the method in finding accurate approximate solutions without a finer mesh requirement. In the magnetohydrodynamics flow problem, an algorithm is developed by applying a variant of the penalty-projection scheme with the grad-div stabilization technique. We choose this method due to the achievement of the splitting methods in approximate solutions.

The second goal in this work is to construct the algorithms being stable over long time intervals for these multiphysics flow problems as well as for the Navier-Stokes

equations (NSE). The aim is to achieve the stability at all times without any restriction on the size of the time step.

This thesis is organized as follows:

**Chapter 2** focuses on a variant of the projection based VMS algorithm, which decouples the system of equations in an effective way. We provide the stability and convergence analysis of the method. The numerical tests are presented to validate the theoretical findings.

**Chapter 3** provides the numerical approximation of the MHD flow in Elsässer variables. The scheme is constructed by using the penalty projection method with the grad-div stabilization parameter. A complete mathematical analysis is presented, consisting of the proof of the unconditional stability, and optimal convergence of the method. Numerical experiments are provided to support the analytical results.

**Chapter 4** studies the stability behavior of three multiphysics flow problems at all times. We first focus on the long time stability analysis of the NSE with linearly extrapolated two steps backward Euler formula (BDF2LE). We then provide a numerical experiment to compare the long time stability behaviors of BDF2LE and linearly extrapolated Crank-Nicolson (CNLE) scheme. Additionally, we present the long time stability analysis for the Boussinesq system and MHD flow in primitive and Elsässer variables. We present a numerical experiment for the MHD flow in Elsässer variables to test the stability time step restriction. Chapter 4 concludes with numerical experiments to compare the mass conservation property of the NSE with different finite elements over long time intervals.

**Chapter 5** contains conclusions along with the future works. We note that numerical experiments in this thesis are made with the *FreeFem* ++ software by using the UMFPACK [56].

## 1.1 Three Multiphysics Flow Problems

Since this thesis studies three different flow problems, this section is devoted to the derivation of three multiphysics flow problems: the NSE, the Boussinesq system, and MHD flow. In addition, we give some useful definitions which are important in fluid dynamics and present the dimensionless form of the equations.

### 1.1.1 Definition of Some Physical Notions

- **Fluid** is a substance that deforms continuously when subjected to a shear stress. Fluids can be categorized as liquids and gases.
- **Stress** at a point is defined as the elemental force per unit elemental area enclosing that point such that the elemental area tend to zero. Stresses have both magnitude and direction, and the direction is relative to the surface on which the stress acts.
- **Dynamic (Absolute) viscosity** is a force per unit area per unit velocity gradient. It is denoted by  $\mu$ .
- **Kinematic viscosity** is the ratio of the dynamic viscosity to the fluid density:

$$\nu := \frac{\mu}{\rho}.$$

- **Incompressible fluid** is a fluid with constant density.
- **Homogeneous fluid** is a fluid such that mass density is constant in space.
- **Forces** on a fluid flow can be grouped as internal and external forces. External ( or body ) forces can be gravity, buoyancy and electromagnetic forces. Internal forces are viscous and pressure forces.

In fluid kinematics, fluid motion can be described in two ways: Lagrangian and Eulerian description. In the Lagrangian description, the position of a fluid particle at any time is defined by its initial position [37], and the properties of a fluid particle such as velocity and density are determined by following each fluid particle individually. In the Eulerian description, on the other hand, the field variables such as velocity, density and pressure, are described as functions of space and time within the control volume [21].

We use Eulerian approach which enables us to write fluid variables as a function of space and time. In addition, we assume that fluid variables are smooth functions in finite time interval  $(0, T]$ , and on the domain  $\Omega$ . In the derivation of the system of equations, we frequently make use of *divergence theorem* which is given by the following:

**Theorem 1.1.1** Let  $\mathbf{F}$  be a differentiable vector field in a domain  $\Omega \subset \mathbb{R}^3$  with smooth boundary  $\partial\Omega$ . Then

$$\int_{\Omega} (\nabla \cdot \mathbf{F}) dx = \int_{\partial\Omega} \mathbf{F} \cdot \mathbf{n} ds \quad (1.1)$$

where  $\mathbf{n}$  is the outward unit normal vector.

### 1.1.2 The Navier Stokes Equations

The NSE for *steady or unsteady, homogeneous, incompressible, viscous, Newtonian fluid motion*, and are derived by continuum mechanics, in particular as laws for the conservation of mass and conservation of linear momentum. These equations either alone, or together with other equations, have applications across the engineering and science spectrum, including flows in pipes and channels, plasma physics, the petroleum industry, thermo-hydraulics, atmospheric movement, and ocean currents. From the mathematical point of view, they consist of non-linear PDE, and are expressed as follows [77]:

$$\frac{\partial \mathbf{u}}{\partial t} + (\mathbf{u} \cdot \nabla) \mathbf{u} + \nabla p - \frac{\mu}{\rho} \Delta \mathbf{u} = \mathbf{f}, \quad (1.2)$$

$$\nabla \cdot \mathbf{u} = 0, \quad (1.3)$$

where  $\mathbf{u}$  is the fluid velocity,  $p$  is the pressure,  $\mu$  is the dynamic kinematic viscosity,  $\rho$  is the density, and  $\mathbf{f}$  is the body force acting on the fluid flow.

The equation (1.2) is the momentum equation. The second equation (1.3) is the continuity equation which is called *the incompressibility constraint*. The term  $(\mathbf{u} \cdot \nabla) \mathbf{u}$ , responsible for the non-linearity of the NSE, is called the convective term, and  $\nu \Delta \mathbf{u}$  the diffusion term.

#### **Step 1: The Derivation of Continuity Equation**

Let  $V$  be an arbitrary control volume in  $\Omega \subset \mathbb{R}^3$  with smooth surface  $\partial V$ . By using Eulerian approach, the mass density of the fluid, and its velocity are defined as a function of space  $\mathbf{x}$  and time  $t$ . Then, the total mass, and the rate of change of mass in  $\Omega$  are given by, respectively,

$$m(t) = \int_V \rho(t, \mathbf{x}) d\mathbf{x},$$

and

$$\frac{dm(t)}{dt} = \frac{d}{dt} \int_V \rho(t, \mathbf{x}) d\mathbf{x} = \int_V \frac{\partial \rho(t, \mathbf{x})}{\partial t} d\mathbf{x}. \quad (1.4)$$

The physical law of the mass conservation states that *mass is neither created nor destroyed in any chemical reaction*. Since mass is conserved inside  $V$ , the rate of change of mass in  $V$  must be equal to the flux of mass  $\rho \mathbf{u}(t, \mathbf{x})$  across the boundary  $\partial V$ . Thus, one can obtain

$$\frac{dm(t)}{dt} = - \int_{\partial V} (\rho \mathbf{u})(t, \mathbf{s}) \cdot \mathbf{n}(\mathbf{s}) d\mathbf{s}. \quad (1.5)$$

The application of the divergence theorem on the right hand side of (1.5) along with the use of (1.4) produces

$$\int_V \left( \nabla \cdot (\rho \mathbf{u})(t, \mathbf{x}) + \frac{\partial \rho(t, \mathbf{x})}{\partial t} \right) d\mathbf{x} = 0.$$

Since  $V$  is arbitrary, which results in

$$\nabla \cdot (\rho \mathbf{u}) + \frac{\partial \rho}{\partial t} = 0, \quad \forall (t, \mathbf{x}) \in (0, T] \times \Omega,$$

and the fluid is incompressible and homogeneous, i.e.,  $\rho(t, \mathbf{x})$  is constant, we have the continuity equation:

$$\nabla \cdot \mathbf{u} = 0, \quad \text{in } (0, T] \times \Omega. \quad (1.6)$$

### ***Step 2: The Derivation of Momentum Equation***

Let the position of a fluid particle, its velocity and acceleration at any time  $t$  be given as follows, respectively,

$$\begin{aligned} \mathbf{x} &= (x(t), y(t), z(t)), \\ \mathbf{u} &= (u(x(t), y(t), z(t)), v(x(t), y(t), z(t)), w(x(t), y(t), z(t))), \\ \mathbf{a}(t) &= a(x(t), y(t), z(t)) = \left( \frac{\partial \mathbf{u}}{\partial x} \frac{\partial x}{\partial t} + \frac{\partial \mathbf{u}}{\partial y} \frac{\partial y}{\partial t} + \frac{\partial \mathbf{u}}{\partial z} \frac{\partial z}{\partial t} + \frac{\partial \mathbf{u}}{\partial t} \right) \\ &= \mathbf{u} \cdot \nabla \mathbf{u} + \frac{\partial \mathbf{u}}{\partial t} =: \frac{D\mathbf{u}}{dt}. \end{aligned}$$



The linear momentum inside  $V$  is given by

$$\int_V (\rho \mathbf{u})(t, \mathbf{x}) d\mathbf{x}.$$

Then, the application of Newton's second law in  $V$ , giving that '*the rate of change of linear momentum inside  $V$  is equal to the net force acting on the fluid*' [21], produces

$$\frac{d}{dt} \int_V (\rho \mathbf{u})(t, \mathbf{x}) d\mathbf{x} = - \int_{\partial V} (\rho \mathbf{u})(\mathbf{u} \cdot \mathbf{n})(t, \mathbf{s}) d\mathbf{s} + \int_V F_{net}(t, \mathbf{x}) d\mathbf{x}. \quad (1.7)$$

By using the following identity

$$\begin{aligned} \mathbf{u}(\mathbf{u} \cdot \mathbf{n}) &= \begin{bmatrix} u_1 \\ u_2 \\ u_3 \end{bmatrix} \begin{bmatrix} u_1 n_1 + u_2 n_2 + u_3 n_3 \end{bmatrix} = \begin{bmatrix} u_1 u_1 n_1 + u_1 u_2 n_2 + u_1 u_3 n_3 \\ u_2 u_1 n_1 + u_2 u_2 n_2 + u_2 u_3 n_3 \\ u_3 u_1 n_1 + u_3 u_2 n_2 + u_3 u_3 n_3 \end{bmatrix} \\ &= \begin{bmatrix} u_1 u_1 + u_1 u_2 + u_1 u_3 \\ u_2 u_1 + u_2 u_2 + u_2 u_3 \\ u_3 u_1 + u_3 u_2 + u_3 u_3 \end{bmatrix} \begin{bmatrix} n_1 \\ n_2 \\ n_3 \end{bmatrix} \\ &= \mathbf{u} \mathbf{u}^T \mathbf{n}, \end{aligned}$$

and applying divergence theorem to the first term on the right hand side of (1.7) yields

$$\int_V \left( \frac{\partial}{\partial t} (\rho \mathbf{u}) + \nabla \cdot (\rho \mathbf{u} \mathbf{u}^T)(t, \mathbf{x}) \right) d\mathbf{x} = \int_V F_{net}(t, \mathbf{x}) d\mathbf{x}. \quad (1.8)$$

Using product rule along with the incompressibility of the fluid, we have

$$\begin{aligned} \frac{\partial}{\partial t} (\rho \mathbf{u}) &= \frac{\partial \rho}{\partial t} \mathbf{u} + \rho \frac{\partial \mathbf{u}}{\partial t} \\ &= \rho \frac{\partial \mathbf{u}}{\partial t}, \\ \nabla \cdot (\rho \mathbf{u} \mathbf{u}^T) &= \mathbf{u} \mathbf{u}^T \nabla \rho + \rho (\nabla \cdot \mathbf{u}) \mathbf{u} + \rho (\mathbf{u} \cdot \nabla) \mathbf{u} \\ &= \rho (\mathbf{u} \cdot \nabla) \mathbf{u}, \end{aligned}$$

Substituting these into (1.8) gives

$$\int_V \rho \left( \frac{\partial \mathbf{u}}{\partial t} + (\mathbf{u} \cdot \nabla) \mathbf{u} \right) (t, \mathbf{x}) d\mathbf{x} = \int_V F_{net}(t, \mathbf{x}) d\mathbf{x}. \quad (1.9)$$

On the other hand, the net force acting on the fluid inside  $V$  consists of body (external) forces and internal forces. Thus

$$\int_V F_{net}(t, \mathbf{x}) d\mathbf{x} = \int_V F_{ext}(t, \mathbf{x}) d\mathbf{x} + \int_{\partial V} \mathbf{t}(t, \mathbf{s}) d\mathbf{s}, \quad (1.10)$$

where  $\mathbf{t}$  is the internal force vector, called *Cauchy stress vector*. The linear dependence of Cauchy stress vector gives the following relation:

$$\mathbf{t} = \mathbb{S}\mathbf{n},$$

here  $\mathbb{S}$  is called Cauchy stress tensor such that it is defined by

$$\mathbb{S} = \begin{bmatrix} \sigma_{11} & \tau_{12} & \tau_{13} \\ \tau_{21} & \sigma_{22} & \tau_{23} \\ \tau_{31} & \tau_{32} & \sigma_{33} \end{bmatrix}, \quad \tau_{ij} = \tau_{ji}; \quad i, j = 1, 2, 3, (i \neq j)$$

here  $\sigma_{ii}$  is called normal stress tensor,  $\tau_{ij}$  shear stresses. Cauchy stress tensor is decomposed into

$$\mathbb{S} = \mathbb{V} - P\mathbb{I},$$

here  $\mathbb{V}$  is viscous stress tensor,  $P$  is the pressure. The pressure  $P$  acts only on a surface of a fluid volume  $V$ , and it is normal to that surface, and directed into  $V$ . Thus, we have

$$-\int_{\partial V} P\mathbf{n}ds = -\int_V \nabla P dx = -\int_V \nabla \cdot (P\mathbb{I})dx.$$

**Remark 1.1.2** *Friction between fluid particles can only occur if the particles move with different velocities. For this reason, the viscous stress tensor is modeled to depend on the gradient of the velocity. For the reason of the symmetry of the stress, the viscous stress tensor is the symmetric part of the gradient, the so-called velocity deformation tensor.*

*If the velocity gradient are not too large, one can assume that first the dependency is linear and second that higher derivatives can be neglected. Since there is no friction for a flow with constant velocity, such that  $\mathbb{V}$  vanishes in this case, lower order terms than first order derivatives of the velocity should not appear in the model. Introducing first order viscosity  $\mu$ , and the second order viscosity  $\eta$ , one writes this tensor in fluid dynamics in the form :*

$$\mathbb{V} = 2\mu\mathbb{D}(\mathbf{u}) - \left(\eta - \frac{2\mu}{3}\right) (\nabla \cdot \mathbf{u})$$

*where  $\mu$  is called dynamic viscosity or shear viscosity, and  $\mathbb{D}(\mathbf{u})$  is the velocity deformation tensor defined by  $\mathbb{D}(\mathbf{u}) = (\nabla\mathbf{u} + (\nabla\mathbf{u})^T)/2$ .*

This linear relation is only an approximation for a real fluid. In general, the relation will be non-linear. Only for small stresses, a linear approximation of the general stress-deformation relation can be used. A fluid satisfying this assumption is called *Newtonian fluid*.

For incompressible ( $\nabla \cdot \mathbf{u} = 0$ ), Newtonian fluids, viscous stress tensor is given by

$$\mathbb{V} = 2\mu\mathbb{D}(\mathbf{u}).$$

Therefore,

$$\begin{aligned} \int_{\partial V} \mathbf{t}(t, \mathbf{s}) d\mathbf{s} &= \int_{\partial V} (\mathbb{S}\mathbf{n})(t, \mathbf{s}) d\mathbf{s} = \int_V (\nabla \cdot \mathbb{S}) d\mathbf{x} \\ &= \int_V \nabla \cdot (2\mu\mathbb{D}(\mathbf{u})) d\mathbf{x} - \int_V \nabla \cdot (P\mathbb{I}) d\mathbf{x} \\ &= \int_V \nabla \cdot (2\mu\mathbb{D}(\mathbf{u})) d\mathbf{x} - \int_V \nabla P d\mathbf{x}. \end{aligned}$$

Since  $\mu$  is constant, and the flow is incompressible one can have

$$\begin{aligned} \nabla \cdot (2\mu\mathbb{D}(\mathbf{u})) &= \nabla \cdot \left( 2\mu \frac{\nabla\mathbf{u} + \nabla\mathbf{u}^T}{2} \right) \\ &= \mu \nabla \cdot (\nabla\mathbf{u} + \nabla\mathbf{u}^T) = \mu \nabla \cdot \nabla\mathbf{u} + \mu \nabla \cdot \nabla\mathbf{u}^T \\ &= \mu \Delta\mathbf{u}, \end{aligned}$$

which gives

$$\int_{\partial V} \mathbf{t}(t, \mathbf{s}) d\mathbf{s} = \int_V \mu \Delta\mathbf{u} d\mathbf{x} - \int_V \nabla P d\mathbf{x}. \quad (1.11)$$

Substitute (1.11) into (1.10). Then (1.9) becomes

$$\int_V \left[ \rho \left( \frac{\partial\mathbf{u}}{\partial t} + (\mathbf{u} \cdot \nabla)\mathbf{u} \right) - \mu \Delta\mathbf{u} + \nabla P \right] (t, \mathbf{x}) d\mathbf{x} = \int_V f_{ext}(t, \mathbf{x}) d\mathbf{x}. \quad (1.12)$$

Since  $V$  is arbitrary, one has

$$\frac{\partial\mathbf{u}}{\partial t} + (\mathbf{u} \cdot \nabla)\mathbf{u} - \frac{\mu}{\rho} \Delta\mathbf{u} + \nabla p = \mathbf{f} \quad \text{in } (0, T] \times \Omega, \quad (1.13)$$

here  $\mathbf{f} := \frac{\mathbf{f}_{ext}}{\rho}$ , and  $p := \frac{P}{\rho}$ . Thus, equation (1.13) along with (1.6) gives for unsteady flow of incompressible, viscous, Newtonian fluid:

$$\frac{\partial \mathbf{u}}{\partial t} + (\mathbf{u} \cdot \nabla) \mathbf{u} - \frac{\mu}{\rho} \Delta \mathbf{u} + \nabla p = \mathbf{f}, \quad (1.14)$$

$$\nabla \cdot \mathbf{u} = 0, \quad (1.15)$$

in  $(0, T] \times \Omega$ .

### 1.1.2.1 The Nondimensional Form of the NSE

To obtain the dimensionless form of the (1.14)-(1.15) in three dimensions, we first define  $\mathbf{u} = (u, v, w)$ , and write the x, y and z-components of the equations (1.2)-(1.3)

$$\frac{\partial u}{\partial t} + u \frac{\partial u}{\partial x} + v \frac{\partial u}{\partial y} + w \frac{\partial u}{\partial z} - \nu \Delta u + \frac{1}{\rho} \frac{\partial P}{\partial x} = 0 \quad (1.16)$$

$$\frac{\partial v}{\partial t} + u \frac{\partial v}{\partial x} + v \frac{\partial v}{\partial y} + w \frac{\partial v}{\partial z} - \nu \Delta v + \frac{1}{\rho} \frac{\partial P}{\partial y} = 0, \quad (1.17)$$

$$\frac{\partial w}{\partial t} + u \frac{\partial w}{\partial x} + v \frac{\partial w}{\partial y} + w \frac{\partial w}{\partial z} - \nu \Delta w + \frac{1}{\rho} \frac{\partial P}{\partial z} = g_z, \quad (1.18)$$

$$\frac{\partial u}{\partial x} + \frac{\partial v}{\partial y} + \frac{\partial w}{\partial z} = 0. \quad (1.19)$$

Define dimensionless variables as follows:

$$x^* = \frac{x}{L}, \quad y^* = \frac{y}{L}, \quad z^* = \frac{z}{L},$$

$$u^* = \frac{u}{U}, \quad v^* = \frac{v}{U}, \quad w^* = \frac{w}{U}, \quad t^* = \frac{t}{L/U}, \quad p^* = \frac{P}{\rho U^2}, \quad g_z^* = \frac{g_z}{g_0},$$

where  $U$ ,  $L$  and  $g_0$  represent the characteristic velocity, length and the magnitude of gravity, respectively. Then

$$\frac{\partial u}{\partial t} = \frac{U^2}{L} \frac{\partial u^*}{\partial t^*}, \quad u \frac{\partial u}{\partial x} = \frac{U^2}{L} u^* \frac{\partial u^*}{\partial x^*},$$

$$\nu \Delta u = \frac{\nu U}{L^2} \Delta u^*, \quad \frac{1}{\rho} \frac{\partial P}{\partial x} = \frac{U^2}{L} \frac{\partial p^*}{\partial x^*}.$$

Rewriting the remaining terms in (1.16)-(1.19), and plugging them into (1.16)-(1.19) gives the following:

$$\begin{aligned} \frac{U^2}{L} \frac{\partial u^*}{\partial t^*} + \frac{U^2}{L} u^* \frac{\partial u^*}{\partial x^*} + \frac{U^2}{L} v^* \frac{\partial u^*}{\partial y^*} + \frac{U^2}{L} w^* \frac{\partial u^*}{\partial z^*} - \frac{\nu U}{L^2} \Delta u^* \\ + \frac{\rho U^2}{\rho L} \frac{\partial p^*}{\partial x^*} = 0 \end{aligned} \quad (1.20)$$

$$\begin{aligned} \frac{U^2}{L} \frac{\partial v^*}{\partial t^*} + \frac{U^2}{L} u^* \frac{\partial v^*}{\partial x^*} + \frac{U^2}{L} v^* \frac{\partial v^*}{\partial y^*} + \frac{U^2}{L} w^* \frac{\partial v^*}{\partial z^*} - \frac{\nu U}{L^2} \Delta v^* \\ + \frac{\rho U^2}{\rho L} \frac{\partial p^*}{\partial y^*} = 0, \end{aligned} \quad (1.21)$$

$$\begin{aligned} \frac{U^2}{L} \frac{\partial w^*}{\partial t^*} + \frac{U^2}{L} u^* \frac{\partial w^*}{\partial x^*} + \frac{U^2}{L} v^* \frac{\partial w^*}{\partial y^*} + \frac{U^2}{L} w^* \frac{\partial w^*}{\partial z^*} - \frac{\nu U}{L^2} \Delta w^* \\ + \frac{\rho U^2}{\rho L} \frac{\partial p^*}{\partial z^*} = g_0 g_z^*, \end{aligned} \quad (1.22)$$

$$\frac{U}{L} \left( \frac{\partial u^*}{\partial x^*} + \frac{\partial v^*}{\partial y^*} + \frac{\partial w^*}{\partial z^*} \right) = 0, \quad (1.23)$$

First, multiply the first three equations by  $\frac{L}{U^2}$ , and the last equation by  $\frac{L}{U}$ . Next, drop the notation (\*), define  $Re := \frac{UL}{\nu}$ , and  $\mathbf{f} := (0, 0, \frac{1}{Fr^2} g_z^*)$ , where  $Fr := \frac{U}{\sqrt{g_0 L}}$ . Then, rewriting the equations in the vector form produces the following equations:

$$\frac{\partial \mathbf{u}}{\partial t} + (\mathbf{u} \cdot \nabla) \mathbf{u} - \frac{1}{Re} \Delta \mathbf{u} + \nabla p = \mathbf{f}, \quad (1.24)$$

$$\nabla \cdot \mathbf{u} = 0. \quad (1.25)$$

In the rest of the thesis,  $1/Re$  is denoted by the letter  $\nu$  for the stability and convergence analysis.

**Remark 1.1.3** *The dimensionless parameter  $Re$  is called Reynolds number, and is the ratio of the inertial forces to viscous force. The size of the  $Re$  plays a key role in distinguishing laminar flows from turbulent ones. When  $Re$  decreases, the flow becomes smooth and more easily predictable because of the dominance of the viscous term. However, as  $Re$  increases, the convective force dominates, and makes the flow unstable and chaotic. Such flows are called turbulent, and they have complex fluid structure. When  $Re < 2300$ , the flow is laminar, and  $Re > 2300$ , the flow turbulent.*

### 1.1.3 Incompressible non-isothermal fluid flow driven by natural convection

Incompressible non-isothermal fluid flows are important research areas in convective heat transfer, and are controlled by the NSE along with the heat transfer equation. Therefore, we need some information about heat transfer.

#### 1.1.3.1 Heat Transfer Fundamentals

There are three mechanism in which heat transfers: conduction, convection, and radiation.

- **Conduction** is the transfer of the energy from the more energetic particles of a substance to the adjacent, less energetic ones as a result of interactions between the particles.
- **Convection** is the mode of the heat transfer between a solid surface and the adjacent liquid or gas that is in the motion. It involves the combined effects of conduction and fluid motion.
- **Radiation** is the transfer of energy due to the emission of electromagnetic waves (or photons).

**Heat transfer rate** is the amount of heat transferred per unit time, and denoted by  $\dot{Q}$ . If the rate of heat transfer is available, then the total amount of heat transfer during a time interval  $\Delta t$  can be determined from

$$Q = \int_0^{\Delta t} \dot{Q} dt.$$

The basic requirement in the heat transfer is the existence of a temperature difference. The rate of heat transfer in a certain direction depends on the magnitude of the temperature gradient in that direction. The larger the temperature gradient, the higher the rate of heat transfer.

In a gravitational field, there exist a net force that pushes upward a light fluid placed in a heavier fluid. The upward force exerted by a fluid on a body completely or partially immersed in it is called the **buoyancy force**.

**Heat flux** is the rate of the heat transfer per unit area which is normal to the direction of heat transfer. Average heat flux is expressed as

$$\dot{q} = \frac{\dot{Q}}{A}$$

where  $A$  is the heat transfer area.

**Thermal diffusivity** represents how fast heat diffuses through a material, and it is defined as

$$\kappa = \frac{\text{Heat conducted}}{\text{Heat stored}} = \frac{k}{\rho C_p} \quad (m^2/s^2)$$

Note that thermal conductivity  $k$  represents how well a material conducts heat, and heat capacity  $\rho C_p$  represents how much energy a material stores per unit volume.

**Volume (or Thermal) Expansion Coefficient** is a measure of the change in volume of a substance with temperature at constant pressure, defined as [63]

$$\beta := \frac{1}{\nu} \left( \frac{\partial \nu}{\partial \theta} \right)_P = -\frac{1}{\rho} \left( \frac{\partial \rho}{\partial \theta} \right)_P,$$

where  $\nu$  is the kinematic viscosity, and  $\rho$  the fluid density.

### 1.1.3.2 Derivation of the Non-Isothermal Fluid Flows

Derivation of incompressible, non-isothermal, Newtonian fluid flows with constant properties, including density, driven by natural convection depends on the conservation of mass, the linear momentum and the energy. Thus, the system of equations with Boussinesq assumption and external force  $\mathbf{f}$  are expressed by the NSE together with heat transport equation. The Boussinesq approximation states that *the density differences can be neglected everywhere except in the buoyancy force*, With this assumption, the thermal expansion coefficient is written as follows [21]:

$$\beta = -\frac{1}{\rho} \frac{\rho_\infty - \rho}{\theta_\infty - \theta},$$

where  $\rho$  is the fluid density,  $\rho_\infty$  and  $\theta_\infty$  are the reference density, and the reference temperature away from the surface. Similarly, this assumption enables us to rewrite the gravity force as

$$\rho \mathbf{f} = \rho \mathbf{g} = (\rho_\infty - \rho) \mathbf{g}.$$

This reduces the equation of the fluid motion to the following:

$$\frac{\partial \mathbf{u}}{\partial t} + (\mathbf{u} \cdot \nabla) \mathbf{u} + \frac{1}{\rho} \nabla P - \frac{\mu}{\rho} \Delta \mathbf{u} = \mathbf{g} \beta (\theta - \theta_\infty) + \mathbf{f}, \quad (1.26)$$

$$\nabla \cdot \mathbf{u} = 0. \quad (1.27)$$

The last step is the derivation of the heat transport equation. From the energy balance, the first law of thermodynamics, meaning *energy is neither created nor destroyed, it can only changes the form*, one can get the following for any control volume  $V$  in  $\mathbb{R}^3$ :

$$\begin{aligned} & \left( \begin{array}{c} \text{the rate of} \\ \text{heat accumulation} \\ \text{inside } V \end{array} \right) \\ &= \left( \begin{array}{c} \text{the net heat transfer rate} \\ \text{by conduction} \\ \text{into } V \end{array} \right) + \left( \begin{array}{c} \text{the net heat transfer rate} \\ \text{by convection} \\ \text{into } V \end{array} \right) \\ & \quad + \left( \begin{array}{c} \text{the net heat generation rate} \\ \text{inside } V \end{array} \right). \end{aligned}$$

Under the assumption that density  $\rho$ , viscosity  $\mu$ , thermal conductivity  $k$  and specific heat  $c_p$  of the fluid are constant, the fluid heat per unit mass is expressed by  $c_p \theta$ . Then, the energy balance in  $\Omega$  can be expressed mathematically as follows:

$$\frac{\partial}{\partial t} \iiint_{\Omega} (\rho c_p \theta) dx = \iint_S q \cdot \mathbf{n} ds + \iint_S (\rho c_p \theta) (\mathbf{u} \cdot \mathbf{n}) ds + \iiint_{\Omega} \mu G dx,$$

where  $G$  is the volumetric energy rate,  $q$  is the heat flux, which is defined as the heat transfer rate per unit area and is given by

$$q = \frac{Q}{A} = -k \nabla \theta, \quad (1.28)$$

where  $Q$  represents the heat transfer rate per unit time. Now with the application of the divergence theorem along with the relation (1.28) produces

$$\iiint_{\Omega} \rho c_p \frac{\partial \theta}{\partial t} dx = \iiint_{\Omega} k \nabla \cdot \nabla \theta dx - \iiint_{\Omega} \rho c_p \nabla \cdot (\theta \mathbf{u}) dx + \iiint_{\Omega} \mu G dx. \quad (1.29)$$

Now, using the following

$$\nabla \cdot (\theta \mathbf{u}) = (\mathbf{u} \cdot \nabla) \theta + (\theta \cdot \nabla) \mathbf{u}, \quad (\nabla \cdot \nabla) \theta = \Delta \theta,$$



along with the incompressibility of the fluid ( $\nabla \cdot \mathbf{u} = 0$ ) reduces the integral equation (1.29) to

$$\iiint_{\Omega} \rho c_p \frac{\partial \theta}{\partial t} dV = \iiint_{\Omega} k \Delta \theta dV - \iiint_{\Omega} \rho c_p (\mathbf{u} \cdot \nabla) \theta dV + \iiint_{\Omega} \mu G dx. \quad (1.30)$$

Finally, dividing (1.30) by  $\rho c_p$  produces the heat transport equation:

$$\frac{\partial \theta}{\partial t} - \frac{k}{\rho c_p} \Delta \theta + (\mathbf{u} \cdot \nabla) \theta = \mu \frac{1}{\rho c_p} G, \quad (1.31)$$

This equation together with (1.26) and (1.27) gives the governing dimensional equations for the Boussinesq system:

$$\frac{\partial \mathbf{u}}{\partial t} + (\mathbf{u} \cdot \nabla) \mathbf{u} + \frac{1}{\rho} \nabla P - \nu \Delta \mathbf{u} = \mathbf{g} \beta (\theta - \theta_{\infty}) + \mathbf{f}, \quad (1.32)$$

$$\nabla \cdot \mathbf{u} = 0, \quad (1.33)$$

$$\frac{\partial \theta}{\partial t} + (\mathbf{u} \cdot \nabla) \theta - \kappa \Delta \theta = \Gamma, \quad (1.34)$$

where  $\Gamma := \mu \frac{1}{\rho c_p} G$ , and  $\kappa := \frac{k}{\rho c_p}$ .

### 1.1.3.3 Dimensionless Form of the Boussinesq System

To derive the dimensionless form of the Boussinesq system in 2D without the forcing terms, define the dimensionless variables as follows [21]:

$$\begin{aligned} x^* &= \frac{x}{L}, \quad y^* = \frac{y}{L}, \\ u^* &= \frac{u}{U}, \quad v^* = \frac{v}{U}, \quad t^* = \frac{tU}{L}, \quad p^* = \frac{P}{\rho U^2}, \quad \theta^* = \frac{\theta - \theta_{\infty}}{\theta_s - \theta_{\infty}}, \end{aligned}$$

here  $U$  is the characteristic velocity,  $L$  the characteristic length,  $\theta_s$  the temperature of the surface,  $\nu$  the kinematic viscosity,  $g$  the gravitational acceleration. Substituting these with appropriate calculations, and dropping the notation (\*), we have

$$\frac{U^2}{L} \frac{\partial \mathbf{u}}{\partial t} + \frac{U^2}{L} (\mathbf{u} \cdot \nabla) \mathbf{u} - \frac{\nu U}{L^2} \Delta \mathbf{u} + \frac{U^2}{L} \nabla p = \langle 0, g \beta (\theta_s - \theta_{\infty}) \rangle \theta, \quad (1.35)$$

$$\frac{U}{L} \nabla \cdot \mathbf{u} = 0, \quad (1.36)$$

$$\frac{U(\theta_s - \theta_{\infty})}{L} \frac{\partial \theta}{\partial t} + \frac{U(\theta_s - \theta_{\infty})}{L} (\mathbf{u} \cdot \nabla) \theta - \frac{\kappa(\theta_s - \theta_{\infty})}{L^2} \Delta \theta = \mu \frac{U^2}{L^2 \rho c_p} G. \quad (1.37)$$

First, divide the first equation by  $\frac{U^2}{L}$ , the second equation by  $\frac{U}{L}$ , and the third equation by  $\frac{U(\theta_s - \theta_\infty)}{L}$ . Next consider the following:

$$\begin{aligned}\frac{g\beta(\theta_s - \theta_\infty)L}{U^2} &= \frac{g\beta(\theta_s - \theta_\infty)L L^2\nu^2}{U^2 L^2\nu^2} \\ &= \frac{g\beta(\theta_s - \theta_\infty)L^3}{\nu^2} \frac{1}{(UL/\nu)^2} \\ \frac{\kappa(\theta_s - \theta_\infty)}{L^2} \frac{L}{U(\theta_s - \theta_\infty)} &= \frac{\kappa(\theta_s - \theta_\infty)}{L^2} \frac{L}{U(\theta_s - \theta_\infty)} \frac{\nu}{\nu} \\ &= -\frac{1}{\nu/\kappa} \frac{1}{UL/\nu}, \\ \frac{\mu U}{L\rho c_p(\theta_s - \theta_\infty)} &= \frac{\mu U}{L\rho c_p(\theta_s - \theta_\infty)} \frac{U}{U} = \frac{U^2}{c_p(\theta_s - \theta_\infty)} \frac{\mu/\rho}{UL}, \\ &= \frac{Ec}{Re}.\end{aligned}$$

Then, (1.35)-(1.37) reduces to the following, which is the *dimensionless form* of (1.32)-(1.34) without forcing terms:

$$\frac{\partial \mathbf{u}}{\partial t} + (\mathbf{u} \cdot \nabla) \mathbf{u} - \nu \Delta \mathbf{u} - \nabla p = \frac{Gr}{Re^2} \langle 0, \theta \rangle, \quad (1.38)$$

$$\nabla \cdot \mathbf{u} = 0, \quad (1.39)$$

$$\frac{\partial \theta}{\partial t} + (\mathbf{u} \cdot \nabla) \theta - \frac{1}{Pr Re} \Delta \theta = \frac{Ec}{Re} G. \quad (1.40)$$

where  $\nu = 1/Re$ ,  $Pr := \nu/\kappa$ ,  $Gr := \frac{g\beta(\theta_s - \theta_\infty)L^3}{\nu^2}$ , and  $Ec := \frac{U^2}{c_p(\theta_s - \theta_\infty)}$ , called Eckert number. In the rest of the thesis,  $\frac{Gr}{Re^2}$  and  $\frac{1}{Pr Re}$  are denoted by the letters  $Ri$  and  $\kappa$ , respectively.

**Remark 1.1.4** *In the system of equations (1.38)-(1.40),*

- $Ri = Gr/Re^2$  is called *Richardson number*, and  $Gr$  is called the *Grashof number*.  $Ri$  is the ratio of the buoyancy force to the viscous force, and accounts for the gravitational force as well as the thermal expansion of the fluid. In addition to that,  $Ri$  plays a key role in determining the flow as forced, natural, and mixed convection. For  $Ri \ll 1$ , the flow is called forced convection; for  $Ri \gg 1$ , the natural convection; and  $Ri \approx 1$ , the mixed convection.
- $Pr$  is called *Prandtl number*, is the ratio of the molecular momentum diffusivity to the molecular thermal diffusivity. For air,  $Pr \approx 0.71$ ; for water,  $Pr \approx 7$ .

### 1.1.4 Magnetohydrodynamic Equations

The study of MHD flow deals with the interaction between a magnetic field and electrically conducting fluid, such as in plasmas, liquid metals and electrolytes. The evolution *dimensional* equations describing MHD flows use both fluid mechanics and electromagnetism theory, and consist of the Navier-Stokes and pre-Maxwell equations [76, 9]:

$$\mathbf{u}_t + (\mathbf{u} \cdot \nabla)\mathbf{u} - s(\mathbf{B} \cdot \nabla)\mathbf{B} - \nu\Delta\mathbf{u} + \nabla p = \mathbf{f}, \quad (1.41)$$

$$\nabla \cdot \mathbf{u} = 0, \quad (1.42)$$

$$\mathbf{B}_t + (\mathbf{u} \cdot \nabla)\mathbf{B} - (\mathbf{B} \cdot \nabla)\mathbf{u} - \nu_m\Delta\mathbf{B} = \nabla \times \mathbf{g}, \quad (1.43)$$

$$\nabla \cdot \mathbf{B} = 0, \quad (1.44)$$

in  $(0, T] \times \Omega$ . Here  $\mathbf{u}$  is the velocity of the fluid,  $p$  is a modified pressure,  $\mathbf{B}$  is the magnetic field,  $\nu$  is the kinematic viscosity. In addition  $s = \frac{1}{\rho\tilde{\mu}}$ ,  $\tilde{\mu}$  is the magnetic permeability,  $\rho$  density, and  $\nu_m = \frac{1}{\tilde{\mu}\sigma}$ , called the magnetic resistivity,  $\sigma$  the electrical conductivity,  $\mathbf{f}$  is external force and  $\nabla \times \mathbf{g}$  is the external forces acting on the magnetic field.

#### 1.1.4.1 Derivation of MHD Equations in Primitive Variables

A non-magnetic, conducting particle moving with velocity  $\mathbf{u}$ , and carrying a charge  $q$  in a magnetic field  $\mathbf{B}$  is exposed to the following three forces ([31]):

$$\mathbf{f} = q\mathbf{E}_s + q\mathbf{E}_i + q\mathbf{u} \times \mathbf{B}$$

here

- $q\mathbf{E}_s$  is called Coulomb (electrostatic) force resulting from the repulsion or attraction of electric charges;  $\mathbf{E}_s$  the electrostatic field,
- $q\mathbf{E}_i$  is the force which the charge experiences in the presence of a time-varying magnetic field;  $\mathbf{E}_i$  the electric field induced by the changing magnetic field,
- $q\mathbf{u} \times \mathbf{B}$  is the Lorentz force resulting from the motion of charge in a magnetic field.

The application of Coulomb and Gauss's law yields

$$\nabla \cdot \mathbf{E}_s = \rho_e / \epsilon_0, \quad \nabla \times \mathbf{E}_s = 0,$$

here  $\rho_e$  is the total charge density, and  $\epsilon_0$  is the permittivity of free space. On the other hand, induced electric field has zero divergence and by Faraday's law,

$$\nabla \cdot \mathbf{E}_i = 0, \quad \nabla \times \mathbf{E}_i = -\frac{\partial \mathbf{B}}{\partial t}.$$

Define the total electric field by  $\mathbf{E} = \mathbf{E}_s + \mathbf{E}_i$ . Then

$$\mathbf{f} = q(\mathbf{E} + \mathbf{u} \times \mathbf{B}), \quad (1.45)$$

$$\nabla \cdot \mathbf{E} = \frac{\rho_e}{\epsilon_0}, \quad \nabla \times \mathbf{E} = -\frac{\partial \mathbf{B}}{\partial t}. \quad (1.46)$$

Form the second equation of (1.46), one can obtain that  $\nabla \cdot \mathbf{B} = 0$ . By Ohm's law,

$$\mathbf{J} = \sigma(\mathbf{E} + \mathbf{u} \times \mathbf{B}),$$

here  $\sigma$  is the electrical conductivity of the fluid. In addition, the conservation of charge in stationary conductor, that states that the electric charge is neither created nor destroyed, the rate of total charge in a volume is equal to the the rate of charge flowing cross the surface of that volume, gives that

$$\nabla \cdot \mathbf{J} = -\frac{\partial \rho_e}{\partial t}. \quad (1.47)$$

However,  $\rho_e$  is very small in motion which leads to ignoring  $\frac{\partial \rho_e}{\partial t}$ , and reducing (1.47) to  $\nabla \cdot \mathbf{J} = 0$ .

Amperé-Maxwell equation is expressed by

$$\nabla \times \mathbf{B} = \tilde{\mu} \left( \mathbf{J} + \epsilon_0 \frac{\partial \mathbf{E}}{\partial t} \right),$$

where  $\tilde{\mu}$  is the magnetic permeability. Thus, Maxwell's equations for MHD are given as follows:

$$\nabla \cdot \mathbf{E} = -\frac{\rho_e}{\epsilon_0}, \quad \nabla \times \mathbf{E} = -\frac{\partial \mathbf{B}}{\partial t}, \quad (1.48)$$

$$\nabla \times \mathbf{B} = \tilde{\mu} \left( \mathbf{J} + \epsilon_0 \frac{\partial \mathbf{E}}{\partial t} \right), \quad \nabla \cdot \mathbf{B} = 0, \quad (1.49)$$

with additional equations

$$\nabla \cdot \mathbf{J} = -\frac{\partial \rho_e}{\partial t}, \quad \mathbf{F} = q(\mathbf{E} + \mathbf{u} \times \mathbf{B}). \quad (1.50)$$

In MHD, the term  $\partial\rho_e/\partial t$  is can be ignored. This is because of the dominance of the Lorentz force with compared with the electric force  $q\mathbf{E}$ . The term  $\epsilon_0\partial E/\partial t$  can be neglected too, if it is compared with the term current density  $\mathbf{J}$ . Therefore, Maxwell equations are reduced to

$$\nabla \times \mathbf{E} = -\frac{\partial \mathbf{B}}{\partial t}, \quad \nabla \cdot \mathbf{B} = 0, \quad (1.51)$$

$$\nabla \times \mathbf{B} = \tilde{\mu}\mathbf{J}, \quad \nabla \cdot \mathbf{J} = 0, \quad (1.52)$$

$$\mathbf{J} = \sigma(\mathbf{E} + \mathbf{u} \times \mathbf{B}), \quad (1.53)$$

$$\mathbf{F} = \mathbf{J} \times \mathbf{B}. \quad (1.54)$$

Now, we derive full MHD equations for incompressible flow by taking Lorentz force as a body force and  $\mathbf{f}, \nabla \times \mathbf{g}$  as external forces. First, consider the first equation in (1.51), next use (1.53) which yields the following:

$$\begin{aligned} \frac{\partial \mathbf{B}}{\partial t} &= -\nabla \times \mathbf{E} = -\nabla \times [(\mathbf{J}/\sigma) - \mathbf{u} \times \mathbf{B}] = \nabla \times [\mathbf{u} \times \mathbf{B} - \nabla \times \mathbf{B}/\tilde{\mu}\sigma] \\ \frac{\partial \mathbf{B}}{\partial t} &= \nabla \times (\mathbf{u} \times \mathbf{B}) - \frac{1}{\tilde{\mu}\sigma} \nabla \times (\nabla \times \mathbf{B}). \end{aligned} \quad (1.55)$$

Rewrite the right hand side terms of (1.55) along with the solenoidal constraint on  $\mathbf{u}$  and  $\mathbf{B}$  as

$$\begin{aligned} \nabla \times (\mathbf{u} \times \mathbf{B}) &= \mathbf{u}\nabla \cdot \mathbf{B} - \mathbf{B}\nabla \cdot \mathbf{u} + (\mathbf{B} \cdot \nabla)\mathbf{u} - (\mathbf{u} \cdot \nabla)\mathbf{B} \\ &= (\mathbf{B} \cdot \nabla)\mathbf{u} - (\mathbf{u} \cdot \nabla)\mathbf{B}, \\ \nabla \times (\nabla \times \mathbf{B}) &= \nabla(\nabla \cdot \mathbf{B}) - \Delta \mathbf{B} \\ &= -\Delta \mathbf{B}. \end{aligned}$$

Then, equation (1.55) reduces to

$$\frac{\partial \mathbf{B}}{\partial t} = (\mathbf{B} \cdot \nabla)\mathbf{u} - (\mathbf{u} \cdot \nabla)\mathbf{B} + \nu_m \Delta \mathbf{B}, \quad \nu_m = (\tilde{\mu}\sigma)^{-1}, \quad (1.56)$$

$$\nabla \cdot \mathbf{B} = 0. \quad (1.57)$$

On the other hand, the dimensional equations of the fluid motion are given as

$$\frac{\partial \mathbf{u}}{\partial t} = -\mathbf{u} \cdot \nabla \mathbf{u} + \frac{1}{\rho}(\mathbf{J} \times \mathbf{B}) + \nu \Delta \mathbf{u} - \frac{1}{\rho} \nabla P - \mathbf{f}, \quad (1.58)$$

$$\nabla \cdot \mathbf{u} = 0. \quad (1.59)$$

Rewrite the Lorentz force using the first equation in (1.58):

$$-\frac{1}{\rho}(J \times \mathbf{B}) = \frac{1}{\rho}(\mathbf{B} \times J) = \frac{1}{\rho\tilde{\mu}}(\mathbf{B} \times (\nabla \times \mathbf{B})), \quad (1.60)$$

$$\mathbf{B} \times (\nabla \times \mathbf{B}) = \nabla(\mathbf{B} \cdot \mathbf{B}) - (\mathbf{B} \cdot \nabla)\mathbf{B} = \frac{1}{2}|\mathbf{B}|^2 - (\mathbf{B} \cdot \nabla)\mathbf{B}, \quad (1.61)$$

Then use that in (1.58), and denote  $p := 1/\rho \left( \frac{1}{2\tilde{\mu}}|\mathbf{B}|^2 - P \right)$  which produces

$$\frac{\partial \mathbf{u}}{\partial t} + (\mathbf{u} \cdot \nabla)\mathbf{u} - \frac{1}{\rho\tilde{\mu}}(\mathbf{B} \cdot \nabla)\mathbf{B} - \nu\Delta\mathbf{u} + \nabla p = \mathbf{f}, \quad (1.62)$$

$$\nabla \cdot \mathbf{u} = 0. \quad (1.63)$$

Then, the system equations (1.62), (1.63), (1.56) and (1.57) with an external force on the magnetic field form the MHD equations:

$$\frac{\partial \mathbf{u}}{\partial t} + (\mathbf{u} \cdot \nabla)\mathbf{u} - s(\mathbf{B} \cdot \nabla)\mathbf{B} - \nu\Delta\mathbf{u} + \nabla p = \mathbf{f}, \quad (1.64)$$

$$\nabla \cdot \mathbf{u} = 0, \quad (1.65)$$

$$\frac{\partial \mathbf{B}}{\partial t} + (\mathbf{u} \cdot \nabla)\mathbf{B} - (\mathbf{B} \cdot \nabla)\mathbf{u} - \nu_m\Delta\mathbf{B} = \nabla \times g, \quad (1.66)$$

$$\nabla \cdot \mathbf{B} = 0. \quad (1.67)$$

where  $\nu = \frac{\mu}{\rho}$ ,  $s = \frac{1}{\rho\tilde{\mu}}$ , and  $\nu_m = \frac{1}{\tilde{\mu}\sigma}$ , called the magnetic viscosity.

#### 1.1.4.2 Dimensionless form of MHD equations in primitive variables

To produce the dimensionless form of (1.66) without forcing terms in 2D, denote the fluid velocity and the magnetic field by  $\mathbf{u} = (u, v)$  and  $\mathbf{B} = (B_x, B_y)$ , respectively. Then define the dimensionless variables as follows [92], [88]:

$$\begin{aligned} x^* &= \frac{x}{L}, \quad y^* = \frac{y}{L}, \quad t^* = \frac{tU}{L}, \\ u^* &= \frac{u}{U}, \quad v^* = \frac{v}{U}, \quad p^* = \frac{P}{\rho U^2}, \\ B_x^* &= \frac{B_x}{A}, \quad B_y^* = \frac{B_y}{A}, \end{aligned}$$

here  $A$  is the magnitude of  $\mathbf{B}$ . Plugging them into (1.64)-(1.67) yields

$$\begin{aligned} \frac{U^2}{L} \frac{\partial \mathbf{u}^*}{\partial t^*} + \frac{U^2}{L} (\mathbf{u}^* \cdot \nabla) \mathbf{u}^* - \frac{sA^2}{L} (\mathbf{B}^* \cdot \nabla) \mathbf{B}^* - \frac{\nu U}{L^2} \Delta \mathbf{u}^* + \frac{U^2}{L} \nabla p^* &= \mathbf{f}, \\ \frac{U}{L} \nabla \cdot \mathbf{u}^* &= 0, \\ \frac{AU}{L} \frac{\partial \mathbf{B}^*}{\partial t^*} + \frac{AU}{L} (\mathbf{u}^* \cdot \nabla) \mathbf{B}^* - \frac{AU}{L} (\mathbf{B}^* \cdot \nabla) \mathbf{u}^* - \frac{\nu_m A}{L^2} \Delta \mathbf{B}^* &= \nabla \times \mathbf{g}, \\ \frac{A}{L} \nabla \cdot \mathbf{B}^* &= 0. \end{aligned}$$

First multiply the first equation by  $L/U^2$ , the second equation  $L/U$ , the third equation  $L/AU$  and the last equation  $L/A$ . Next denote  $f^* := \frac{f}{U^2/L}$ ,  $g^* := \frac{g}{AU}$ ,  $\nabla^* := L\nabla$ , and consider

$$\begin{aligned} \frac{sA^2}{U^2} &= \frac{1}{\rho} \frac{A^2}{(UL/\nu)(UL\sigma\tilde{\mu})} \frac{L^2\sigma}{\nu} = \frac{\left( AL\sqrt{\frac{\sigma}{\nu\rho}} \right)^2}{(UL/\nu)UL\sigma\tilde{\mu}} =: \frac{Ha^2}{ReRe_m}, \\ Re_m &:= UL\sigma\tilde{\mu}. \end{aligned}$$

Then dropping the  $*$  notation, one can have the dimensionless form of the system equations (1.64)-(1.67):

$$\frac{\partial \mathbf{u}}{\partial t} + \mathbf{u} \cdot \nabla \mathbf{u} - \frac{Ha^2}{ReRe_m} (\mathbf{B} \cdot \nabla) \mathbf{B} - \nu \Delta \mathbf{u} + \nabla p = \mathbf{f}, \quad (1.68)$$

$$\nabla \cdot \mathbf{u} = 0, \quad (1.69)$$

$$\frac{\partial \mathbf{B}}{\partial t} + (\mathbf{u} \cdot \nabla) \mathbf{B} - (\mathbf{B} \cdot \nabla) \mathbf{u} + \frac{1}{Re_m} \Delta \mathbf{B} = \nabla \times \mathbf{g}, \quad (1.70)$$

$$\nabla \cdot \mathbf{B} = 0. \quad (1.71)$$

where  $\nu := 1/Re$ ,  $Re_m = UL\sigma\tilde{\mu}$ , called magnetic Reynolds number.

**Remark 1.1.5** *In the system of equations (1.68)-(1.71), the dimensionless parameter*

- *In the rest of the thesis,  $\frac{1}{Re_m}$  and  $\frac{Ha^2}{ReRe_m}$  are denoted by the letters  $\nu_m$  and  $s$ , respectively.*
- *$Ha$  is called Hartmann number. It is interpreted as the ratio of the electromagnetic force to viscous force,*
- *$s$  is called the coupling number (magnetic force coefficient or interaction parameter),*

- $Re_m$  is called magnetic Reynolds number, the ratio of the advection ( $\nabla \times (\mathbf{u} \times \mathbf{B})$ ) to diffusion ( $\Delta \mathbf{B} / \sigma \tilde{\mu}$ ). If  $Re_m \ll 1$ , then  $\mathbf{u}$  has little effect on  $\mathbf{B}$ , the induced magnetic field being negligible by comparison with the imposed field [31],
- $Pr_m := \nu / \nu_m$  is called the magnetic Prandtl number.

### 1.1.4.3 Derivation of MHD equations in Elsässer variables

The Elsässer formulation of MHD was first proposed by W. Elsässer in 1950 [35]. To derive it, we begin by splitting the magnetic field into mean and fluctuations,

$$\sqrt{s}\mathbf{B} =: \sqrt{s}\mathbf{B}_0 + \sqrt{s}\mathbf{b} \quad \text{with } \mathbf{B}_0 = \mathbf{B}_0(t).$$

and rewriting system (1.68)-(1.71) as

$$\mathbf{u}_t + (\mathbf{u} \cdot \nabla)\mathbf{u} - s(\mathbf{B}_0 \cdot \nabla)\mathbf{b} - s(\mathbf{b} \cdot \nabla)\mathbf{b} - \nu\Delta\mathbf{u} + \nabla p = \mathbf{f}, \quad (1.72)$$

$$\nabla \cdot \mathbf{u} = 0, \quad (1.73)$$

$$\mathbf{b}_t + (\mathbf{u} \cdot \nabla)\mathbf{b} - (\mathbf{B}_0 \cdot \nabla)\mathbf{u} - (\mathbf{b} \cdot \nabla)\mathbf{u} - \nu_m\Delta\mathbf{b} = \nabla \times \mathbf{g} - \frac{d\mathbf{B}_0}{dt}, \quad (1.74)$$

$$\nabla \cdot \mathbf{b} = 0. \quad (1.75)$$

Now, rescale (1.74) by  $\sqrt{s}$ , add (subtract) (1.72) to (from) (1.74) and set

$$\begin{aligned} \mathbf{f}_1 &:= \mathbf{f} + \nabla \times \mathbf{g} - \frac{d\mathbf{B}_0}{dt}, & \mathbf{f}_2 &:= \mathbf{f} - \sqrt{s} \left( \nabla \times \mathbf{g} + \frac{d\mathbf{B}_0}{dt} \right), \\ q &:= P + \sqrt{s}\lambda, & r &:= P - \sqrt{s}\lambda \end{aligned}$$

Then we get

$$\begin{aligned} (\mathbf{u} + \sqrt{s}\mathbf{b})_t + (\mathbf{u} \cdot \nabla)(\mathbf{u} + \sqrt{s}\mathbf{b}) - (\sqrt{s}\mathbf{B}_0 \cdot \nabla)(\mathbf{u} + \sqrt{s}\mathbf{b}) - \nu\Delta\mathbf{u} \\ - (\sqrt{s}\mathbf{b} \cdot \nabla)(\mathbf{u} + \sqrt{s}\mathbf{b}) - \nu_m\Delta(\sqrt{s}\mathbf{b}) + \nabla q = \mathbf{f}_1, \end{aligned}$$

$$\nabla \cdot (\mathbf{u} + \sqrt{s}\mathbf{b}) = 0,$$

$$\begin{aligned} (\mathbf{u} - \sqrt{s}\mathbf{b})_t + (\mathbf{u} \cdot \nabla)(\mathbf{u} - \sqrt{s}\mathbf{b}) + (\sqrt{s}\mathbf{B}_0 \cdot \nabla)(\mathbf{u} - \sqrt{s}\mathbf{b}) - \nu\Delta\mathbf{u} \\ + (\sqrt{s}\mathbf{b} \cdot \nabla)(\mathbf{u} - \sqrt{s}\mathbf{b}) + \nu_m\Delta(\sqrt{s}\mathbf{b}) + \nabla r = \mathbf{f}_2, \end{aligned}$$

$$\nabla \cdot (\mathbf{u} - \sqrt{s}\mathbf{b}) = 0.$$



Now defining  $\mathbf{v} = \mathbf{u} + \sqrt{s}\mathbf{b}$ ,  $\mathbf{w} = \mathbf{u} - \sqrt{s}\mathbf{b}$ ,  $\tilde{\mathbf{B}}_0 = \sqrt{s}\mathbf{B}_0$  produces the Elsässer formulation:

$$\mathbf{v}_t + \mathbf{w} \cdot \nabla \mathbf{v} - (\tilde{\mathbf{B}}_0 \cdot \nabla) \mathbf{v} + \nabla q - \frac{\nu + \nu_m}{2} \Delta \mathbf{v} - \frac{\nu - \nu_m}{2} \Delta \mathbf{w} = \mathbf{f}_1, \quad (1.76)$$

$$\nabla \cdot \mathbf{v} = 0, \quad (1.77)$$

$$\mathbf{w}_t + \mathbf{v} \cdot \nabla \mathbf{w} + (\tilde{\mathbf{B}}_0 \cdot \nabla) \mathbf{w} + \nabla r - \frac{\nu + \nu_m}{2} \Delta \mathbf{w} - \frac{\nu - \nu_m}{2} \Delta \mathbf{v} = \mathbf{f}_2, \quad (1.78)$$

$$\nabla \cdot \mathbf{w} = 0. \quad (1.79)$$



## CHAPTER 2

### AN EXPLICITLY DECOUPLED VARIATIONAL MULTISCALE METHOD FOR INCOMPRESSIBLE NON ISOTHERMAL FLUID FLOWS

In this chapter, we focus on incompressible, non-isothermal flows driven by natural convection, we call the Boussinesq system. Recall from Section 1.1.3.3, *the dimensionless* form of governing equations of the system with appropriate initial velocity and temperature conditions and homogeneous Dirichlet boundary conditions along with forcing term, the equations (1.38)-(1.40) can be given by

$$\begin{aligned} \mathbf{u}_t + (\mathbf{u} \cdot \nabla)\mathbf{u} + \nabla p - \nu \Delta \mathbf{u} &= Ri \langle \mathbf{0}, \theta \rangle + \mathbf{f}, & \text{on } (0, T] \times \Omega, \\ \nabla \cdot \mathbf{u} &= 0, & \text{on } [0, T] \times \Omega, \\ \theta_t - \kappa \Delta \theta + (\mathbf{u} \cdot \nabla)\theta &= \Gamma, & \text{on } (0, T] \times \Omega, \\ \mathbf{u}|_{t=0} = \mathbf{u}_0, \theta|_{t=0} &= \theta_0, & \text{on } \Omega \\ \mathbf{u} = 0, \theta &= 0, & \text{on } \partial\Omega \end{aligned} \tag{2.1}$$

where  $\nu = 1/Re$ ,  $Ri = Gr/Re^2$ ,  $\kappa = 1/PrRe$  and  $Pr = \nu/\kappa$ .

It is clear to see that this system is a coupling of the Navier-Stokes equations and the transport equation. In addition, the complexity of the flow character at small  $\nu$  and the gaps in mathematical theory of incompressible flows make finding analytic solutions of natural convection flows seemingly impossible, and the remedy is to employ numerical methods and/or experimental analysis.

One popular and mathematically sound numerical discretization method for the solution of (2.1) is the finite element method. However, the application of the standard finite element methods leads to two main instabilities in approximate solutions. The

first instability is due to the dominance of the convective term, which is the result of the small  $\nu$  in (2.1), and can be seen as nonphysical oscillations with sharp boundary layers in the velocity and temperature solutions. In this case, the method loses accuracy, and this problem is handled with mesh refinement. However, especially in three dimensions, this effort requires more powerful computers than exist today, or will exist in the foreseeable future. The second numerical instability arises from the violation of the inf-sup (Ladyzhenskaya-Babuska-Brezzi (LBB)) stability condition, given by (2.13), and appears as oscillations, especially in the approximate pressure space.

In recent years, different stabilization techniques have been introduced to reduce the limitations mentioned above. The popular stabilization technique applied more extensively than the others is the residual based ones. The philosophy of the residual based stabilization is to add a control of a strong residual to the standard Galerkin formulation which acts on all scales. The popular residual based stabilization techniques seen in literature are the streamline-upwind/Petrov-Galerkin (SUPG), pressure-stabilizing Petrov-Galerkin (PSPG), grad-div stabilization and projection based variational multiscale (VMS) stabilization.

The SUPG stabilization technique can be applied to both compressible and incompressible flows. For incompressible flows, the stabilization term is added to the Galerkin formulation as a series of integral terms containing the product of the residual momentum equation and the advective term acting on the test functions. The technique was first presented by Hughes and Brooks in 1979 ([16]). In [17], the method was developed in the case of stationary convection dominated flows, and extended to the stationary incompressible Navier-Stokes equations. In addition, the accuracy of the SUPG was tested with numerical experiments in this study. The application of the technique for the incompressible flows based on the vorticity-stream function and velocity-pressure formulations was reported in [102], and for the linear advection-dominated flow problems in [73]. On the other hand, the technique was applied to the stationary scalar linear convection-dominated convection-diffusion problem and the extension to the case of time dependent, variable coefficient was studied in [72]. The more studies about SUPG for time-dependent multi-dimensional advective-diffusive, scalar advection-diffusion and convection-diffusion as well as transport problems can be seen, respectively in [61, 11, 101, 19]. The comparison of the method with

some stabilization techniques to the diffusion-convection-reaction is given in [28]. In [27], by using SUPG formulation, the stability and accuracy is analyzed for the one-dimensional convection-diffusion equations along with the forward Euler scheme. The stabilization technique PSPG for the steady-state Stokes and the Navier-Stokes has been reported in [103], and for the unsteady Stokes problem with time step restriction in [10], and for the transient Stokes problem in [20]. Optimal error estimates without time step restriction for the PSPG method for unsteady Stokes equations are presented in [70].

The grad-div stabilization technique was first introduced by Franca and Hughes in [42]. The main idea in this technique for the NSE is to add a user-selected penalty term involving the residual of the continuity equation into the Galerkin finite element formulation. By this way, it is obtained a control on the lack of the mass conservation, and aimed to prevent the negative effect of the pressure on the velocity error. Standard error analysis for the grad-div stabilization with the choice of the LBB-stable finite element pairs, for example Taylor Hood element, shows that this penalty-parameter should be chosen as  $\mathcal{O}(1)$  to achieve optimal convergence order. This method with subgrid pressure models for the incompressible NSE is applied in [86]. The application of the method for the NSE in rotation form and for the Stokes problem can be seen in [78, 87], respectively. These studies [78, 87, 86] reveal that the technique improves the accuracy of the finite element solutions for the Stokes and the NSE by reducing the effect of the pressure error on velocity. Grad-div stabilization for Oseen problem with LBB-stable finite element pairs is studied for both the continuous in time and the fully discrete case (backward Euler method, two step backward differentiation formula (BDF2), and Crank-Nicolson schemes) in [43], and for the Bousinesq flow in [32], and thermal convection flow problems in [45].

In literature, there are several papers, reviewing different stabilized method for many different flow problems. For example, Franca et al. in [39] consider these techniques for advection-diffusion equations. In [40], for Stokes problem, and in [13] for Oseen problem, stabilized finite element schemes are reviewed.

One of the recent popular stabilization method is the projection based methods. These methods are closely connected with the framework of the variational multiscale method which was first proposed by Hughes in 1995, [60]. Following from [60], the solution scales in flow can be decomposed as large and small scales. The underlying idea

of VMS methods is the definition of the large scales by using projection into appropriate subspaces. Based on the ideas from [60], Collis [29] proposed multiscale discretization of the NSE for turbulent flows. According to [29], the flow field can be decomposed into three scales (large, small, and unresolved small scales).

Following ideas from [53, 60], there are different realizations of the VMS in literature. One realization is through bubble VMS method. In this method, the finite element spaces satisfying the LBB condition are chosen for the large scales, and the residual bubbles for the small scales. The key point in the usage of the bubble functions is to separate small scales into a number of local problems to obtain an efficient method. However, this choice of small scales does not reflect the true physical behavior of the small scales. Residual-free bubble and an inf-sup stable element was used for the Oseen problem in [41]. Gravemeier et al. in [48] used residual free bubbles with three, and two scales VMS method for the time-dependent NSE, and with three scales VMS for the large eddy simulation of the turbulent flows in [49]. John and Kindl was used them for the NSE on the turbulent channel flow in [68].

Another realization of the VMS is called projection-based VMS method. In this method, the finite element spaces satisfying the LBB condition are chosen for all scales, not only for the large scales, and large scales are defined by projection into appropriate solution spaces. For the large scales either a lower order finite element space than the standard finite element spaces is chosen, or higher ones. In the former case, both large and small scale solutions are computed on the same mesh, which is called one level VMS method (see, [65]). This paper reveals that with suitable conditions on large scales, VMS method can be implemented easily into an existing code for solving the NSE. On the other hand, in the latter case, called two level VMS, the approximate large scale solutions are calculated on a coarser mesh [67]. In [67], the convection-dominated convection-diffusion equations was studied. In this study, VMS introduces an additional diffusion term, uses a fine mesh  $C^0$ -finite element space for all scales, and a coarse mesh discontinuous finite element space for large scales. This study with the choice of large scales concludes two results: first, VMS is implemented in such an efficient way that the computational time for semi-discrete discretization (only time discretization) with VMS does not increase with the use of the finer mesh of large scale space compared to fully implicit discretization. Second, the convergence rate for the method gives similar results for the streamline

diffusion finite element method if it is used with appropriate scaling of fine and coarse mesh. The extension of the method to the NSE can be given in [66], which presents finite element error analysis of the method with the constant depends on the reduced Reynolds number. The application of the VMS of the non-isothermal free convection problems with a priori error estimate and the standard benchmark problem in a two-dimensional differentially heated two-dimensional cavity was reported in [85], and to the MHD in [7], steady-state natural convection in [25], and to the Darcy-Brinkman equations in [26].

The studies about the VMS method reveal that it gives much more accurate approximate solutions on coarse meshes, and reduces to the requirement of the computational memory. Recently, a variant of VMS was proposed for Navier-Stokes simulations by Layton et. al. in [79], which is in essence a post-processing step to be used after each time step in a Navier-Stokes solver, but is cleverly constructed in such a way that it recovers the (discretized) VMS eddy viscosity, and thus truncates scales at the correct location. The purpose of this chapter is to extend this novel idea from [79] of decoupled, post-processing VMS to the Boussinesq system by introducing two decoupled (post processing) VMS steps: one each for velocity and temperature, in order to efficiently truncate velocity and temperature scales. We note that related studies of VMS methods for transport equations have been performed in [53]. In addition, for non-isothermal free convection problems with large-eddy simulation was reported in [85]. The novelty of our proposed method is that it is a fully discrete method that fully decouples the transport equation and the VMS steps from the mass/momentum equations. In addition, the proposed method truncates scales with an *explicitly decoupled stabilization*, which can thus be considered as a post-processing step that one can implement VMS steps into an existing code without changing original (existing) codes. We present details about the algorithm in Section 2.2.

## 2.1 Mathematical Preliminaries

In this section, we present some necessary definitions and inequalities which are essential in our stability and convergence analysis. Through this thesis, we assume that  $\Omega$  represents simply connected, bounded region in  $\mathbb{R}^d$ ,  $d \in \{2, 3\}$ , with smooth

boundary  $\partial\Omega$ .

**Definition 2.1.1** A measurable function  $f$  defined on  $\Omega$  is said to be essentially bounded if there exists a constant  $M$  such that

$$|f(x)| \leq M, \text{ for almost everywhere (a.e.) on } \Omega.$$

The greatest lower bound of such constants  $M$  is called the essential supremum of  $\Omega$ , and is denoted by [1]

$$\|f\|_{\infty} := \text{ess sup}_{x \in \Omega} |f(x)|.$$

**Definition 2.1.2** The Lebesgue spaces, denoted by  $L^p(\Omega)$ ,  $1 \leq p \leq \infty$ , are defined as follows [1]:

$$L^p(\Omega) : \{f : f \text{ is real-Lebesgue measurable function, } \|f\|_{L^p} < \infty\}, \quad (2.2)$$

here

$$\|f\|_{L^p} = \left( \int_{\Omega} |f(x)|^p dx \right)^{1/p}, \quad p \in [1, \infty),$$
$$\|f\|_{\infty} = \text{ess sup}_{x \in \Omega} |f(x)|, \quad p = \infty.$$

**Definition 2.1.3** Let  $V$  be a inner product space. If  $V$  is complete under the norm induced by the inner product on  $V$ , then  $V$  is called Hilbert space.

**Definition 2.1.4** Let  $V$  be a vector space. The dual space of  $V$  is denoted by  $V^*$ , and defined by

$$V^* := \{f : f : V \rightarrow \mathbb{R} \text{ is linear functional}\}.$$

Our special interest is  $L^2(\Omega)$ -space for  $p = 2$ , which is a Hilbert space with the following induced norm:

$$\|f\| = (f, f)^{1/2}, \quad (f, g) = \left( \int_{\Omega} f(x)g(x)dx \right).$$



**Definition 2.1.5** The zero-mean subspace of  $L^2(\Omega)$  is defined as:

$$L_0^2(\Omega) := \left\{ q \in L^2(\Omega) : \int_{\Omega} q dx = 0 \right\}.$$

**Lemma 2.1.6** Let  $a, b$  be non-negative numbers. Then,

$$ab \leq \frac{a^p}{p} + \frac{a^q}{q}, \quad (2.3)$$

where  $\frac{1}{p} + \frac{1}{q} = 1$  with  $p, q \in [1, \infty)$ .

**Proof:** Consider

$$f(t) = \frac{t^q}{q} - t + \frac{1}{p} \text{ on } [0, \infty).$$

Then for all  $t \geq 0$ ,  $f(t) \geq 0$ . Take  $t = b/a^{p-1}$  such that  $\frac{1}{p} + \frac{1}{q} = 1$ . Then using  $(p-1)q = p$ , one can have

$$\begin{aligned} f(b/a^{p-1}) &\geq 0 \\ \frac{b^q}{qa^{(p-1)q}} - \frac{b}{a^{p-1}} + \frac{1}{p} &\geq 0, \\ \frac{b^q}{qa^p} - \frac{b}{a^{p-1}} + \frac{1}{p} &\geq 0. \end{aligned}$$

Multiply the above inequality by  $a^p$  gives the desired inequality.  $\square$

The important inequality in  $L^p$ -spaces, also employed frequently in this study, is the Hölder's inequality (see the proof [1].), which is given below:

**Lemma 2.1.7 (The Hölder's Inequality)** Suppose that  $f \in L^p(\Omega)$  and  $g \in L^q(\Omega)$  with  $\frac{1}{p} + \frac{1}{q} = 1$  for  $p, q \in [1, \infty]$ . Then  $fg \in L^1(\Omega)$  and

$$\|fg\|_{L^1} \leq \|f\|_{L^p} \|g\|_{L^q}. \quad (2.4)$$

**Proof:** If either  $\|f\|_{L^p} = 0$  or  $\|g\|_{L^q} = 0$ , then  $f(x)g(x) = 0$  a.e. in  $\Omega$ . Then (2.4) is satisfied. Otherwise, set  $a = |f(x)|/\|f\|_{L^p}$  and  $b = |g(x)|/\|g\|_{L^q}$ . Then, use (2.3) and integrate over  $\Omega$ :

$$\frac{1}{\|f\|_{L^p} \|g\|_{L^q}} \int_{\Omega} |f(x)g(x)| dx \leq \frac{1}{p \|f\|_{L^p}^p} \int_{\Omega} |f(x)|^p dx + \frac{1}{q \|g\|_{L^q}^q} \int_{\Omega} |g(x)|^q dx.$$

Then multiplying the above inequality by  $\|f\|_{L^p}\|g\|_{L^q}$  and using the fact that  $1/p + 1/q = 1$  gives the desired inequality.  $\square$

We now state the Young's Inequality without proving it, which is the generalization of the Lemma 2.1.6:

**Lemma 2.1.8 (Young's Inequality)** *Let  $a, b, \varepsilon$  be non-negative numbers. Then,*

$$ab \leq \frac{\varepsilon^p}{p} a^p + \frac{\varepsilon^{-p/q}}{q} a^q, \quad (2.5)$$

where  $\frac{1}{p} + \frac{1}{q} = 1$  with  $p, q \in [1, \infty)$ .

**Definition 2.1.9** *Let  $\Omega$  be an open subset of  $\mathbb{R}^d$ , and  $f \in C(\Omega)$ .*

- *Then the support of  $f$  is defined as follows:*

$$\text{supp}(f) = \overline{\{x \in \Omega : f(x) \neq 0\}}.$$

- *If  $\text{supp}(f)$  is compact in  $\mathbb{R}^d$ , and  $\text{supp}(f) \subset \Omega$ , then we say that  $f$  has a compact support in  $\Omega$  [1].*
- $C_0^\infty(\Omega) := \{f \in C^\infty(\Omega) : f \text{ has a compact support in } \Omega\}$ .

**Definition 2.1.10** *Let  $\Omega \subset \mathbb{R}^d$ . Then a multi-index is a vector defined by*

$$\alpha = (\alpha_1, \dots, \alpha_d), \quad \alpha_i \in \mathbb{N} \cup 0, \quad i = 1, 2, \dots, d.$$

*Derivatives are defined by*

$$D^\alpha = \frac{\partial^{|\alpha|}}{\partial x_1^{\alpha_1} \dots \partial x_d^{\alpha_d}}.$$

here  $|\alpha| = \sum_{i=1}^d \alpha_i$ .

**Definition 2.1.11 (The Sobolev Spaces)** *Let  $k \in \mathbb{N}$ , and  $p \in [1, \infty]$ . The Sobolev spaces are defined by*

$$W_k^p(\Omega) := \{f : \Omega \rightarrow \mathbb{R} : D^\alpha f \in L^p(\Omega), \quad \forall 0 \leq |\alpha| \leq k\}.$$

We now state some useful information about the Sobolev spaces:

**Remark 2.1.12**

- *The Sobolev spaces are Banach spaces with the following norm:*

$$\|f\|_k^p := \left( \sum_{0 \leq |\alpha| \leq k} \left( \int_{\Omega} |D^\alpha f(x)|^p dx \right) \right)^{1/p}, \quad 1 \leq p < \infty,$$

$$\|f\|_k^\infty := \max_{0 \leq |\alpha| \leq k} (\text{ess sup}_{x \in \Omega} |D^\alpha f(x)|), \quad p = \infty.$$

- $W_0^p = L^p(\Omega)$ .
- *For  $p = 2$ , the Sobolev spaces and their norms are denoted as follows:*

$$H^k(\Omega) := W_k^2(\Omega), \quad \text{and} \quad \|f\|_k := \|f\|_k^p.$$

$H^k(\Omega)$  are Hilbert spaces.

- $H_0^k(\Omega) := \{v \in H^k(\Omega) : v = 0 \text{ on } \partial\Omega\}$  is a closed subspace of  $H^k(\Omega)$ .  
Thus, it is a Hilbert space.

**Lemma 2.1.13 (The Poincaré-Friedrichs' Inequality [44])** *Let  $\Omega \subset L_d$ ,  $L_d = \{x \in \mathbb{R}^d : -d/2 < x_n < d/2\}$ , for some  $d > 0$ . Then for all  $\varphi \in H_0^1(\Omega)$ ,  $1 \leq q \leq \infty$*

$$\|\varphi\| \leq (C_{PF}) \|\nabla\varphi\|. \quad (2.6)$$

**Proof:** It is enough to show that  $\varphi \in C_0^\infty(\Omega)$ . For such functions one has

$$|\varphi(x)| \leq (1/2) \int_{-d/2}^{d/2} |\nabla\varphi(x)| dx_n,$$

which implies (2.6) for  $q = \infty$ . If  $q \in [1, \infty)$ , employing the Hölder inequality yields

$$|\varphi(x)|^q \leq (d^{q-1}/2^q) \int_{-d/2}^{d/2} |\nabla\varphi(x)| dx_n$$

which, after integrating over  $L_d$ , proves (2.6). □

**Lemma 2.1.14** *The norms on  $H^1(\Omega)$  and  $H_0^1(\Omega)$  are equivalent.*

**Proof:** The norms on  $H^1(\Omega)$  and  $H_0^1(\Omega)$  are given by, respectively

$$\|\varphi\|_1 = (\|\varphi\|^2 + \|\nabla\varphi\|^2)^{1/2}, \quad \|\varphi\|_0^1 = \|\nabla\varphi\|.$$

Let  $\varphi \in H_0^1$  be given. Then by using the Poincaré-Friedrichs' inequality, one can have

$$\|\varphi\|_1^2 \leq (1 + C_{PF}^2)\|\nabla\varphi\|^2,$$

and taking the square root of both sides yields

$$\|\varphi\|_1 \leq \sqrt{(1 + C_{PF}^2)}\|\nabla\varphi\|. \quad (2.7)$$

On the other hand,

$$\|\varphi\|_1 \geq \|\nabla\varphi\|. \quad (2.8)$$

From (2.7) and (2.8), one can get the equivalence of these norms.  $\square$

**Definition 2.1.15** *For any function  $v(x, t)$  defined  $\Omega \times (0, T]$  (either scalar or vector valued), we use the following norms:*

$$\|v\|_{m,k} := \left( \int_0^T \|v(t, \cdot)\|_k^m dt \right)^{1/m}, \quad \text{and} \quad \|v\|_{\infty,k} := \text{ess sup}_{0 \leq t \leq T} \|v(t, \cdot)\|_k, \quad (2.9)$$

where  $T > 0$  is a given finite end time. We also make use of the notation

$$t^n = n\Delta t, \quad \forall n = 1, \dots, M,$$

where  $\Delta t$  represents a given time step such that  $M = T\Delta t$ . Furthermore, for any continuous function  $v$  in time, we use the following notation:

$$v(t^n) =: v^n, \quad \forall n = 1, \dots, M.$$

Since the mathematical analysis requires a time discretization, we define discrete forms of the norms in (2.9) as follows:

$$\|v\|_{m,k} := \left( \Delta t \sum_{n=0}^{M-1} \|v^{n+1}\|_k^m \right)^{1/m}, \quad \text{and} \quad \|v\|_{\infty,k} := \max_{0 \leq n \leq M-1} \|v^{n+1}\|_k, \quad (2.10)$$

We use bold character notation to distinguish the vector valued functions and their spaces than the scalar ones. Since the finite element method is used in the stability and convergence analysis, we choose the standard function spaces for the continuous velocity field, pressure and temperature spaces as

$$\mathbf{X} := \mathbf{H}_0^1(\Omega), \quad Q := L_0^2(\Omega), \quad W := H_0^1(\Omega),$$

The weakly-divergence free subspace  $\mathbf{V} \subset \mathbf{X}$  is defined by:

$$\mathbf{V} := \{\mathbf{v} \in \mathbf{X} : (\nabla \cdot q, \mathbf{v}) = 0, \quad \forall q \in Q\}$$

The estimate below plays an important role, which gives a relation between the divergence and  $H^1$ -norms.

**Lemma 2.1.16** *For any  $\varphi \in H^1(\Omega)$ , we have the following relation:*

$$\|\nabla \cdot \varphi\| \leq \sqrt{d} \|\nabla \varphi\|, \quad (2.11)$$

where  $d$  is the dimension of the domain  $\Omega$ .

**Proof:** We show only the validity of the estimate for  $d = 3$  since the proof is similar for  $d = 2$ . Let  $\varphi = (u(x, y, z), v(x, y, z), w(x, y, z))$  be in  $\mathbf{H}^1(\Omega)$ . Then from the definition of the divergence operator

$$\nabla \cdot \varphi = \frac{\partial u}{\partial x} + \frac{\partial v}{\partial y} + \frac{\partial w}{\partial z} =: u_x + v_y + w_z$$

and using the Young's inequality yields

$$\begin{aligned} \|\nabla \cdot \varphi\|^2 &= \int_{\Omega} (u_x^2 + v_y^2 + w_z^2 + 2u_x v_y + 2u_x w_z + 2v_y w_z) dx \\ &\leq \int_{\Omega} 3(u_x^2 + v_y^2 + w_z^2) dx = \left( \sqrt{3} \|\nabla \varphi\| \right)^2. \end{aligned}$$

Taking square root of both sides of the inequality gives the estimate.  $\square$

**Remark 2.1.17** *Unless the converse is stated, through this thesis  $C$  denotes a generic constant independent of all parameters, mesh size  $h$  and time step  $\Delta t$ .*

Another important space and norm in this study are the dual space

$$H^{-1}(\Omega) := (H_0^1(\Omega))^*$$

of  $H_0^1(\Omega)$ , and its dual norm  $\|\cdot\|_{-1}$ , which is defined by

$$\|f\|_{-1} := \sup_{\varphi \in X} \frac{(f, \varphi)}{\|\nabla \varphi\|}. \quad (2.12)$$

Due to the application of the finite element method in spacial discretization, we need a generation of a fine mesh  $\pi_h$  of the domain  $\Omega$ . We denote the conforming finite element spaces defined on  $\pi_h$  by

$$\mathbf{X}_h \subset \mathbf{X}, Q_h \subset Q, W_h \subset W.$$

It is assumed that the conforming finite element spaces of the velocity and pressure spaces satisfy the discrete inf-sup condition (or Ladyzenskaya-Brezzi-Babuska (LBB) condition [46]), e.g., there is a constant  $\beta$  independent of the mesh size  $h$  such that

$$\inf_{q_h \in Q_h} \sup_{\mathbf{v}_h \in \mathbf{X}_h} \frac{(q_h, \nabla \cdot \mathbf{v}_h)}{\|\nabla \mathbf{v}_h\| \|q_h\|} \geq \beta > 0. \quad (2.13)$$

and that conforming velocity, pressure and temperature finite element spaces the following well-known approximation properties:

$$\inf_{\mathbf{v}_h \in \mathbf{X}_h} \{\|\mathbf{u} - \mathbf{v}_h\| + h\|\nabla(\mathbf{u} - \mathbf{v}_h)\|\} \leq Ch^{k+1}\|\mathbf{u}\|_{k+1}, \quad \mathbf{u} \in \mathbf{H}^{k+1}, \quad (2.14)$$

$$\inf_{q_h \in Q_h} \|p - q_h\| \leq Ch^k\|p\|_k, \quad p \in H^k, \quad (2.15)$$

$$\inf_{\theta_h \in W_h} \{\|\theta - \theta_h\| + h\|\nabla(\theta - \theta_h)\|\} \leq Ch^{k+1}\|\theta\|_{k+1}, \quad \theta \in H^{k+1}. \quad (2.16)$$

The discretely divergence free subspace  $\mathbf{V}_h \subset \mathbf{X}$  is defined by

$$\mathbf{V}_h = \{\mathbf{v}_h \in \mathbf{X}_h : (q_h, \nabla \cdot \mathbf{v}_h) = 0, \quad \forall q_h \in Q_h\}.$$

**Remark 2.1.18** *Under the inf-sup condition (2.13), the discretely divergence-free subspace  $\mathbf{V}_h$  has the same approximation properties as  $\mathbf{X}_h$  and is nonempty [14]. Note that in general  $\mathbf{V}_h \not\subset \mathbf{V}$ .*

We often make use of the Taylor-Hood element pair, defined as  $(X_h, Q_h) = ((P_k)^d, P_{k-1})$ , i.e.,

$$\mathbf{X}_h := \{\mathbf{v}_h \in \mathbf{X} : v_h|_K \in (P_k)^d(K), \quad \forall K \in \pi_h\}, \quad (2.17)$$

$$Q_h := \{q_h \in Q \cap C^0(\Omega) : q_h|_K \in P_{k-1}(K), \quad \forall K \in \pi_h\}. \quad (2.18)$$

Taylor-Hood finite element pair satisfies LBB-condition if  $k \geq 2$ , [46, 15]. In addition, we use the Scott-Vogelius finite element pair  $(\mathbf{X}_h, Q_h) = ((P_k)^d, P_{k-1}^{disc})$ . The Scott-Vogelius finite element pair is discretely inf-sup stable if one of the following conditions on the mesh  $\pi_h$  holds [113, 114, 115]:

1. In  $2d$ ,  $k \geq 4$  and the mesh has no singular vertices,
2. In  $3d$ ,  $k \geq 6$  on a quasi-uniform tetrahedral mesh,
3. In  $2d$  or  $3d$ , when  $k \geq d$  the mesh is generated as a barycenter refinement of a regular, conforming triangular or tetrahedral mesh, which is obtained by the dividing each triangle  $K \in \pi_h$  into six triangles and drawing the six edges joining the barycenter of  $K$  with the vertices of  $K$  as well as the midpoints of its edges.
4. When the mesh is of Powell-Sabin type and  $k = 1$  in  $2d$  or  $k = 2$  in  $3d$ , [18].

In the computations, we perform the Scott-Vogelius finite element pairs, which are known to be stable on barycenter refined regular triangular meshes [3], given by condition 3. We also use the inverse inequality from [46]: there exists a constant  $C$  such that

$$\|\nabla \mathbf{v}_h\| \leq Ch^{-1} \|\mathbf{v}_h\|, \quad \forall \mathbf{v}_h \in \mathbf{X}_h, \quad (2.19)$$

$$\|\nabla \chi_h\| \leq Ch^{-1} \|\chi_h\|, \quad \forall \chi_h \in W_h. \quad (2.20)$$

In addition, since the proposed numerical scheme uses a variant of the projection based VMS method, a coarse mesh triangulation  $\pi_H$  of the domain  $\Omega$  is needed, as is an additional finite element space  $L_H \subset L := (L^2(\Omega))^{d \times d}$  on  $\pi_H$  with  $H \geq h$ . This space is used to project both continuous and discrete velocity and temperature fields, and is spanned by piecewise polynomials with degree  $k - 1$ .

We now give the definition of the  $L^2$  orthogonal projection into  $L_H$ -space, and the approximation property for that.

**Definition 2.1.19** *The  $L^2$  orthogonal projection  $P_\mu^H$  from  $L$  onto  $L_H$  is defined by*

$$(P_\mu^H \mathbb{L}, v_H) = (\mathbb{L}, v_H), \quad (2.21)$$

for all  $v_H \in L_H$ ,  $\mathbb{L} \in L$ .

For the error arising from this projection, there exists a constant  $C$  such that

$$\|\mathbb{L} - P_\mu^H \mathbb{L}\| \leq CH^k |\mathbb{L}|_{k+1}, \quad (2.22)$$

for all  $\mathbb{L} \in L \cap (H^{k+1}(\Omega))^{d \times d}$ .

**Remark 2.1.20** *The choice of the large scale space  $L_H$  is important, see e.g., [65, 71] for a discussion here. We choose  $L_H$  to be degree  $k-1$  polynomials since we intend it to hold gradients of degree  $k$  polynomials. The choice of  $H$  must be balanced between efficiency and accuracy, since larger  $H$  provides for more efficient projections into  $L_H$  and reduces storage, but accuracy decreases. It is typical that  $H = O(h^q)$ , with  $0 \leq q \leq 1$ , and how large  $q$  can be is typically chosen from balancing terms in the convergence analysis, so that  $H$  is chosen small enough that it does not increase the asymptotic error. For the method proposed herein and with  $k = 2$ , we find  $H = O(h^{1/2})$  is the maximum such  $H$ .*

We also need to define two skew-symmetric trilinear forms, and the bounds on them.

**Definition 2.1.21** *Define  $c_0 : (\mathbf{X} \times \mathbf{X} \times \mathbf{X}) \rightarrow \mathbb{R}$  and  $c_1 : (\mathbf{X} \times W \times W) \rightarrow \mathbb{R}$  such that*

$$c_0(\mathbf{u}, \mathbf{v}, \mathbf{w}) = \frac{1}{2}((\mathbf{u} \cdot \nabla)\mathbf{v}, \mathbf{w}) - \frac{1}{2}((\mathbf{u} \cdot \nabla)\mathbf{w}, \mathbf{v}), \quad (2.23)$$

$$c_1(\mathbf{u}, \theta, \chi) = \frac{1}{2}((\mathbf{u} \cdot \nabla)\theta, \chi) - \frac{1}{2}((\mathbf{u} \cdot \nabla)\chi, \theta), \quad (2.24)$$

for all  $(\mathbf{u}, \mathbf{v}, \mathbf{w}) \in (\mathbf{X} \times \mathbf{X} \times \mathbf{X})$  and  $(\mathbf{u}, \theta, \chi) \in (\mathbf{X} \times W \times W)$ , respectively.

By using definition of these skew-symmetric trilinear forms, one can easily show that

$$\begin{aligned} c_0(\mathbf{u}, \mathbf{v}, \mathbf{w}) &= -c_0(\mathbf{u}, \mathbf{w}, \mathbf{v}), & c_0(\mathbf{u}, \mathbf{v}, \mathbf{v}) &= 0, \\ c_1(\mathbf{u}, \theta, \chi) &= -c_1(\mathbf{u}, \chi, \theta), & c_1(\mathbf{u}, \theta, \theta) &= 0. \end{aligned}$$

for all  $(\mathbf{u}, \mathbf{v}, \mathbf{w}) \in \mathbf{X} \times \mathbf{X} \times \mathbf{X}$  and  $(\mathbf{u}, \theta, \psi) \in \mathbf{X} \times W \times W$ . We present the Ladyhenskaya inequality without proving it (see [77]).



**Lemma 2.1.22 (The Ladyhenskaya inequality)** *Let  $\mathbf{u}$  be any vector in  $\mathbb{R}^d$ ,  $d = 2, 3$  with the indicated  $L^p$ -norms are finite. Then*

$$\begin{aligned}\|\mathbf{u}\|_{L^4} &\leq 2^{1/4}\|\mathbf{u}\|_{L^2}^{1/2}\|\nabla\mathbf{u}\|_{L^2}^{1/2}, & d = 2, \\ \|\mathbf{u}\|_{L^4} &\leq \frac{4}{3\sqrt{3}}\|\mathbf{u}\|_{L^2}^{1/4}\|\nabla\mathbf{u}\|_{L^2}^{3/4}, & d = 3, \\ \|\mathbf{u}\|_{L^6} &\leq \frac{2}{\sqrt{3}}\|\nabla\mathbf{u}\|, & d = 3.\end{aligned}$$

**Lemma 2.1.23** *For all  $\mathbf{u}, \mathbf{v}, \mathbf{w} \in \mathbf{X}$  and  $\theta, \psi \in W$ , there exist constants  $C_1 := C_1(\Omega)$  and  $C_2 := C_2(\Omega)$ , i.e., depending only on the size of the domain  $\Omega$ , such that the skew-symmetric trilinear forms satisfy the following bounds*

$$c_0(\mathbf{u}, \mathbf{v}, \mathbf{w}) \leq C_1\|\nabla\mathbf{u}\|\|\nabla\mathbf{v}\|\|\nabla\mathbf{w}\|, \quad (2.25)$$

$$c_1(\mathbf{u}, \theta, \psi) \leq C_2\|\nabla\mathbf{u}\|\|\nabla\theta\|\|\nabla\psi\|. \quad (2.26)$$

**Proof:** We prove only the first inequality of Lemma 2.1.23 for  $d = 3$ . By the definition of the skew-symmetric trilinear form, and the application of the Hölder's and the Ladyzenskaya's inequalities, one can get

$$\begin{aligned}|c_0(\mathbf{u}, \mathbf{v}, \mathbf{w})| &\leq \frac{1}{2}|((\mathbf{u} \cdot \nabla)\mathbf{v}, \mathbf{w})| + \frac{1}{2}|((\mathbf{u} \cdot \nabla)\mathbf{w}, \mathbf{v})| \\ &\leq C\|\mathbf{u}\|_{L^4}\|\nabla\mathbf{v}\|\|\mathbf{w}\|_{L^4} + C\|\mathbf{u}\|_{L^4}\|\nabla\mathbf{w}\|\|\mathbf{v}\|_{L^4} \\ &\leq \frac{4C}{3\sqrt{3}}\|\mathbf{u}\|^{1/4}\|\nabla\mathbf{u}\|^{3/4}\|\nabla\mathbf{v}\|\|\mathbf{w}\|^{1/4}\|\nabla\mathbf{w}\|^{3/4} \\ &\quad + \frac{4C}{3\sqrt{3}}\|\mathbf{u}\|^{1/4}\|\nabla\mathbf{u}\|^{3/4}\|\nabla\mathbf{w}\|\|\mathbf{v}\|^{1/4}\|\nabla\mathbf{v}\|^{3/4}.\end{aligned}$$

Then, using the Poincaré-Friedrichs' inequality gives the desired estimate.  $\square$

The following inequality plays a key role in the convergence analysis, and its proof can be found in [37]:

**Lemma 2.1.24 (Agmon's Inequality)** *Let  $\mathbf{u} \in \mathbf{X} \cap \mathbf{H}^2(\Omega)$ . Then there exist a constant  $C$  only depending on the domain  $\Omega$  such that*

$$\begin{aligned}\|\mathbf{u}\|_{L^\infty} &\leq C\|\mathbf{u}\|_1^{1/2}\|\mathbf{u}\|_2^{1/2}, & d = 2, 3 \\ \|\mathbf{u}\|_{L^\infty} &\leq C\|\mathbf{u}\|^{1/4}\|\mathbf{u}\|_2^{3/4}, & d = 3.\end{aligned}$$

The last two important inequalities are the discrete Gronwall's Lemma (see e.g.,[59]), and the polarization inequality:

**Lemma 2.1.25 (Discrete Gronwall's Lemma)** *Let  $\Delta t$ ,  $B$  and  $a_n, b_n, c_n, d_n$  be finite non-negative numbers such that*

$$a_M + \Delta t \sum_{n=0}^M b_n \leq \Delta t \sum_{n=0}^{M-1} d_n a_n + \Delta t \sum_{n=0}^M c_n + B \quad \text{for } M \geq 1.$$

*Then for all  $\Delta t > 0$ ,*

$$a_M + \Delta t \sum_{n=0}^M b_n \leq \exp\left(\Delta t \sum_{n=0}^{M-1} d_n\right) \left(\Delta t \sum_{n=0}^M c_n + B\right).$$

**Lemma 2.1.26 (The polarization identity)** *Let  $V$  be an inner product space. Then for all  $\phi, \psi \in V$ , the following equality is satisfied:*

$$2(\phi - \psi, \phi) = \|\phi\|^2 - \|\psi\|^2 + \|\phi - \psi\|^2.$$

## 2.2 Numerical Scheme

In this section, we propose a numerical algorithm to the system (2.1) in which the VMS stabilization is implemented as a post-processing step. The algorithm introduces two decoupled VMS steps, one for the velocity and the other for temperature, and decouples the momentum equation from the heat transport equations. The algorithm uses backward Euler time discretization and finite element spacial discretization, which is given below:

### Algorithm 2.2.1

*Let a time step  $\Delta t$ , and finite end time  $T$  be given such that  $T = M\Delta t$  and  $t^{n+1} = (n+1)\Delta t$ ,  $n = 0, 1, 2, \dots, M-1$ . Denote the fully discrete solutions by*

$$\mathbf{u}_h^{n+1} := \mathbf{u}_h(t^{n+1}), \quad p_h^{n+1} := p_h(t^{n+1}), \quad \theta_h^{n+1} := \theta_h(t^{n+1}),$$

*for all  $n = 0, 1, 2, 3, \dots, M-1$ . Define  $\mathbf{u}_h^0$  and  $\theta_h^0$  to be the nodal interpolant of  $\mathbf{u}_0 \in \mathbf{L}^2(\Omega)$  and  $\theta_0 \in L^2(\Omega)$ . Then, find  $(\mathbf{u}_h^{n+1}, p_h^{n+1}, \theta_h^{n+1}) \in (\mathbf{X}_h, Q_h, W_h)$  via the following two steps:*

**Step 1:** Compute  $(\mathbf{w}_h^{n+1}, p_h^{n+1}, \phi_h^{n+1}) \in (\mathbf{X}_h, Q_h, W_h)$  satisfying

$$\begin{aligned} \frac{1}{\Delta t}(\mathbf{w}_h^{n+1} - \mathbf{u}_h^n, \mathbf{v}_h) + \nu(\nabla \mathbf{w}_h^{n+1}, \nabla \mathbf{v}_h) - (p_h^{n+1}, \nabla \cdot \mathbf{v}_h) \\ + c_0(\mathbf{u}_h^n, \mathbf{w}_h^{n+1}, \mathbf{v}_h) = Ri(\langle 0, \theta_h^n \rangle, \mathbf{v}_h) + (\mathbf{f}^{n+1}, \mathbf{v}_h) \end{aligned} \quad (2.27)$$

$$(\nabla \cdot \mathbf{w}_h^{n+1}, q_h) = 0, \quad (2.28)$$

$$\frac{1}{\Delta t}(\phi_h^{n+1} - \theta_h^n, \chi_h) + (\kappa \nabla \phi_h^{n+1}, \nabla \chi_h) + c_1(\mathbf{u}_h^n, \phi_h^{n+1}, \chi_h) = (\Gamma^{n+1}, \chi_h), \quad (2.29)$$

for all  $(\mathbf{v}_h, q_h, \chi_h) \in (\mathbf{X}^h, Q^h, W^h)$ .

**Step 2:** Stabilize  $\mathbf{w}_h^{n+1}$  and  $\phi_h^{n+1}$  to get  $(\mathbf{u}_h^{n+1}, \lambda_h^{n+1}, \theta_h^{n+1}) \in (\mathbf{X}_h, Q_h, W_h)$

$$\begin{aligned} \frac{1}{\Delta t}(\mathbf{w}_h^{n+1} - \mathbf{u}_h^{n+1}, \boldsymbol{\varphi}_h) &= (\lambda_h^{n+1}, \nabla \cdot \boldsymbol{\varphi}_h) + \alpha_1(\nabla \mathbf{u}_h^{n+1}, \nabla \boldsymbol{\varphi}_h) \\ &\quad - \alpha_1(P_u^H \nabla \mathbf{u}_h^n, P_u^H \nabla \boldsymbol{\varphi}_h), \end{aligned} \quad (2.30)$$

$$(\nabla \cdot \mathbf{u}_h^{n+1}, r_h) = 0, \quad (2.31)$$

$$\frac{1}{\Delta t}(\phi_h^{n+1} - \theta_h^{n+1}, \Psi_h) = \alpha_2(\nabla \theta_h^{n+1}, \nabla \Psi_h) - \alpha_2(P_\theta^H \nabla \theta_h^n, P_\theta^H \nabla \Psi_h), \quad (2.32)$$

for all  $(\boldsymbol{\varphi}_h, r_h, \Psi_h) \in (\mathbf{X}^h, Q^h, W^h)$ . Here  $\alpha_1 = \alpha_1(\mathbf{x}, h)$ ,  $\alpha_2 = \alpha_2(\mathbf{x}, h)$  are user-selected eddy viscosity parameters, and  $P_u^H, P_\theta^H$  are  $L^2$ -orthogonal projections defined by (2.21).

### 2.3 Stability and Convergence Analysis

In this section, we first prove that the solutions of the Algorithm 2.2.1 are unconditionally stable over finite time interval. Then we show it has optimal approximation property in time and space provided the stabilization parameters are chosen  $\mathcal{O}(h^2)$ , and the large scale mesh size  $H = \mathcal{O}(\sqrt{h})$ .

#### Lemma 2.3.1 (Stability of the velocity and temperature)

Assume that  $\mathbf{f} \in L^\infty(0, T; \mathbf{H}^{-1}(\Omega))$ ,  $\Gamma \in L^\infty(0, T; H^{-1}(\Omega))$ . Then the scheme (2.27)-(2.32) is unconditionally stable with respect to the time step size in the following sense:  $\forall \Delta t > 0$ , velocity satisfies

$$\begin{aligned}
& \|\mathbf{u}_h^M\|^2 + \alpha_1 \Delta t \|\nabla \mathbf{u}_h^M\|^2 + \Delta t \sum_{n=0}^{M-1} \alpha_1 \|(I - P_u^H) \nabla \mathbf{u}_h^{n+1}\|^2 \\
& \leq \|\mathbf{u}_h^0\|^2 + \alpha_1 \Delta t \|\nabla \mathbf{u}_h^0\|^2 + 2\nu^{-1} \Delta t \sum_{n=0}^{M-1} \|\mathbf{f}^{n+1}\|_{-1}^2 \\
& \quad + 2\tilde{C}T \left( \|\theta_h^0\|^2 + \Delta t \alpha_2 \|\nabla \theta_h^0\|^2 + \kappa^{-1} \Delta t \sum_{n=0}^{M-1} \|\Gamma^{n+1}\|_{-1}^2 \right), \quad (2.33)
\end{aligned}$$

and temperature satisfies

$$\begin{aligned}
& \|\theta_h^M\|^2 + \alpha_2 \Delta t \|\nabla \theta_h^M\|^2 + \Delta t \sum_{n=0}^{M-1} \alpha_2 \|(I - P_\theta^H) \nabla \theta_h^{n+1}\|^2 \\
& \leq \|\theta_h^0\|^2 + \alpha_2 \Delta t \|\nabla \theta_h^0\|^2 + \kappa^{-1} \Delta t \sum_{n=0}^{M-1} \|\Gamma^{n+1}\|_{-1}^2, \quad (2.34)
\end{aligned}$$

where  $\tilde{C} = C\nu^{-1} Ri^2$ .

**Remark 2.3.2** This stability lemma and with the application of the Lax-Milgram Theorem [77] implies the algorithm is well-posed, since it is linear and finite dimensional at each time step.

**Proof:** To begin with the stability analysis, first choose  $\mathbf{v}_h = \mathbf{w}_h^{n+1}$  in (2.27),  $q_h = p_h^{n+1}$  in (2.28),  $\chi_h = \phi_h^{n+1}$  in (2.29),  $\varphi_h = \mathbf{u}_h^{n+1}$  in (2.30),  $r_h = \lambda_h^{n+1}$  in (2.31) and  $\Psi_h = \theta_h^{n+1}$  in (2.32), which kills the pressure term  $(p_h^{n+1}, \nabla \cdot \mathbf{v}_h)$ , and skew-symmetric trilinear forms:

$$\begin{aligned}
c_0(\mathbf{u}_h^n, \mathbf{w}_h^{n+1}, \mathbf{w}_h^{n+1}) &= 0, \\
c_1(\mathbf{u}_h^n, \phi_h^{n+1}, \phi_h^{n+1}) &= 0.
\end{aligned}$$

Applying the Cauchy-Schwarz inequality to the right hand side terms produces

$$\begin{aligned}
\|\mathbf{w}_h^{n+1}\|^2 + \nu \Delta t \|\nabla \mathbf{w}_h^{n+1}\|^2 &\leq \|\mathbf{u}_h^n\| \|\mathbf{w}_h^{n+1}\| + \Delta t Ri \|\theta_h^n\| \|\mathbf{w}_h^{n+1}\| \\
&\quad + \Delta t \|\mathbf{f}^{n+1}\|_{-1} \|\nabla \mathbf{w}_h^{n+1}\|, \quad (2.35)
\end{aligned}$$

$$\|\phi_h^{n+1}\|^2 + \kappa \Delta t \|\nabla \phi_h^{n+1}\|^2 \leq \|\theta_h^n\| \|\phi_h^{n+1}\| + \Delta t \|\Gamma^{n+1}\|_{-1} \|\nabla \phi_h^{n+1}\|, \quad (2.36)$$

$$\begin{aligned}
\|\mathbf{u}_h^{n+1}\|^2 + \alpha_1 \Delta t \|\nabla \mathbf{u}_h^{n+1}\|^2 &\leq \|\mathbf{w}_h^{n+1}\| \|\mathbf{u}_h^{n+1}\| \\
&\quad + \alpha_1 \Delta t \|P_u^H \nabla \mathbf{u}_h^n\| \|P_u^H \nabla \mathbf{u}_h^{n+1}\|, \quad (2.37)
\end{aligned}$$

$$\begin{aligned}
\|\theta_h^{n+1}\|^2 + \alpha_2 \Delta t \|\nabla \theta_h^{n+1}\|^2 &\leq \|\phi_h^{n+1}\| \|\theta_h^{n+1}\| \\
&\quad + \alpha_2 \Delta t \|P_\theta^H \nabla \theta_h^n\| \|P_\theta^H \nabla \theta_h^{n+1}\|. \quad (2.38)
\end{aligned}$$

Now, use the Young's inequality on the right hand side terms of (2.35)-(2.36) to get

$$\begin{aligned} \|\mathbf{w}_h^{n+1}\|^2 + \nu\Delta t\|\nabla\mathbf{w}_h^{n+1}\|^2 &\leq \frac{1}{2}\|\mathbf{w}_h^{n+1}\|^2 + \frac{1}{2}\|\mathbf{u}_h^n\|^2 + \frac{\nu}{2}\|\nabla\mathbf{w}_h^{n+1}\|^2 \\ &\quad + \nu^{-1}\Delta t\|\mathbf{f}^{n+1}\|_{-1}^2 + \tilde{C}\Delta t\|\theta_h^n\|^2, \end{aligned} \quad (2.39)$$

and

$$\begin{aligned} \|\phi_h^{n+1}\|^2 + \kappa\Delta t\|\nabla\phi_h^{n+1}\|^2 &\leq \frac{1}{2}\|\phi_h^{n+1}\|^2 + \frac{1}{2}\|\theta_h^n\|^2 + \frac{\kappa\Delta t}{2}\|\nabla\phi_h^{n+1}\|^2 \\ &\quad + \frac{\kappa^{-1}\Delta t}{2}\|\Gamma^{n+1}\|_{-1}^2, \end{aligned} \quad (2.40)$$

where  $\tilde{C} = C\nu^{-1}Ri^2$ , and rearranging the terms gives

$$\frac{1}{2}\|\mathbf{w}_h^{n+1}\|^2 + \frac{\nu\Delta t}{2}\|\nabla\mathbf{w}_h^{n+1}\|^2 \leq \frac{1}{2}\|\mathbf{u}_h^n\|^2 + \nu^{-1}\Delta t\|\mathbf{f}^{n+1}\|_{-1}^2 + \tilde{C}\Delta t\|\theta_h^n\|^2, \quad (2.41)$$

$$\frac{1}{2}\|\phi_h^{n+1}\|^2 + \frac{\kappa\Delta t}{2}\|\nabla\phi_h^{n+1}\|^2 \leq \frac{1}{2}\|\theta_h^n\|^2 + \frac{\kappa^{-1}\Delta t}{2}\|\Gamma^{n+1}\|_{-1}^2. \quad (2.42)$$

On the other hand, by the properties of the orthogonal projection, one can have

$$\begin{aligned} \|P_u^H\varphi\| &\leq 1, \quad \text{for all } \varphi \in \mathbf{L}, \\ \|P_\theta^H\psi\| &\leq 1, \quad \text{for all } \psi \in L. \end{aligned}$$

Thus, the application of the Young's inequality with appropriate  $\varepsilon$  to the right hand side terms of (2.37) and (2.38) along with above fact results in

$$\begin{aligned} \|\mathbf{u}_h^{n+1}\|^2 + \alpha_1\Delta t\|\nabla\mathbf{u}_h^{n+1}\|^2 + \frac{\alpha_1\Delta t}{2}(\|\nabla\mathbf{u}_h^{n+1}\|^2 + \|\nabla\mathbf{u}_h^{n+1}\|^2) \\ \leq \frac{1}{2}\|\mathbf{u}_h^{n+1}\|^2 + \frac{1}{2}\|\mathbf{w}_h^{n+1}\|^2 + \frac{\alpha_1\Delta t}{2}\|P_u^H\nabla\mathbf{u}_h^{n+1}\|^2 + \frac{\alpha_1\Delta t}{2}\|\nabla\mathbf{u}_h^n\|^2, \end{aligned} \quad (2.43)$$

and

$$\begin{aligned} \|\theta_h^{n+1}\|^2 + \frac{\alpha_2\Delta t}{2}(\|\nabla\theta_h^{n+1}\|^2 + \|\nabla\theta_h^{n+1}\|^2) \\ \leq \frac{1}{2}\|\theta_h^{n+1}\|^2 + \frac{1}{2}\|\phi_h^{n+1}\|^2 + \frac{\alpha_2\Delta t}{2}\|P_\theta^H\nabla\theta_h^{n+1}\|^2 + \frac{\alpha_2\Delta t}{2}\|\nabla\theta_h^n\|^2. \end{aligned} \quad (2.44)$$

Now rearrange the terms, and use the properties of orthogonal projection

$$\begin{aligned} \|P_u^H\varphi\|^2 + \|(I - P_u^H)\varphi\|^2 &= \|\varphi\|^2, \quad \text{for all } \varphi \in \mathbf{L}, \\ \|P_\theta^H\psi\|^2 + \|(I - P_\theta^H)\psi\|^2 &= \|\psi\|^2, \quad \text{for all } \psi \in L, . \end{aligned}$$

Then, equations (2.43) and (2.44) reduces to

$$\begin{aligned} \frac{1}{2}\|\mathbf{u}_h^{n+1}\|^2 + \frac{\alpha_1\Delta t}{2}(\|\nabla\mathbf{u}_h^{n+1}\|^2 - \|\nabla\mathbf{u}_h^n\|^2) + \frac{\alpha_1\Delta t}{2}\|(I - P_u^H)\nabla\mathbf{u}_h^{n+1}\|^2 \\ \leq \frac{1}{2}\|\mathbf{w}_h^{n+1}\|^2, \end{aligned} \quad (2.45)$$

and

$$\begin{aligned} \frac{1}{2}\|\theta_h^{n+1}\|^2 + \frac{\alpha_2\Delta t}{2}(\|\nabla\theta_h^{n+1}\|^2 - \|\nabla\theta_h^n\|^2) + \frac{\alpha_2\Delta t}{2}\|(I - P_\theta^H)\nabla\theta_h^{n+1}\|^2 \\ \leq \frac{1}{2}\|\phi_h^{n+1}\|^2. \end{aligned} \quad (2.46)$$

Using estimate (2.42) on the left hand side of (2.46) results in

$$\begin{aligned} \frac{1}{2}\|\theta_h^{n+1}\|^2 + \frac{\alpha_2\Delta t}{2}(\|\nabla\theta_h^{n+1}\|^2 - \|\nabla\theta_h^n\|^2) + \frac{\alpha_2\Delta t}{2}\|(I - P_\theta^H)\nabla\theta_h^{n+1}\|^2 \\ \leq \frac{1}{2}\|\theta_h^n\|^2 + \frac{\kappa^{-1}\Delta t}{2}\|\Gamma^{n+1}\|_{-1}^2, \end{aligned}$$

and summing the resulting inequality from  $n = 0$  to  $M - 1$  gives the second estimate. To get the first claim, plug estimate (2.41) to the right hand side of (2.45), and sum the resulting inequality from  $n = 0$  to  $M - 1$  to have

$$\begin{aligned} \|\mathbf{u}_h^M\|^2 + \alpha_1\Delta t\|\nabla\mathbf{u}_h^M\|^2 + \Delta t\sum_{n=0}^{M-1}\alpha_1\|(I - P_u^H)\nabla\mathbf{u}_h^{n+1}\|^2 \\ \leq \|\mathbf{u}_h^0\|^2 + \alpha_1\Delta t\|\nabla\mathbf{u}_h^0\|^2 + 2\nu^{-1}\Delta t\sum_{n=0}^{M-1}\|\mathbf{f}^{n+1}\|_{-1}^2 + \tilde{C}\Delta t\sum_{n=0}^{M-1}\|\theta_h^n\|^2. \end{aligned} \quad (2.47)$$

Note that from the stability bound on temperature, one can write

$$\Delta t\sum_{n=0}^{M-1}\|\theta_h^n\|^2 \leq \Delta tM\left(\|\theta_h^0\|^2 + \alpha_2\Delta t\|\nabla\theta_h^0\|^2 + \kappa^{-1}\Delta t\sum_{n=0}^{M-1}\|\Gamma^{n+1}\|_{-1}^2\right).$$

Considering this in (2.47) proves the second claim.  $\square$

By using Lemma 2.3.1, we can also get bounds on  $\mathbf{w}_h^{n+1}$  and  $\phi_h^{n+1}$ .

**Lemma 2.3.3** *Suppose  $\mathbf{f} \in L^\infty(0, T; \mathbf{H}^{-1}(\Omega))$ ,  $\Gamma \in L^\infty(0, T; H^{-1}(\Omega))$ . Then  $\forall \Delta t > 0$ ,  $\mathbf{w}_h^{n+1}$  and  $\phi_h^{n+1}$  satisfy the following:*

$$\begin{aligned} \|\mathbf{w}_h^M\|^2 + \nu\Delta t\sum_{n=0}^{M-1}\|\nabla\mathbf{w}_h^{n+1}\|^2 \\ \leq \|\mathbf{w}_h^0\|^2 + \|\mathbf{u}_h^0\|^2 + \alpha_1\Delta t\|\nabla\mathbf{u}_h^0\|^2 + 2\nu^{-1}\Delta t\sum_{n=0}^{M-1}\|\mathbf{f}^{n+1}\|_{-1}^2 \\ + 2\tilde{C}T\left(\|\theta_h^0\|^2 + \alpha_2\Delta t\|\nabla\theta_h^0\|^2 + \kappa^{-1}\Delta t\sum_{n=0}^{M-1}\|\Gamma^{n+1}\|_{-1}^2\right), \end{aligned} \quad (2.48)$$

and

$$\begin{aligned} \|\phi_h^M\|^2 + \kappa\Delta t \sum_{n=0}^{M-1} \|\nabla\phi_h^{n+1}\|^2 &\leq \|\phi_h^0\|^2 + \|\theta_h^0\|^2 + \alpha_2\Delta t\|\nabla\theta_h^0\|^2 \\ &\quad + \kappa^{-1}\Delta t \sum_{n=0}^{M-1} \|\Gamma^{n+1}\|_{-1}^2. \end{aligned} \quad (2.49)$$

where  $\tilde{C} = C\nu^{-1}Ri^2$ .

**Proof:** Since the proof of (2.48) and (2.49) are similar, we obtain only the bound on  $\phi_h^{n+1}$ . First sum estimate (2.46) from  $n = 0$  to  $M - 2$  to get

$$\begin{aligned} \sum_{n=0}^{M-2} \|\theta_h^{n+1}\|^2 + \alpha_2\Delta t\|\nabla\theta_h^{M-1}\|^2 + \Delta t \sum_{n=0}^{M-2} \alpha_2\|(I - P_\theta^H)\nabla\theta_h^{n+1}\|^2 \\ \leq \alpha_2\Delta t\|\nabla\theta_h^0\|^2 + \sum_{n=0}^{M-2} \|\phi_h^{n+1}\|^2, \end{aligned}$$

next change the index and drop the non-negative left hand side terms to obtain

$$\sum_{n=1}^{M-1} \|\theta_h^n\|^2 \leq \alpha_2\Delta t\|\nabla\theta_h^0\|^2 + \sum_{n=1}^{M-1} \|\phi_h^n\|^2. \quad (2.50)$$

Summing (2.40) from  $n = 0$  to  $M - 1$  yields

$$\sum_{n=0}^{M-1} \|\phi_h^{n+1}\|^2 + \kappa\Delta t \sum_{n=0}^{M-1} \|\nabla\phi_h^{n+1}\|^2 \leq \sum_{n=0}^{M-1} \|\theta_h^n\|^2 + \kappa^{-1}\Delta t \sum_{n=0}^{M-1} \|\Gamma^{n+1}\|_{-1}^2, \quad (2.51)$$

Adding the term  $\|\theta_h^0\|^2$  to the right hand side of (2.51), and considering estimate (2.50) gives the bound on  $\phi_h^{n+1}$ .  $\square$

### 2.3.1 Convergence Analysis

We proceed to present an á priori error estimate for the explicitly decoupled method for the approximate solutions of (2.27)-(2.32). For ease of notation, we will denote by  $\mathbf{u}^{n+1}, \theta^{n+1}$  the true solutions of (2.1) at time  $t^{n+1} = (n + 1)\Delta t$ , i.e.,

$$\mathbf{u}^{n+1} := \mathbf{u}(t^{n+1}), \theta^{n+1} := \theta(t^{n+1}).$$

Similarly,  $\mathbf{u}_t^{n+1}$  and  $\theta_t^{n+1}$  stand for the time derivatives of the true solutions of (2.1) at time  $t^{n+1}$ . For convergence, we assume the following regularity assumptions hold

for the true solutions:

$$\begin{aligned}
\mathbf{u}, \theta &\in L^\infty(0, T; H^2 \cap H^{k+1}(\Omega)), \\
\mathbf{u}_t, \theta_t &\in L^\infty(0, T; H^{k+1}(\Omega)), \\
\mathbf{u}_{tt}, \theta_{tt} &\in L^\infty(0, T; L^2(\Omega)), \\
p &\in L^2(0, T; H^k(\Omega)).
\end{aligned} \tag{2.52}$$

If the assumed regularity does not hold, then the results of the following convergence theorem will (likely) not hold. We can see why from the analysis, since reduced accuracy in the interpolation estimates, and assumptions that certain norms are bounded. In the numerical experiments section, we consider convergence in a test problem without the assumed smoothness, and observe convergence, however with suboptimal rates in space. In the error analysis, we use the following error decompositions:

$$\begin{aligned}
\mathbf{u}^{n+1} - \mathbf{w}_h^{n+1} &= (\mathbf{u}^{n+1} - \tilde{\mathbf{U}}^{n+1}) - (\mathbf{w}_h^{n+1} - \tilde{\mathbf{U}}^{n+1}) =: \boldsymbol{\eta}_u^{n+1} - \boldsymbol{\epsilon}_u^{n+1} \\
\mathbf{u}^{n+1} - \mathbf{u}_h^{n+1} &= (\mathbf{u}^{n+1} - \tilde{\mathbf{U}}^{n+1}) - (\mathbf{u}_h^{n+1} - \tilde{\mathbf{U}}^{n+1}) =: \boldsymbol{\eta}_u^{n+1} - \mathbf{e}_u^{n+1} \\
\theta^{n+1} - \phi_h^{n+1} &= (\theta^{n+1} - \tilde{\theta}^{n+1}) - (\phi_h^{n+1} - \tilde{\theta}^{n+1}) =: \eta_\theta^{n+1} - \epsilon_\theta^{n+1} \\
\theta^{n+1} - \theta_h^{n+1} &= (\theta^{n+1} - \tilde{\theta}^{n+1}) - (\theta_h^{n+1} - \tilde{\theta}^{n+1}) =: \eta_\theta^{n+1} - e_\theta^{n+1}
\end{aligned} \tag{2.53}$$

Here  $\tilde{\mathbf{U}}$  and  $\tilde{\theta}$  are approximations of  $\mathbf{u}$  and  $\theta$  in  $\mathbf{V}^h$  and  $W^h$ , respectively.

**Theorem 2.3.4** *Assume continuous solutions  $(\mathbf{u}, p, \theta)$  of (2.1) satisfy the regularity assumptions (2.52). In addition, let the time step  $\Delta t > 0$ , and end time  $T = M\Delta t$  be given, and  $\mathbf{u}_h^{n+1}, \mathbf{w}_h^{n+1}, p_h^{n+1}, \lambda_h^{n+1}, \theta_h^{n+1}, \phi_h^{n+1}$  be the solutions of (2.27)-(2.32) for all  $n = 0, 1, \dots, M-1$ . If eddy viscosity parameters  $\alpha_1, \alpha_2$  are chosen as  $\mathcal{O}(h^2)$ , then there exists a constant  $C$ , independent of mesh size  $h$  and time step  $\Delta t$ , such that the errors satisfy the following:*

$$\begin{aligned}
\|\mathbf{e}_u^M\|^2 + \|e_\theta^M\|^2 &+ \sum_{n=0}^{M-1} \left( \|\boldsymbol{\epsilon}_u^{n+1} - \mathbf{e}_u^n\|^2 + \|\boldsymbol{\epsilon}_u^{n+1} - \mathbf{e}_u^{n+1}\|^2 \right) \\
&+ \sum_{n=0}^{M-1} \left( \|\epsilon_\theta^{n+1} - e_\theta^n\|^2 + \|\epsilon_\theta^{n+1} - e_\theta^{n+1}\|^2 \right) \\
&+ \Delta t \sum_{n=0}^{M-1} \left( \nu \|\nabla \boldsymbol{\epsilon}_u^{n+1}\|^2 + \kappa \|\nabla \epsilon_\theta^{n+1}\|^2 + \alpha_1 \|\nabla \mathbf{e}_u^{n+1}\|^2 + \alpha_2 \|\nabla e_\theta^{n+1}\|^2 \right) \\
&\leq \tilde{C} \left( (\Delta t)^2 + h^2 (\Delta t)^2 + h^{2k} + h^2 H^{2k} + h^{2k+2} \right),
\end{aligned}$$

$$\tilde{C} := \tilde{C}(\mathbf{u}, p, \theta, \mathbf{u}_t, \mathbf{u}_{tt}, \theta_t, \theta_{tt}, T, C_{PF}).$$



We now state the corollary of the Theorem 2.3.4.

**Remark 2.3.5** *We note that our convergence analysis can be extended with homogeneous Neumann boundary conditions without difficulty.*

**Corollary 2.3.6** *Under the assumptions of Theorem 2.3.4, choose  $(\mathbf{X}_h, Q_h) = (\mathbf{P}_2, P_1)$  Taylor-Hood elements, i.e.,  $k = 2$ ,  $W_h = W \cap P_2$  finite elements, and  $H \leq \mathcal{O}(\sqrt{h})$ . Then, the errors in velocity and temperature satisfy, for every  $\Delta t > 0$ ,*

$$\begin{aligned} \|\mathbf{u}(T) - \mathbf{u}_h^M\|^2 + \|\theta(T) - \theta_h^M\|^2 + \Delta t \sum_{n=1}^M \left( \nu \|\mathbf{u}^n - \mathbf{w}_h^n\|^2 + \kappa \|\theta^n - \phi_h^n\|^2 \right) \\ \leq \tilde{C} \left( (\Delta t)^2 + h^4 \right), \end{aligned} \quad (2.54)$$

$$\tilde{C} := \tilde{C}(\mathbf{u}, p, \theta, \mathbf{u}_t, \mathbf{u}_{tt}, \theta_t, \theta_{tt}, T, C_{PF}).$$

**Proof:** First applying the inequality  $(a+b)^2 \leq 2(a^2+b^2)$  to the errors  $\|\mathbf{u}(T) - \mathbf{u}_h^M\|^2$ ,  $\|\theta(T) - \theta_h^M\|^2$ ,  $\|\mathbf{u}^n - \mathbf{w}_h^n\|^2$ , and  $\|\theta^n - \phi_h^n\|^2$ . Then using the conclusion of the previous theorem along with the choice of the  $k = 2$  gives the desired result.  $\square$

**Remark 2.3.7** *The theorem and corollary above, which lead to our choices of  $H$ ,  $\alpha_1$  and  $\alpha_2$ , are based on the smoothness assumptions of a true solution. If these assumptions do not hold, then optimal choices of these parameters will generally change as well. Due to the delicate nature of the nonlinearities involved, it is difficult to make a general statement about what the optimal values will be for a given regularity. However, in such cases, the choices we make are likely good starting points, and testing/tuning should be done to improve them.*

**Proof:** The first aim is to obtain error equations. Since the true solutions  $(\mathbf{u}^{n+1}, p^{n+1}, \theta^{n+1})$  of (2.1) at time  $t^{n+1}$  satisfies

$$\begin{aligned} \frac{1}{\Delta t} (\mathbf{u}^{n+1} - \mathbf{u}^n, \mathbf{v}_h) + \nu (\nabla \mathbf{u}^{n+1}, \nabla \mathbf{v}_h) + c_0 (\mathbf{u}^{n+1}, \mathbf{u}^{n+1}, \mathbf{v}_h) - (p^{n+1} - q_h, \nabla \cdot \mathbf{v}_h) \\ = \left( \frac{\mathbf{u}^{n+1} - \mathbf{u}^n}{\Delta t} - \mathbf{u}_t^{n+1}, \mathbf{v}_h \right) + (Ri \langle 0, \theta^{n+1} \rangle, \mathbf{v}_h) + (\mathbf{f}^{n+1}, \mathbf{v}_h), \end{aligned} \quad (2.55)$$

and

$$\begin{aligned} & \frac{1}{\Delta t} (\theta^{n+1} - \theta^n, \chi_h) + (\kappa \nabla \theta^{n+1}, \nabla \chi_h) + c_1(\mathbf{u}^{n+1}, \theta^{n+1}, \chi_h) \\ &= \left( \frac{\theta^{n+1} - \theta^n}{\Delta t} - \theta_t^{n+1}, \chi_h \right) + (\Gamma^{n+1}, \chi_h), \end{aligned} \quad (2.56)$$

for all  $(\mathbf{v}_h, q_h, \chi_h) \in (\mathbf{W}_h, Q_h, W_h)$ , subtracting (2.27) from (2.55), and (2.29) from (2.56) results in

$$\begin{aligned} & \frac{1}{\Delta t} ((\mathbf{u}^{n+1} - \mathbf{w}_h^{n+1}) - (\mathbf{u}^n - \mathbf{u}_h^n), \mathbf{v}_h) + \nu (\nabla(\mathbf{u}^{n+1} - \mathbf{w}_h^{n+1}), \nabla \mathbf{v}_h) \\ & \quad + c_0(\mathbf{u}^{n+1}, \mathbf{u}^{n+1}, \mathbf{v}_h) - c_0(\mathbf{u}_h^n, \mathbf{w}_h^{n+1}, \mathbf{v}_h) - (p^{n+1} - q_h, \nabla \cdot \mathbf{v}_h) \\ &= \left( \frac{\mathbf{u}^{n+1} - \mathbf{u}^n}{\Delta t} - \mathbf{u}_t^{n+1}, \mathbf{v}_h \right) + (Ri \langle 0, \theta^{n+1} - \theta^n \rangle, \mathbf{v}_h) + (Ri \langle 0, \theta^n - \theta_h^n \rangle, \mathbf{v}_h), \end{aligned} \quad (2.57)$$

and

$$\begin{aligned} & \frac{1}{\Delta t} ((\theta^{n+1} - \phi_h^{n+1}) - (\theta^n - \theta_h^n), \chi_h) + \kappa (\nabla(\theta^{n+1} - \phi_h^{n+1}), \nabla \chi_h) \\ & \quad + c_1(\mathbf{u}^{n+1}, \theta^{n+1}, \chi_h) - c_1(\mathbf{u}_h^n, \phi_h^{n+1}, \chi_h) = \left( \frac{\theta^{n+1} - \theta^n}{\Delta t} - \theta_t^{n+1}, \chi_h \right), \end{aligned} \quad (2.58)$$

for all  $(\mathbf{v}_h, q_h, \chi_h) \in (\mathbf{V}_h, Q_h, W_h)$ . Using the error decompositions (2.53) in (2.57) and (2.58) produce

$$\begin{aligned} & \frac{1}{\Delta t} (\boldsymbol{\epsilon}_u^{n+1} - \mathbf{e}_u^n, \mathbf{v}_h) + \nu (\nabla \boldsymbol{\epsilon}_u^{n+1}, \nabla \mathbf{v}_h) \\ &= \left( \frac{\boldsymbol{\eta}_u^{n+1} - \boldsymbol{\eta}_u^n}{\Delta t}, \mathbf{v}_h \right) + \nu (\nabla \boldsymbol{\eta}_u^{n+1}, \nabla \mathbf{v}_h) - (p^{n+1} - q_h, \nabla \cdot \mathbf{v}_h) + c_0(\mathbf{u}^{n+1}, \mathbf{u}^{n+1}, \mathbf{v}_h) \\ & \quad - c_0(\mathbf{u}_h^n, \mathbf{w}_h^{n+1}, \mathbf{v}_h) - (Ri \langle 0, \eta_\theta^n \rangle, \mathbf{v}_h) + (Ri \langle 0, e_\theta^n \rangle, \mathbf{v}_h) \\ & \quad - (Ri \langle 0, (\theta^{n+1} - \theta^n) \rangle, \mathbf{v}_h) - \left( \frac{\mathbf{u}^{n+1} - \mathbf{u}^n}{\Delta t} - \mathbf{u}_t^{n+1}, \mathbf{v}_h \right), \end{aligned} \quad (2.59)$$

and

$$\begin{aligned} & \frac{1}{\Delta t} (\epsilon_\theta^{n+1} - e_\theta^n, \chi_h) + \kappa (\nabla \epsilon_\theta^{n+1}, \nabla \chi_h) \\ &= \left( \frac{\eta_\theta^{n+1} - \eta_\theta^n}{\Delta t}, \chi_h \right) + \kappa (\nabla \eta_\theta^{n+1}, \nabla \chi_h) + c_1(\mathbf{u}^{n+1}, \theta^{n+1}, \chi_h) \\ & \quad - c_1(\mathbf{u}_h^n, \phi_h^{n+1}, \chi_h) - \left( \frac{\theta^{n+1} - \theta^n}{\Delta t} - \theta_t^{n+1}, \chi_h \right). \end{aligned} \quad (2.60)$$

Choose test functions  $\mathbf{v}_h = \boldsymbol{\epsilon}_u^{n+1}$  in (2.59), and  $\chi_h = \epsilon_\theta^{n+1}$  in (2.60), along with the use of polarization identity yields

$$\begin{aligned}
& \frac{1}{2\Delta t} (\|\boldsymbol{\epsilon}_u^{n+1}\|^2 - \|\mathbf{e}_u^n\|^2 + \|\boldsymbol{\epsilon}_u^{n+1} - \mathbf{e}_u^n\|^2) + \nu \|\nabla \boldsymbol{\epsilon}_u^{n+1}\|^2 \\
&= \left( \frac{\boldsymbol{\eta}_u^{n+1} - \boldsymbol{\eta}_u^n}{\Delta t}, \boldsymbol{\epsilon}_u^{n+1} \right) + \nu (\nabla \boldsymbol{\eta}_u^{n+1}, \nabla \boldsymbol{\epsilon}_u^{n+1}) - (p^{n+1} - q_h, \nabla \cdot \boldsymbol{\epsilon}_u^{n+1}) \\
&+ c_0 (\mathbf{u}^{n+1}, \mathbf{u}^{n+1}, \boldsymbol{\epsilon}_u^{n+1}) - c_0 (\mathbf{u}_h^n, \mathbf{w}_h^{n+1}, \boldsymbol{\epsilon}_u^{n+1}) - (Ri \langle 0, \eta_\theta^n - e_\theta^n \rangle, \boldsymbol{\epsilon}_u^{n+1}) \\
&\quad - (Ri \langle 0, (\theta^{n+1} - \theta^n) \rangle, \boldsymbol{\epsilon}_u^{n+1}) - \left( \frac{\mathbf{u}^{n+1} - \mathbf{u}^n}{\Delta t} - \mathbf{u}_t^{n+1}, \boldsymbol{\epsilon}_u^{n+1} \right), \quad (2.61)
\end{aligned}$$

and

$$\begin{aligned}
& \frac{1}{2\Delta t} (\|\epsilon_\theta^{n+1}\|^2 - \|e_\theta^n\|^2 + \|\epsilon_\theta^{n+1} - e_\theta^n\|^2) + \kappa \|\nabla \epsilon_\theta^{n+1}\|^2 \\
&= \left( \frac{\eta_\theta^{n+1} - \eta_\theta^n}{\Delta t}, \epsilon_\theta^{n+1} \right) + \kappa (\nabla \eta_\theta^{n+1}, \nabla \epsilon_\theta^{n+1}) + c_1 (\mathbf{u}^{n+1}, \theta^{n+1}, \epsilon_\theta^{n+1}) \\
&\quad - c_1 (\mathbf{u}_h^n, \phi_h^{n+1}, \epsilon_\theta^{n+1}) - \left( \frac{\theta^{n+1} - \theta^n}{\Delta t} - \theta_t^{n+1}, \epsilon_\theta^{n+1} \right). \quad (2.62)
\end{aligned}$$

We now proceed to bound the right hand side terms of the equation (2.61). By using Taylor's expansion with integral remainder, we get

$$\begin{aligned}
\boldsymbol{\eta}_u^{n+1} - \boldsymbol{\eta}_u^n &= \int_{t^n}^{t^{n+1}} \partial_t \boldsymbol{\eta}_u dt, \\
\frac{\boldsymbol{\eta}_u^{n+1} - \boldsymbol{\eta}_u^n}{\Delta t} &= \frac{1}{\Delta t} \int_{t^n}^{t^{n+1}} \partial_t \boldsymbol{\eta}_u dt.
\end{aligned}$$

Then using the Cauchy-Schwarz, the Poincaré-Friedrichs' and the Young's inequalities on the first three right hand side terms of (2.61) yields

$$\begin{aligned}
& \left| \left( \frac{\boldsymbol{\eta}_u^{n+1} - \boldsymbol{\eta}_u^n}{\Delta t}, \boldsymbol{\epsilon}_u^{n+1} \right) \right| \leq \frac{1}{\Delta t} \left\| \int_{t^n}^{t^{n+1}} \partial_t \boldsymbol{\eta}_u dt \right\| \|\boldsymbol{\epsilon}_u^{n+1}\| \\
&\leq \frac{\nu}{26} \|\nabla \boldsymbol{\epsilon}_u^{n+1}\|^2 + \frac{C\nu^{-1}}{\Delta t} \int_{t^n}^{t^{n+1}} \|\partial_t \boldsymbol{\eta}_u\|^2 dt, \\
&\leq \nu |(\nabla \boldsymbol{\eta}_u^{n+1}, \nabla \boldsymbol{\epsilon}_u^{n+1})| \leq \nu \|\nabla \boldsymbol{\eta}_u^{n+1}\| \|\nabla \boldsymbol{\epsilon}_u^{n+1}\| \\
&\quad \frac{\nu}{26} \|\nabla \boldsymbol{\epsilon}_u^{n+1}\|^2 + C\nu \|\nabla \boldsymbol{\eta}_u^{n+1}\|^2, \\
& |(p^{n+1} - q_h, \nabla \cdot \boldsymbol{\epsilon}_u^{n+1})| \leq \inf_{q_h \in Q_h} \|p^{n+1} - q_h\| \|\nabla \cdot \boldsymbol{\epsilon}_u^{n+1}\| \\
&\leq \sqrt{d} \inf_{q_h \in Q_h} \|p^{n+1} - q_h\| \|\nabla \boldsymbol{\epsilon}_u^{n+1}\| \\
&\leq \frac{\nu}{26} \|\nabla \boldsymbol{\epsilon}_u^{n+1}\|^2 + C\nu^{-1} \inf_{q_h \in Q_h} \|p^{n+1} - q_h\|^2.
\end{aligned}$$

To bound the nonlinear terms, we first write them as follows:

$$\begin{aligned}
& c_0(\mathbf{u}^{n+1}, \mathbf{u}^{n+1}, \boldsymbol{\epsilon}_u^{n+1}) - c_0(\mathbf{u}_h^n, \mathbf{w}_h^{n+1}, \boldsymbol{\epsilon}_u^{n+1}) \\
&= c_0(\mathbf{u}^{n+1} - \mathbf{u}^n, \mathbf{u}^{n+1}, \boldsymbol{\epsilon}_u^{n+1}) + c_0(\mathbf{u}^n - \mathbf{u}_h^n, \mathbf{u}^{n+1}, \boldsymbol{\epsilon}_u^{n+1}) + c_0(\mathbf{u}_h^n, \mathbf{u}^{n+1} - \mathbf{w}_h^{n+1}, \boldsymbol{\epsilon}_u^{n+1}) \\
&= c_0(\mathbf{u}^{n+1} - \mathbf{u}^n, \mathbf{u}^{n+1}, \boldsymbol{\epsilon}_u^{n+1}) + c_0(\boldsymbol{\eta}_u^n, \mathbf{u}^{n+1}, \boldsymbol{\epsilon}_u^{n+1}) \\
&\quad - c_0(\mathbf{e}_u^n, \mathbf{u}^{n+1}, \boldsymbol{\epsilon}_u^{n+1}) + c_0(\mathbf{u}_h^n, \boldsymbol{\eta}_u^{n+1} - \boldsymbol{\epsilon}_u^{n+1}, \boldsymbol{\epsilon}_u^{n+1}).
\end{aligned}$$

By Taylor expansion, we have

$$\mathbf{u}^{n+1} - \mathbf{u}^n = (\Delta t)\mathbf{u}_t(t^*), \quad t^* \in (t^n, t^{n+1}).$$

Then using the bound on the skew-symmetric trilinear form (2.25) on the first two nonlinear and the last one gives

$$\begin{aligned}
|c_0(\mathbf{u}^{n+1} - \mathbf{u}^n, \mathbf{u}^{n+1}, \boldsymbol{\epsilon}_u^{n+1})| &= |\Delta t c_0(\mathbf{u}_t(t^*), \mathbf{u}^{n+1}, \boldsymbol{\epsilon}_u^{n+1})| \\
&\leq C\Delta t \|\nabla \mathbf{u}_t(t^*)\| \|\nabla \mathbf{u}^{n+1}\| \|\nabla \boldsymbol{\epsilon}_u^{n+1}\| \\
&\leq \frac{\nu}{26} \|\nabla \boldsymbol{\epsilon}_u^{n+1}\|^2 + C\nu^{-1}(\Delta t)^2 \|\nabla \mathbf{u}^{n+1}\|^2 \|\mathbf{u}_t\|_{L^\infty(0,T;H^1(\Omega))}^2,
\end{aligned}$$

$$\begin{aligned}
|c_0(\boldsymbol{\eta}_u^n, \mathbf{u}^{n+1}, \boldsymbol{\epsilon}_u^{n+1})| &\leq C \|\nabla \boldsymbol{\eta}_u^n\| \|\nabla \mathbf{u}^{n+1}\| \|\nabla \boldsymbol{\epsilon}_u^{n+1}\| \\
&\leq \frac{\nu}{26} \|\nabla \boldsymbol{\epsilon}_u^{n+1}\|^2 + C\nu^{-1} \|\nabla \mathbf{u}^{n+1}\|^2 \|\nabla \boldsymbol{\eta}_u^n\|^2,
\end{aligned}$$

$$\begin{aligned}
|c_0(\mathbf{u}_h^n, \boldsymbol{\eta}_u^{n+1} - \boldsymbol{\epsilon}_u^{n+1}, \boldsymbol{\epsilon}_u^{n+1})| &= |c_0(\mathbf{u}_h^n, \boldsymbol{\eta}_u^{n+1}, \boldsymbol{\epsilon}_u^{n+1})| \\
&\leq C \|\nabla \mathbf{u}_h^n\| \|\nabla \boldsymbol{\eta}_u^{n+1}\| \|\nabla \boldsymbol{\epsilon}_u^{n+1}\| \\
&\leq \frac{\nu}{26} \|\nabla \boldsymbol{\epsilon}_u^{n+1}\|^2 + C\nu^{-1} \|\nabla \mathbf{u}_h^n\|^2 \|\nabla \boldsymbol{\eta}_u^{n+1}\|^2.
\end{aligned}$$

Now we find a bound on the nonlinear term  $c_0(\mathbf{e}_u^n, \mathbf{u}^{n+1}, \boldsymbol{\epsilon}_u^{n+1})$ . To do that, we first use the definition of the skew-symmetric trilinear form. Then we apply the Cauchy-Schwarz, Young's and the Poincaré-Friedrich's, Ladyzhenskaya's and Agmon's inequalities, respectively, to get

$$\begin{aligned}
|c_0(\mathbf{e}_u^n, \mathbf{u}^{n+1}, \boldsymbol{\epsilon}_u^{n+1})| &= \frac{1}{2} |((\mathbf{e}_u^n \cdot \nabla \mathbf{u}^{n+1}, \boldsymbol{\epsilon}_u^{n+1}) - (\mathbf{e}_u^n \cdot \nabla \boldsymbol{\epsilon}_u^{n+1}, \mathbf{u}^{n+1}))| \\
&\leq \frac{1}{2} (\|\mathbf{e}_u^n\| \|\nabla \mathbf{u}^{n+1}\|_{L^6} \|\boldsymbol{\epsilon}_u^{n+1}\|_{L^3} + \|\mathbf{e}_u^n\| \|\nabla \boldsymbol{\epsilon}_u^{n+1}\| \|\mathbf{u}^{n+1}\|_{L^\infty}) \\
&\leq \frac{1}{2} (C \|\mathbf{e}_u^n\| \|\mathbf{u}^{n+1}\|_{H^2} \|\boldsymbol{\epsilon}_u^{n+1}\|^{1/2} \|\nabla \boldsymbol{\epsilon}_u^{n+1}\|^{1/2} + C \|\mathbf{e}_u^n\| \|\nabla \boldsymbol{\epsilon}_u^{n+1}\| \|\mathbf{u}^{n+1}\|_{H^1}^{1/2} \|\mathbf{u}^{n+1}\|_{H^2}^{1/2}) \\
&\leq \frac{1}{2} (C \|\mathbf{e}_u^n\| \|\mathbf{u}^{n+1}\|_{H^2} \|\nabla \boldsymbol{\epsilon}_u^{n+1}\| + C \|\mathbf{e}_u^n\| \|\nabla \boldsymbol{\epsilon}_u^{n+1}\| \|\mathbf{u}^{n+1}\|_{H^2}) \\
&\leq \frac{\nu}{26} \|\nabla \boldsymbol{\epsilon}_u^{n+1}\|^2 + C\nu^{-1} \|\mathbf{u}^{n+1}\|_{H^2}^2 \|\mathbf{e}_u^n\|^2.
\end{aligned}$$

By using Taylor's theorem

$$\frac{\mathbf{u}^{n+1} - \mathbf{u}^n}{\Delta t} - \mathbf{u}_t^{n+1} = -\frac{\Delta t}{2} \mathbf{u}_{tt}(t^{**}), \quad \theta^{n+1} - \theta^n = \Delta t \theta_t(s^*); \quad t^{**}, s^* \in (t^{n+1}, t^{n+1})$$

and the standard estimates, we have the following bounds on the remaining right hand side terms of (2.61):

$$\begin{aligned} |(Ri\langle 0, \eta_\theta^n - e_\theta^n \rangle, \epsilon_u^{n+1})| &\leq Ri(\|\eta_\theta^n\| + \|e_\theta^n\|)\|\epsilon_u^{n+1}\| \\ &\leq C_{PF} Ri(\|\eta_\theta^n\| + \|e_\theta^n\|)\|\nabla \epsilon_u^{n+1}\| \\ &\leq \frac{\nu}{26} \|\nabla \epsilon_u^{n+1}\|^2 + C_{PF}^2 Ri^2 \nu^{-1} (\|\eta_\theta^n\|^2 + \|e_\theta^n\|^2), \\ |(Ri\langle 0, \theta^{n+1} - \theta^n \rangle, \epsilon_u^{n+1})| &\leq Ri \Delta t \|\theta_t(s^*)\| \|\epsilon_u^{n+1}\| \\ &\leq C_{PF} Ri \Delta t \|\theta_t(s^*)\| \|\nabla \epsilon_u^{n+1}\| \\ &\leq \frac{\nu}{26} \|\nabla \epsilon_u^{n+1}\|^2 + C \nu^{-1} Ri^2 (\Delta t)^2 \|\theta_t\|_{L^\infty(t^n, t^{n+1}; L^2(\Omega))}^2, \\ \left| \left( \frac{\mathbf{u}^{n+1} - \mathbf{u}^n}{\Delta t} - \mathbf{u}_t^{n+1}, \epsilon_u^{n+1} \right) \right| &\leq \frac{\nu}{26} \|\nabla \epsilon_u^{n+1}\|^2 + C \nu^{-1} (\Delta t)^2 \|\mathbf{u}_{tt}\|_{L^\infty(t^n, t^{n+1}; L^2(\Omega))}^2. \end{aligned}$$

Plugging these estimates into (2.61) gives

$$\begin{aligned} &\frac{1}{2\Delta t} (\|\epsilon_u^{n+1}\|^2 - \|e_u^n\|^2 + \|\epsilon_u^{n+1} - e_u^n\|^2) + \nu \|\nabla \epsilon_u^{n+1}\|^2 \\ &\leq \frac{\nu}{2} \|\nabla \epsilon_u^{n+1}\|^2 + \frac{C\nu^{-1}}{\Delta t} \int_{t^n}^{t^{n+1}} \|\partial_t \eta_u\|^2 dt + C\nu \|\nabla \eta_u^{n+1}\|^2 + C\nu^{-1} \inf_{q_h \in Q_h} \|p^{n+1} - q_h\|^2 \\ &\quad + C\nu^{-1} (\Delta t)^2 \|\nabla \mathbf{u}^{n+1}\|^2 \|\mathbf{u}_t\|_{L^\infty(0, T; \mathbf{H}^1(\Omega))}^2 + C\nu^{-1} \|\nabla \mathbf{u}^{n+1}\|^2 \|\nabla \eta_u^n\|^2 \\ &\quad + C\nu^{-1} \|\nabla \mathbf{u}_h^n\|^2 \|\nabla \eta_u^{n+1}\|^2 + C\nu^{-1} \|\mathbf{u}^{n+1}\|_{\mathbf{H}^2}^2 \|e_u^n\|^2 + C_{PF}^2 Ri^2 \nu^{-1} (\|\eta_\theta^n\|^2 + \|e_\theta^n\|^2) \\ &\quad + C\nu^{-1} (\Delta t)^2 \left( \|\mathbf{u}_{tt}\|_{L^\infty(t^n, t^{n+1}; L^2(\Omega))}^2 + Ri^2 \|\theta_t\|_{L^\infty(t^n, t^{n+1}; L^2(\Omega))}^2 \right). \quad (2.63) \end{aligned}$$

Using the approximation properties and rearranging the terms yields

$$\begin{aligned} &\frac{1}{2\Delta t} (\|\epsilon_u^{n+1}\|^2 - \|e_u^n\|^2 + \|\epsilon_u^{n+1} - e_u^n\|^2) + \frac{\nu}{2} \|\nabla \epsilon_u^{n+1}\|^2 \\ &\leq \frac{C\nu^{-1} h^{2k+2}}{\Delta t} \int_{t^n}^{t^{n+1}} \|\mathbf{u}_t\|_{k+1}^2 dt + C\nu h^{2k} \|\mathbf{u}^{n+1}\|_{k+1}^2 + C\nu^{-1} h^{2k} \|p^{n+1}\|_k^2 \\ &\quad + C\nu^{-1} (\Delta t)^2 \|\nabla \mathbf{u}^{n+1}\|^2 \|\mathbf{u}_t\|_{L^\infty(0, T; \mathbf{H}^1(\Omega))}^2 + C\nu^{-1} h^{2k} \|\nabla \mathbf{u}^{n+1}\|^2 \|\mathbf{u}\|_{k+1}^2 \\ &\quad + C\nu^{-1} h^{2k} \|\nabla \mathbf{u}_h^n\|^2 \|\mathbf{u}^{n+1}\|_{k+1}^2 + C\nu^{-1} \|\mathbf{u}^{n+1}\|_{\mathbf{H}^2}^2 \|e_u^n\|^2 \\ &\quad + C_{PF}^2 Ri^2 \nu^{-1} (Ch^{2k+2} \|\theta^n\|_{k+1}^2 + \|e_\theta^n\|^2) \\ &\quad + C\nu^{-1} (\Delta t)^2 \left( \|\mathbf{u}_{tt}\|_{L^\infty(0, T; L^2(\Omega))}^2 + Ri^2 \|\theta_t\|_{L^\infty(0, T; L^2(\Omega))}^2 \right). \quad (2.64) \end{aligned}$$

Multiplying the above inequality by  $2\Delta t$ , dropping the non-negative third left hand side term, and summing from  $n = 0$  to  $M - 1$  along with the use of the regularity assumptions gives

$$\begin{aligned}
& \sum_{n=0}^{M-1} (\|\epsilon_u^{n+1}\|^2 - \|\mathbf{e}_u^n\|^2) + \nu \Delta t \sum_{n=0}^{M-1} \|\nabla \epsilon_u^{n+1}\|^2 \\
& \leq C\nu^{-1}h^{2k+2} \int_0^T \|\mathbf{u}_t\|_{k+1}^2 dt + C\nu h^{2k} \|\mathbf{u}\|_{\infty, k+1}^2 + C\nu^{-1}h^{2k} \|p\|_{2,k}^2 \\
& + C\nu^{-1} \left( (\Delta t)^2 \|\mathbf{u}_t\|_{L^\infty(0,T; \mathbf{H}^1(\Omega))}^2 + C\nu^{-1}h^{2k} \|\mathbf{u}\|_{\infty, k+1}^2 \right) \left( \Delta t \sum_{n=0}^{M-1} \|\nabla \mathbf{u}^{n+1}\|^2 \right) \\
& + C\nu^{-1}h^{2k} \|\mathbf{u}\|_{\infty, k+1}^2 \left( \Delta t \sum_{n=0}^{M-1} \|\nabla \mathbf{u}_h^{n+1}\|^2 \right) + CC_{PF}^2 Ri^2 \nu^{-1} h^{2k+2} \|\theta\|_{\infty, k}^2 \\
& + C\nu^{-1} \left( \Delta t \sum_{n=0}^{M-1} \|\mathbf{u}^{n+1}\|_{\mathbf{H}^2}^2 \|\mathbf{e}_u^n\|^2 + C_{PF}^2 Ri^2 \|\mathbf{e}_\theta^n\|^2 \right) \\
& + C\nu^{-1} (\Delta t)^2 (\Delta t M) \left( \|\mathbf{u}_{tt}\|_{L^\infty(0,T; L^2(\Omega))}^2 + Ri^2 \|\theta_t\|_{L^\infty(0,T; L^2(\Omega))}^2 \right). \quad (2.65)
\end{aligned}$$

Using the similar technique and estimates to the right hand side of (2.62) provides

$$\begin{aligned}
& \sum_{n=0}^{M-1} (\|\epsilon_\theta^{n+1}\|^2 - \|\mathbf{e}_\theta^n\|^2) + \nu \Delta t \sum_{n=0}^{M-1} \|\nabla \epsilon_\theta^{n+1}\|^2 \\
& \leq C\nu^{-1}h^{2k+2} \int_0^T \|\theta_t\|_{k+1}^2 dt + C\nu h^{2k} \|\theta\|_{\infty, k+1}^2 \\
& + C\nu^{-1} \left( (\Delta t)^2 \|\mathbf{u}_t\|_{L^\infty(0,T; \mathbf{H}^1(\Omega))}^2 + C\nu^{-1}h^{2k} \|\mathbf{u}\|_{\infty, k+1}^2 \right) \left( \Delta t \sum_{n=0}^{M-1} \|\nabla \theta^{n+1}\|^2 \right) \\
& + C\nu^{-1}h^{2k} \|\theta\|_{\infty, k+1}^2 \left( \Delta t \sum_{n=0}^{M-1} \|\nabla \mathbf{u}_h^n\|^2 \right) + C\nu^{-1} \Delta t \sum_{n=0}^{M-1} \|\theta^{n+1}\|_{H^2}^2 \|\mathbf{e}_u^n\|^2 \\
& + C\nu^{-1} (\Delta t)^2 (\Delta t M) \|\theta_{tt}\|_{L^\infty(0,T; L^2(\Omega))}^2. \quad (2.66)
\end{aligned}$$

Sum these two inequality noting that  $\Delta t M = T$ , and rearrange the terms to have

$$\begin{aligned}
& \sum_{n=0}^{M-1} (\|\epsilon_u^{n+1}\|^2 + \|\epsilon_\theta^{n+1}\|^2) - \sum_{n=0}^{M-1} (\|\mathbf{e}_u^n\|^2 + \|\mathbf{e}_\theta^n\|^2) + \nu \Delta t \sum_{n=0}^{M-1} (\|\nabla \epsilon_u^{n+1}\|^2 + \|\nabla \epsilon_\theta^{n+1}\|^2) \\
& \leq \tilde{C}\nu^{-1} \Delta t \sum_{n=0}^{M-1} \left( (\|\mathbf{u}^{n+1}\|_{\mathbf{H}^2}^2 + \|\theta^{n+1}\|_{H^2}^2) \|\mathbf{e}_u^n\|^2 + C_{PF}^2 Ri^2 \|\mathbf{e}_\theta^n\|^2 \right) \\
& + \tilde{C}\nu^{-1}h^{2k} \Delta t \sum_{n=0}^{M-1} \|\nabla \mathbf{u}_h^n\|^2 + C(\nu^{-1}h^{2k+2} + (\nu + \nu^{-1})h^{2k}) + C\nu^{-1}(\Delta t)^2, \quad (2.67)
\end{aligned}$$

where  $\tilde{C} := \tilde{C}(\mathbf{u}, p, \theta, \mathbf{u}_t, \mathbf{u}_{tt}, \theta_t, \theta_{tt}, T, C_{PF})$ .  $\square$

The next step is to obtain relations between  $\|\epsilon_u^{n+1}\|$  and  $\|e_u^{n+1}\|$ ,  $\|\epsilon_\theta^{n+1}\|$  and  $\|e_\theta^{n+1}\|$  by using *Step 2* of Algorithm 2.2.1.

**Lemma 2.3.8** *It holds that*

$$\begin{aligned} \frac{1}{2\Delta t} \|\epsilon_u^{n+1}\|^2 &= \frac{1}{2\Delta t} (\|e_u^{n+1}\|^2 + \|\epsilon_u^{n+1} - e_u^{n+1}\|^2) + \alpha_1 \|\nabla e_u^{n+1}\|^2 - \alpha_1 (\nabla \eta_u^{n+1}, \nabla e_u^{n+1}) \\ &\quad + \alpha_1 (\nabla(\mathbf{u}^{n+1} - \mathbf{u}^n), \nabla e_u^{n+1}) + \alpha_1 ((I - P_u^H) \nabla \mathbf{u}^n, \nabla e_u^{n+1}) \\ &\quad + \alpha_1 (P_u^H \nabla \eta_u^n, \nabla e_u^{n+1}) - \alpha_1 (P_u^H \nabla e_u^n, \nabla e_u^{n+1}), \end{aligned} \quad (2.68)$$

and

$$\begin{aligned} \frac{1}{2\Delta t} \|\epsilon_\theta^{n+1}\|^2 &= \frac{1}{2\Delta t} (\|e_\theta^{n+1}\|^2 + \|\epsilon_\theta^{n+1} - e_\theta^{n+1}\|^2) + \alpha_2 \|\nabla e_\theta^{n+1}\|^2 - \alpha_2 (\nabla \eta_\theta^{n+1}, \nabla e_\theta^{n+1}) \\ &\quad + \alpha_2 (\nabla(\theta^{n+1} - \theta^n), \nabla e_\theta^{n+1}) + \alpha_2 ((I - P_\theta^H) \nabla \theta^n, \nabla e_\theta^{n+1}) \\ &\quad + \alpha_2 (P_\theta^H \nabla \eta_\theta^n, \nabla e_\theta^{n+1}) - \alpha_2 (P_\theta^H \nabla e_\theta^n, \nabla e_\theta^{n+1}). \end{aligned} \quad (2.69)$$

**Proof:** Choosing  $r_h = \lambda_h^{n+1}$  in (2.31), equation (2.30) becomes

$$\frac{1}{\Delta t} (\mathbf{w}_h^{n+1} - \mathbf{u}_h^{n+1}, \boldsymbol{\varphi}_h) = \alpha_1 (\nabla \mathbf{u}_h^{n+1}, \nabla \boldsymbol{\varphi}_h) - \alpha_1 (P_u^H \nabla \mathbf{u}_h^n, \nabla \boldsymbol{\varphi}_h).$$

Adding and subtracting terms on the right hand side of the above equation, and on the right hand side of (2.32) gives

$$\begin{aligned} \frac{1}{\Delta t} (\mathbf{w}_h^{n+1} - \mathbf{u}_h^{n+1}, \boldsymbol{\varphi}_h) &= \alpha_1 (\nabla(\mathbf{u}_h^{n+1} - \mathbf{u}_h^{n+1}), \nabla \boldsymbol{\varphi}_h) + \alpha_1 (\nabla(\mathbf{u}^{n+1} - \mathbf{u}^n), \nabla \boldsymbol{\varphi}_h) \\ &\quad + \alpha_1 (\nabla \mathbf{u}^n, \nabla \boldsymbol{\varphi}_h) - \alpha_1 (P_u^H \nabla \mathbf{u}^n, \nabla \boldsymbol{\varphi}_h) + \alpha_1 (P_u^H \nabla \mathbf{u}^n, \nabla \boldsymbol{\varphi}_h) - \alpha_1 (P_u^H \nabla \mathbf{u}_h^n, \nabla \boldsymbol{\varphi}_h) \\ &= \alpha_1 (\nabla(\mathbf{u}_h^{n+1} - \mathbf{u}_h^{n+1}), \nabla \boldsymbol{\varphi}_h) + \alpha_1 (\nabla(\mathbf{u}^{n+1} - \mathbf{u}^n), \nabla \boldsymbol{\varphi}_h) \\ &\quad + ((I - P_u^H) \nabla \mathbf{u}^n, \nabla \boldsymbol{\varphi}_h) + \alpha_1 (P_u^H \nabla(\mathbf{u}^n - \mathbf{u}_h^n), \nabla \boldsymbol{\varphi}_h) \end{aligned} \quad (2.70)$$

and

$$\begin{aligned} \frac{1}{\Delta t} (\phi_h^{n+1} - \theta_h^{n+1}, \Psi_h) &= \alpha_2 (\nabla(\theta_h^{n+1} - \theta_h^{n+1}), \nabla \Psi_h) + \alpha_2 (\nabla(\mathbf{u}^{n+1} - \mathbf{u}^n), \nabla \Psi_h) \\ &\quad + \alpha_2 (\nabla \theta^n, \nabla \Psi_h) - \alpha_2 (P_\theta^H \nabla \theta^n, \nabla \Psi_h) + \alpha_2 (P_\theta^H \nabla \theta^n, \nabla \Psi_h) - \alpha_2 (P_\theta^H \nabla \theta_h^n, \nabla \Psi_h) \\ &= \alpha_2 (\nabla(\theta_h^{n+1} - \theta_h^{n+1}), \nabla \Psi_h) + \alpha_2 (\nabla(\theta^{n+1} - \theta^n), \nabla \Psi_h) \\ &\quad + ((I - P_\theta^H) \nabla \theta^n, \nabla \Psi_h) + \alpha_2 (P_\theta^H \nabla(\theta^n - \theta_h^n), \nabla \Psi_h). \end{aligned} \quad (2.71)$$

□

To continue error analysis, first multiply (2.68) and (2.69) by  $2\Delta t$ , next sum over time step, and then add the resulting equality to (2.67). Then we get

$$\begin{aligned}
& \sum_{n=0}^{M-1} (\|\mathbf{e}_u^{n+1}\|^2 + \|e_\theta^{n+1}\|^2) - \sum_{n=0}^{M-1} (\|\mathbf{e}_u^n\|^2 + \|e_\theta^n\|^2) \\
& + \sum_{n=0}^{M-1} (\|\boldsymbol{\epsilon}_u^{n+1} - \mathbf{e}_u^{n+1}\|^2 + \|\epsilon_\theta^{n+1} - e_\theta^{n+1}\|^2) + \nu \Delta t \sum_{n=0}^{M-1} (\|\nabla \boldsymbol{\epsilon}_u^{n+1}\|^2 + \|\nabla \epsilon_\theta^{n+1}\|^2) \\
& \quad + \Delta t \sum_{n=0}^{M-1} \left( 2\alpha_1 \|\nabla \mathbf{e}_u^{n+1}\|^2 + 2\alpha_2 \|\nabla e_\theta^{n+1}\|^2 \right) \\
& \leq \tilde{C}\nu^{-1} \left( \Delta t \sum_{n=0}^{M-1} \left( \|\mathbf{u}^{n+1}\|_{\mathbf{H}^2}^2 + \|\theta^{n+1}\|_{H^2}^2 \right) \|\mathbf{e}_u^n\|^2 + C_{PF}^2 Ri^2 \|e_\theta^n\|^2 \right) \\
& + \tilde{C}\nu^{-1} h^{2k} \left( \Delta t \sum_{n=0}^{M-1} \|\nabla \mathbf{u}_h^n\|^2 \right) + \tilde{C} (\nu^{-1} h^{2k+2} + (\nu + \nu^{-1}) h^{2k}) + C\nu^{-1} (\Delta t)^2 \\
& \quad + 2\Delta t \sum_{n=0}^{M-1} (RT1 + RT2 + RT3 + RT4 + RT5). \quad (2.72)
\end{aligned}$$

Observe that the last four terms in the right of (2.72) can be controlled by using the Cauchy-Schwarz, the Young's inequalities with using the fact that  $\|P_u^H\| \leq 1$ , and using the approximating properties

$$\begin{aligned}
|RT1| & \leq |\alpha_1 (\nabla \boldsymbol{\eta}_u^{n+1}, \nabla \mathbf{e}_u^{n+1})| + |\alpha_2 (\nabla \eta_\theta^{n+1}, \nabla e_\theta^{n+1})| \\
& \leq \alpha_1 \|\nabla \boldsymbol{\eta}_u^{n+1}\| \|\nabla \mathbf{e}_u^{n+1}\| + \alpha_2 \|\nabla \eta_\theta^{n+1}\| \|\nabla e_\theta^{n+1}\| \\
& \leq \frac{\alpha_1}{10} \|\nabla \mathbf{e}_u^{n+1}\|^2 + \frac{\alpha_2}{10} \|\nabla e_\theta^{n+1}\|^2 + C\alpha_1 \|\nabla \boldsymbol{\eta}_u^{n+1}\|^2 + C\alpha_2 \|\nabla \eta_\theta^{n+1}\|^2, \\
& \leq \frac{\alpha_1}{10} \|\nabla \mathbf{e}_u^{n+1}\|^2 + \frac{\alpha_2}{10} \|\nabla e_\theta^{n+1}\|^2 + C\alpha_1 h^{2k} \|\mathbf{u}^n\|_{k+1}^2 + C\alpha_1 h^{2k} \|\theta^n\|_{k+1}^2, \\
|RT2| & = |\alpha_1 (\nabla (\mathbf{u}^{n+1} - \mathbf{u}^n), \nabla \mathbf{e}_u^{n+1})| + |\alpha_2 (\nabla (\theta^{n+1} - \theta^n), \nabla e_\theta^{n+1})| \\
& \leq \alpha_1 \|\nabla (\mathbf{u}^{n+1} - \mathbf{u}^n)\| \|\nabla \mathbf{e}_u^{n+1}\| + \alpha_2 \|\nabla (\theta^{n+1} - \theta^n)\| \|\nabla e_\theta^{n+1}\| \\
& \leq \frac{\alpha_1}{10} \|\nabla \mathbf{e}_u^{n+1}\|^2 + \frac{\alpha_2}{10} \|\nabla e_\theta^{n+1}\|^2 \\
& \quad + C(\Delta t)^2 \left( \alpha_1 \|\mathbf{u}_t\|_{L^\infty(0,T;\mathbf{H}^1(\Omega))}^2 + \alpha_2 \|\theta_t\|_{L^\infty(0,T;H^1(\Omega))}^2 \right),
\end{aligned}$$



$$\begin{aligned}
|RT3| &= |\alpha_1((I - P_u^H)\nabla \mathbf{u}^n, \nabla \mathbf{e}_u^{n+1})| + |\alpha_2((I - P_\theta^H)\nabla \theta^n, \nabla e_\theta^{n+1})| \\
&\leq \frac{\alpha_1}{10} \|\nabla \mathbf{e}_u^{n+1}\|^2 + \frac{\alpha_2}{10} \|\nabla e_\theta^{n+1}\|^2 + C\alpha_1 \|(I - P_u^H)\nabla \mathbf{u}^n\|^2 \\
&\quad + C\alpha_2 \|(I - P_\theta^H)\nabla \theta^n\|^2, \\
&\leq \frac{\alpha_1}{10} \|\nabla \mathbf{e}_u^{n+1}\|^2 + \frac{\alpha_2}{10} \|\nabla e_\theta^{n+1}\|^2 + C\alpha_1 H^{2k} \|\mathbf{u}^n\|_{k+1}^2 + C\alpha_2 H^{2k} \|\theta^n\|_{k+1}^2,
\end{aligned}$$

$$\begin{aligned}
|RT4| &= |\alpha_1(P_u^H \nabla \boldsymbol{\eta}_u^n, P_u^H \nabla \mathbf{e}_u^{n+1})| + |\alpha_2(P_\theta^H \nabla \eta_\theta^n, P_\theta^H \nabla e_\theta^{n+1})| \\
&\leq \frac{\alpha_1}{10} \|\nabla \mathbf{e}_u^{n+1}\|^2 + \frac{\alpha_2}{10} \|\nabla e_\theta^{n+1}\|^2 + C\alpha_1 \|\nabla \boldsymbol{\eta}_u^n\|^2 + C\alpha_2 \|\nabla \eta_\theta^n\|^2 \\
&\leq \frac{\alpha_1}{10} \|\nabla \mathbf{e}_u^{n+1}\|^2 + \frac{\alpha_2}{10} \|\nabla e_\theta^{n+1}\|^2 + C\alpha_1 h^{2k} \|\mathbf{u}^n\|_{k+1}^2 + C\alpha_2 h^{2k} \|\theta^n\|_{k+1}^2
\end{aligned}$$

To evaluate the last term, we use standard inequalities with inverse inequality to obtain

$$\begin{aligned}
|RT5| &= |\alpha_1(P_u^H \nabla \mathbf{e}_u^n, \nabla \mathbf{e}_u^{n+1})| + |\alpha_2(P_\theta^H \nabla e_\theta^n, \nabla e_\theta^{n+1})| \\
&\leq \alpha_1 \|P_u^H \nabla \mathbf{e}_u^n\| \|\nabla \mathbf{e}_u^{n+1}\| + \alpha_2 \|P_\theta^H \nabla e_\theta^n\| \|\nabla e_\theta^{n+1}\| \\
&\leq \alpha_1 C h^{-1} \|\mathbf{e}_u^n\| \|\nabla \mathbf{e}_u^{n+1}\| + \alpha_2 C h^{-1} \|e_\theta^n\| \|\nabla e_\theta^{n+1}\| \\
&\leq \frac{\alpha_1}{10} \|\nabla \mathbf{e}_u^{n+1}\|^2 + \frac{\alpha_2}{10} \|\nabla e_\theta^{n+1}\|^2 + C h^{-2} \alpha_1 \|\mathbf{e}_u^n\|^2 + C h^{-2} \alpha_2 \|e_\theta^n\|^2.
\end{aligned}$$

Plugging these estimates into (2.72) along with the use of approximation properties and regularity assumptions yields

$$\begin{aligned}
&\sum_{n=0}^{M-1} (\|\mathbf{e}_u^{n+1}\|^2 + \|e_\theta^{n+1}\|^2) - \sum_{n=0}^{M-1} (\|\mathbf{e}_u^n\|^2 + \|e_\theta^n\|^2) \\
&\quad + \sum_{n=0}^{M-1} (\|\boldsymbol{\epsilon}_u^{n+1} - \mathbf{e}_u^{n+1}\|^2 + \|\epsilon_\theta^{n+1} - e_\theta^{n+1}\|^2) \\
&+ \nu \Delta t \sum_{n=0}^{M-1} (\|\nabla \boldsymbol{\epsilon}_u^{n+1}\|^2 + \|\nabla \epsilon_\theta^{n+1}\|^2) + \nu \Delta t \sum_{n=0}^{M-1} (\alpha_1 \|\nabla \mathbf{e}_u^{n+1}\|^2 + \alpha_2 \|\nabla e_\theta^{n+1}\|^2) \\
&\leq \tilde{C} \Delta t \sum_{n=0}^{M-1} \left( (\nu^{-1} \|\mathbf{u}^{n+1}\|_{\mathbf{H}^2}^2 + \nu^{-1} \|\theta^{n+1}\|_{H^2}^2 + \alpha_1 h^{-2}) \|\mathbf{e}_u^n\|^2 \right. \\
&\quad \left. + (\nu^{-1} C_{PF}^2 Ri^2 + h^{-2} \alpha_2) \|e_\theta^n\|^2 \right) \\
&+ \tilde{C} \nu^{-1} h^{2k} \left( \Delta t \sum_{n=0}^{M-1} \|\nabla \mathbf{u}_h^n\|^2 \right) + \tilde{C} \left( \nu^{-1} h^{2k+2} + (\nu + \nu^{-1}) h^{2k} \right) + \nu^{-1} (\Delta t)^2 \\
&\quad + (\alpha_1 + \alpha_2) h^{2k} + (\alpha_1 + \alpha_2) H^{2k} + (\alpha_1 + \alpha_2) (\Delta t)^2. \quad (2.73)
\end{aligned}$$

Finally, choosing  $\alpha_1 = \alpha_2 = \mathcal{O}(h^2)$ , using stability result on discrete velocity and temperature solutions, and then applying Lemma 2.1.25 completes the proof.

## 2.4 Numerical Experiments

We provide two numerical experiments in this section. In the first one, we verify the theoretical results obtained in Section 2.3 by choosing the coarse mesh size as  $H = h$ , and the large scale space  $L_H$  as  $P_1$ . In the second numerical experiment, the effectiveness of the algorithm on Marsigli's flow is revealed.

### 2.4.1 Convergence Rate Verification

In the first test problem we verify the convergence rates predicted by Theorem 2.3.4.

We fix the following solutions

$$\begin{aligned}\mathbf{u} &= \begin{pmatrix} \cos(\pi y) \\ \sin(\pi x) \end{pmatrix} (1 + 0.1t), \\ p &= \sin(\pi(x + y))(1 + 0.2t), \\ \theta &= \sin(\pi x) + y \exp(t).\end{aligned}$$

on the region  $\Omega = (0, 1) \times (0, 1)$  with the boundary conditions which are true solutions on  $\partial\Omega$ . We calculate  $\mathbf{f}$  and  $\Gamma$  from (2.1) by taking the parameters as

$$Re = Ri = Pr = \kappa = 1.$$

We choose

$$(\mathbf{X}_h, Q_h, w_h) = (\mathbf{P}_2, P_1, P_1), H = h, \alpha_1 = h^2, \alpha_1 = h^2, \mathbf{L}_H = P_1.$$

To test spacial convergence rate, we first isolate the spatial error by choosing a fixed time step  $\Delta t = T/8$ , and end time  $T = 1e - 4$ . Next we compute approximate solutions on successive uniform meshes. Results are shown in Table 2.1 and Table 2.2. We observe second order convergence for both velocity and temperature in  $L^2(0, T; \mathbf{H}^1(\Omega))$ -norm. Third order convergence of velocity and temperature is found in the  $L^\infty(0, T; \mathbf{H}^1(\Omega))$ -norm, which is consistent with an  $L^2$ -lift, although we did prove such a result herein. Figure 2.1 shows that the discrete velocity and temperature solutions converge to continuous velocity and temperature solution when mesh size  $h$  goes to zero. In addition to this, Figure 2.1 shows that the spatial errors in velocity and temperature goes to zero when mesh size  $h$  goes to zero.

For the temporal convergence rate verification, we first fix mesh size as  $h = 1/64$ , and end time  $T = 1$ . We next compute discrete solutions using successively smaller time steps. Errors and rates are presented in Table 2.3 and Table 2.4. We observe first order convergence in all norms, as expected. Figure 2.2 shows that the temporal velocity and temperature errors goes to zero when time step  $\Delta t$  goes to zero.

Table 2.1: Velocity errors with fixed time step and small  $T$  to isolate the spatial errors.

$h^{-1}$	$\ \mathbf{u} - \mathbf{u}_h\ $	rate	$\ \ \mathbf{u} - \mathbf{u}_h\ \ _{2,1}$	rate
4	2.561e-3	--	7.129e-4	—
8	3.210e-4	2.995	1.771e-4	2.009
16	3.991e-5	3.008	4.351e-5	2.025
32	5.728e-6	2.800	1.117e-5	1.961
64	7.505e-7	2.932	2.904e-6	1.943
128	9.838e-8	2.931	7.411e-7	1.970

Table 2.2: Temperature errors with fixed time step and small  $T$  to isolate the spatial errors.

$h^{-1}$	$\ \theta - \theta_h\ $	rate	$\ \ \theta - \theta_h\ \ _{2,1}$	rate
4	1.812e-3	—	5.045e-4	—
8	2.273e-4	2.994	1.256e-4	2.005
16	2.817e-5	3.012	3.069e-5	2.033
32	3.434e-6	3.036	7.458e-6	2.040
64	4.234e-7	3.020	1.844e-6	2.015
128	5.288e-8	3.001	4.601e-7	2.003

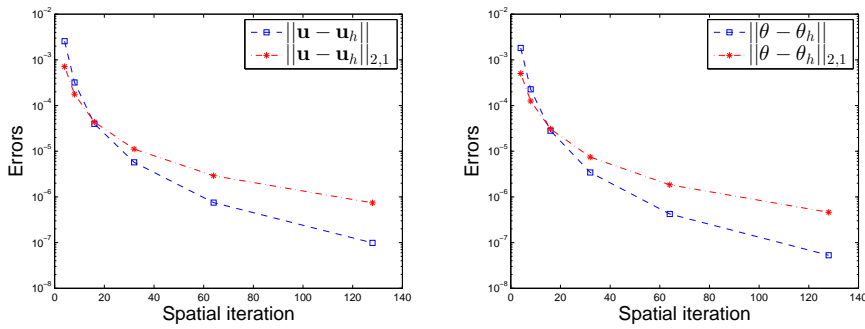


Figure 2.1: Spatial velocity and temperature errors with fixed time step and small  $T$ .

Table 2.3: Velocity errors with fixed fine mesh and large  $T = 1.0$  to isolate the temporal errors.

$\Delta t$	$\ \mathbf{u} - \mathbf{u}_h\ $	rate	$\ \ \mathbf{u} - \mathbf{u}_h\ \ _{2,1}$	rate
1	2.407e-3	–	2.508e-1	–
1/2	1.625e-3	0.566	1.602e-1	0.646
1/4	1.121e-3	0.535	1.042e-1	0.621
1/8	7.473e-4	0.585	6.638e-2	0.650
1/16	4.670e-4	0.678	3.875e-2	0.776
1/32	2.723e-4	0.778	2.125e-2	0.866
1/64	1.498e-4	0.861	1.126e-2	0.916
1/128	7.922e-5	0.920	5.851e-3	0.944

Table 2.4: Temperature errors with fixed fine mesh and large  $T = 1.0$  to isolate the temporal errors.

$\Delta t$	$\ \theta - \theta_h\ $	rate	$\ \ \theta - \theta_h\ \ _{2,1}$	rate
1	2.8e-2	–	2.031e-1	–
1/2	1.571e-2	0.833	9.479e-2	1.100
1/4	8.277e-3	0.924	4.122e-2	1.201
1/8	4.252e-3	0.961	1.704e-2	1.273
1/16	2.155e-3	0.980	7.463e-3	1.191
1/32	1.085e-3	0.989	3.524e-3	1.082
1/64	5.446e-4	0.994	1.733e-3	1.023
1/128	2.728e-4	0.997	8.761e-3	0.984

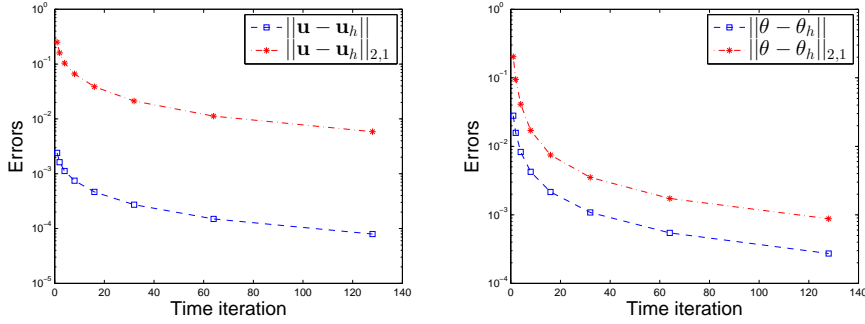


Figure 2.2: Temporal velocity and temperature errors with fixed mesh size.

## 2.4.2 Luigi Ferdinando Marsigli's physical model of gravity driven, two-layer flow

The undercurrent in the Bosphorus Strait that flows between The Black Sea and the Bosphorus Strait is one of the example of the gravity driven currents. In 1679, Marsigli revealed that this current is due to the density differences. He performed a laboratory experiment: a container was initially divided by a partition. The left side contained dyed water taken from the undercurrent in the Bosphorous, while the right side contained water having the density of surface water in the Black Sea. Two holes were placed in the partition to observe the resulting flow. The flow through the lower hole was in the direction of the undercurrent in the Bosphorous, while the flow through the upper hole was in the direction of the surface flow [98].

### 2.4.2.1 Marsigli's experiment set-up

The aim is to simulate this physical situation described by Marsigli in 1679. In the problem set up, we follow the paper written by H. Johnston et. al. in [84], where fourth order finite difference discretizations has been numerically simulated on this experiment. Using the Boussinesq assumption that the densities can be measured as temperatures, this problem can be modeled with the Boussinesq equations studied herein.

**Remark 2.4.1** *We note that the stability and convergence analysis in Section 2.3 is suitable for the Neumann type of boundary conditions when the normal derivatives of unknowns for the system (2.1) is zero on the whole boundary.*

The problem's set up is given as follows:

- The region is the perpendicular cross-section of one of the tanks which contains either pure water or salty water. The perpendicular cross section of the pipe is drawn in Figure 2.3.
- $\mathbf{u} = 0$ ,  $\nabla\theta \cdot \mathbf{n} = 0$  on  $\partial\Omega$ ,
- The initial velocity is taken to be at rest, and the initial temperature is discontinuous, with  $\theta = 1.5$  on the left half of the box ( $x \leq 4$ ) and  $\theta = 1.0$  for the right half ( $x > 4$ ).

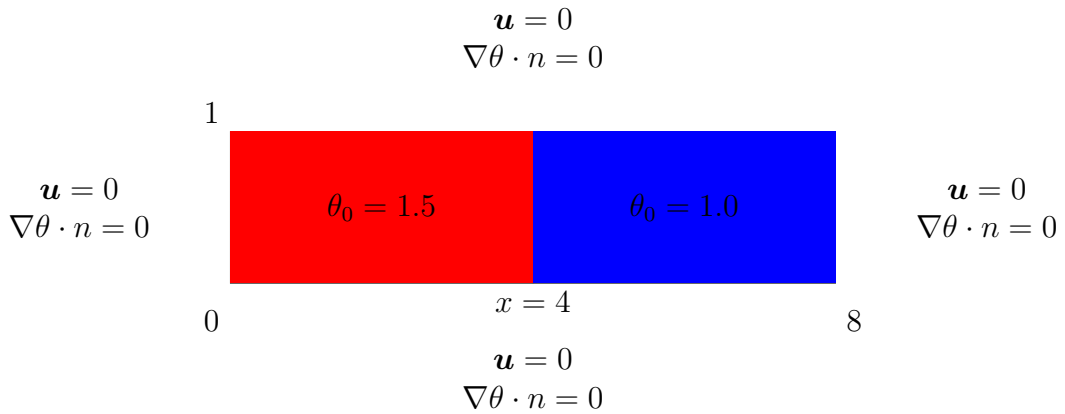


Figure 2.3: The Marsigli's Flow Setup

We chose flow parameters of  $Re = 1,000$ ,  $Ri=4$ , and  $Pr=1$ . More details about the physical problem can be found in [84].

For a resolved direct numerical simulation (DNS), we used  $(\mathbf{P}_2, P_1^{disc}, P_2)$  velocity-pressure-temperature elements on a mesh of 60,000 barycenter-refined triangles, which provided 241,162 velocity degrees of freedom (dof), 180,000 pressure dof, and 120,581 temperature dof. That such an element is LBB stable on this type of mesh is proven in [90, 3]. For the DNS, we used the same algorithm as proposed herein, but without the post-processing, with  $\Delta t = 0.01$ , and we compute to an end time of  $T=8$ . The temperature contours and velocity streamlines of the DNS are shown in Figures 2.4 at  $T = 2, 4$  and 8. We observe that as time progresses, the fluids mix at the warm/cold interface, and the warmer fluid spreads out on top of the colder fluid. We also ran this DNS test on a finer mesh with over 1 million total dof and time step  $\Delta t = 0.005$ , and also with those same parameters and the BDF2 time stepping discretization, and got

identical plots.

The goal of the model and associated discretization we study herein is to be able to find good approximations on much coarser discretizations than are needed by a DNS. For the coarse discretization, we use a time step of  $\Delta t = 0.02$ , and  $(\mathbf{P}_2, P_1, P_2)$  velocity-pressure-temperature elements on a mesh that provides just 14,782 velocity dof, 1,891 pressure dof, and 7,381 temperature dof.

On the coarse discretization, the DNS (i.e. ‘no-model’) performs very poorly. Results are shown in Figure 2.5, and it is clear that significant oscillations build in the temperature and velocity, and create a very poor solution. At  $T = 2$ , significant oscillations are present in the temperature contour, which causes the temperature at some areas to be above 1.5 or below 1, which is non-physical. By  $T = 8$ , the coarse mesh DNS predicted temperature contour has no physical meaning, as it predicts temperatures almost entirely out of the interval  $[1, 1.5]$ .

We next run the proposed algorithm/model using the coarse discretization, with  $\alpha_1 = \alpha_2 = 0.02$ , which was chosen because  $h^2 \approx 0.02$  (nearly identical results were found with  $\alpha_1 = \alpha_2 = 0.01$  and  $\alpha_1 = \alpha_2 = 0.005$ ). Results are shown in Figure 2.6, and we observe the proposed algorithm predicts well the overall flow pattern and temperature distribution of the resolved DNS. Some of the fine scale detail is lost, which is expected.



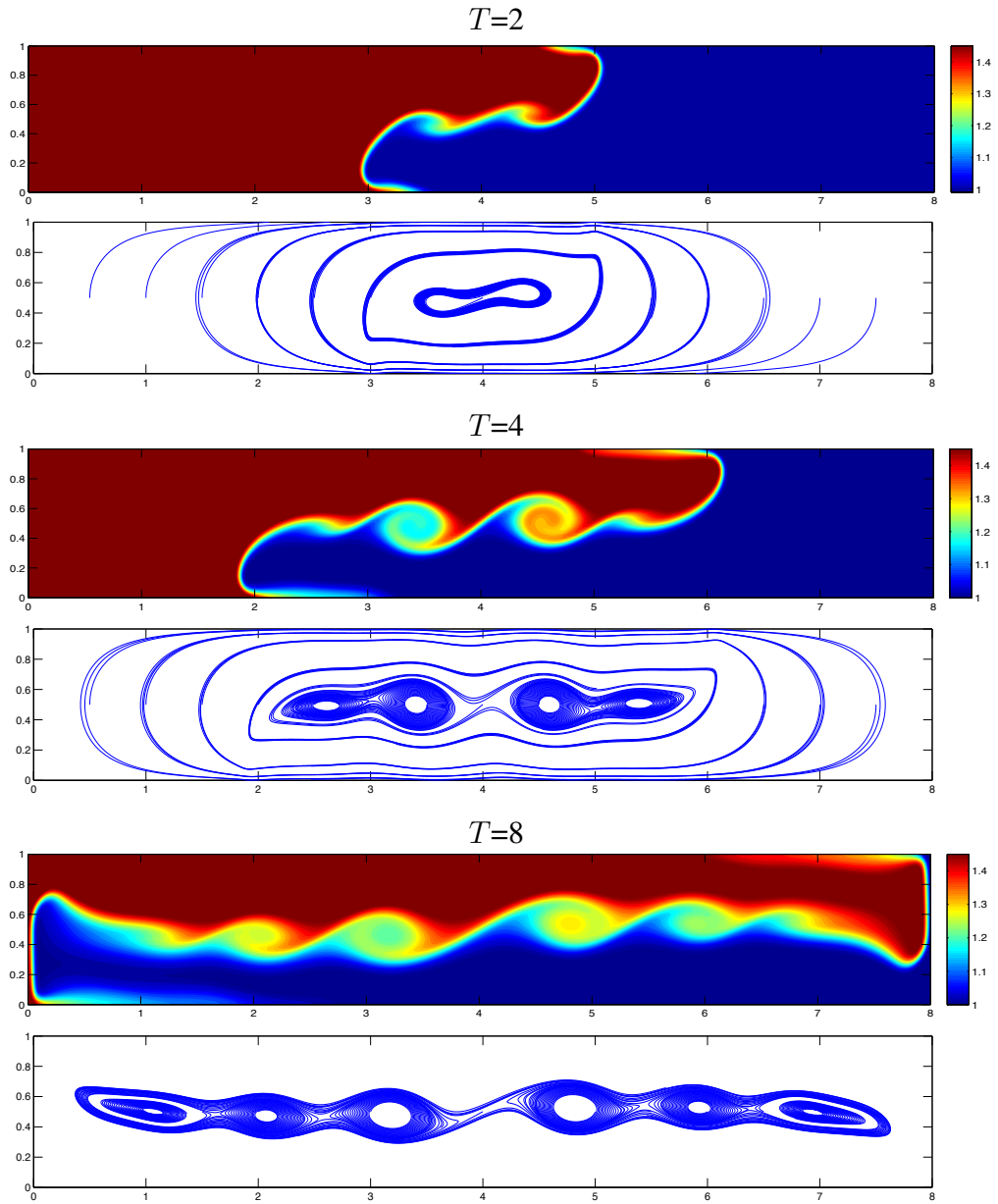


Figure 2.4: Resolved temperature contours and velocity streamlines for the  $Re=1,000$ ,  $Ri=4$ ,  $Pr = 1$  Marsigli flow test with  $T = 2, 4$ , and  $8$ .

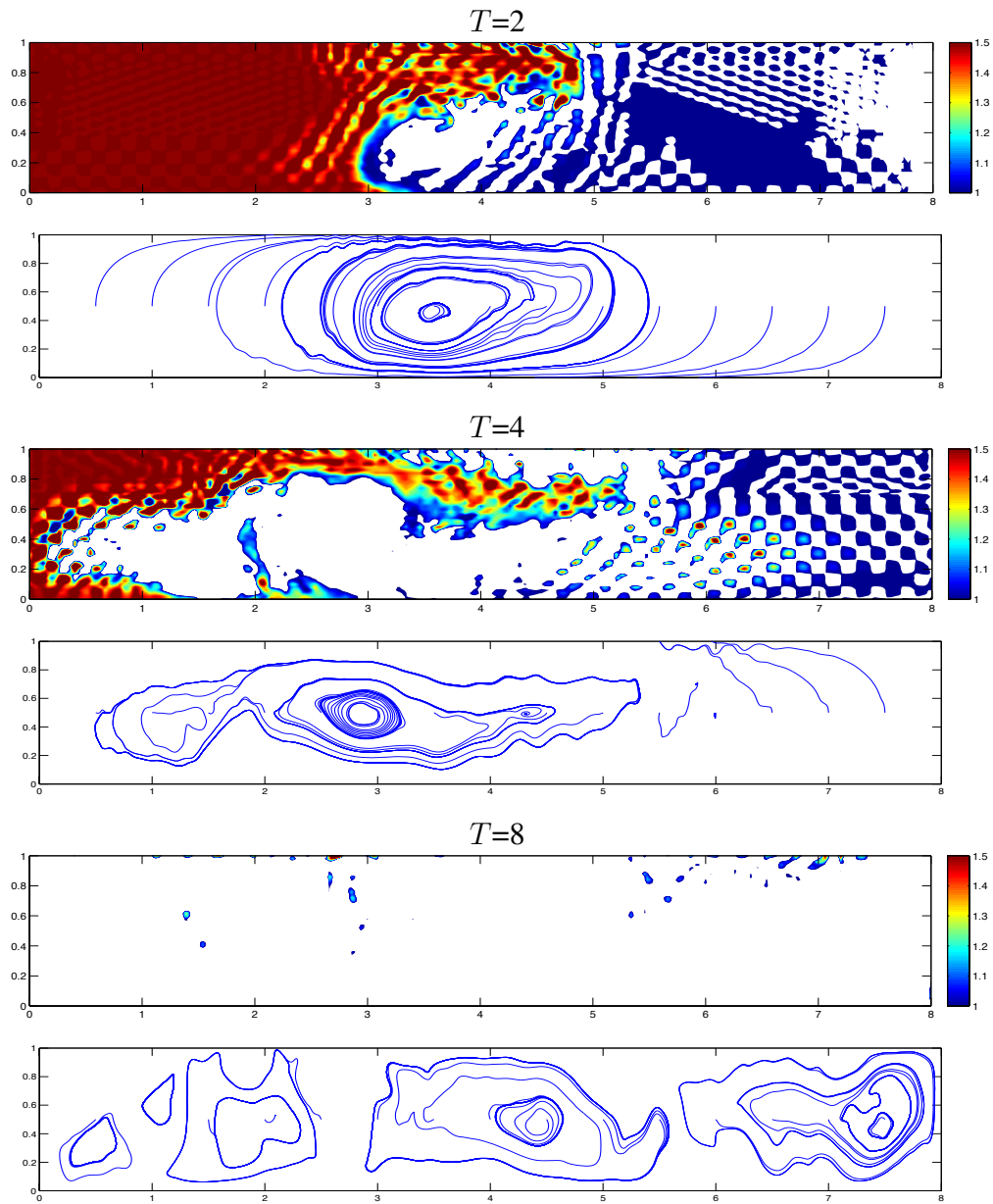


Figure 2.5: Coarse mesh DNS (no model) solutions for temperature contours and velocity streamlines for the  $Re=1,000$ ,  $Ri=4$ ,  $Pr = 1$  Marsigli flow test with  $T = 2$ , 4, and 8.

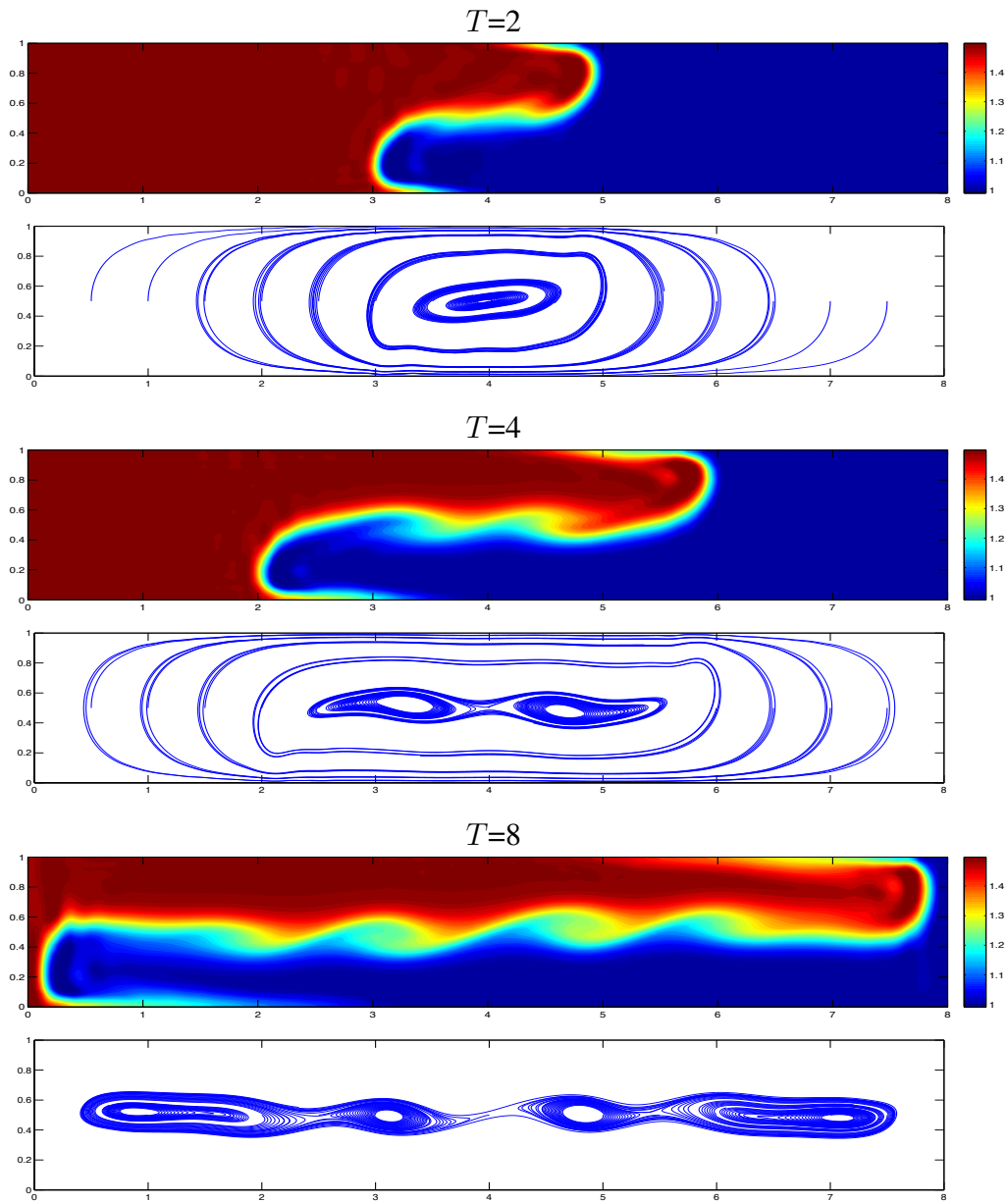


Figure 2.6: Coarse mesh model solutions for temperature contours and velocity streamlines for the  $Re=1,000$ ,  $Ri=4$ ,  $Pr = 1$  Marsigli flow test with  $T = 2, 4$ , and 8.



## CHAPTER 3

### NUMERICAL ANALYSIS OF MHD IN ELSÄSSER VARIABLES

We consider an efficient and accurate numerical approximation of magnetohydrodynamic (MHD) flow. Recall from Section 1.1.4.2 (equations (1.76)-(1.79)), the system of governing equations for MHD in Elsässer variables, [76, 9], are given by

$$\mathbf{v}_t + \mathbf{w} \cdot \nabla \mathbf{v} - (\tilde{\mathbf{B}}_0 \cdot \nabla) \mathbf{v} + \nabla q - \frac{\nu + \nu_m}{2} \Delta \mathbf{v} - \frac{\nu - \nu_m}{2} \Delta \mathbf{w} = \mathbf{f}_1, \quad (3.1)$$

$$\nabla \cdot \mathbf{v} = 0, \quad (3.2)$$

$$\mathbf{w}_t + \mathbf{v} \cdot \nabla \mathbf{w} + (\tilde{\mathbf{B}}_0 \cdot \nabla) \mathbf{w} + \nabla r - \frac{\nu + \nu_m}{2} \Delta \mathbf{w} - \frac{\nu - \nu_m}{2} \Delta \mathbf{v} = \mathbf{f}_2, \quad (3.3)$$

$$\nabla \cdot \mathbf{w} = 0, \quad (3.4)$$

in  $(0, T] \times \Omega$ .

A fundamental difficulty in simulating of MHD flow is solving the fully coupled linear systems that arise in common discretizations of (1.41)-(1.44). It is an open problem how to decouple the equations in an unconditionally stable way (with respect to the timestep size), and usually timestepping methods that decouple the equations are prone to unstable behavior without using excessively small sizes. To confront this issue, an excellent idea was presented by Trenchea in [109]: if one rewrites the MHD system in terms of Elsässer variables, then an unconditionally stable, decoupled, timestepping algorithm can be created. In [82], the second order in time finite element method for MHD Elsässer formulation was proposed, and it is obtained that the scheme is conditionally stable, and optimal convergence. In [112], this system is studied with spectral deferred correction (SDC) method, and SDC is compared with Runge-Kutta methods and linear multistep methods based on BDFs.

However, difficulties with MHD Elsässer formulation is that the solutions  $\mathbf{v}$  and  $\mathbf{w}$

are coupled with the pressure through by the incompressibility conditions  $\nabla \cdot \boldsymbol{v} = 0$  and  $\nabla \cdot \boldsymbol{w} = 0$ , making the MHD-Elsässer formulations difficult to solve numerically. This obstacle is also shared with the NSE. In the late of 1960's, Chorin and Temam [23, 100] proposed the projection method to handle this problem for the NSE. The novelty of these methods for the NSE is to stably decouple the velocity and pressure by producing two decoupled steps. In the first step, the elliptic equation for the velocity is solved, and the predicted (mean) velocity solution independent of the div-free constraint is obtained. In the second step, this velocity solution is projected onto the div-free space, and the approximate velocity solution satisfying the Neumann boundary condition is obtained. Applying the divergence operator to the second step, one can get Poisson equation for the pressure which satisfies the homogeneous Neumann boundary condition. The efficiency of the method is obvious since it converts the saddle point problem into a linear problem, which is easier to solve than coupled schemes, and reduces the CPU time. Due to the these advantages, the classical and different forms of this method have been studied extensively. Chorin used this method with periodic boundary conditions for the NSE in [24]. The classical projection method with semi-implicit discretization for the NSE was reported in [50, 51], and semi-explicit first order discretization along with the homogeneous Neumann boundary condition in [94]. In [75], Kim and Moin applied this method for the NSE using different intermediate-velocity boundary condition. The application of the pressure-correction type of method with higher semi-explicit discretization was presented in [110]. Shen modified the scheme from [110] by using fully implicit semi discretization, and combined the method with penalty method in [95]. In addition, he applied the method with pressure stabilization in [96]. The method is applied to fully discretization for the NSE in [34], which reveals that the numerical error in the method has the same structure as in the semi-discrete case analyzed in [33].

Besides the advantages of the projection methods, they sacrifice the optimal pressure error in time, and suffer from pressure error boundary layers (see [52] ), and produces splitting error resulting from the predicted velocity due to the independence of the incompressibility constraint. In [89], Prohl proposed a new form of the method, called Chorin-Penalty method, which gives first-order pressure approximation and removes the pressure error arising close to the boundary. On the other hand, Bowers et al. studied this method with a the sparse grad-div stabilization for the NSE in [12].

The purpose of this chapter is to extend the analysis of Trenchea's algorithm [109] to a fully discrete setting, i.e. together with a finite element spatial discretization by proposing a more efficient variation of the algorithm based on projection method, and is to show that projection method is equivalent to the coupled scheme. More precisely, with the use of grad-div stabilization, our aim is to show that the approximate solutions satisfying true boundary condition of the projection method converges to the coupled scheme solutions when penalty-parameter  $\gamma \rightarrow \infty$ . By this way, the projection method ensures the coupled scheme's accuracy if it is used large penalty-parameter.

To realize these aims, this chapter is organized as follows. Section 3.1 is devoted to mathematical preliminaries necessary for the mathematical analysis while Section 3.2 to the numerical algorithm for the system (3.1)-(3.4). Section 3.3 studies the stability and converge analysis of the proposed algorithm. Section 3.4 provides two numerical experiments to show the validity of the numerical scheme and efficiency of that.

### 3.1 Mathematical Preliminaries

In this chapter, we choose the natural function spaces for our problem as

$$\begin{aligned}\mathbf{X} &:= \mathbf{H}_0^1(\Omega) = \{\mathbf{v} \in (L^2(\Omega))^d : \nabla \mathbf{v} \in L^2(\Omega)^{d \times d}, \mathbf{v} = 0 \text{ on } \partial\Omega\}, \\ Q &:= L_0^2(\Omega) = \{q \in L^2(\Omega) : \int_{\Omega} q \, dx = 0\},\end{aligned}$$

and

$$\mathbf{Y} := \{\mathbf{v} \in \mathbf{H}^1(\Omega) : \mathbf{v} \cdot \mathbf{n} = 0 \text{ on } \partial\Omega\},$$

where  $\mathbf{n}$  denote the outward unit normal vector normal to the boundary  $\partial\Omega$ . The space of weakly-divergence free functions is given by

$$\mathbf{V} := \{\mathbf{v} \in \mathbf{X} : \nabla \cdot \mathbf{v} = 0\}.$$

Let  $\mathbf{X}_h \subset \mathbf{X}$ ,  $Q_h \subset Q$  denote conforming velocity, pressure finite element spaces based on an edge to edge triangulations of  $\Omega$  with maximum triangle diameter  $h$ . The velocity-pressure FEM spaces  $(\mathbf{X}_h, Q_h)$  are assumed to satisfy the usual discrete inf-sup condition (2.13) for stability of the discrete pressure, and the approximation

properties typical of piecewise polynomials of degree  $(k, k - 1)$ , (2.14)-(2.15)

$$\inf_{\mathbf{v}_h \in \mathbf{X}_h} \{ \|\mathbf{u} - \mathbf{v}_h\| + h \|\nabla(\mathbf{u} - \mathbf{v}_h)\| \} \leq Ch^{k+1} |\mathbf{u}|_{k+1}, \quad \mathbf{u} \in \mathbf{H}^{k+1}(\Omega), \quad (3.5)$$

$$\inf_{q_h \in Q_h} \|p - q_h\| \leq Ch^k |p|_k, \quad p \in H^k(\Omega). \quad (3.6)$$

The discretely divergence free subspace of  $\mathbf{X}_h$  is

$$\mathbf{V}_h := \{ \mathbf{v}_h \in \mathbf{X}_h : (\nabla \cdot \mathbf{v}_h, q_h) = 0, \text{ for all } q_h \in Q_h \}.$$

To help simplify a very technical analysis, we choose the Scott-Vogelius finite element pairs  $(\mathbf{X}_h, Q_h) = (\mathbf{P}_k, P_{k-1}^{disc})$  to approximate velocity-pressure spaces, which are known to fulfill inf-sup condition under certain restrictions on the mesh and polynomial degree, e.g. [3, 91, 114, 113]. However, our analysis can be extended without difficulty (but with more terms) to any inf-sup stable element choice. With the use of Scott-Vogelius finite element pairs,  $\mathbf{V}_h$  is conforming to  $\mathbf{V}$ , i.e.,  $\mathbf{V}_h \subset \mathbf{V}$  and the functions in  $\mathbf{V}_h$  are divergence-free pointwise, and there is no need to use the skew-symmetric trilinear form for the non-linear terms in (3.1)-(3.3). Because of the splitting of equations, it is necessary to define an additional velocity space:

$$\mathbf{Y}_h = (P_k)^d \cap (H_0^{div}(\Omega))^d.$$

where

$$(H_0^{div}(\Omega))^d := \{ \mathbf{u} \in \mathbf{L}^2(\Omega)^d : \nabla \cdot \mathbf{u} \in L^2(\Omega), \mathbf{u} \cdot \mathbf{n} = 0 \text{ on } \partial\Omega \}.$$

The only difference between  $\mathbf{Y}_h$  and  $\mathbf{X}_h$  is simply that the boundary condition of  $\mathbf{Y}_h$  is only enforced in the normal direction, while for  $\mathbf{X}_h$  it is enforced in all directions. Let  $\mathbf{R}_h \subset \mathbf{X}_h$  be the orthogonal complement of the  $\mathbf{V}_h$  according to the  $\mathbf{H}^1$ -norm. The following lemma gives the equivalence of the divergence and gradient norms in the space  $\mathbf{R}_h$ , which is proven in [46] in a very general setting, and a simpler proof for the case of Scott-Vogelius elements is given in [83].

**Lemma 3.1.1** *Let  $(\mathbf{X}_h, Q_h) \subset (X, Q)$  be finite element pairs satisfying the inf-sup condition (2.13) and the divergence-free property, i.e.,  $\nabla \cdot \mathbf{X}_h \subset Q_h$ . Then there exists a constant  $C_R$  independent of  $h$  such that*

$$\|\nabla \mathbf{v}_h\| \leq C_R \|\nabla \cdot \mathbf{v}_h\|, \quad \forall \mathbf{v}_h \in \mathbf{R}_h.$$



### 3.2 Numerical Scheme

In this section, we propose a variation of Algorithm 3.3.2 that uses a penalty-projection method for each decoupled problem. This is typically more efficient, as the linear systems that arise are much easier to solve:

#### Algorithm 3.2.1 (Grad-div stabilized penalty projection scheme)

Let time step  $\Delta t > 0$  and end time  $T > 0$  be given. Set  $M = T/\Delta t$ , and start with  $\tilde{\mathbf{v}}^0 = \mathbf{v}(0)$ ,  $\tilde{\mathbf{w}}^0 = \mathbf{w}(0) \in \mathbf{H}^2 \cup \mathbf{V}$ . For all  $n = 0, 1, \dots, M - 1$ , compute  $\hat{\mathbf{v}}_h^{n+1}$ ,  $\hat{\mathbf{w}}_h^{n+1}$ ,  $\hat{p}_h^{n+1}$ ,  $\hat{q}_h^{n+1}$  via:

**Step 1:** Find  $\hat{\mathbf{v}}_h^{n+1} \in \mathbf{X}_h$  satisfying for all  $\boldsymbol{\chi}_h \in \mathbf{X}_h$ ,

$$\begin{aligned} \left( \frac{\hat{\mathbf{v}}_h^{n+1} - \tilde{\mathbf{v}}_h^n}{\Delta t}, \boldsymbol{\chi}_h \right) + b^*(\hat{\mathbf{w}}_h^n, \hat{\mathbf{v}}_h^{n+1}, \boldsymbol{\chi}_h) - (\tilde{\mathbf{B}}_0(t^{n+1}) \cdot \nabla \hat{\mathbf{v}}_h^{n+1}, \boldsymbol{\chi}_h) \\ + \frac{\nu + \nu_m}{2} (\nabla \hat{\mathbf{v}}_h^{n+1}, \nabla \boldsymbol{\chi}_h) + \frac{\nu - \nu_m}{2} (\nabla \hat{\mathbf{w}}_h^n, \nabla \boldsymbol{\chi}_h) \\ + \gamma (\nabla \cdot \hat{\mathbf{v}}_h^{n+1}, \nabla \cdot \boldsymbol{\chi}_h) = (\mathbf{f}_1(t^{n+1}), \boldsymbol{\chi}_h). \end{aligned} \quad (3.7)$$

**Step 2:** Find  $(\tilde{\mathbf{v}}_h^{n+1}, \hat{q}_h^{n+1}) \in (\mathbf{Y}_h \times Q_h)$  satisfying for all  $(\mathbf{v}_h, q_h) \in (\mathbf{Y}_h \times Q_h)$ ,

$$\left( \frac{\tilde{\mathbf{v}}_h^{n+1} - \hat{\mathbf{v}}_h^{n+1}}{\Delta t}, \mathbf{v}_h \right) - (\hat{q}_h^{n+1}, \nabla \cdot \mathbf{v}_h) = 0, \quad (3.8)$$

$$(\nabla \cdot \tilde{\mathbf{v}}_h^{n+1}, q_h) = 0. \quad (3.9)$$

**Step 3:** Compute  $\hat{\mathbf{w}}_h^{n+1} \in \mathbf{X}_h$  for all  $\mathbf{l}_h \in \mathbf{X}_h$ ,

$$\begin{aligned} \left( \frac{\hat{\mathbf{w}}_h^{n+1} - \tilde{\mathbf{w}}_h^n}{\Delta t}, \mathbf{l}_h \right) + b^*(\hat{\mathbf{v}}_h^n, \hat{\mathbf{w}}_h^{n+1}, \mathbf{l}_h) + (\tilde{\mathbf{B}}_0(t^{n+1}) \cdot \nabla \hat{\mathbf{w}}_h^{n+1}, \mathbf{l}_h) \\ + \frac{\nu + \nu_m}{2} (\nabla \hat{\mathbf{w}}_h^{n+1}, \nabla \mathbf{l}_h) + \frac{\nu - \nu_m}{2} (\nabla \hat{\mathbf{v}}_h^n, \nabla \mathbf{l}_h) \\ + \gamma (\nabla \cdot \hat{\mathbf{w}}_h^{n+1}, \nabla \cdot \mathbf{l}_h) = (\mathbf{f}_2(t^{n+1}), \mathbf{l}_h). \end{aligned} \quad (3.10)$$

**Step 4:** Find  $(\tilde{\mathbf{w}}_h^{n+1}, \hat{\lambda}_h^{n+1}) \in (\mathbf{Y}_h \times Q_h)$  satisfying for all  $(\mathbf{s}_h, r_h) \in (\mathbf{Y}_h \times Q_h)$ ,

$$\left( \frac{\tilde{\mathbf{w}}_h^{n+1} - \hat{\mathbf{w}}_h^{n+1}}{\Delta t}, \mathbf{s}_h \right) - (\hat{\lambda}_h^{n+1}, \nabla \cdot \mathbf{s}_h) = 0, \quad (3.11)$$

$$(\nabla \cdot \tilde{\mathbf{w}}_h^{n+1}, r_h) = 0. \quad (3.12)$$

Note that  $\mathbf{X}_h \subset \mathbf{Y}_h$ . This enables us choosing  $\mathbf{v}_h = \boldsymbol{\chi}_h$  in (3.8),  $\mathbf{s}_h = \mathbf{l}_h$  in (3.11) and combining these with equations (3.7) and (3.10), respectively, yields

$$\begin{aligned} & \left( \frac{\hat{\mathbf{v}}_h^{n+1} - \hat{\mathbf{v}}_h^n}{\Delta t}, \boldsymbol{\chi}_h \right) + b^*(\hat{\mathbf{w}}_h^n, \hat{\mathbf{v}}_h^{n+1}, \boldsymbol{\chi}_h) - (\tilde{\mathbf{B}}_0(t^{n+1}) \cdot \nabla \hat{\mathbf{v}}_h^{n+1}, \boldsymbol{\chi}_h) \\ & + \frac{\nu + \nu_m}{2} (\nabla \hat{\mathbf{v}}_h^{n+1}, \nabla \boldsymbol{\chi}_h) + \frac{\nu - \nu_m}{2} (\nabla \hat{\mathbf{w}}_h^n, \nabla \boldsymbol{\chi}_h) + \gamma (\nabla \cdot \hat{\mathbf{v}}_h^{n+1}, \nabla \cdot \boldsymbol{\chi}_h) \\ & - (\hat{q}_h^n, \nabla \cdot \boldsymbol{\chi}_h) = (\mathbf{f}_1(t^{n+1}), \boldsymbol{\chi}_h), \quad (3.13) \end{aligned}$$

$$\begin{aligned} & \left( \frac{\hat{\mathbf{w}}_h^{n+1} - \hat{\mathbf{w}}_h^n}{\Delta t}, \mathbf{l}_h \right) + b^*(\hat{\mathbf{v}}_h^n, \hat{\mathbf{w}}_h^{n+1}, \mathbf{l}_h) + (\tilde{\mathbf{B}}_0(t^{n+1}) \cdot \nabla \hat{\mathbf{w}}_h^{n+1}, \mathbf{l}_h) \\ & + \frac{\nu + \nu_m}{2} (\nabla \hat{\mathbf{w}}_h^{n+1}, \nabla \mathbf{l}_h) + \frac{\nu - \nu_m}{2} (\nabla \hat{\mathbf{v}}_h^n, \nabla \mathbf{l}_h) + \gamma (\nabla \cdot \hat{\mathbf{w}}_h^{n+1}, \nabla \cdot \mathbf{l}_h) \\ & - (\hat{\lambda}_h^n, \nabla \cdot \mathbf{l}_h) = (\mathbf{f}_2(t^{n+1}), \mathbf{l}_h), \quad (3.14) \end{aligned}$$

for all  $\boldsymbol{\chi}_h \in \mathbf{X}_h$  and  $\mathbf{l}_h \in \mathbf{X}_h$ .

### 3.3 Stability and Convergence Analysis

We first prove unconditional stability of the grad-div stabilized penalty projection scheme. However, accuracy in projection type methods is often an issue, but we prove in Section 3.3.1 that the penalty-projection scheme gives the same solution as Algorithm 3.3.2 as  $\gamma \rightarrow \infty$ .

#### Lemma 3.3.1 (Unconditional Stability of Algorithm 3.2.1)

Assume  $\mathbf{f}_1, \mathbf{f}_2 \in L^\infty(0, T, \mathbf{H}^{-1}(\Omega))$  and let  $(\hat{\mathbf{v}}_h^{n+1}, \hat{\mathbf{w}}_h^{n+1}, \hat{q}_h^{n+1}, \hat{\lambda}_h^{n+1})$  be the discrete solutions of Algorithm 3.2.1. For all  $\Delta t > 0$ , we have the following bound:

$$\begin{aligned} & \|\hat{\mathbf{v}}_h^M\|^2 + \|\hat{\mathbf{w}}_h^M\|^2 + \frac{(\nu - \nu_m)^2}{2(\nu + \nu_m)} \Delta t (\|\nabla \hat{\mathbf{v}}_h^M\|^2 + \|\nabla \hat{\mathbf{w}}_h^M\|^2) \\ & + \frac{\nu \nu_m}{\nu + \nu_m} \Delta t \sum_{n=0}^{M-1} (\|\nabla \hat{\mathbf{v}}_h^{n+1}\|^2 + \|\nabla \hat{\mathbf{w}}_h^{n+1}\|^2) \\ & + \Delta t \sum_{n=0}^{M-1} \gamma (\|\nabla \cdot \hat{\mathbf{v}}_h^{n+1}\|^2 + \|\nabla \cdot \hat{\mathbf{w}}_h^{n+1}\|^2) \\ & \leq \|\hat{\mathbf{v}}_h^0\|^2 + \|\hat{\mathbf{w}}_h^0\|^2 + \frac{(\nu - \nu_m)^2}{2(\nu + \nu_m)} \Delta t (\|\nabla \hat{\mathbf{v}}_h^0\|^2 + \|\nabla \hat{\mathbf{w}}_h^0\|^2) \\ & + \frac{\nu + \nu_m}{\nu \nu_m} \Delta t \sum_{n=0}^{M-1} (\|\mathbf{f}_1(t^{n+1})\|_{-1}^2 + \|\mathbf{f}_2(t^{n+1})\|_{-1}^2). \quad (3.15) \end{aligned}$$

**Proof:** Taking  $\chi_h = \hat{\mathbf{v}}_h^{n+1}$  in (3.7) and  $\mathbf{l}_h = \hat{\mathbf{w}}_h^{n+1}$  in (3.10) with the polarization identity, we get

$$\begin{aligned} \frac{1}{2\Delta t} (\|\hat{\mathbf{v}}_h^{n+1}\|^2 - \|\tilde{\mathbf{v}}_h^n\|^2 + \|\hat{\mathbf{v}}_h^{n+1} - \tilde{\mathbf{v}}_h^n\|^2) + \frac{\nu + \nu_m}{2} \|\nabla \hat{\mathbf{v}}_h^{n+1}\|^2 + \gamma \|\nabla \cdot \hat{\mathbf{v}}_h^{n+1}\|^2 \\ = -\frac{\nu - \nu_m}{2} (\nabla \hat{\mathbf{w}}_h^n, \nabla \hat{\mathbf{v}}_h^{n+1}) + (\mathbf{f}_1(t^{n+1}), \hat{\mathbf{v}}_h^{n+1}), \end{aligned} \quad (3.16)$$

and

$$\begin{aligned} \frac{1}{2\Delta t} (\|\hat{\mathbf{w}}_h^{n+1}\|^2 - \|\tilde{\mathbf{w}}_h^n\|^2 + \|\hat{\mathbf{w}}_h^{n+1} - \tilde{\mathbf{w}}_h^n\|^2) + \frac{\nu + \nu_m}{2} \|\nabla \hat{\mathbf{w}}_h^{n+1}\|^2 + \gamma \|\nabla \cdot \hat{\mathbf{w}}_h^{n+1}\|^2 \\ = -\frac{\nu - \nu_m}{2} (\nabla \hat{\mathbf{v}}_h^n, \nabla \hat{\mathbf{w}}_h^{n+1}) + (\mathbf{f}_2(t^{n+1}), \hat{\mathbf{w}}_h^{n+1}). \end{aligned} \quad (3.17)$$

Applying the Cauchy-Schwarz and the Young's inequalities on the right hand sides terms of (3.16) and (3.17) gives

$$\begin{aligned} \frac{|\nu - \nu_m|}{2} |(\nabla \hat{\mathbf{w}}_h^n, \nabla \hat{\mathbf{v}}_h^{n+1})| &\leq \frac{|\nu - \nu_m|}{2} \|\nabla \hat{\mathbf{w}}_h^n\| \|\nabla \hat{\mathbf{v}}_h^{n+1}\| \\ &\leq \frac{\nu + \nu_m}{4} \|\nabla \hat{\mathbf{v}}_h^{n+1}\|^2 + \frac{(\nu - \nu_m)^2}{4(\nu + \nu_m)} \|\nabla \hat{\mathbf{w}}_h^n\|^2, \\ |(\mathbf{f}_1(t^{n+1}), \hat{\mathbf{v}}_h^{n+1})| &\leq \|\mathbf{f}_1(t^{n+1})\|_{-1} \|\nabla \hat{\mathbf{v}}_h^{n+1}\| \\ &\leq \frac{\nu \nu_m}{2(\nu + \nu_m)} \|\nabla \hat{\mathbf{v}}_h^{n+1}\|^2 + \frac{(\nu + \nu_m)}{2(\nu \nu_m)} \|\mathbf{f}_1(t^{n+1})\|_{-1}^2, \\ \frac{|\nu - \nu_m|}{2} |(\nabla \hat{\mathbf{v}}_h^n, \nabla \hat{\mathbf{w}}_h^{n+1})| &\leq \frac{|\nu - \nu_m|}{2} \|\nabla \hat{\mathbf{v}}_h^n\| \|\nabla \hat{\mathbf{w}}_h^{n+1}\| \\ &\leq \frac{\nu + \nu_m}{4} \|\nabla \hat{\mathbf{w}}_h^{n+1}\|^2 + \frac{(\nu - \nu_m)^2}{4(\nu + \nu_m)} \|\nabla \hat{\mathbf{v}}_h^n\|^2, \\ |(\mathbf{f}_2(t^{n+1}), \hat{\mathbf{w}}_h^{n+1})| &\leq \|\mathbf{f}_2(t^{n+1})\|_{-1} \|\nabla \hat{\mathbf{w}}_h^{n+1}\| \\ &\leq \frac{\nu \nu_m}{2(\nu + \nu_m)} \|\nabla \hat{\mathbf{w}}_h^{n+1}\|^2 + \frac{(\nu + \nu_m)}{2(\nu \nu_m)} \|\mathbf{f}_2(t^{n+1})\|_{-1}^2. \end{aligned}$$

Plugging these estimates into (3.16) and (3.17), respectively, and dropping the non-negative left hand side terms yields

$$\begin{aligned} \frac{1}{2\Delta t} (\|\hat{\mathbf{v}}_h^{n+1}\|^2 - \|\tilde{\mathbf{v}}_h^n\|^2) + \frac{\nu + \nu_m}{4} \|\nabla \hat{\mathbf{v}}_h^{n+1}\|^2 + \gamma \|\nabla \cdot \hat{\mathbf{v}}_h^{n+1}\|^2 \\ \leq \frac{(\nu - \nu_m)^2}{4(\nu + \nu_m)} \|\nabla \hat{\mathbf{w}}_h^n\|^2 + \frac{(\nu + \nu_m)}{2(\nu \nu_m)} \|\mathbf{f}_1(t^{n+1})\|_{-1}^2, \end{aligned} \quad (3.18)$$

and

$$\begin{aligned} \frac{1}{2\Delta t} (\|\hat{\mathbf{w}}_h^{n+1}\|^2 - \|\tilde{\mathbf{w}}_h^n\|^2) + \frac{\nu + \nu_m}{4} \|\nabla \hat{\mathbf{w}}_h^{n+1}\|^2 + \gamma \|\nabla \cdot \hat{\mathbf{w}}_h^{n+1}\|^2 \\ \leq \frac{(\nu - \nu_m)^2}{4(\nu + \nu_m)} \|\nabla \hat{\mathbf{v}}_h^n\|^2 + \frac{(\nu + \nu_m)}{2(\nu \nu_m)} \|\mathbf{f}_2(t^{n+1})\|_{-1}^2. \end{aligned} \quad (3.19)$$

Now choose  $\mathbf{v}_h = \tilde{\mathbf{v}}_h^{n+1}$  in (3.8),  $q_h = \hat{q}_h^{n+1}$  in (3.9) and  $\mathbf{s}_h = \tilde{\mathbf{w}}_h^{n+1}$  in (3.11),  $r_h = \hat{\lambda}_h^{n+1}$  in (3.12). Then apply the Cauchy-Schwarz and the Young's inequalities to obtain

$$\|\tilde{\mathbf{v}}_h^{n+1}\|^2 \leq \|\hat{\mathbf{v}}_h^{n+1}\|^2, \quad \forall n = 0, 1, \dots, M-1 \quad (3.20)$$

$$\|\tilde{\mathbf{w}}_h^{n+1}\|^2 \leq \|\hat{\mathbf{w}}_h^{n+1}\|^2, \quad \forall n = 0, 1, \dots, M-1. \quad (3.21)$$

and use (3.20) in (3.18) and (3.21) in (3.19) to produce

$$\begin{aligned} & \frac{1}{2\Delta t} (\|\hat{\mathbf{v}}_h^{n+1}\|^2 - \|\hat{\mathbf{v}}_h^n\|^2) + \frac{(\nu - \nu_m)^2}{4(\nu + \nu_m)} \|\nabla \hat{\mathbf{v}}_h^{n+1}\|^2 + \frac{\nu\nu_m}{2(\nu + \nu_m)} \|\nabla \hat{\mathbf{v}}_h^{n+1}\|^2 \\ & + \gamma \|\nabla \cdot \hat{\mathbf{v}}_h^{n+1}\|^2 \leq \frac{(\nu - \nu_m)^2}{4(\nu + \nu_m)} \|\nabla \hat{\mathbf{w}}_h^n\|^2 + \frac{\nu + \nu_m}{2\nu\nu_m} \|\mathbf{f}_1(t^{n+1})\|_{-1}^2, \end{aligned} \quad (3.22)$$

and

$$\begin{aligned} & \frac{1}{2\Delta t} (\|\hat{\mathbf{w}}_h^{n+1}\|^2 - \|\hat{\mathbf{w}}_h^n\|^2) + \frac{(\nu - \nu_m)^2}{4(\nu + \nu_m)} \|\nabla \hat{\mathbf{w}}_h^{n+1}\|^2 + \frac{\nu\nu_m}{2(\nu + \nu_m)} \|\nabla \hat{\mathbf{w}}_h^{n+1}\|^2 \\ & + \gamma \|\nabla \cdot \hat{\mathbf{w}}_h^{n+1}\|^2 \leq \frac{(\nu - \nu_m)^2}{4(\nu + \nu_m)} \|\nabla \hat{\mathbf{v}}_h^n\|^2 + \frac{\nu + \nu_m}{2\nu\nu_m} \|\mathbf{f}_2(t^{n+1})\|_{-1}^2. \end{aligned} \quad (3.23)$$

Adding these two equations, multiplying by  $2\Delta t$  and summing over time steps finishes the proof.  $\square$

### 3.3.1 Convergence Analysis

In this section, we prove that approximate solutions of Algorithm 3.2.1 converge to the solutions of the fully coupled scheme as the penalty parameter  $\gamma \rightarrow \infty$ , which is given below:

#### Algorithm 3.3.2 (Fully Coupled Scheme)

Let time step  $\Delta t > 0$  and end time  $T > 0$  be given. Set  $M = T/\Delta t$  and start with  $\mathbf{v}_h^0 = \mathbf{v}(0)$ ,  $\mathbf{w}_h^0 = \mathbf{w}(0) \in \mathbf{H}^2 \cup \mathbf{V}$ . For all  $n = 0, 1, \dots, M-1$ , compute  $(\mathbf{v}_h^{n+1}, \mathbf{w}_h^{n+1}) \in \mathbf{V}_h \times \mathbf{V}_h$  satisfying for all  $(\boldsymbol{\chi}_h, \mathbf{l}_h) \in \mathbf{V}_h \times \mathbf{V}_h$ ,

$$\begin{aligned} & \left( \frac{\mathbf{v}_h^{n+1} - \mathbf{v}_h^n}{\Delta t}, \boldsymbol{\chi}_h \right) + (\mathbf{w}_h^n \cdot \nabla \mathbf{v}_h^{n+1}, \boldsymbol{\chi}_h) - (\tilde{\mathbf{B}}_0(t^{n+1}) \cdot \nabla \mathbf{v}_h^{n+1}, \boldsymbol{\chi}_h) \\ & + \frac{\nu + \nu_m}{2} (\nabla \mathbf{v}_h^{n+1}, \nabla \boldsymbol{\chi}_h) + \frac{\nu - \nu_m}{2} (\nabla \mathbf{w}_h^n, \nabla \boldsymbol{\chi}_h) = (\mathbf{f}_1(t^{n+1}), \boldsymbol{\chi}_h), \end{aligned} \quad (3.24)$$

and

$$\begin{aligned} & \left( \frac{\mathbf{w}_h^{n+1} - \mathbf{w}_h^n}{\Delta t}, \mathbf{l}_h \right) + (\mathbf{v}_h^n \cdot \nabla \mathbf{w}_h^{n+1}, \mathbf{l}_h) + (\tilde{\mathbf{B}}_0(t^{n+1}) \cdot \nabla \mathbf{w}_h^{n+1}, \mathbf{l}_h) \\ & + \frac{\nu + \nu_m}{2} (\nabla \mathbf{w}_h^{n+1}, \nabla \mathbf{l}_h) + \frac{\nu - \nu_m}{2} (\nabla \mathbf{v}_h^n, \nabla \mathbf{l}_h) = (\mathbf{f}_2(t^{n+1}), \mathbf{l}_h). \end{aligned} \quad (3.25)$$

Even though this scheme is decoupled into 2 sub-problems, it is unconditionally stable with respect to a given timestep size  $\Delta t$ , and it converges optimally both in space and in time under the smoothness assumptions of the true solutions (3.26), which are given by Lemma 3.3.3 and Theorem 3.3.4 ( see for the proof [2] ).

**Lemma 3.3.3 (Unconditional Stability of Algorithm 3.3.2)**

Suppose  $\mathbf{f}_1, \mathbf{f}_2 \in L^\infty(0, T; \mathbf{H}^{-1}(\Omega))$ ,  $\mathbf{v}_h^0, \mathbf{w}_h^0 \in \mathbf{H}^1(\Omega)$ . Then for any  $\Delta t > 0$ , solutions to (3.24)-(3.25) satisfy

$$\begin{aligned} & \|\mathbf{v}_h^M\|^2 + \|\mathbf{w}_h^M\|^2 + \frac{(\nu - \nu_m)^2}{2(\nu + \nu_m)} \Delta t (\|\nabla \mathbf{v}_h^M\|^2 + \|\nabla \mathbf{w}_h^M\|^2) \\ & + \frac{\nu \nu_m}{\nu + \nu_m} \Delta t \sum_{n=0}^{M-1} (\|\nabla \mathbf{v}_h^{n+1}\|^2 + \|\nabla \mathbf{w}_h^{n+1}\|^2) \\ & \leq \|\mathbf{v}_h^0\|^2 + \|\mathbf{w}_h^0\|^2 + \frac{(\nu - \nu_m)^2}{2(\nu + \nu_m)} (\|\nabla \mathbf{v}_h^0\|^2 + \|\nabla \mathbf{w}_h^0\|^2) \\ & + \frac{\nu + \nu_m}{\nu \nu_m} \Delta t \sum_{n=0}^{M-1} (\|\mathbf{f}_1(t^{n+1})\|_{-1}^2 + \|\mathbf{f}_2(t^{n+1})\|_{-1}^2). \end{aligned}$$

**Theorem 3.3.4** Assume  $(\mathbf{v}, \mathbf{w}, p)$  solves (3.1)-(3.4) and satisfying

$$\begin{aligned} & \mathbf{v}, \mathbf{w} \in L^\infty(0, T; \mathbf{H}^m(\Omega)), \quad m = \max\{2, k + 1\}, \\ & \mathbf{v}_t, \mathbf{w}_t \in L^\infty(0, T; \mathbf{H}^{k+1}(\Omega)), \\ & \mathbf{v}_{tt}, \mathbf{w}_{tt} \in L^\infty(0, T; \mathbf{L}^2(\Omega)). \end{aligned} \quad (3.26)$$

Then the solution  $(\mathbf{v}_h, \mathbf{w}_h)$  to Algorithm 3.3.2 converges to the true solution: for any  $\Delta t > 0$ ,

$$\begin{aligned} & \|\mathbf{v}(T) - \mathbf{v}_h^M\| + \|\mathbf{w}(T) - \mathbf{w}_h^M\| + \frac{\nu^2 + \nu_m^2}{4(\nu + \nu_m)} \Delta t (\|\nabla(\mathbf{v}(T) - \mathbf{v}_h^M)\| + \|\nabla(\mathbf{w}(T) - \mathbf{w}_h^M)\|) \\ & + \frac{\nu \nu_m}{2(\nu + \nu_m)} \left\{ \Delta t \sum_{n=1}^{M-1} (\|\nabla(\mathbf{v}(t^n) - \mathbf{v}_h^n)\|^2 + \|\nabla(\mathbf{w}(t^n) - \mathbf{w}_h^n)\|^2) \right\}^{\frac{1}{2}} \leq C(h^k + \Delta t). \end{aligned} \quad (3.27)$$

Before we prove the convergence of Algorithm 3.2.1 to Algorithm 3.3.2 as  $\gamma \rightarrow \infty$ , we state the following assumptions for the discrete solutions of these algorithms, which are essential for our convergence analysis.

**Assumption 3.3.5** Assume that there exists a constant  $C_*$  which is independent of  $h, \Delta t$  and  $\gamma$ , such that for sufficiently small  $h$  and  $\Delta t$ , the solutions of Algorithm 3.3.2 and Algorithm 3.2.1 satisfy

$$\begin{aligned} \max_{1 \leq n \leq M} (\|\nabla \mathbf{v}_h^n\|_{L^3} + \|\nabla \mathbf{w}_h^n\|_{L^3} + \|\mathbf{v}_h^n\|_\infty + \|\mathbf{w}_h^n\|_\infty) &\leq C_*, \\ \max_{1 \leq n \leq M} (\|\nabla \hat{\mathbf{v}}_h^n\| + \|\nabla \hat{\mathbf{w}}_h^n\|) &\leq C_*. \end{aligned}$$

**Theorem 3.3.6** Let  $(\mathbf{v}_h^{n+1}, \mathbf{w}_h^{n+1}, q_h^{n+1})$  and  $(\hat{\mathbf{v}}_h^{n+1}, \hat{\mathbf{w}}_h^{n+1}, \hat{q}_h^{n+1})$  be solutions of the Algorithm 3.3.2 and Algorithm 3.2.1, respectively, for  $n = 0, 1, 2, \dots, M-1$ . We then have the following:

$$\begin{aligned} &\left( \Delta t \sum_{n=0}^{M-1} (\|\nabla(\mathbf{v}_h^{n+1} - \hat{\mathbf{v}}_h^{n+1})\|^2 + \|\nabla(\mathbf{w}_h^{n+1} - \hat{\mathbf{w}}_h^{n+1})\|^2) \right)^{1/2} \\ &\leq \gamma^{-1} C \max\left\{ C_* \left( \frac{\nu + \nu_m}{\nu \nu_m} \right)^{1/2}, (\Delta t)^{-1/2} \right\} \\ &\quad \times \left( \Delta t \sum_{n=0}^{M-1} (\|q_h^{n+1} - \hat{q}_h^n\|^2 + \|\lambda_h^{n+1} - \hat{\lambda}_h^n\|^2) \right)^{1/2}. \end{aligned}$$

**Remark 3.3.7** The theorem shows that on a fixed mesh and timestep, penalty-projection solutions have first order convergence to the Algorithm 3.3.2 solution as  $\gamma \rightarrow \infty$ . This shows that for large penalty parameters, we can use the penalty-projection method and get the same accuracy as Algorithm 3.3.2.

**Proof:** Denote  $\mathbf{e}^{n+1} := \mathbf{v}_h^{n+1} - \hat{\mathbf{v}}_h^{n+1}$  and  $\boldsymbol{\epsilon}^{n+1} := \mathbf{w}_h^{n+1} - \hat{\mathbf{w}}_h^{n+1}$  and decompose the errors orthogonally as follows:

$$\mathbf{e}^{n+1} := \mathbf{e}_0^{n+1} + \mathbf{e}_R^{n+1}, \quad \boldsymbol{\epsilon}^{n+1} := \boldsymbol{\epsilon}_0^{n+1} + \boldsymbol{\epsilon}_R^{n+1}$$

with  $\mathbf{e}_0^{n+1}, \boldsymbol{\epsilon}_0^{n+1} \in \mathbf{V}_h$  and  $\mathbf{e}_R^{n+1}, \boldsymbol{\epsilon}_R^{n+1} \in \mathbf{R}_h, n = 0, 1, \dots, M-1$ .

**Step 1:** Estimate of  $\mathbf{e}_R^{n+1}, \boldsymbol{\epsilon}_R^{n+1}$ :

Subtracting the equation (3.24), (3.25) from (3.13) and (3.14) produces

$$\begin{aligned} & \frac{1}{\Delta t} \left( (\mathbf{v}_h^{n+1} - \hat{\mathbf{v}}_h^{n+1}) - (\mathbf{v}_h^n - \hat{\mathbf{v}}_h^n), \boldsymbol{\chi}_h \right) + \frac{\nu + \nu_m}{2} (\nabla(\mathbf{v}_h^{n+1} - \hat{\mathbf{v}}_h^{n+1}), \nabla \boldsymbol{\chi}_h) \\ & + \gamma (\nabla \cdot (\mathbf{v}_h^{n+1} - \hat{\mathbf{v}}_h^{n+1}), \nabla \cdot \boldsymbol{\chi}_h) + \frac{\nu + \nu_m}{2} (\nabla(\mathbf{w}_h^n - \hat{\mathbf{w}}_h^n), \nabla \boldsymbol{\chi}_h) + b^*(\mathbf{w}_h^n, \mathbf{v}_h^{n+1}, \boldsymbol{\chi}_h) \\ & - b^*(\hat{\mathbf{w}}_h^n, \hat{\mathbf{v}}_h^{n+1}, \boldsymbol{\chi}_h) - (\mathbf{B}_0(\tilde{t}^{n+1}) \cdot \nabla(\mathbf{v}_h^{n+1} - \hat{\mathbf{v}}_h^{n+1}), \boldsymbol{\chi}_h) - (q_h^{n+1} - \hat{q}_h^n, \nabla \cdot \boldsymbol{\chi}_h) = 0, \end{aligned} \quad (3.28)$$

and

$$\begin{aligned} & \frac{1}{\Delta t} \left( (\mathbf{w}_h^{n+1} - \hat{\mathbf{w}}_h^{n+1}) - (\mathbf{w}_h^n - \hat{\mathbf{w}}_h^n), \mathbf{l}_h \right) + \frac{\nu + \nu_m}{2} (\nabla(\mathbf{w}_h^{n+1} - \hat{\mathbf{w}}_h^{n+1}), \nabla \mathbf{l}_h) \\ & + \gamma (\nabla \cdot (\mathbf{w}_h^{n+1} - \hat{\mathbf{w}}_h^{n+1}), \nabla \cdot \mathbf{l}_h) + \frac{\nu + \nu_m}{2} (\nabla(\mathbf{v}_h^n - \hat{\mathbf{v}}_h^n), \nabla \mathbf{l}_h) + b^*(\mathbf{v}_h^n, \mathbf{w}_h^{n+1}, \mathbf{l}_h) \\ & - b^*(\hat{\mathbf{v}}_h^n, \hat{\mathbf{w}}_h^{n+1}, \mathbf{l}_h) - (\mathbf{B}_0(\tilde{t}^{n+1}) \cdot \nabla(\mathbf{w}_h^{n+1} - \hat{\mathbf{w}}_h^{n+1}), \mathbf{l}_h) - (\lambda_h^{n+1} - \hat{\lambda}_h^n, \nabla \cdot \mathbf{l}_h) = 0, \end{aligned} \quad (3.29)$$

for all  $(\boldsymbol{\chi}_h, \mathbf{l}_h) \in (\mathbf{X}_h, Q_h)$ . Now rewrite the non-linear terms as follows:

$$\begin{aligned} & b^*(\mathbf{w}_h^n, \mathbf{v}_h^{n+1}, \boldsymbol{\chi}_h) - b^*(\hat{\mathbf{w}}_h^n, \hat{\mathbf{v}}_h^{n+1}, \boldsymbol{\chi}_h) = b^*(\mathbf{w}_h^n - \hat{\mathbf{w}}_h^n, \mathbf{v}_h^{n+1}, \boldsymbol{\chi}_h) \\ & \quad + b^*(\mathbf{w}_h^n, \mathbf{v}_h^{n+1} - \hat{\mathbf{v}}_h^{n+1}, \boldsymbol{\chi}_h) \\ & b^*(\mathbf{v}_h^n, \mathbf{w}_h^{n+1}, \mathbf{l}_h) - b^*(\hat{\mathbf{v}}_h^n, \hat{\mathbf{w}}_h^{n+1}, \mathbf{l}_h) = b^*(\mathbf{v}_h^n - \hat{\mathbf{v}}_h^n, \mathbf{w}_h^{n+1}, \mathbf{l}_h) + b^*(\mathbf{v}_h^n, \mathbf{w}_h^{n+1} - \hat{\mathbf{w}}_h^{n+1}, \mathbf{l}_h). \end{aligned}$$

Then equations (3.28) and (3.29) becomes

$$\begin{aligned} & \frac{1}{\Delta t} \left( \boldsymbol{\epsilon}^{n+1} - \boldsymbol{\epsilon}^n, \boldsymbol{\chi}_h \right) + \frac{\nu + \nu_m}{2} (\nabla \boldsymbol{\epsilon}^{n+1}, \nabla \boldsymbol{\chi}_h) + \gamma (\nabla \cdot \boldsymbol{\epsilon}_R^{n+1}, \nabla \cdot \boldsymbol{\chi}_h) \\ & \quad + \frac{\nu - \nu_m}{2} (\nabla \boldsymbol{\epsilon}^n, \nabla \boldsymbol{\chi}_h) - (\tilde{\mathbf{B}}_0(t^{n+1}) \cdot \nabla \boldsymbol{\epsilon}^{n+1}, \boldsymbol{\chi}_h) + b^*(\boldsymbol{\epsilon}^n, \mathbf{v}_h^{n+1}, \boldsymbol{\chi}_h) \\ & \quad + b^*(\hat{\mathbf{w}}_h^n, \boldsymbol{\epsilon}^{n+1}, \boldsymbol{\chi}_h) - (q_h^{n+1} - \hat{q}_h^n, \nabla \cdot \boldsymbol{\chi}_h) = 0, \end{aligned} \quad (3.30)$$

and

$$\begin{aligned} & \frac{1}{\Delta t} \left( \boldsymbol{\epsilon}^{n+1} - \boldsymbol{\epsilon}^n, \mathbf{l}_h \right) + \frac{\nu + \nu_m}{2} (\nabla \boldsymbol{\epsilon}^{n+1}, \nabla \mathbf{l}_h) + \gamma (\nabla \cdot \boldsymbol{\epsilon}_R^{n+1}, \nabla \cdot \mathbf{l}_h) \\ & \quad + \frac{\nu - \nu_m}{2} (\nabla \boldsymbol{\epsilon}^n, \nabla \mathbf{l}_h) + (\tilde{\mathbf{B}}_0(t^{n+1}) \cdot \nabla \boldsymbol{\epsilon}^{n+1}, \mathbf{l}_h) + b^*(\boldsymbol{\epsilon}^n, \mathbf{w}_h^{n+1}, \mathbf{l}_h) \\ & \quad + b^*(\hat{\mathbf{v}}_h^n, \boldsymbol{\epsilon}^{n+1}, \mathbf{l}_h) - (\lambda_h^{n+1} - \hat{\lambda}_h^n, \nabla \cdot \mathbf{l}_h) = 0. \end{aligned} \quad (3.31)$$

Taking  $\boldsymbol{\chi}_h = \boldsymbol{\epsilon}^{n+1}$  in (3.30),  $\mathbf{l}_h = \boldsymbol{\epsilon}^{n+1}$  in (3.31), which kills the non-linear terms

$$\begin{aligned} & b^*(\hat{\mathbf{w}}_h^n, \boldsymbol{\epsilon}^{n+1}, \boldsymbol{\epsilon}^{n+1}) = 0, \quad b^*(\hat{\mathbf{v}}_h^n, \boldsymbol{\epsilon}^{n+1}, \boldsymbol{\epsilon}^{n+1}) = 0, \\ & (\tilde{\mathbf{B}}_0(t^{n+1}) \cdot \nabla \boldsymbol{\epsilon}^{n+1}, \boldsymbol{\epsilon}^{n+1}) = 0, \quad (\tilde{\mathbf{B}}_0(t^{n+1}) \cdot \nabla \boldsymbol{\epsilon}^{n+1}, \boldsymbol{\epsilon}^{n+1}) = 0, \end{aligned}$$

and using the polarization identity yields

$$\begin{aligned} & \frac{1}{2\Delta t} \left( \|e^{n+1}\|^2 - \|e^n\|^2 + \|e^{n+1} - e^n\|^2 \right) + \frac{\nu + \nu_m}{2} \|\nabla e^{n+1}\|^2 + \gamma \|\nabla \cdot e_R^{n+1}\|^2 \\ &= -\frac{\nu - \nu_m}{2} (\nabla e^n, \nabla e^{n+1}) + (q_h^{n+1} - \hat{q}_h^n, \nabla \cdot e_R^{n+1}) - b^*(e^n, v_h^{n+1}, e^{n+1}), \end{aligned} \quad (3.32)$$

$$\begin{aligned} & \frac{1}{2\Delta t} \left( \|e^{n+1}\|^2 - \|e^n\|^2 + \|e^{n+1} - e^n\|^2 \right) + \frac{\nu + \nu_m}{2} \|\nabla e^{n+1}\|^2 + \gamma \|\nabla \cdot e_R^{n+1}\|^2 \\ &= -\frac{\nu - \nu_m}{2} (\nabla e^n, \nabla e^{n+1}) + (\lambda_h^{n+1} - \hat{\lambda}_h^n, \nabla \cdot e_R^{n+1}) - b^*(e^n, w_h^{n+1}, e^{n+1}). \end{aligned} \quad (3.33)$$

Applying the Cauchy-Schwarz and the Young's inequalities to the first two terms of (3.32) and (3.33) provides

$$\frac{|\nu - \nu_m|}{2} |(\nabla e^n, \nabla e^{n+1})| \leq \frac{(\nu - \nu_m)^2}{4(\nu + \nu_m)} \|\nabla e^n\|^2 + \frac{\nu + \nu_m}{4} \|\nabla e^{n+1}\|^2, \quad (3.34)$$

$$|(q_h^{n+1} - \hat{q}_h^n, \nabla \cdot e_R^{n+1})| \leq \frac{\gamma^{-1}}{2} \|q_h^{n+1} - \hat{q}_h^n\|^2 + \frac{\gamma}{2} \|\nabla \cdot e_R^{n+1}\|^2, \quad (3.35)$$

$$\frac{|\nu - \nu_m|}{2} |(\nabla e^n, \nabla e^{n+1})| \leq \frac{(\nu - \nu_m)^2}{4(\nu + \nu_m)} \|\nabla e^n\|^2 + \frac{\nu + \nu_m}{4} \|\nabla e^{n+1}\|^2, \quad (3.36)$$

$$|(\lambda_h^{n+1} - \hat{\lambda}_h^n, \nabla \cdot e_R^{n+1})| \leq \frac{\gamma^{-1}}{2} \|\lambda_h^{n+1} - \hat{\lambda}_h^n\|^2 + \frac{\gamma}{2} \|\nabla \cdot e_R^{n+1}\|^2. \quad (3.37)$$

To bound the non-linear terms, use Hölder's, Sobolev embedding theorem between  $L^6(\Omega)$  and  $H^1(\Omega)$ , i.e  $L^6(\Omega) \hookrightarrow H^1(\Omega)$ , the Poincaré-Friedrichs', and the Young's inequalities along with Assumption 4.1 to get

$$\begin{aligned} |b^*(e^n, v_h^{n+1}, e^{n+1})| &= \frac{1}{2} \left| \left( (e^n \cdot \nabla v_h^{n+1}, e^{n+1}) + (e^n \cdot \nabla e_h^{n+1}, v_h^{n+1}) \right) \right| \\ &\leq C \left( \|e^n\| \|\nabla v_h^{n+1}\|_{L^3} \|\nabla e^{n+1}\| + \|e^n\| \|v_h^{n+1}\|_{L^\infty} \|\nabla e^{n+1}\| \right) \\ &\leq C \left( \|e^n\| \|\nabla v_h^{n+1}\|_{L^3} \|\nabla e^{n+1}\| + \|e^n\| \|v_h^{n+1}\|_{L^\infty} \|\nabla e^{n+1}\| \right) \\ &\leq CC_* \|e^n\| \|\nabla e^{n+1}\| \\ &\leq \frac{\nu \nu_m}{2(\nu + \nu_m)} \|\nabla e^{n+1}\|^2 + \frac{CC_*^2(\nu + \nu_m)}{\nu \nu_m} \|e^n\|^2, \end{aligned} \quad (3.38)$$



and

$$\begin{aligned}
|b^*(\mathbf{e}^n, \mathbf{w}_h^{n+1}, \boldsymbol{\epsilon}^{n+1})| &= \frac{1}{2} \left| \left( \mathbf{e}^n \cdot \nabla \mathbf{w}_h^{n+1}, \boldsymbol{\epsilon}^{n+1} \right) + \left( \mathbf{e}^n \cdot \nabla \boldsymbol{\epsilon}_h^{n+1}, \mathbf{w}_h^{n+1} \right) \right| \\
&\leq C \left( \|\mathbf{e}^n\| \|\nabla \mathbf{w}_h^{n+1}\|_{L^3} \|\nabla \boldsymbol{\epsilon}^{n+1}\| + \|\mathbf{e}^n\| \|\mathbf{w}_h^{n+1}\|_{L^\infty} \|\nabla \boldsymbol{\epsilon}^{n+1}\| \right) \\
&\leq C \left( \|\mathbf{e}^n\| \|\nabla \mathbf{w}_h^{n+1}\|_{L^3} \|\nabla \boldsymbol{\epsilon}^{n+1}\| + \|\mathbf{e}^n\| \|\mathbf{w}_h^{n+1}\|_{L^\infty} \|\nabla \boldsymbol{\epsilon}^{n+1}\| \right) \\
&\leq CC_* \|\mathbf{e}^n\| \|\nabla \boldsymbol{\epsilon}^{n+1}\| \\
&\leq \frac{\nu \nu_m}{2(\nu + \nu_m)} \|\nabla \boldsymbol{\epsilon}^{n+1}\|^2 + \frac{CC_*^2(\nu + \nu_m)}{\nu \nu_m} \|\mathbf{e}^n\|^2. \tag{3.39}
\end{aligned}$$

First substitute estimates (3.34), (3.35) and (3.38) in (3.32), next drop the non-negative term  $\|\mathbf{e}^{n+1} - \mathbf{e}^n\|^2$ , and add the term  $\frac{\nu \nu_m}{2(\nu + \nu_m)} \|\nabla \boldsymbol{\epsilon}^{n+1}\|^2$  to both side of the resulting inequality. Then (3.32) becomes

$$\begin{aligned}
&\frac{1}{2\Delta t} (\|\mathbf{e}^{n+1}\|^2 - \|\mathbf{e}^n\|^2) + \frac{(\nu - \nu_m)^2}{4(\nu + \nu_m)} \|\nabla \mathbf{e}^{n+1}\|^2 + \frac{\nu \nu_m}{2(\nu + \nu_m)} \|\nabla \mathbf{e}^{n+1}\|^2 \\
&+ \frac{\gamma}{2} \|\nabla \cdot \mathbf{e}_R^{n+1}\|^2 \leq \frac{(\nu - \nu_m)^2}{4(\nu + \nu_m)} \|\nabla \mathbf{e}^n\|^2 + \frac{CC_*^2(\nu + \nu_m)}{\nu \nu_m} \|\boldsymbol{\epsilon}^n\|^2 + \frac{\gamma^{-1}}{2} \|q_h^{n+1} - \hat{q}_h^n\|^2. \tag{3.40}
\end{aligned}$$

Similarly, plugg (3.36), (3.37) and (3.39) into (3.33), add the term  $\frac{\nu \nu_m}{2(\nu + \nu_m)} \|\nabla \boldsymbol{\epsilon}^{n+1}\|^2$  to both sides of the resulting inequality. Then dropping the non-negative term  $\|\boldsymbol{\epsilon}^{n+1} - \boldsymbol{\epsilon}^n\|^2$  provides

$$\begin{aligned}
&\frac{1}{2\Delta t} (\|\boldsymbol{\epsilon}^{n+1}\|^2 - \|\boldsymbol{\epsilon}^n\|^2) + \frac{(\nu - \nu_m)^2}{4(\nu + \nu_m)} \|\nabla \boldsymbol{\epsilon}^{n+1}\|^2 + \frac{\nu \nu_m}{2(\nu + \nu_m)} \|\nabla \boldsymbol{\epsilon}^{n+1}\|^2 + \frac{\gamma}{2} \|\nabla \cdot \boldsymbol{\epsilon}_R^{n+1}\|^2 \\
&\leq \frac{(\nu - \nu_m)^2}{4(\nu + \nu_m)} \|\nabla \boldsymbol{\epsilon}^n\|^2 + \frac{CC_*^2(\nu + \nu_m)}{\nu \nu_m} \|\boldsymbol{\epsilon}^n\|^2 + \frac{\gamma^{-1}}{2} \|\lambda_h^{n+1} - \hat{\lambda}_h^n\|^2. \tag{3.41}
\end{aligned}$$

Now add the equations (3.40) and (3.41), multiply by  $2\Delta t$  and sum over time steps to obtain

$$\begin{aligned}
&\|\mathbf{e}^M\|^2 + \|\boldsymbol{\epsilon}^M\|^2 + \frac{(\nu - \nu_m)^2}{2(\nu + \nu_m)} \Delta t \left( \|\nabla \mathbf{e}^M\|^2 + \|\nabla \boldsymbol{\epsilon}^M\|^2 \right) \\
&+ \frac{\nu \nu_m}{\nu + \nu_m} \Delta t \sum_{n=0}^{M-1} (\|\nabla \mathbf{e}^{n+1}\|^2 + \|\nabla \boldsymbol{\epsilon}^{n+1}\|^2) + \Delta t \sum_{n=0}^{M-1} \gamma (\|\nabla \cdot \mathbf{e}_R^{n+1}\|^2 + \|\nabla \cdot \boldsymbol{\epsilon}_R^{n+1}\|^2) \\
&\leq \Delta t \sum_{n=0}^{M-1} \frac{CC_*^2(\nu + \nu_m)}{\nu \nu_m} (\|\mathbf{e}^n\|^2 + \|\boldsymbol{\epsilon}^n\|^2) \\
&\quad + \Delta t \sum_{n=0}^{M-1} \gamma^{-1} \left( \|q_h^{n+1} - \hat{q}_h^n\|^2 + \|\lambda_h^{n+1} - \hat{\lambda}_h^n\|^2 \right),
\end{aligned}$$

and apply discrete Gronwall Lemma to get

$$LHS \leq \gamma^{-1} \exp \left( CC_*^2 \frac{(\nu + \nu_m)}{\nu \nu_m} \right) \left( \Delta t \sum_{n=0}^{M-1} (\|q_h^{n+1} - \hat{q}_h^n\|^2 + \|\lambda_h^{n+1} - \hat{\lambda}_h^n\|^2) \right). \quad (3.42)$$

Using Lemma 3.1.1 with (3.42) yields the following desired bound:

$$\begin{aligned} & \Delta t \sum_{n=0}^{M-1} (\|\nabla e_R^{n+1}\|^2 + \|\nabla \epsilon_R^{n+1}\|^2) \\ & \leq C_R^2 \left( \Delta t \sum_{n=0}^{M-1} (\|\nabla \cdot e_R^{n+1}\|^2 + \|\nabla \cdot \epsilon_R^{n+1}\|^2) \right) \\ & \leq \gamma^{-2} C_R^2 \exp \left( CC_*^2 \frac{(\nu + \nu_m)}{\nu \nu_m} \right) \left( \Delta t \sum_{n=0}^{M-1} (\|q_h^{n+1} - \hat{q}_h^n\|^2 + \|\lambda_h^{n+1} - \hat{\lambda}_h^n\|^2) \right). \end{aligned} \quad (3.43)$$

**Step 2: Estimates of  $e_0^{n+1}, \epsilon_0^{n+1}$  :**

To find a bound on  $\left( \Delta t \sum_{n=0}^{M-1} (\|\nabla e_0^{n+1}\|^2 + \|\nabla \epsilon_0^{n+1}\|^2) \right)$ , we begin with choosing  $\chi_h = e_0^{n+1}$  in (3.30). This yields

$$\gamma (\nabla \cdot e_R^{n+1}, \nabla \cdot e_0^{n+1}) = 0, \quad (q_h^{n+1} - \hat{q}_h^n, \nabla \cdot e_0^{n+1}) = 0,$$

since  $e_0^{n+1} \in \mathbf{V}_h$ . In addition, by the orthogonal decomposition of  $\mathbf{H}^1(\Omega)$ , the orthogonal error decomposition and by the definition of the skew-symmetric trilinear form, one can obtain

$$\begin{aligned} (\nabla e^{n+1}, \nabla e_0^{n+1}) &= (\nabla e_R^{n+1}, \nabla e_0^{n+1}) + (\nabla e_0^{n+1}, \nabla e_0^{n+1}), \\ b^*(\hat{\mathbf{w}}_h^n, e^{n+1}, e_0^{n+1}) &= b^*(\hat{\mathbf{w}}_h^n, e_R^{n+1}, e_0^{n+1}) + b^*(\hat{\mathbf{w}}_h^n, e_0^{n+1}, e_0^{n+1}) \\ &= b^*(\hat{\mathbf{w}}_h^n, e_R^{n+1}, e_0^{n+1}). \end{aligned}$$

Therefore, equation (3.30) reduces to

$$\begin{aligned} & \frac{1}{\Delta t} (e^{n+1} - e^n, e_0^{n+1}) + \frac{\nu + \nu_m}{2} \|\nabla e_0^{n+1}\|^2 = -\frac{\nu - \nu_m}{2} (\nabla \epsilon_0^n, \nabla e_0^{n+1}) \\ & + (\tilde{\mathbf{B}}_0(t^{n+1}) \cdot \nabla e_R^{n+1}, e_0^{n+1}) - b^*(\epsilon^n, \mathbf{v}_h^{n+1}, e_0^{n+1}) - b^*(\hat{\mathbf{w}}_h^n, e_R^{n+1}, e_0^{n+1}), \end{aligned} \quad (3.44)$$

Similarly, taking  $\mathbf{l}_h = \epsilon_0^{n+1}$  in (3.31) yields

$$\begin{aligned} & \frac{1}{\Delta t} (\epsilon^{n+1} - \epsilon^n, \epsilon_0^{n+1}) + \frac{\nu + \nu_m}{2} \|\nabla \epsilon_0^{n+1}\|^2 = -\frac{\nu - \nu_m}{2} (\nabla e_0^n, \nabla \epsilon_0^{n+1}) \\ & + (\tilde{\mathbf{B}}_0(t^{n+1}) \cdot \nabla \epsilon_R^{n+1}, \epsilon_0^{n+1}) - b^*(e^n, \mathbf{w}_h^{n+1}, \epsilon_0^{n+1}) - b^*(\hat{\mathbf{v}}_h^n, \epsilon_R^{n+1}, \epsilon_0^{n+1}). \end{aligned} \quad (3.45)$$

Applying the Cauchy-Schwarz and the Hölder's inequalities with (2.25) on the right hand side terms of (3.44) and (3.45) gives

$$\begin{aligned}
& \frac{1}{\Delta t}(\mathbf{e}^{n+1} - \mathbf{e}^n, \mathbf{e}_0^{n+1}) + \frac{\nu + \nu_m}{2} \|\nabla \mathbf{e}_0^{n+1}\|^2 \\
& \leq \frac{|\nu - \nu_m|}{2} \|\nabla \boldsymbol{\epsilon}_0^n\| \|\nabla \mathbf{e}_0^{n+1}\| + C \|\tilde{\mathbf{B}}_0(t^{n+1})\|_\infty \|\nabla \mathbf{e}_R^{n+1}\| \|\mathbf{e}_0^{n+1}\| \\
& \quad + |b^*(\boldsymbol{\epsilon}^n, \mathbf{v}_h^{n+1}, \mathbf{e}_0^{n+1})| + C \|\nabla \hat{\mathbf{w}}_h^n\| \|\nabla \mathbf{e}_R^{n+1}\| \|\nabla \mathbf{e}_0^{n+1}\|, \quad (3.46)
\end{aligned}$$

$$\begin{aligned}
& \frac{1}{\Delta t}(\boldsymbol{\epsilon}^{n+1} - \boldsymbol{\epsilon}^n, \boldsymbol{\epsilon}_0^{n+1}) + \frac{\nu + \nu_m}{2} \|\nabla \boldsymbol{\epsilon}_0^{n+1}\|^2 \\
& \leq \frac{|\nu - \nu_m|}{2} \|\nabla \mathbf{e}_0^n\| \|\nabla \boldsymbol{\epsilon}_0^{n+1}\| + C \|\tilde{\mathbf{B}}_0(t^{n+1})\|_\infty \|\nabla \boldsymbol{\epsilon}_R^{n+1}\| \|\boldsymbol{\epsilon}_0^{n+1}\| \\
& \quad + |b^*(\boldsymbol{\epsilon}^n, \mathbf{w}_h^{n+1}, \boldsymbol{\epsilon}_0^{n+1})| + C \|\nabla \hat{\mathbf{v}}_h^n\| \|\nabla \boldsymbol{\epsilon}_R^{n+1}\| \|\nabla \boldsymbol{\epsilon}_0^{n+1}\|. \quad (3.47)
\end{aligned}$$

To bound the non-linear terms in (3.46) and (3.47), first use the definition of the skew-symmetric trilinear form, next apply the Cauchy-Schwarz and the Hölder inequalities. Then use the Sobolev embedding theorem between  $\mathbf{L}^6(\Omega)$  and  $\mathbf{H}^1(\Omega)$ , i.e  $\mathbf{L}^6(\Omega) \hookrightarrow \mathbf{H}^1(\Omega)$ , and the Assumption 3.3.5 to get

$$\begin{aligned}
|b^*(\boldsymbol{\epsilon}^n, \mathbf{v}_h^{n+1}, \mathbf{e}_0^{n+1})| &= \frac{1}{2} \left| \left( \boldsymbol{\epsilon}^n \cdot \nabla \mathbf{v}_h^{n+1}, \mathbf{e}_0^{n+1} \right) - \left( \mathbf{e}^n \cdot \nabla \mathbf{e}_0^{n+1}, \mathbf{v}_h^{n+1} \right) \right| \\
&\leq C \left( \|\boldsymbol{\epsilon}^n\| \|\nabla \mathbf{v}_h^{n+1}\|_{\mathbf{L}^3} \|\mathbf{e}_0^{n+1}\| + \|\boldsymbol{\epsilon}^n\| \|\nabla \mathbf{v}_h^{n+1}\|_{\mathbf{L}^\infty} \|\nabla \mathbf{e}_0^{n+1}\| \right) \\
&\leq C \left( \|\boldsymbol{\epsilon}^n\| \|\nabla \mathbf{v}_h^{n+1}\|_{\mathbf{L}^3} \|\nabla \mathbf{e}_0^{n+1}\| + \|\boldsymbol{\epsilon}^n\| \|\nabla \mathbf{v}_h^{n+1}\|_{\mathbf{L}^\infty} \|\nabla \mathbf{e}_0^{n+1}\| \right) \\
&\leq CC^* \|\boldsymbol{\epsilon}^n\| \|\nabla \mathbf{e}_0^{n+1}\|, \quad (3.48)
\end{aligned}$$

and

$$\begin{aligned}
|b^*(\boldsymbol{\epsilon}^n, \mathbf{w}_h^{n+1}, \boldsymbol{\epsilon}_0^{n+1})| &= \frac{1}{2} \left| \left( \boldsymbol{\epsilon}^n \cdot \nabla \mathbf{w}_h^{n+1}, \boldsymbol{\epsilon}_0^{n+1} \right) - \left( \mathbf{e}^n \cdot \nabla \boldsymbol{\epsilon}_0^{n+1}, \mathbf{w}_h^{n+1} \right) \right| \\
&\leq C \left( \|\boldsymbol{\epsilon}^n\| \|\nabla \mathbf{w}_h^{n+1}\|_{\mathbf{L}^3} \|\boldsymbol{\epsilon}_0^{n+1}\|_{\mathbf{L}^6} + \|\boldsymbol{\epsilon}^n\| \|\mathbf{w}_h^{n+1}\|_{\mathbf{L}^\infty} \|\nabla \boldsymbol{\epsilon}_0^{n+1}\| \right) \\
&\leq C \left( \|\boldsymbol{\epsilon}^n\| \|\nabla \mathbf{w}_h^{n+1}\|_{\mathbf{L}^3} \|\nabla \boldsymbol{\epsilon}_0^{n+1}\| + \|\boldsymbol{\epsilon}^n\| \|\mathbf{w}_h^{n+1}\|_{\mathbf{L}^\infty} \|\nabla \boldsymbol{\epsilon}_0^{n+1}\| \right) \\
&\leq CC^* \|\boldsymbol{\epsilon}^n\| \|\nabla \boldsymbol{\epsilon}_0^{n+1}\|. \quad (3.49)
\end{aligned}$$

Now first use the Poincaré-Friedrichs' inequality along with the Assumption 3.3.5 on the second and third right hand side terms of (3.46) and (3.47), respectively. Next,

plug the bounds (3.48) and (3.49) to obtain

$$\begin{aligned}
& \frac{1}{\Delta t}(\mathbf{e}^{n+1} - \mathbf{e}^n, \mathbf{e}_0^{n+1}) + \frac{\nu + \nu_m}{2} \|\nabla \mathbf{e}_0^{n+1}\|^2 \\
& \leq \frac{|\nu - \nu_m|}{2} \|\nabla \boldsymbol{\epsilon}_0^n\| \|\nabla \mathbf{e}_0^{n+1}\| + CC_{PF}^2 C^* \|\nabla \mathbf{e}_R^{n+1}\| \|\nabla \mathbf{e}_0^{n+1}\| \\
& \quad + CC^* \|\boldsymbol{\epsilon}^n\| \|\nabla \mathbf{e}_0^{n+1}\| + C \|\nabla \hat{\mathbf{w}}_h^n\| \|\nabla \mathbf{e}_R^{n+1}\| \|\nabla \mathbf{e}_0^{n+1}\|, \quad (3.50)
\end{aligned}$$

and

$$\begin{aligned}
& \frac{1}{\Delta t}(\boldsymbol{\epsilon}^{n+1} - \boldsymbol{\epsilon}^n, \boldsymbol{\epsilon}_0^{n+1}) + \frac{\nu + \nu_m}{2} \|\nabla \boldsymbol{\epsilon}_0^{n+1}\|^2 \\
& \leq \frac{|\nu - \nu_m|}{2} \|\nabla \mathbf{e}_0^n\| \|\nabla \boldsymbol{\epsilon}_0^{n+1}\| + CC_{PF}^2 C^* \|\nabla \boldsymbol{\epsilon}_R^{n+1}\| \|\nabla \boldsymbol{\epsilon}_0^{n+1}\| \\
& \quad + CC^* \|\mathbf{e}^n\| \|\nabla \boldsymbol{\epsilon}_0^{n+1}\| + C \|\nabla \hat{\boldsymbol{\theta}}_h^n\| \|\nabla \boldsymbol{\epsilon}_R^{n+1}\| \|\nabla \boldsymbol{\epsilon}_0^{n+1}\|. \quad (3.51)
\end{aligned}$$

Applying the Young's inequality with appropriate  $\varepsilon$  on the right hand side terms of (3.50) and (3.51) produces

$$\begin{aligned}
& \frac{1}{\Delta t}(\mathbf{e}^{n+1} - \mathbf{e}^n, \mathbf{e}_0^{n+1}) + \frac{\nu + \nu_m}{2} \|\nabla \mathbf{e}_0^{n+1}\|^2 \leq \frac{(\nu - \nu_m)^2}{4(\nu + \nu_m)} \|\nabla \boldsymbol{\epsilon}_0^n\|^2 + \frac{\nu + \nu_m}{4} \|\nabla \mathbf{e}_0^{n+1}\|^2, \\
& \quad + \frac{\nu \nu_m}{2(\nu + \nu_m)} \|\nabla \mathbf{e}_0^{n+1}\|^2 + CC_*^2 \frac{\nu + \nu_m}{\nu \nu_m} (\|\mathbf{e}^n\|^2 + \|\nabla \mathbf{e}_R^{n+1}\|^2) \quad (3.52)
\end{aligned}$$

and

$$\begin{aligned}
& \frac{1}{\Delta t}(\boldsymbol{\epsilon}^{n+1} - \boldsymbol{\epsilon}^n, \boldsymbol{\epsilon}_0^{n+1}) + \frac{\nu + \nu_m}{2} \|\nabla \boldsymbol{\epsilon}_0^{n+1}\|^2 \leq \frac{(\nu - \nu_m)^2}{4(\nu + \nu_m)} \|\nabla \mathbf{e}_0^n\|^2 \\
& + \frac{\nu + \nu_m}{4} \|\nabla \boldsymbol{\epsilon}_0^{n+1}\|^2 + \frac{\nu \nu_m}{2(\nu + \nu_m)} \|\nabla \boldsymbol{\epsilon}_0^{n+1}\|^2 + CC_*^2 \frac{\nu + \nu_m}{\nu \nu_m} (\|\mathbf{e}^n\|^2 + \|\nabla \boldsymbol{\epsilon}_R^{n+1}\|^2). \quad (3.53)
\end{aligned}$$

To evaluate the time derivative in (3.52), add and subtract the term  $\mathbf{e}_R^{n+1}$ , and use the polarization identity. Then applying the Cauchy-Schwarz, the Young's and the Poincaré-Friedrichs' inequalities gives us the following bound :

$$\begin{aligned}
& \frac{1}{\Delta t}(\mathbf{e}^{n+1} - \mathbf{e}^n, \mathbf{e}_0^{n+1}) = \frac{1}{\Delta t}(\mathbf{e}^{n+1} - \mathbf{e}^n, \mathbf{e}^{n+1}) - \frac{1}{\Delta t}(\mathbf{e}^{n+1} - \mathbf{e}^n, \mathbf{e}_R^{n+1}) \\
& \geq \frac{1}{2\Delta t} (\|\mathbf{e}^{n+1}\|^2 - \|\mathbf{e}^n\|^2) + \frac{1}{2\Delta t} \|\mathbf{e}^{n+1} - \mathbf{e}^n\|^2 - \frac{1}{\Delta t} (\mathbf{e}^{n+1} - \mathbf{e}^n, \mathbf{e}_R^{n+1}) \\
& \geq \frac{1}{2\Delta t} (\|\mathbf{e}^{n+1}\|^2 - \|\mathbf{e}^n\|^2) - \frac{1}{2\Delta t} \|\mathbf{e}_R^{n+1}\|^2 \\
& \geq \frac{1}{2\Delta t} (\|\mathbf{e}^{n+1}\|^2 - \|\mathbf{e}^n\|^2) - \frac{C}{2\Delta t} \|\nabla \mathbf{e}_R^{n+1}\|^2.
\end{aligned}$$

Similarly, the time derivative in (3.53) becomes

$$\begin{aligned}
\frac{1}{\Delta t}(\boldsymbol{\epsilon}^{n+1} - \boldsymbol{\epsilon}^n, \boldsymbol{\epsilon}_0^{n+1}) &= \frac{1}{\Delta t}(\boldsymbol{\epsilon}^{n+1} - \boldsymbol{\epsilon}^n, \boldsymbol{\epsilon}^{n+1}) - \frac{1}{\Delta t}(\boldsymbol{\epsilon}^{n+1} - \boldsymbol{\epsilon}^n, \boldsymbol{\epsilon}_R^{n+1}) \\
&\geq \frac{1}{2\Delta t}(\|\boldsymbol{\epsilon}^{n+1}\|^2 - \|\boldsymbol{\epsilon}^n\|^2) + \frac{1}{2\Delta t}\|\boldsymbol{\epsilon}^{n+1} - \boldsymbol{\epsilon}^n\|^2 - \frac{1}{\Delta t}(\boldsymbol{\epsilon}^{n+1} - \boldsymbol{\epsilon}^n, \boldsymbol{\epsilon}_R^{n+1}) \\
&\geq \frac{1}{2\Delta t}(\|\boldsymbol{\epsilon}^{n+1}\|^2 - \|\boldsymbol{\epsilon}^n\|^2) - \frac{1}{2\Delta t}\|\boldsymbol{\epsilon}_R^{n+1}\|^2 \\
&\geq \frac{1}{2\Delta t}(\|\boldsymbol{\epsilon}^{n+1}\|^2 - \|\boldsymbol{\epsilon}^n\|^2) - \frac{C}{2\Delta t}\|\nabla\boldsymbol{\epsilon}_R^{n+1}\|^2.
\end{aligned}$$

Plugging time derivative estimates into (3.52), and (3.53) with adding and subtracting the terms  $\frac{\nu\nu_m}{2(\nu+\nu_m)}\|\nabla\boldsymbol{e}_0^{n+1}\|^2$  and  $\frac{\nu\nu_m}{2(\nu+\nu_m)}\|\nabla\boldsymbol{\epsilon}_0^{n+1}\|^2$  to (3.52), and to (3.53), respectively results in

$$\begin{aligned}
&\frac{1}{2\Delta t}(\|\boldsymbol{e}^{n+1}\|^2 - \|\boldsymbol{e}^n\|^2) + \frac{(\nu - \nu_m)^2}{4(\nu + \nu_m)}\|\nabla\boldsymbol{e}_0^{n+1}\|^2 + \frac{\nu\nu_m}{2(\nu + \nu_m)}\|\nabla\boldsymbol{e}_0^{n+1}\|^2 \\
&\leq \frac{(\nu - \nu_m)^2}{4(\nu + \nu_m)}\|\nabla\boldsymbol{\epsilon}_0^n\|^2 + CC_*^2\frac{\nu + \nu_m}{\nu\nu_m}\|\boldsymbol{\epsilon}^n\|^2 + C\left(C_*^2\frac{\nu + \nu_m}{\nu\nu_m} + (\Delta t)^{-1}\right)\|\nabla\boldsymbol{e}_R^{n+1}\|^2,
\end{aligned} \tag{3.54}$$

and

$$\begin{aligned}
&\frac{1}{2\Delta t}(\|\boldsymbol{\epsilon}^{n+1}\|^2 - \|\boldsymbol{\epsilon}^n\|^2) + \frac{(\nu - \nu_m)^2}{4(\nu + \nu_m)}\|\nabla\boldsymbol{\epsilon}_0^{n+1}\|^2 + \frac{\nu\nu_m}{2(\nu + \nu_m)}\|\nabla\boldsymbol{\epsilon}_0^{n+1}\|^2 \\
&\leq \frac{(\nu - \nu_m)^2}{4(\nu + \nu_m)}\|\nabla\boldsymbol{e}_0^n\|^2 + CC_*^2\frac{\nu + \nu_m}{\nu\nu_m}\|\boldsymbol{e}^n\|^2 + C\left(C_*^2\frac{\nu + \nu_m}{\nu\nu_m} + (\Delta t)^{-1}\right)\|\nabla\boldsymbol{\epsilon}_R^{n+1}\|^2.
\end{aligned} \tag{3.55}$$

Adding the equations (3.54) and (3.55), multiplying both sides of the resulting inequalities by  $2\Delta t$ , summing over time steps and rearranging the terms results in

$$\begin{aligned}
&\|\boldsymbol{e}^M\|^2 + \|\boldsymbol{\epsilon}^M\|^2 + \frac{(\nu - \nu_m)^2}{2(\nu + \nu_m)}\Delta t(\|\nabla\boldsymbol{e}_0^M\|^2 + \|\nabla\boldsymbol{\epsilon}_0^M\|^2) \\
&\quad + \frac{\nu\nu_m}{(\nu + \nu_m)}\Delta t\sum_{n=0}^{M-1}(\|\nabla\boldsymbol{e}_0^{n+1}\|^2 + \|\nabla\boldsymbol{\epsilon}_0^{n+1}\|^2) \\
&\quad \leq \Delta t\sum_{n=0}^{M-1}CC_*^2\frac{(\nu + \nu_m)}{\nu\nu_m}(\|\boldsymbol{e}^n\|^2 + \|\boldsymbol{\epsilon}^n\|^2) \\
&\quad + \Delta t\sum_{n=0}^{M-1}C\left(C_*^2\frac{(\nu + \nu_m)}{\nu\nu_m} + (\Delta t)^{-1}\right)\left(\|\nabla\boldsymbol{e}_R^{n+1}\|^2 + \|\nabla\boldsymbol{\epsilon}_R^{n+1}\|^2\right).
\end{aligned}$$

Now drop the non-negative terms on the left hand side, apply Lemma 3.1.1 and the discrete Gronwall Lemma to get

$$\begin{aligned} & \|e^M\|^2 + \|\epsilon^M\|^2 + \frac{\nu\nu_m}{(\nu + \nu_m)} \Delta t \sum_{n=0}^{M-1} (\|\nabla e_0^{n+1}\|^2 + \|\nabla \epsilon_0^{n+1}\|^2) \\ & \leq \exp\left(C C_*^2 \frac{\nu + \nu_m}{\nu\nu_m}\right) C C_R^2 \left(C_*^2 \frac{\nu + \nu_m}{\nu\nu_m} + (\Delta t)^{-1}\right) \\ & \quad \times \left(\Delta t \sum_{n=0}^{M-1} (\|\nabla \cdot e_R^{n+1}\|^2 + \|\nabla \cdot \epsilon_R^{n+1}\|^2)\right), \end{aligned} \quad (3.56)$$

and then use (3.43) in (3.56), which produces

$$\begin{aligned} & \Delta t \sum_{n=0}^{M-1} (\|\nabla e_0^{n+1}\|^2 + \|\nabla \epsilon_0^{n+1}\|^2) \\ & \leq \gamma^{-2} C \left(C_*^2 \frac{\nu + \nu_m}{\nu\nu_m} + (\Delta t)^{-1}\right) \left(\Delta t \sum_{n=0}^{M-1} (\|q_h^{n+1} - \hat{q}_h^n\|^2 + \|\lambda_h^{n+1} - \hat{\lambda}_h^n\|^2)\right). \end{aligned} \quad (3.57)$$

Now first use the definitions of

$$\nabla(\mathbf{v}_h^{n+1} - \hat{\mathbf{v}}_h^{n+1}) = \mathbf{e}^{n+1}, \quad \nabla(\mathbf{w}_h^{n+1} - \hat{\mathbf{w}}_h^{n+1}) = \boldsymbol{\epsilon}^{n+1}$$

and use the orthogonal decomposition of these errors, i.e.  $\mathbf{e}^{n+1} = \mathbf{e}_0^{n+1} + \mathbf{e}_R^{n+1}$  and  $\boldsymbol{\epsilon}^{n+1} = \boldsymbol{\epsilon}_0^{n+1} + \boldsymbol{\epsilon}_R^{n+1}$ . Next apply the following inequality

$$(a + b)^2 \leq 2(a^2 + b^2), \quad \forall a, b \geq 0,$$

to the terms  $\|\nabla(\mathbf{v}_h^{n+1} - \hat{\mathbf{v}}_h^{n+1})\|^2$ ,  $\|\nabla(\mathbf{w}_h^{n+1} - \hat{\mathbf{w}}_h^{n+1})\|^2$ , and sum the resulting equations which yields

$$\begin{aligned} & \|\nabla(\mathbf{v}_h^{n+1} - \hat{\mathbf{v}}_h^{n+1})\|^2 + \|\nabla(\mathbf{w}_h^{n+1} - \hat{\mathbf{w}}_h^{n+1})\|^2 \\ & \leq 2 \left(\|\nabla e_0^{n+1}\|^2 + \|\nabla \epsilon_0^{n+1}\|^2 + \|\nabla e_R^{n+1}\|^2 + \|\nabla \epsilon_R^{n+1}\|^2\right). \end{aligned} \quad (3.58)$$

Then multiplying by  $\Delta t$ , summing over time steps, and combining the results (3.43) and (3.57) finishes the proof.  $\square$

### 3.4 Numerical Experiments

In this section, we implement two numerical experiments to test the proposed scheme and theory presented in Section 3.3.1. We first test the convergence of the grad-

div stabilized penalty projection scheme to the coupled scheme as  $\gamma \rightarrow \infty$ . We then test the proposed scheme on a test problem of channel flow over step. For all of our simulations, we choose  $(\mathbf{P}_2, P_1^{disc})$  Scott-Vogelius elements. These elements remove the effect of the (often large in MHD) pressure discretization error on the velocity/magnetic field errors.

### 3.4.1 Numerical Experiment 1: Convergence of grad-div stabilized penalty projection scheme to coupled scheme as $\gamma \rightarrow \infty$

To test the convergence in Section 3.3.1, we pick  $\nu = \nu_m = s = 1$ , and compute the errors between the solutions of Algorithm 3.2.1 and Algorithm 3.3.2 in  $H^1$ -norm with end time  $T = 1$ . We obtained that the error between these solutions goes to zero when  $\gamma \rightarrow 0$ . The results are shown in Table 3.1. In addition, Figure 3.1 shows that the penalty projection scheme solutions converge to coupled scheme solutions when  $\gamma$  goes to infinity. Furthermore, it shows that the divergence of the solutions for the penalty projection scheme converges to zero when penalty parameter  $\gamma$  goes to infinity.

Table 3.1: Shown above are differences between the penalty-projection and coupled schemes solutions for varying  $\gamma$ , and the divergence of solutions for Algorithm 3.2.1.

$\gamma$	$\ \mathbf{v}_h^N - \hat{\mathbf{v}}_h^N\ $	$\ \nabla \cdot \hat{\mathbf{v}}_h^N\ $	$\ \mathbf{w}_h^N - \hat{\mathbf{w}}_h^N\ $	$\ \nabla \cdot \hat{\mathbf{w}}_h^N\ $
0	7.593e-2	2.807e-1	7.426e-2	2.676e-1
1	5.850e-2	1.996e-1	5.665e-2	1.874e-1
10	2.024e-2	6.451e-2	1.922e-2	5.854e-2
$10^2$	5.854e-3	8.653e-3	2.582e-3	7.744e-3
$10^3$	2.836e-4	2.676e-4	2.676e-4	8.015e-4
$10^4$	2.846e-5	9.007e-5	2.686e-5	8.043e-5
$10^5$	2.845e-6	9.011e-6	2.685e-6	8.046e-6

### 3.4.2 Numerical experiment 2: MHD Channel flow with full step

In the second numerical experiment, we test Algorithm 3.2.1 on two dimensional channel flow over a forward and backward facing step (or full step) in the presence

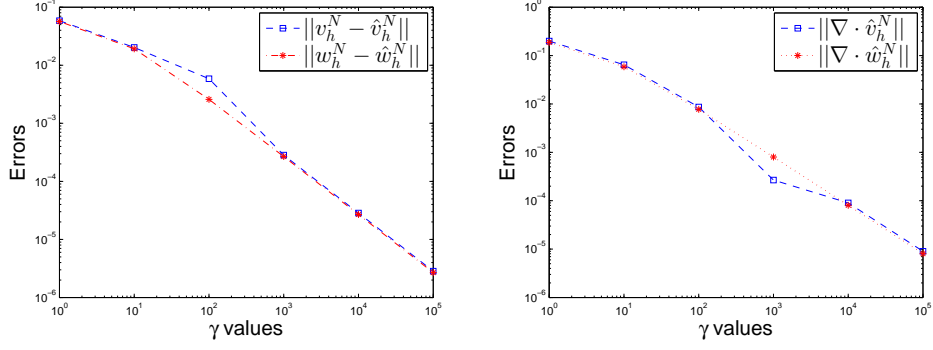


Figure 3.1: Differences between the penalty-projection and coupled schemes solutions, and the divergence of solutions for Algorithm 3.2.1 for varying  $\gamma$ .

of a magnetic field, which is similar to the NSE benchmark problem in  $2d$  considered in [54]. The true physical expectation in this numerical experiment for the NSE, when  $Re \approx 600$ , is the formation and detachment of the eddies behind the step, and movement into flow, and the formation of new eddies. In the implementation, the left boundary can be taken as the inflow of the flow and the right boundary as the outflow of the flow. In most application, the bottom boundary and the top boundary are taken as a solid wall. However, the top boundary can be taken as a boundary at which the flow is inviscid ( more information see [54]).

Channel flow is a popular, and preferable test problem since it is used for modeling in numerous industrial and engineering problems such as in the study of air pollution, cooling of electronic devices. In [38], to calculate the pressure distribution of air along the sides of greenhouses in agricultural areas, the NSE with the Galerkin finite element method and free outflow boundary condition was tested on  $2d$ -channel flow. Besides applications of this numerical experiment in industry, it is commonly used to show the effectiveness of algorithms and to test the accuracy of approximate solutions in  $2d$  or  $3d$ , which means to test whether there exists unexpected wiggles (or eddies) or not. In [78],  $2d$  channel flow is implemented to show the effectiveness of the grad-div stabilization for the NSE in the rotation form, and it is known that it gives much more worse solutions due to the requirement of the usage of Bernoulli pressure. In this work, the behavior of the NSE at  $Re = 600$  was tested and compared by using Crank-Nicholson finite element scheme in convective form, the skew-symmetric form, rotation form and the rotation form with grad-div stabilization. To model  $2d$  channel flow, a box  $[0, 40] \times [0, 10]$  is used in  $2d$ , and the top and bottom boundary of



the box was taken as a solid wall, left boundary as the inflow of the flow with parabolic velocity profile, and the right boundary as the outflow of the flow with zero-traction boundary condition (implemented as a do-nothing condition). In this numerical experiment, the value of *Reynolds number* plays an important role since eddies above or at  $Re = 600$  are shed from the step.

The behavior of the NSE in velocity-vorticity and helicity formulation, proposed in [81], was tested with 3d-full step channel, modeled by a  $[0, 10] \times [0, 40] \times [0, 10]$  rectangular box, by enforcing constant velocity profile for the inflow of the flow, which is the steady state channel flow profile at  $Re = 20$ , [64]. The main aim to use this experiment in this work is to reveal that the proposed scheme is reasonable and gives acceptable solutions. For more applications, one can see [69, 30, 8].

### 3.4.2.1 Experiment setup

In our simulation, we take

- the domain  $\Omega := 40 \times 10$  rectangle with a  $1 \times 1$  step five units into the channel at the bottom.
- initial velocity  $\mathbf{u} = \langle y(10 - y)/25, 0 \rangle^T$ , and initial induced magnetic field  $\mathbf{B} = 0$ .
- enforce
  - i) parabolic velocity profile  $\mathbf{u} = \langle y(10 - y)/25, 0 \rangle^T$  at the inflow and outflow.
  - ii) homogeneous Dirichlet velocity boundary condition at the top and bottom walls of the channel.
- impose  $\langle 0, 1 \rangle^T$  as a boundary condition for the magnetic field.
- choose  $P_2$  for velocity and magnetic field,  $P_1$  the pressure, use a mesh provided 568, 535 total degrees of freedom.

#### Remark 3.4.1

*Notice that our plots represent until  $30 \times 10$ -domain since our concern concentrates*

on the behavior of the flow behind the step.

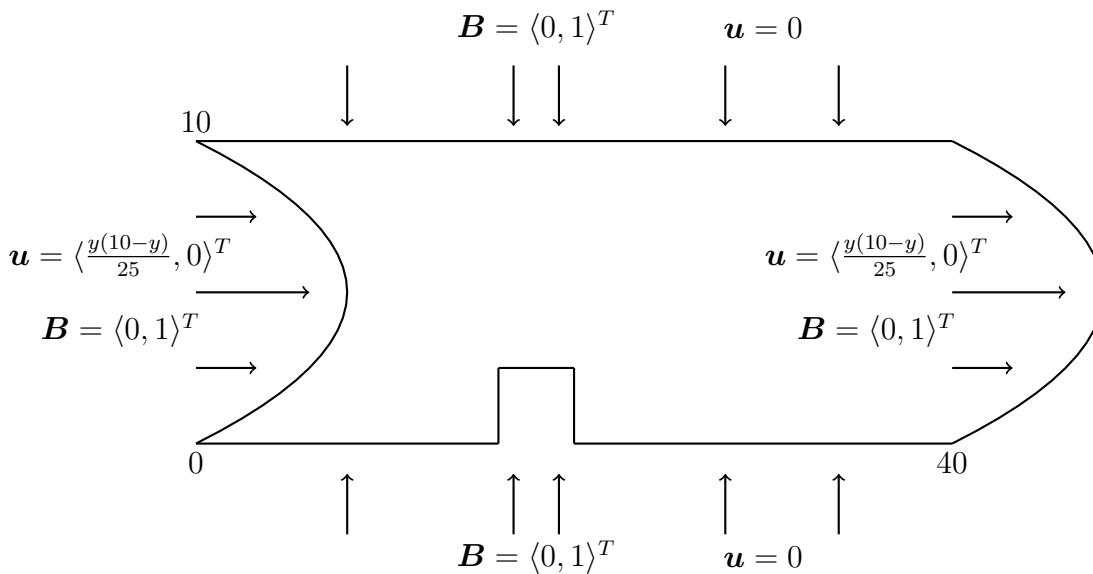


Figure 3.2: Geometry of the problem for channel flow

Recall from Section 1.1.4.2 that the dimensionless parameter  $s = \frac{Ha^2}{ReRe_m}$ , and the Hartmann number  $Ha$  contains the magnitude of the induced magnetic field.

The aim in this numerical experiment is to show how the velocity and magnetic field solutions of Algorithm 3.2.1 change when Hartmann number  $Ha$  increases. To show that, we first fix  $Re, Re_m$  to 1, and next compute the solutions of Algorithm 3.2.1 for varying  $s$ . All computations are carried out by taking time step  $\Delta t = 0.025$  with end time  $T = 40$ .

For  $s = 0$  (see Figure 3.3), which means that there is no effect of the induced magnetic field, we get eddies forming behind the step, which is the expected result. For  $s = 0.01$ , the second plot in Figure 3.3, it can be seen that the effect of the magnetic field is very small. However, when  $s$  increases, the shedding of eddies behind the step is inhibited, and the eddies change to steady and shortens. This is because of the retarding effect of Lorentz force. In addition, the change in velocity profile is clearly altered away from a parabolic shape to plug like. On the other hand, the magnetic field plots show a clear interaction between the flow and the induced magnetic field.

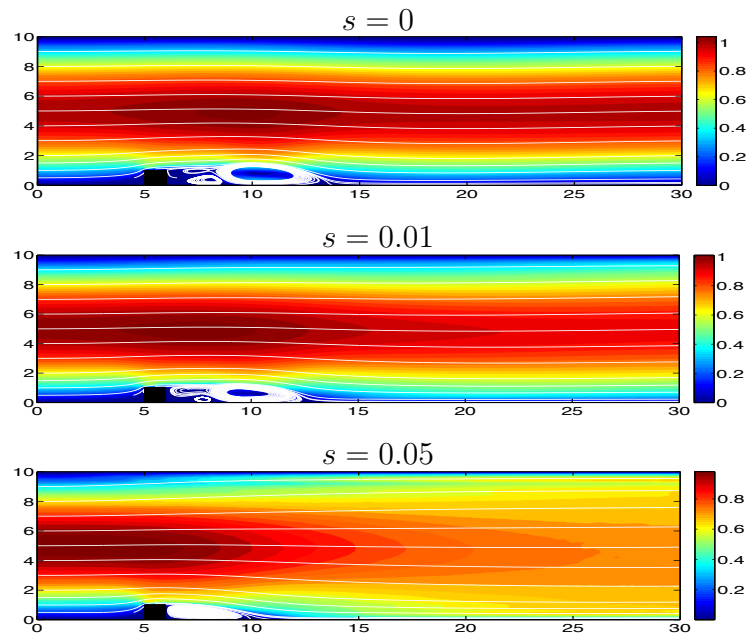


Figure 3.3: Velocity solutions (shown as streamlines over velocity) for MHD channel flow over full step with varying  $s$  at  $T = 40$ .

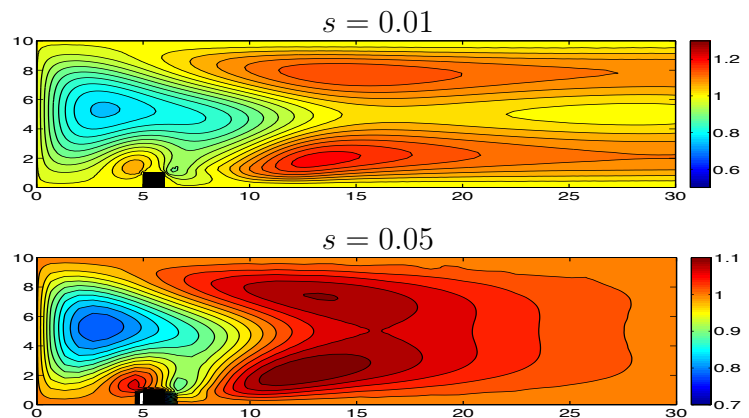


Figure 3.4: Magnetic field magnitudes for MHD channel flow over full step with varying  $s$  at  $T = 40$ .

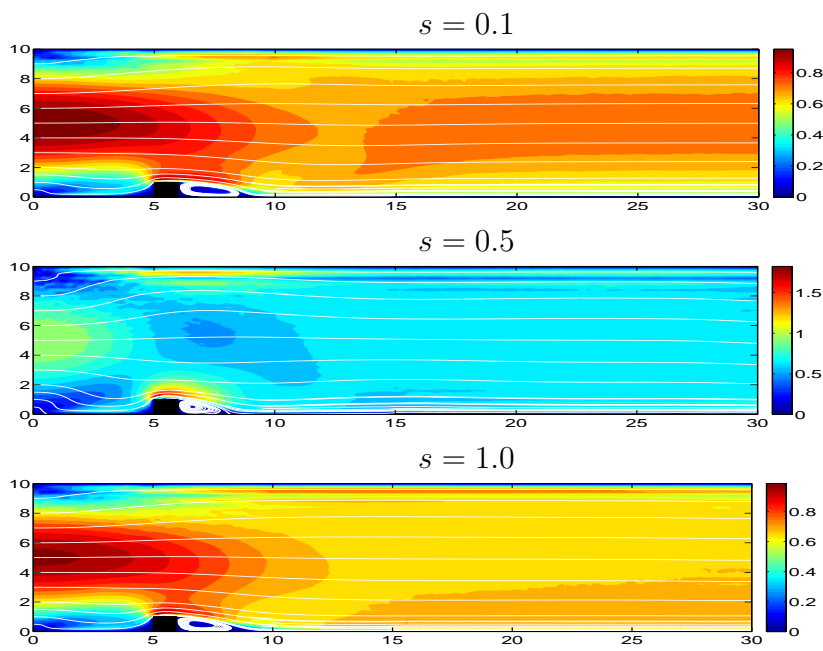


Figure 3.5: Velocity solutions (shown as streamlines over velocity) for MHD channel flow over full step with varying  $s$  at  $T = 40$ .

## CHAPTER 4

### LONG TIME STABILITY ANALYSIS OF MULTIPHYSICS FLOW PROBLEMS

In this chapter, we focus on long time-stability notion of some multiphysics flow problems. This topic has an important place in the improving of the long time statistic such as weather prediction, and is essential for the accuracy of longer time simulations, especially in the simulation of the flow at high *Reynolds number*. Therefore, it is important to develop numerical algorithms for multiphysics problems possessing such a property without time step restriction.

The long time stability notion of a numerical algorithm is not a new research area, but has received an increasing attention in recent years. If we look at the literature, the works of J. Heywood and R. Rannacher [58, 59] can be given as primary studies in this topic, which reveal the approximate solution of the NSE with Crank-Nicolson time and Galerkin finite element spatial discretization is stable over long time interval in the energy norm. The works of J. Shen [93], and J. Simo and F. Armero [97] follows these works. In [93], the long time stability and error analysis of the NSE was studied by using a fully discrete non-linear Galerkin method, and this notion was explored for the NSE with time integration algorithms, containing couples schemes and fractional step/projection methods in [97]. In [74], the long time stability for linear backward Euler time discretization with homogeneous and periodic boundary conditions of the NSE was studied in  $V$  and  $D(A)$ -spaces, which are defined by  $V := \{v \in H_0^1(\Omega) : \nabla \cdot v = 0\}$ ,  $D(A) = H^2(\Omega) \cap V$ .

On the other hand, recent works of F. Tone, X. Wang, S. Gottlieb, D. Wirosoetisno and co-workers ([108, 104, 106, 4]) have made great strides in understanding long-time stability results for several commonly used discretizations of incompressible

flow problems. In [108], F. Tone and D. Wirosoetisno analyzed the long time stability of the implicit Euler schemes for the NSE in  $2d$  with homogeneous Dirichlet boundary conditions. They proved that the solutions are long time stable in  $\mathbf{H}^1$ -norm under time step restriction. Tone showed that in [105] the approximate velocity solution of implicit Euler scheme for the NSE with space-periodic boundary condition are bounded at all time in  $\mathbf{H}^2$ -norm. Furthermore, in [104], she proved the long time velocity solution of the NSE with Crank-Nicolson time discretization is conditionally stable in  $L^2$  and  $\mathbf{H}_0^1$ -norms. The extension of the ideas from [108, 104] to the MHD flow in  $2d$  can be seen in [106]. The stability at all times for the NSE was explored with VMS in  $\mathbf{H}_0^1$ -norm in [4].

In the past five years, long-time stability notion with several schemes has been studied, e.g. for the incompressible NSE in [47, 111, 6], and also for the Boussinesq equations in [36]. Gottlieb et al. in [47] studied the NSE in vorticity-streamline formulation with first order semi discretization, i.e., the discretization only in time, and they obtained that the proposed scheme has long time stability property in  $L^2$  and  $\mathbf{H}^1$ -norms under time step restriction. In addition to this, the same problem with second order temporal discretization was examined by Wang in [111], where the vorticity solution is stable at all times in  $\mathbf{H}^1$ -norm with the time step restriction. In [99], Tachim Medjo and Tone proved that approximate solutions for the implicit Euler scheme of the two-phase flow model are uniformly bounded in time. For BDF2 type schemes, unconditional long-time stability has been proven for a Stokes-Darcy system in [80, 22],  $2d$  double-diffusive convection problems with numerical experiment in [107]. In addition to these, Heister et al. studied the NSE in  $2d$  with a particular velocity-vorticity formulation with implicit-explicit BDF2 time discretization in [57], and they proved that the method is long time stable in  $L^2$  and  $\mathbf{H}^1$ -norms without time step-restriction.

A common theme of the studies mentioned above is that the stability property at all times is subjected to a time step restriction. In addition, the studies in this area are lack of numerical simulation over long time intervals. In this thesis, we try to fill this gap in this topic by proving the stability property of a popular algorithm over long time interval achieved without any time step restriction.

In this chapter, we study three-multiphysics flow problems: the Navier-Stokes equations, incompressible non-isothermal fluid flow and MHD in primitive and Elsässer

variables. For each of these systems/schemes, we prove unconditional long-time  $L^2$  stability of velocity / temperature / magnetic field, provided external forces (and sources) are uniformly bounded in time. Here, we take advantage of the  $G$ -norm theory from [55] in order to prove unconditional long time stability of the scheme. In addition to our analytical stability results, we also provide numerical experiments. This chapter is organized as follows. Section 4.1 is devoted to mathematical preliminaries. Section 4.2 presents the long time stability results for the NSE with linearly extrapolated BDF2 (BDF2LE) finite element scheme as well as two numerical experiments. In the first numerical experiment in Section 4.2, we compare the stability of BDF2LE to linearly extrapolated Crank-Nicolson schemes (CNLE), and find that BDF2LE has better stability properties, particularly for smaller viscosity values. In the second numerical experiment, we display the importance of discrete mass conservation in long-time simulations of the incompressible Navier-Stokes equations. With a simple numerical experiment using a finite element in space, linear extrapolated Crank-Nicolson in time discretization, we show that using elements that enforce strong mass conservation can provide significantly more accurate solutions compared to those that enforce it weakly, particularly over long time intervals. On the other hand, Section 4.3, Section 4.4 and Section 4.5 study the long time stability of the BDF2LE finite element scheme for the Boussinesq system, MHD in primitive variables and MHD in Elsässer variables, respectively.

#### 4.1 Mathematical Preliminaries

Let  $\Omega$  be an open, connected bounded Lipschitz domain in  $\mathbb{R}^d$ ,  $d = 2, 3$ . We denote the usual  $L^2$  inner product and its induced norm by  $(\cdot, \cdot)$  and  $\|\cdot\|$ , respectively. We use the following function spaces:

$$\begin{aligned} \mathbf{X} &:= (H_0^1(\Omega))^d = \{\mathbf{v} \in (L^p(\Omega))^d : \nabla \mathbf{v} \in L^2(\Omega)^{d \times d}, \mathbf{v} = 0 \text{ on } \partial\Omega\}, \\ Q &:= L_0^2(\Omega) = \{q \in L^2(\Omega) : \int_{\Omega} q \, dx = 0\}, \\ W &:= H_0^1(\Omega). \end{aligned}$$

Let  $\pi_h$  be a regular, conforming, triangulation of the domain, and  $\mathbf{X}_h \subset \mathbf{X}$ ,  $Q_h \subset Q$ ,  $W_h \subset W$  be conforming finite element spaces defined on  $\pi_h$ . We assume that velocity-pressure finite element spaces  $(\mathbf{X}_h, Q_h)$  are inf-sup stable. Another inequal-

ity used frequently in the long time stability analysis is inverse inequality: There exists a constant  $C_I$ , dependent on the minimum angle of the mesh but independent of  $h$ , such that

$$\|\nabla \phi_h\| \leq C_I h^{-1} \|\phi_h\|, \quad \forall \phi_h \in \mathbf{X}_h. \quad (4.1)$$

The discretely divergence free subspace of  $\mathbf{X}_h$  is defined as

$$\mathbf{V}_h = \{\mathbf{v}_h \in \mathbf{X}_h : (q_h, \nabla \cdot \mathbf{v}_h) = 0 \quad \forall q_h \in Q_h\}.$$

We denote  $\mathbf{V}_h^*$  as the dual space of  $\mathbf{V}_h$  and its norm by  $\|\cdot\|_{\mathbf{V}_h^*}$ :

$$\|\Phi\|_{\mathbf{V}_h^*} := \sup_{\mathbf{v}_h \in \mathbf{V}_h} \frac{(\Phi, \mathbf{v}_h)}{\|\nabla \mathbf{v}_h\|}.$$

In the discretization of non-linear terms for the proposed flow problems, we use the following skew-symmetric trilinear forms:

$$\begin{aligned} b^*(\mathbf{u}, \mathbf{v}, \mathbf{w}) &:= \frac{1}{2} ((\mathbf{u} \cdot \nabla \mathbf{v}, \mathbf{w}) - (\mathbf{u} \cdot \nabla \mathbf{w}, \mathbf{v})) \quad \forall \mathbf{u}, \mathbf{v}, \mathbf{w} \in \mathbf{X}, \\ c^*(\mathbf{u}, \theta, \psi) &:= \frac{1}{2} ((\mathbf{u} \cdot \nabla \theta, \psi) - (\mathbf{u} \cdot \nabla \psi, \theta)) \quad \forall \mathbf{u} \in \mathbf{X} \text{ and } \theta, \psi \in W. \end{aligned}$$

We also define the space

$$L^\infty(\mathbb{R}_+, V_h^*) := \{f : \Omega^d \times \mathbb{R}_+ \rightarrow \mathbb{R}^d, \exists C < \infty \text{ with } \|f(t)\|_{V_h^*} < C \text{ a.e. } t > 0\}.$$

The schemes we consider are of BDF2 type, and the analysis is greatly simplified if we use the  $G$ -stability framework, as in [55]. Hence, we define here the  $G$ -matrix

$$G := \begin{pmatrix} 1/2 & -1 \\ -1 & 5/2 \end{pmatrix},$$

and its associated  $G$ -norm

$$\|\chi\|_G^2 = (\chi, G\chi), \quad \chi \in \mathbb{R}^{2n}.$$

It is well known [55] that the  $L^2$  and the  $G$ -norms are equivalent in the following sense:  $\exists C_u, C_l > 0$  such that

$$C_l \|\chi\|_G \leq \|\chi\| \leq C_u \|\chi\|_G. \quad (4.2)$$

Set  $\chi_v^n := [v^{n-1}, v^n]^T$  and  $\chi_v^{n+1} := [v^n, v^{n+1}]^T$ . Then if each  $v^i \in L^2(\Omega)$  the following relation holds (see, e.g. [55]):

$$\left( \frac{3}{2} v^{n+1} - 2v^n + \frac{1}{2} v^{n-1}, v^{n+1} \right) = \frac{1}{2} (\|\chi_v^{n+1}\|_G^2 - \|\chi_v^n\|_G^2) + \frac{\|v^{n+1} - 2v^n + v^{n-1}\|^2}{4}. \quad (4.3)$$



## 4.2 Long time stability of the NSE

We first show the BDF2LE finite element scheme for the NSE is unconditionally long time stable, i.e., stability is independent of end time and the time step  $\Delta t$ . This is a widely-used algorithm, and is given as follows:

**Algorithm 4.2.1 (BDF2LE for the NSE)** *Let the forcing  $\mathbf{f} \in L^\infty(\mathbb{R}_+; \mathbf{V}_h^*)$ , and an initial condition  $\mathbf{u}_0 \in L^2(\Omega)$  be given. Define  $\mathbf{u}_h^{-1} = \mathbf{u}_h^0$  to be nodal interpolant of  $\mathbf{u}_0$ . Choose a time step  $\Delta t$ . For all  $n = 0, 1, 2, \dots$ , find  $(\mathbf{u}_h^{n+1}, p_h^{n+1})$  satisfying for all  $(\mathbf{v}_h, q_h) \in (\mathbf{X}_h, Q_h)$*

$$\begin{aligned} \frac{1}{2\Delta t}(3\mathbf{u}_h^{n+1} - 4\mathbf{u}_h^n + \mathbf{u}_h^{n-1}, \mathbf{v}_h) + b^*(2\mathbf{u}_h^n - \mathbf{u}_h^{n-1}, \mathbf{u}_h^{n+1}, \mathbf{v}_h) + \nu(\nabla \mathbf{u}_h^{n+1}, \nabla \mathbf{v}_h) \\ - (p_h^{n+1}, \nabla \cdot \mathbf{v}_h) = (\mathbf{f}^{n+1}, \mathbf{v}_h) \end{aligned} \quad (4.4)$$

$$(\nabla \cdot \mathbf{u}_h^{n+1}, q_h) = 0. \quad (4.5)$$

**Theorem 4.2.2** *Let  $(\mathbf{u}_h^{n+1}, p_h^{n+1})$  be the solutions of Algorithm 4.2.1 for all  $n = 0, 1, 2, \dots$ . Then for any  $\Delta t > 0$ , we have*

$$\begin{aligned} \|\chi_u^{n+1}\|_G^2 + \frac{\nu\Delta t}{4}\|\nabla \mathbf{u}_h^{n+1}\|^2 \leq (1 + \alpha)^{-(n+1)} \left( \|\chi_u^0\|_G^2 + \frac{\nu\Delta t}{4}\|\nabla \mathbf{u}_h^0\|^2 \right) \\ + \nu^{-1}\alpha^*\|\mathbf{f}\|_{L^\infty(\mathbb{R}_+; \mathbf{V}_h^*)}^2, \end{aligned}$$

where  $\alpha = \min\{2, \frac{\nu\Delta t C_i^2}{4C_{PF}^2}\} > 0$ ,  $\alpha^* = \max\{\frac{1}{2}\Delta t, \frac{4C_{PF}^2}{\nu C_i^2}\} > 0$ ,  $C_{PF}$  is the Poincaré's-Friedrichs' constant from (2.6) and  $C_i$  is given by (4.2).

**Proof:** Take as test functions  $\mathbf{v}_h = 2\Delta t \mathbf{u}_h^{n+1}$  in (4.4),  $q_h = p_h^{n+1}$  in (4.5). Using relation (4.3), and applying the Cauchy-Schwarz inequality and the Young's inequality yields

$$\left( \|\chi_u^{n+1}\|_G^2 - \|\chi_u^n\|_G^2 \right) + \frac{\|\mathbf{u}_h^{n+1} - 2\mathbf{u}_h^n + \mathbf{u}_h^{n-1}\|^2}{2} + \nu\Delta t\|\nabla \mathbf{u}_h^{n+1}\|^2 \leq \nu^{-1}\Delta t\|\mathbf{f}^{n+1}\|_{\mathbf{V}_h^*}^2.$$

Drop the non-negative term  $\frac{\|\mathbf{u}_h^{n+1} - 2\mathbf{u}_h^n + \mathbf{u}_h^{n-1}\|^2}{2}$  and add  $\frac{\nu\Delta t}{4}\|\nabla \mathbf{u}_h^n\|^2$  to both sides to produce

$$\begin{aligned} \left( \|\chi_u^{n+1}\|_G^2 + \frac{\nu\Delta t}{4}\|\nabla \mathbf{u}_h^{n+1}\|^2 \right) + \frac{\nu\Delta t}{4} \left( \|\nabla \mathbf{u}_h^{n+1}\|^2 + \|\nabla \mathbf{u}_h^n\|^2 \right) + \frac{\nu\Delta t}{2}\|\nabla \mathbf{u}_h^{n+1}\|^2 \\ \leq \left( \|\chi_u^n\|_G^2 + \frac{\nu\Delta t}{4}\|\nabla \mathbf{u}_h^n\|^2 \right) + \nu^{-1}\Delta t\|\mathbf{f}^{n+1}\|_{\mathbf{V}_h^*}^2. \end{aligned} \quad (4.6)$$

By using the Poincaré's-Friedrichs' inequality and the equivalence of the  $L^2$  and the  $G$ -norms, the last two terms on the left hand side can be written as

$$\begin{aligned}
& \frac{\nu\Delta t}{4} \left( \|\nabla \mathbf{u}_h^{n+1}\|^2 + \|\nabla \mathbf{u}_h^n\|^2 \right) + \frac{\nu\Delta t}{2} \|\nabla \mathbf{u}_h^{n+1}\|^2 \\
& \geq \frac{\nu\Delta t}{4C_{PF}^2} \|\chi_u^{n+1}\|^2 + \frac{\nu\Delta t}{2} \|\nabla \mathbf{u}_h^{n+1}\|^2 \\
& \geq \frac{\nu\Delta t C_l^2}{4C_{PF}^2} \|\chi_u^{n+1}\|_G^2 + \frac{\nu\Delta t}{2} \|\nabla \mathbf{u}_h^{n+1}\|^2 \\
& \geq \alpha \left( \|\chi_u^{n+1}\|_G^2 + \frac{\nu\Delta t}{4} \|\nabla \mathbf{u}_h^{n+1}\|^2 \right),
\end{aligned}$$

where  $\alpha := \min\{\frac{1}{2}, \frac{\nu\Delta t C_l^2}{4C_{PF}^2}\}$ . Inserting the last estimate in (4.6) and using induction results gives

$$\begin{aligned}
\|\chi_u^{n+1}\|_G^2 + \frac{\nu\Delta t}{4} \|\nabla \mathbf{u}_h^{n+1}\|^2 \leq (1 + \alpha)^{-(n+1)} & \left( \|\chi_u^0\|_G^2 + \frac{\nu\Delta t}{4} \|\nabla \mathbf{u}_h^0\|^2 \right) \\
& + \frac{\nu^{-1}\Delta t}{\alpha} \|\mathbf{f}\|_{L^\infty(\mathbb{R}_+; \mathbf{V}_h^*)}^2.
\end{aligned}$$

Setting  $\frac{\Delta t}{\alpha} = \max\{2\Delta t, \frac{4C_{PF}^2}{\nu C_l^2}\} =: \alpha^*$  and using the equivalence of the  $L^2$  and  $G$ -norms (4.2) completes the proof.  $\square$

#### 4.2.1 Numerical Experiment

In this section, we present two numerical experiments. In these numerical experiments, we consider the NSE with the CNLE finite element discretization, which is given below by Algorithm 4.2.3. This scheme has been studied recently in [77, 5, 62, 6]. In [6], it is shown that the discrete solution of Algorithm 4.2.3 is conditionally long time stable, which is stated in Lemma 4.2.4.

**Algorithm 4.2.3 (CNLE for the NSE)** *Let  $\mathbf{f} \in L^\infty(\mathbb{R}_+; \mathbf{V}_h^*)$  and the initial velocity  $\mathbf{u}_0 \in \mathbf{L}^2(\Omega)$  be given. Define  $\mathbf{u}_h^{-1} = \mathbf{u}_h^0$  to be the nodal interpolant of  $\mathbf{u}_0$  and choose a time step  $\Delta t > 0$ . For  $n = 0, 1, 2, 3, \dots$ , find  $(\mathbf{u}_h^{n+1}, p_h^{n+1}) \in (\mathbf{X}_h, Q_h)$  satisfying*

for every  $(\mathbf{v}_h, q_h) \in (\mathbf{X}_h, Q_h)$ ,

$$\begin{aligned} \left( \frac{\mathbf{u}_h^{n+1} - \mathbf{u}_h^n}{\Delta t}, \mathbf{v}_h \right) + b^*(\mathbf{u}_h^*, \mathbf{u}_h^{n+1/2}, \mathbf{v}_h) + \nu(\nabla \mathbf{u}_h^{n+1/2}, \nabla \mathbf{v}_h) \\ - (p_h^{n+1}, \nabla \cdot \mathbf{v}_h) = (\mathbf{f}(t^{n+1/2}), \mathbf{v}_h), \end{aligned} \quad (4.7)$$

$$(\nabla \cdot \mathbf{u}_h^{n+1}, q_h) = 0, \quad (4.8)$$

where  $\mathbf{u}_h^* = \frac{3}{2}\mathbf{u}_h^n - \frac{1}{2}\mathbf{u}_h^{n-1}$ ,  $\mathbf{u}_h^{n+1/2} = \frac{1}{2}(\mathbf{u}_h^{n+1} + \mathbf{u}_h^n)$  and  $p_h^{n+1}$  is understood to be an approximation of  $p_h^{n+1/2}$ .

**Lemma 4.2.4** Set  $K := \left( \|\mathbf{u}_0\|^2 + \frac{C_{PF}^2}{\nu^2} \|\mathbf{f}\|_{L^\infty(\mathbb{R}_+; \mathbf{V}_h^*)}^2 \right)^{1/2}$ . If

$$\Delta t \leq \min \left\{ \frac{h^2}{4\nu C_I^2}, \frac{\nu h^d}{20C_0^2 K^2 C_I} \right\},$$

then

$$\begin{aligned} \|\mathbf{u}_h^n\|^2 \leq \left( 1 + \frac{\nu}{2C_{PF}^2} \Delta t \right)^{-n} \|\mathbf{u}_0\|^2 + \frac{C_{PF}^2}{\nu^2} \|\mathbf{f}\|_{L^\infty(\mathbb{R}_+; \mathbf{V}_h^*)}^2 \left[ 1 - \left( 1 + \frac{\nu}{2C_{PF}^2} \right)^{-n} \right] \\ \leq K^2, \end{aligned} \quad (4.9)$$

where  $C_0$  is a constant independent of the mesh size  $h$  and time step  $\Delta t$ ,  $d$  the dimension of the domain,  $C_{PF}$  is the Poincaré's-Friedrichs' constant from (2.6) and  $C_I$  is given by (4.1).

We now present the corollary of Lemma 4.2.4, which is the main idea of the second numerical experiment.

**Remark 4.2.5** In addition to the time step restrictions of Lemma 4.2.4, if the time step restriction  $\Delta t \leq \frac{2C_{PF}^2}{\nu}$  holds, then for all

$$n\Delta t \geq \frac{8C_{PF}^2}{\nu} \ln \left( \frac{\nu \|\mathbf{u}_0\|}{C_{PF} \|\mathbf{f}\|_{L^\infty(\mathbb{R}_+; \mathbf{V}_h^*)}} \right),$$

one can have the following:

$$\|\mathbf{u}_h^n\| \leq \sqrt{2} C_{PF} \nu^{-1} \|\mathbf{f}\|_{L^\infty(\mathbb{R}_+; \mathbf{V}_h^*)}. \quad (4.10)$$

### 4.2.1.1 Numerical Experiment 1: Comparison of the stability of the solutions of BDF2LE and CNLE schemes for the NSE over long time interval

In this numerical experiment, we compare the stability of the BDF2LE and the CNLE for the NSE using  $(P_2, P_1^{disc})$  Scott-Vogelius finite elements. We choose an initial velocity and a body force as follows:

$$\mathbf{u}_0 = \begin{pmatrix} \sin(\pi x) \sin(\pi y) \\ \cos(\pi x) \cos(\pi y) \end{pmatrix}, \quad f = \begin{pmatrix} y^2 \cos(xy^2) + \sin(x) \sin(y) \\ 2xy \cos(xy^2) + \cos(x) \cos(y) \end{pmatrix}.$$

We calculate approximate velocity solutions of Algorithm 4.2.1 and Algorithm 4.2.3 on the same  $16 \times 16$  barycenter refined uniform mesh of  $\Omega := (0, 1)^2$  by taking time step  $\Delta t = 0.25$  with end time  $T = 500$  for varying  $\nu$ . The results are shown in Figure ?? and Figure ?? as plots of  $\|u_h^n\|$  versus time.

We observe that for larger  $\nu$  ( $\nu = 1$  and  $\nu = 0.004$ ), the schemes produce very similar stability properties. For  $\nu = 0.002$ , the schemes are similar until around  $T = 70$ , when CNLE deviates: the  $L^2$ -norm of the solution grows for the CNLE but remains constant for the BDF2LE. For  $\nu = 0.001$ , we observe similar results as for  $\nu = 0.002$ , but the deviation happens sooner.

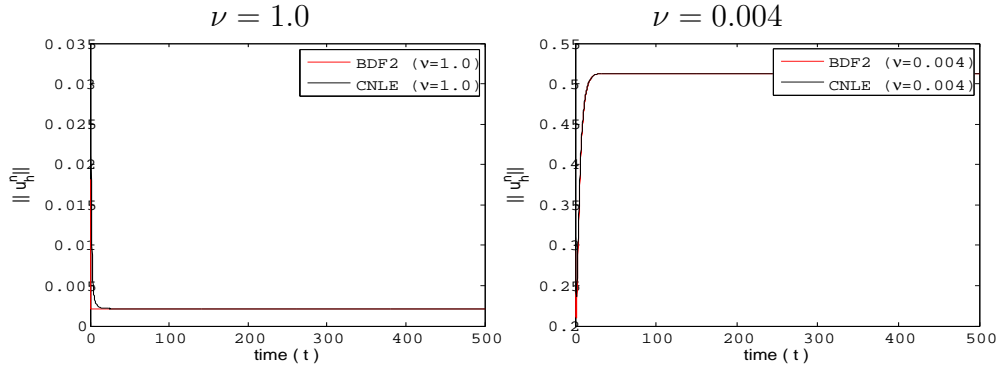


Figure 4.1: Discrete velocity solutions of the BDF2LE and the CNLE schemes for the NSE with  $\Delta t = 0.25$  varying  $\nu$ .

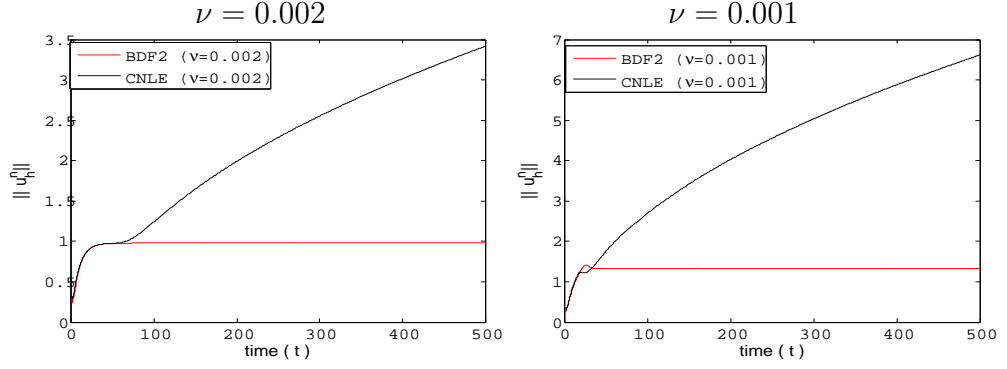


Figure 4.2: Discrete velocity solutions of the BDF2LE and the CNLE schemes for the NSE with  $\Delta t = 0.25$  varying  $\nu$ .

#### 4.2.1.2 Numerical Experiment 2 : Comparison of the mass conservation in long-time simulation of the NSE with different finite elements

The main objective of this section is to discuss how divergence-free elements can provide more accurate solutions over long-time intervals for the NSE, compared to more commonly used elements such as Taylor-Hood, which only enforce the divergence constraint (1.25) weakly, and Scott-Vogelius, enforce divergence free condition strongly. For this aim, we consider CNLE finite element discretization of the system (1.2)-(1.3).

The idea underlying why div-free finite elements provide much more accurate solution is that the divergence-free elements handle the irrotational part of the forcing  $\mathbf{f}$  correctly; they enforce that this part of the forcing affects only the pressure, and with elements that only weakly enforce (1.25), however, the discrete velocity solution is affected by the irrotational part of the forcing, and over long time intervals causing significant error. To verify this theory, we consider the following simple numerical example to illustrate the above theory. On a domain  $\Omega = (0, 1)^2$ , set the initial condition and forcing to be

$$\mathbf{u}_0 = \begin{pmatrix} \sin(\pi x) \sin(\pi y) \\ \cos(\pi x) \cos(\pi y) \end{pmatrix}, \quad \mathbf{f} = 5\nabla(\sin(2x) + \sin(2y))$$

Noting that the forcing is purely irrotational. If homogeneous Dirichlet boundary conditions is enforced, the long-time solution of the NSE is

$$\mathbf{u} = 0, \quad p = 5(\sin(2x) + \sin(2y)),$$

for any positive viscosity  $\nu$ .

We compute approximate solutions of the Algorithm 4.2.3 using both the Scott-Vogelius  $(\mathbf{P}_2, P_1^{disc})$  and the Taylor-Hood  $(\mathbf{P}_2, P_1)$  elements, with  $\Delta t = 1.0$  (but we note we got the same long-time solutions with  $\Delta t = 0.25, 0.05, 0.01$ ). The simulations were run on the same  $16 \times 16$  barycenter refined uniform mesh of  $\Omega$  with 2,754 degrees of freedom (dof) for Scott-Vogelius (SV) elements and 1,811 dof for Taylor-Hood (TH).

Figure 4.4 below shows the evolution of  $\|\mathbf{u}_h^n\|$  with time for several choices of  $\nu$ , and we observe that the Scott-Vogelius solutions all converge to the correct long-time solution of  $\mathbf{u}_h = 0$  (up to the accuracy of the linear solver), whereas the Taylor-Hood solutions are inaccurate due to the mass conservation error, and converge instead to

$$\nu = 0.01 : \|\mathbf{u}_h^n\| \rightarrow 9.427e - 3,$$

$$\nu = 0.002 : \|\mathbf{u}_h^n\| \rightarrow 4.716e - 2,$$

$$\nu = 0.001 : \|\mathbf{u}_h^n\| \rightarrow 8.927e - 2.$$

For small times with  $\nu = 0.01$  and  $0.002$ , we observe that the norms of the Scott-Vogelius and Taylor-Hood solutions are nearly identical, as the plots lay on top of each other.

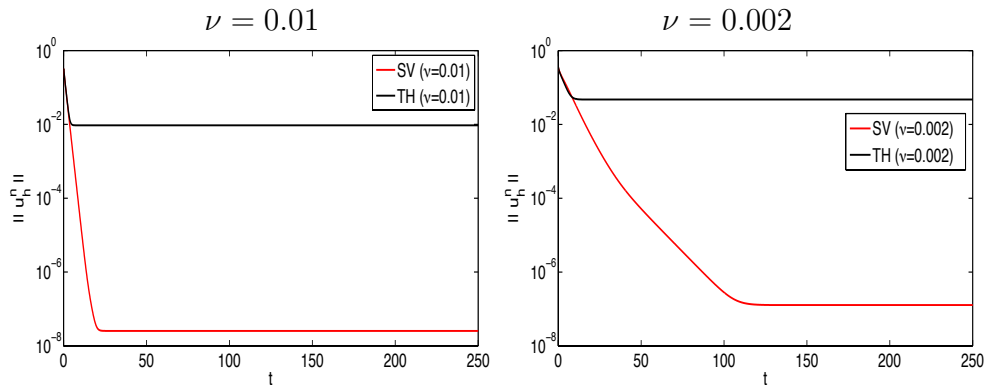


Figure 4.3: Shown above plots of the  $L^2$ -norm of the computed solution  $\|\mathbf{u}_h^n\|$  versus time, for viscosities  $\nu = \frac{1}{100}, \frac{1}{500}$ .

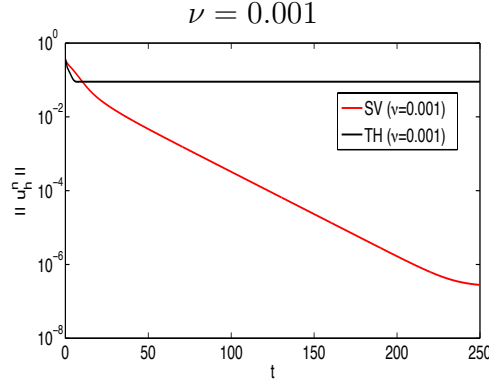


Figure 4.4: Shown above plots of the  $L^2$ -norm of the computed solution  $\|u_h^n\|$  versus time, for viscosity  $\nu = \frac{1}{1000}$ .

### 4.3 Long time stability analysis of the Boussinesq System

In this section, we focus on the Boussinesq system which describes incompressible non-isothermal fluid flow. The linearly extrapolated BDF2 approximation of the system (2.1) reads as follows:

**Algorithm 4.3.1 (BDF2 for the Boussinesq system)** *Let the forcing  $\mathbf{f}$ , the heat source  $\gamma$  and the initial conditions  $\mathbf{u}_0, \theta_0$  be given. Define  $\mathbf{u}_h^{-1} = \mathbf{u}_h^0$  and  $\theta_h^{-1} = \theta_h^0$  to be the nodal interpolants of  $\mathbf{u}_0$  and  $\theta_0$ , respectively. Choose a time step  $\Delta t > 0$ , and for all  $n = 0, 1, 2, 3, \dots$ , find  $(\mathbf{u}_h^{n+1}, p_h^{n+1}, \theta_h^{n+1})$  satisfying for all  $(\mathbf{v}_h, q_h, w_h) \in (\mathbf{X}_h, Q_h, W_h)$*

$$\begin{aligned} \frac{1}{2\Delta t}(3\mathbf{u}_h^{n+1} - 4\mathbf{u}_h^n + \mathbf{u}_h^{n-1}, \mathbf{v}_h) + b^*(2\mathbf{u}_h^n - \mathbf{u}_h^{n-1}, \mathbf{u}_h^{n+1}, \mathbf{v}_h) + \nu(\nabla \mathbf{u}_h^{n+1}, \nabla \mathbf{v}_h) \\ - (p_h^{n+1}, \nabla \cdot \mathbf{v}_h) = (Ri \langle 0, 2\theta_h^n - \theta_h^{n-1} \rangle, \mathbf{v}_h) + (\mathbf{f}^{n+1}, \mathbf{v}_h), \end{aligned} \quad (4.11)$$

$$(\nabla \cdot \mathbf{u}_h^{n+1}, q_h) = 0, \quad (4.12)$$

$$\frac{1}{2\Delta t}(3\theta_h^{n+1} - 4\theta_h^n + \theta_h^{n-1}, w_h) + c^*(\mathbf{u}_h^n, \theta_h^{n+1}, w_h) + \kappa(\nabla \theta_h^{n+1}, \nabla w_h) = (\gamma^{n+1}, w_h). \quad (4.13)$$

We now present the long time stability of Algorithm 4.3.1.

**Theorem 4.3.2** *Let  $\mathbf{f} \in L^\infty(\mathbb{R}_+; \mathbf{V}_h^*)$  and  $\gamma \in L^\infty(\mathbb{R}_+; W_h^*)$ . Then for any  $\Delta t > 0$  and for  $n$  sufficiently large, the velocity and temperature solutions of Algorithm 4.3.1*

satisfy :

$$\|\mathbf{x}_u^{n+1}\|_G^2 + \frac{\nu\Delta t}{4}\|\nabla\mathbf{u}_h^{n+1}\|^2 \leq \left(\frac{1}{1+\beta}\right)^{n+1} \left(\|\mathbf{x}_u^0\|_G^2 + \frac{\nu\Delta t}{4}\|\nabla\mathbf{u}_h^0\|^2\right) + \nu^{-1}\beta^*M^*, \quad (4.14)$$

$$\begin{aligned} \|\mathbf{x}_\theta^{n+1}\|_G^2 + \frac{\kappa\Delta t}{4}\|\nabla\theta_h^{n+1}\|^2 &\leq \left(\frac{1}{1+\eta}\right)^{n+1} \left(\|\mathbf{x}_\theta^0\|_G^2 + \frac{\kappa\Delta t}{4}\|\nabla\theta_h^0\|^2\right) \\ &+ \kappa^{-1}\eta^*\|\gamma\|_{L^\infty(\mathbb{R}_+;W_h^*)}^2, \end{aligned} \quad (4.15)$$

where  $\beta := \min\{2, \frac{\nu\Delta t C_l^2}{4C_{PF}^2}\}$ ,  $\beta^* = \max\{\frac{1}{2}\Delta t, \frac{4C_{PF}^2}{\nu C_l^2}\}$ ,  $\eta := \min\{2, \frac{\kappa\Delta t C_l^2}{4C_{PF}^2}\}$ ,  $\eta^* = \max\{\frac{1}{2}\Delta t, \frac{4C_{PF}^2}{\kappa C_l^2}\}$ , and

$$M^* = 2 \left(10Ri^2 C_{PF}^2 \max\{\|\theta_h^0\|^2, M^2\} + \|\mathbf{f}\|_{L^\infty(\mathbb{R}_+;V_h^*)}^2\right).$$

Moreover, if

$$n\Delta t > \frac{2}{\kappa\eta_{**}} \ln \left( \frac{\|\mathbf{x}_\theta^0\|_G^2 + \frac{\kappa\Delta t}{4}\|\nabla\theta_h^0\|^2}{\kappa^{-2}\eta_{**}^{-1}\|\gamma\|_{L^\infty(\mathbb{R}_+;W_h^*)}^2} \right), \quad \text{and} \quad \kappa\Delta t < 1 \quad (4.16)$$

then for all  $n$  sufficiently large

$$\|\theta_h^n\| \leq \sqrt{2\eta_{**}^{-1}C_u\kappa^{-1}\|\gamma\|_{L^\infty(\mathbb{R}_+;W_h^*)}} =: M, \quad (4.17)$$

where  $\eta_{**} = \min\{\frac{1}{2}, \frac{C_l^2}{4C_{PF}^2}\}$ ,  $C_{PF}$  is the Poincaré's-Friedrichs' constant from (2.6),  $C_l$  and  $C_u$  are given by (4.2).

**Proof:** The proof of Theorem 4.3.2 consists of three steps. In Step 1, we first show the long time stability of the temperature and we obtain the bound on the temperature in Step 2. In Step 3, to obtain the long time stability of velocity we use the results of Step 1 and Step 2.

**Step 1:** (Long-time  $L^2$ -stability of the temperature)

We choose  $w_h = 2\Delta t\theta_h^{n+1}$  in (4.13) and use the relation (4.3). Application of the Cauchy-Schwarz and Young's inequalities gives

$$\begin{aligned} (\|\mathbf{x}_\theta^{n+1}\|_G^2 - \|\mathbf{x}_\theta^n\|_G^2) + \frac{\|\theta_h^{n+1} - 2\theta_h^n + \theta_h^{n-1}\|^2}{2} + \kappa\Delta t\|\nabla\theta_h^{n+1}\|^2 \\ \leq \kappa^{-1}\Delta t\|\gamma^{n+1}\|_{W_h^*}^2. \end{aligned} \quad (4.18)$$



Dropping the non-negative term  $\frac{\|\theta_h^{n+1} - 2\theta_h^n + \theta_h^{n-1}\|^2}{2}$  and adding the term  $\frac{\kappa\Delta t}{4}\|\nabla\theta_h^{n+1}\|^2$  to the both sides of (4.18) leads to

$$\begin{aligned} & \left( \|\chi_\theta^{n+1}\|_G^2 + \frac{\kappa\Delta t}{4}\|\nabla\theta_h^{n+1}\|^2 \right) + \frac{\kappa\Delta t}{4} (\|\nabla\theta_h^{n+1}\|^2 + \|\nabla\theta_h^n\|^2) + \frac{\kappa\Delta t}{2}\|\nabla\theta_h^{n+1}\|^2 \\ & \leq \left( \|\chi_\theta^n\|_G^2 + \frac{\kappa\Delta t}{4}\|\nabla\theta_h^n\|^2 \right) + \kappa^{-1}\Delta t\|\gamma^{n+1}\|_{W_h^*}^2. \end{aligned} \quad (4.19)$$

The last two terms on the left hand side of (4.19) are bounded by the Poincaré's-Friedrichs' inequality and the relation (4.2):

$$\begin{aligned} & \frac{\kappa\Delta t}{4} (\|\nabla\theta_h^{n+1}\|^2 + \|\nabla\theta_h^n\|^2) + \frac{\kappa\Delta t}{2}\|\nabla\theta_h^{n+1}\|^2 \\ & \geq \frac{\kappa\Delta t}{4C_{PF}^2} (\|\theta_h^{n+1}\|^2 + \|\theta_h^n\|^2) + \frac{\kappa\Delta t}{2}\|\nabla\theta_h^{n+1}\|^2 \\ & = \frac{\kappa\Delta t}{4C_{PF}^2} \|\chi_\theta^{n+1}\|^2 + \frac{\kappa\Delta t}{2}\|\nabla\theta_h^{n+1}\|^2 \\ & \geq \frac{\kappa\Delta t C_l^2}{4C_{PF}^2} \|\chi_\theta^{n+1}\|_G^2 + \frac{\kappa\Delta t}{2}\|\nabla\theta_h^{n+1}\|^2 \\ & \geq \eta \left( \|\chi_\theta^{n+1}\|_G^2 + \frac{\kappa\Delta t}{4}\|\nabla\theta_h^{n+1}\|^2 \right), \end{aligned} \quad (4.20)$$

where  $\eta := \min\{\frac{1}{2}, \frac{\kappa\Delta t C_l^2}{4C_{PF}^2}\}$ . We then insert (4.20) into (4.19) and use induction to produce

$$\begin{aligned} & \|\chi_\theta^{n+1}\|_G^2 + \frac{\kappa\Delta t}{4}\|\nabla\theta_h^{n+1}\|^2 \\ & \leq \left( \frac{1}{1+\eta} \right)^{n+1} \left( \|\chi_\theta^0\|_G^2 + \frac{\kappa\Delta t}{4}\|\nabla\theta_h^0\|^2 \right) \\ & \quad + \kappa^{-1}\Delta t\|\gamma\|_{L^\infty(\mathbb{R}_+; W_h^*)}^2 \left[ \frac{1}{1+\eta} + \left( \frac{1}{1+\eta} \right)^2 + \dots + \left( \frac{1}{1+\eta} \right)^{n+1} \right] \\ & \leq \left( \frac{1}{1+\eta} \right)^{n+1} \left( \|\chi_\theta^0\|_G^2 + \frac{\kappa\Delta t}{4}\|\nabla\theta_h^0\|^2 \right) + \frac{\kappa^{-1}\Delta t}{\eta} \|\gamma\|_{L^\infty(\mathbb{R}_+; W_h^*)}^2. \end{aligned}$$

Noting that  $\frac{\Delta t}{\eta} = \max\{2\Delta t, \frac{4C_{PF}^2}{\kappa C_l^2}\} =: \eta^*$ , applying the equivalence of the  $L^2$  and the  $G$ -norms (4.2), and dropping the non-negative term  $\frac{\kappa\Delta t}{4}\|\nabla\theta_h^n\|^2$  gives the long time stability of temperature (4.15).

**Step 2:** (*Bound for the temperature*)

Using the Poincaré-Friedrich inequality and relation (4.2) along with the assumption

$\kappa\Delta t \leq 1$ , the last two term on the left hand side of (4.19) can be written as:

$$\begin{aligned}
& \frac{\kappa\Delta t}{4} (\|\nabla\theta_h^{n+1}\|^2 + \|\nabla\theta_h^n\|^2) + \frac{\kappa\Delta t}{2} \|\nabla\theta_h^{n+1}\|^2 \\
& \geq \frac{\kappa\Delta t C_l^2}{4C_{PF}^2} \|\chi_\theta^{n+1}\|_G^2 + \frac{(\kappa\Delta t)^2}{2} \|\nabla\theta_h^{n+1}\|^2 \\
& = \kappa\Delta t \left( \frac{C_l^2}{4C_{PF}^2} \|\chi_\theta^{n+1}\|_G^2 + \frac{\kappa\Delta t}{2} \|\nabla\theta_h^{n+1}\|^2 \right) \\
& \geq \kappa\Delta t \eta_{**} \left( \|\chi_\theta^{n+1}\|_G^2 + \frac{\kappa\Delta t}{4} \|\nabla\theta_h^{n+1}\|^2 \right) \quad (4.21)
\end{aligned}$$

where  $\eta_{**} := \min\{\frac{1}{2}, \frac{C_l^2}{4C_{PF}^2}\}$ . Inserting this into (4.19) and using induction gives

$$\begin{aligned}
& \|\chi_\theta^{n+1}\|_G^2 + \frac{\kappa\Delta t}{4} \|\nabla\theta_h^{n+1}\|^2 \\
& \leq (1 + \kappa\Delta t \eta_{**})^{-(n+1)} \left( \|\chi_\theta^0\|_G^2 + \frac{\kappa\Delta t}{4} \|\nabla\theta_h^0\|^2 \right) + \kappa^{-2} \eta_{**}^{-1} \|\gamma\|_{L^\infty(\mathbb{R}_+; W_h^*)}^2. \quad (4.22)
\end{aligned}$$

By changing the index from  $(n+1)$  to  $(n)$  in (4.22) and using the inequality

$$(1+x) \geq \exp(x/2), \quad x \in (0, 1)$$

along with the assumption (4.16), one obtains

$$\begin{aligned}
LHS & \leq \exp\left(-\frac{\kappa n \Delta t \eta_{**}}{2}\right) \left( \|\chi_\theta^0\|_G^2 + \frac{\kappa\Delta t}{4} \|\nabla\theta_h^0\|^2 \right) + \kappa^{-2} \eta_{**}^{-1} \|\gamma\|_{L^\infty(\mathbb{R}_+; W_h^*)}^2 \\
& \leq \exp\left(-\ln\left(\frac{\|\chi_\theta^0\|_G^2 + \frac{\kappa\Delta t}{4} \|\nabla\theta_h^0\|^2}{\kappa^{-2} \eta_{**}^{-1} \|\gamma\|_{L^\infty(\mathbb{R}_+; W_h^*)}^2}\right)\right) \left( \|\chi_\theta^0\|_G^2 + \frac{\kappa\Delta t}{4} \|\nabla\theta_h^0\|^2 \right) \\
& \quad + \kappa^{-2} \eta_{**}^{-1} \|\gamma\|_{L^\infty(\mathbb{R}_+; W_h^*)}^2
\end{aligned}$$

Using the equivalence of the norms (4.2) gives the required bound on the temperature.

**Step 3:** (Long-time  $L^2$ -stability of the velocity)

To obtain the long time stability of velocity, we take  $\mathbf{v}_h = u_h^{n+1}$  in (4.11),  $q_h = p_h^{n+1}$  in (4.12). By using the relation (4.3), the standard inequalities, dropping the nonlinear term and multiplying the resulting inequality with  $2\Delta t$  gives

$$\begin{aligned}
& \|\chi_u^{n+1}\|_G^2 + \nu\Delta t \|\nabla \mathbf{u}_h^{n+1}\|^2 \\
& \leq \|\chi_u^n\|_G^2 + 2\nu^{-1}\Delta t \left[ 2C_{PF}^2 Ri^2 \left( 4\|\theta_h^n\|^2 + \|\theta_h^{n-1}\|^2 \right) + \|\mathbf{f}^{n+1}\|_{\mathbf{V}_h^*}^2 \right].
\end{aligned}$$

We first add  $\frac{\nu\Delta t}{4}\|\nabla\mathbf{u}_h^n\|^2$  to both sides of (4.3). Then rearranging terms gives

$$\begin{aligned} & \|\mathcal{X}_u^{n+1}\|_G^2 + \frac{\nu\Delta t}{4}\|\nabla\mathbf{u}_h^{n+1}\|^2 + \frac{\nu\Delta t}{4}\left(\|\nabla\mathbf{u}_h^{n+1}\|^2 + \|\nabla\mathbf{u}_h^n\|^2\right) + \frac{\nu\Delta t}{2}\|\nabla\mathbf{u}_h^{n+1}\|^2 \\ & \leq \|\mathcal{X}_u^n\|_G^2 + \frac{\nu\Delta t}{4}\|\nabla\mathbf{u}_h^n\|^2 + 2\nu^{-1}\Delta t\left[2C_{PF}^2 Ri^2\left(4\|\theta_h^n\|^2 + \|\theta_h^{n-1}\|^2\right) + \|\mathbf{f}^{n+1}\|_{V_h^*}^2\right]. \end{aligned} \quad (4.23)$$

Using the same idea used in Step 1, the last two terms on the left hand side can be rewritten as follows:

$$\frac{\nu\Delta t}{4}\left(\|\nabla\mathbf{u}_h^{n+1}\|^2 + \|\nabla\mathbf{u}_h^n\|^2\right) + \frac{\nu\Delta t}{2}\|\nabla\mathbf{u}_h^{n+1}\|^2 \geq \beta\left(\|\mathcal{X}_u^{n+1}\|_G^2 + \frac{\nu\Delta t}{4}\|\nabla\mathbf{u}_h^{n+1}\|^2\right),$$

where  $\beta := \min\{\frac{1}{2}, \frac{\nu\Delta t C_l^2}{4C_{PF}^2}\}$ . Inserting the last estimate in (4.23), using induction and (4.17) yields

$$\|\mathcal{X}_u^{n+1}\|_G^2 + \frac{\nu\Delta t}{4}\|\nabla\mathbf{u}_h^{n+1}\|^2 \leq \left(\frac{1}{1+\beta}\right)^{n+1}\left(\|\mathcal{X}_u^0\|_G^2 + \frac{\nu\Delta t}{4}\|\nabla\mathbf{u}_h^0\|^2\right) + \frac{\nu^{-1}\Delta t}{\beta}M^*$$

where  $M^* = 2\left(10Ri^2C_{PF}^2\max\{\|\theta_h^0\|^2, M^2\} + \|\mathbf{f}\|_{L^\infty(\mathbb{R}_+; \mathbf{V}_h^*)}^2\right)$ . Noting that  $\frac{\Delta t}{\beta} = \max\{2\Delta t, \frac{4C_{PF}^2}{\nu C_l^2}\} =: \beta^*$  completes the proof.  $\square$

#### 4.4 Long time stability of MHD in primitive variables

The linearized BDF2 finite element of the system (1.41)-(1.44) is given as follows:

##### Algorithm 4.4.1 (BDF2LE for MHD in primitive variables)

Let the body forces  $\mathbf{f}, \mathbf{g}$  and initial conditions  $\mathbf{u}_0, \mathbf{B}_0$  be given. Define  $\mathbf{u}_h^{-1} = \mathbf{u}_h^0$  and  $\mathbf{B}_h^{-1} = \mathbf{B}_h^0$  to be the nodal interpolant of  $\mathbf{u}_0$  and  $\mathbf{B}_0$ , respectively. Set a time step  $\Delta t > 0$ . For all  $n = 0, 1, 2, 3, \dots$ , calculate  $(\mathbf{u}_h^{n+1}, P_h^{n+1}, \mathbf{B}_h^{n+1}, \lambda_h^{n+1}) \in$

$(\mathbf{X}_h, Q_h, \mathbf{X}_h, Q_h)$  satisfying for every  $(\mathbf{v}_h, q_h, \mathbf{w}_h, \lambda_h) \in (\mathbf{X}_h, Q_h, \mathbf{X}_h, Q_h)$ ,

$$\begin{aligned} & \frac{1}{2\Delta t} \left( 3\mathbf{u}_h^{n+1} - 4\mathbf{u}_h^n + \mathbf{u}_h^{n-1}, \mathbf{v}_h \right) + \nu (\nabla \mathbf{u}_h^{n+1}, \nabla \mathbf{v}_h) + b^*(2\mathbf{u}_h^n - \mathbf{u}_h^{n-1}, \mathbf{u}_h^{n+1}, \mathbf{v}_h) \\ & - sb^*(2\mathbf{B}_h^n - \mathbf{B}_h^{n-1}, \mathbf{B}_h^{n+1}, \mathbf{v}_h) - (P_h^{n+1}, \nabla \cdot \mathbf{v}_h) = (\mathbf{f}^{n+1}, \mathbf{v}_h) \end{aligned} \quad (4.24)$$

$$(\nabla \cdot \mathbf{u}_h^{n+1}, q_h) = 0, \quad (4.25)$$

$$\begin{aligned} & \frac{1}{2\Delta t} \left( 3\mathbf{B}_h^{n+1} - 4\mathbf{B}_h^n + \mathbf{B}_h^{n-1}, \mathbf{w}_h \right) + \nu_m (\nabla \mathbf{B}_h^{n+1}, \nabla \mathbf{w}_h) + (\lambda_h^{n+1}, \nabla \cdot \mathbf{w}_h) \\ & + b^*(2\mathbf{u}_h^n - \mathbf{u}_h^{n-1}, \mathbf{B}_h^{n+1}, \mathbf{w}_h) - b^*(2\mathbf{B}_h^n - \mathbf{B}_h^{n-1}, \mathbf{u}_h^{n+1}, \mathbf{w}_h) = (\nabla \times \mathbf{g}^{n+1}, \mathbf{w}_h), \end{aligned} \quad (4.26)$$

$$(\nabla \cdot \mathbf{B}_h^{n+1}, l_h) = 0. \quad (4.27)$$

**Theorem 4.4.2** Let  $\mathbf{f}, \nabla \times \mathbf{g} \in L^\infty(\mathbb{R}_+; \mathbf{V}_h^*)$ ,  $\mathbf{u}_0, B_0 \in \mathbf{L}^2(\Omega)$ . Then the solutions of Algorithm 4.4.1 satisfy

$$\begin{aligned} & \|\mathbf{x}_u^{n+1}\|_G^2 + s\|\mathbf{x}_B^{n+1}\|_G^2 + \frac{\Delta t}{4} \left( \nu \|\nabla \mathbf{u}_h^{n+1}\|^2 + s\nu_m \|\nabla \mathbf{B}_h^{n+1}\|^2 \right) \\ & \leq \left( \frac{1}{1+\mu} \right)^{n+1} \left[ \|\mathbf{x}_u^0\|_G^2 + s\|\mathbf{x}_B^0\|_G^2 + \frac{\Delta t}{4} \left( \nu \|\nabla \mathbf{u}_h^0\|^2 + s\nu_m \|\nabla \mathbf{B}_h^0\|^2 \right) \right] \\ & \quad + \mu^* \left( \nu^{-1} \|\mathbf{f}\|_{L^\infty(\mathbb{R}_+; \mathbf{V}_h^*)}^2 + s\nu_m^{-1} \|\nabla \times \mathbf{g}\|_{L^\infty(\mathbb{R}_+; \mathbf{V}_h^*)}^2 \right) \end{aligned}$$

where  $\mu = \min\{\frac{1}{2}, \frac{\nu C_l^2 \Delta t}{4C_{PF}^2}, \frac{\nu_m C_l^2 \Delta t}{4C_{PF}^2}\}$ ,  $\mu^* = \max\{2\Delta t, \frac{4C_{PF}^2}{\nu C_l^2}, \frac{4C_{PF}^2}{\nu_m C_l^2}\}$ ,  $C_{PF}$  is the Poincaré's-Friedrichs' constant from (2.6), and  $C_l$  is given by (4.2).

**Proof:** The proof starts by choosing  $\mathbf{v}_h = 2\Delta t \mathbf{u}_h^{n+1}$  in (4.24),  $q_h = P_h^{n+1}$  in (4.25),  $\mathbf{w}_h = 2\Delta t \mathbf{B}_h^{n+1}$  in (4.26) and  $l_h = \lambda_h^{n+1}$  in (4.27). A straight forward calculation with relation (4.3) gives that

$$\begin{aligned} & \|\mathbf{x}_u^{n+1}\|_G^2 - \|\mathbf{x}_u^n\|_G^2 + \frac{\|\mathbf{u}_h^{n+1} - 2\mathbf{u}_h^n + \mathbf{u}_h^{n-1}\|^2}{2} - 2s\Delta t b^*(2\mathbf{B}_h^n - \mathbf{B}_h^{n-1}, \mathbf{B}_h^{n+1}, \mathbf{u}_h^{n+1}) \\ & + 2\nu\Delta t \|\nabla \mathbf{u}_h^{n+1}\|^2 = 2\Delta t (\mathbf{f}^{n+1}, \mathbf{u}_h^{n+1}), \end{aligned} \quad (4.28)$$

and

$$\begin{aligned} & \|\mathbf{x}_B^{n+1}\|_G^2 - \|\mathbf{x}_B^n\|_G^2 + \frac{\|\mathbf{B}_h^{n+1} - 2\mathbf{B}_h^n + \mathbf{B}_h^{n-1}\|^2}{2} - 2\Delta t b^*(2\mathbf{B}_h^n - \mathbf{B}_h^{n-1}, \mathbf{u}_h^{n+1}, \mathbf{B}_h^{n+1}) \\ & + 2\nu_m \Delta t \|\nabla \mathbf{B}_h^{n+1}\|^2 = 2\Delta t (\nabla \times \mathbf{g}^{n+1}, \mathbf{B}_h^{n+1}). \end{aligned} \quad (4.29)$$

Multiplying equation (4.29) by  $s$  and adding it to (4.28), taking into account the skew-symmetry of nonlinear term yields

$$\begin{aligned} & \left( \|\chi_u^{n+1}\|_G^2 + s\|\chi_B^{n+1}\|_G^2 \right) + 2\Delta t \left( \nu\|\nabla \mathbf{u}_h^{n+1}\|^2 + s\nu_m\|\nabla \mathbf{B}_h^{n+1}\|^2 \right) \\ & \leq \left( \|\chi_u^n\|_G^2 + s\|\chi_B^n\|_G^2 \right) + 2\Delta t \left( (\mathbf{f}^{n+1}, \mathbf{u}_h^{n+1}) + s(\nabla \times \mathbf{g}^{n+1}, \mathbf{B}_h^{n+1}) \right). \end{aligned} \quad (4.30)$$

Applying now the Cauchy-Schwarz and the Young's inequalities on the forcing terms gives

$$\begin{aligned} & 2\Delta t \left( (\mathbf{f}^{n+1}, \mathbf{u}_h^{n+1}) + s(\nabla \times \mathbf{g}^{n+1}, \mathbf{B}_h^{n+1}) \right) \\ & \leq \Delta t \left( \nu\|\nabla \mathbf{u}_h^{n+1}\|^2 + s\nu_m\|\nabla \mathbf{B}_h^{n+1}\|^2 \right) + \Delta t \left( \nu^{-1}\|\mathbf{f}^{n+1}\|_{\mathbf{V}_h^*}^2 + s\nu_m^{-1}\|\nabla \times \mathbf{g}^{n+1}\|_{\mathbf{V}_h^*}^2 \right). \end{aligned}$$

Using this last estimate in (4.30), and adding  $\frac{\Delta t}{4} \left( \nu\|\nabla \mathbf{u}_h^n\|^2 + s\nu_m\|\nabla \mathbf{B}_h^n\|^2 \right)$  to the both sides of the inequality produces

$$\begin{aligned} & \|\chi_u^{n+1}\|_G^2 + s\|\chi_B^{n+1}\|_G^2 + \frac{\Delta t}{4} \left( \nu\|\nabla \mathbf{u}_h^{n+1}\|^2 + s\nu_m\|\nabla \mathbf{B}_h^{n+1}\|^2 \right) \\ & + \frac{\Delta t}{4} \left( \nu \left( \|\nabla \mathbf{u}_h^{n+1}\|^2 + \|\nabla \mathbf{u}_h^n\|^2 \right) + s\nu_m \left( \|\nabla \mathbf{B}_h^{n+1}\|^2 + \|\nabla \mathbf{B}_h^n\|^2 \right) \right) \\ & + \frac{\Delta t}{2} \left( \nu\|\nabla \mathbf{u}_h^{n+1}\|^2 + s\nu_m\|\nabla \mathbf{B}_h^{n+1}\|^2 \right) \\ & \leq \left( \|\chi_u^n\|_G^2 + s\|\chi_B^n\|_G^2 \right) + \frac{\Delta t}{4} \left( \nu\|\nabla \mathbf{u}_h^n\|^2 + s\nu_m\|\nabla \mathbf{B}_h^n\|^2 \right) \\ & + \Delta t \left( \nu^{-1}\|\mathbf{f}^{n+1}\|_{\mathbf{V}_h^*}^2 + s\nu_m^{-1}\|\nabla \times \mathbf{g}^{n+1}\|_{\mathbf{V}_h^*}^2 \right). \end{aligned}$$

Next, we rewrite the last two terms on the left hand side of above estimate by using the Poincaré's inequality and the relation (4.2):

$$\begin{aligned} & \frac{\Delta t}{4} \left( \nu \left( \|\nabla \mathbf{u}_h^{n+1}\|^2 + \|\nabla \mathbf{u}_h^n\|^2 \right) + s\nu_m \left( \|\nabla \mathbf{B}_h^{n+1}\|^2 + \|\nabla \mathbf{B}_h^n\|^2 \right) \right) \\ & + \frac{\Delta t}{2} \left( \nu\|\nabla \mathbf{u}_h^{n+1}\|^2 + s\nu_m\|\nabla \mathbf{B}_h^{n+1}\|^2 \right) \\ & \geq \frac{\nu C_i^2 \Delta t}{4C_{PF}^2} \|\chi_u^{n+1}\|_G^2 + \frac{\nu \Delta t}{2} \|\nabla \mathbf{u}_h^{n+1}\|^2 + \frac{s\nu_m C_i^2 \Delta t}{4C_{PF}^2} \|\chi_B^{n+1}\|_G^2 + \frac{s\nu_m \Delta t}{2} \|\nabla \mathbf{B}_h^{n+1}\|^2 \\ & \geq \mu \left( \|\chi_u^{n+1}\|_G^2 + s\|\chi_B^{n+1}\|_G^2 + \frac{\Delta t}{4} \left( \nu\|\nabla \mathbf{u}_h^{n+1}\|^2 + s\nu_m\|\nabla \mathbf{B}_h^{n+1}\|^2 \right) \right), \end{aligned}$$

where  $\mu = \min\{\frac{1}{2}, \frac{\nu C_l^2 \Delta t}{4C_{PF}^2}, \frac{\nu_m C_l^2 \Delta t}{4C_{PF}^2}\}$ . The last estimate produces

$$\begin{aligned}
& (1 + \mu) \left( \left( \|\boldsymbol{\chi}_u^{n+1}\|_G^2 + \frac{\nu \Delta t}{4} \|\nabla \mathbf{u}_h^{n+1}\|^2 \right) + s \left( \|\boldsymbol{\chi}_B^{n+1}\|_G^2 + \frac{\nu_m \Delta t}{4} \|\nabla \mathbf{B}_h^{n+1}\|^2 \right) \right) \\
& \leq \|\boldsymbol{\chi}_u^n\|_G^2 + \frac{\nu \Delta t}{4} \|\nabla \mathbf{u}_h^n\|^2 + s \left( \|\boldsymbol{\chi}_B^n\|_G^2 + \frac{\nu_m \Delta t}{4} \|\nabla \mathbf{B}_h^n\|^2 \right) \\
& + \Delta t \left( \nu^{-1} \|\mathbf{f}^{n+1}\|_{\mathbf{V}_h^*}^2 + s \nu_m^{-1} \|\nabla \times \mathbf{g}^{n+1}\|_{\mathbf{V}_h^*}^2 \right), \tag{4.31}
\end{aligned}$$

and then we use induction to get

$$\begin{aligned}
LHS & \leq \left( \frac{1}{1 + \mu} \right)^{n+1} \left( \|\boldsymbol{\chi}_u^0\|_G^2 + s \|\boldsymbol{\chi}_B^0\|_G^2 + \frac{\Delta t}{4} \left( \nu \|\nabla \mathbf{u}_h^0\|^2 + s \nu_m \|\nabla \mathbf{B}_h^0\|^2 \right) \right) \\
& + \frac{\Delta t}{\mu} \left( \nu^{-1} \|\mathbf{f}\|_{L^\infty(\mathbb{R}_+; \mathbf{V}_h^*)}^2 + s \nu_m^{-1} \|\nabla \times \mathbf{g}\|_{L^\infty(\mathbb{R}_+; \mathbf{V}_h^*)}^2 \right). \tag{4.32}
\end{aligned}$$

The final step of the proof consists of considering  $\mu^* := \frac{\Delta t}{\mu} = \max\{2\Delta t, \frac{4C_{PF}^2}{\nu C_l^2}, \frac{4C_{PF}^2}{\nu_m C_l^2}\}$  and using the equivalence of the  $G$  and the  $L^2$ -norms.  $\square$

#### 4.5 The long time stability of MHD in Elsässer variables

In this section, we study the long time behavior of MHD in Elsässer variables. The linearized BDF2 algorithm for the system (3.1)-(3.4) is given as below. It is a very interesting algorithm since it decouples the equations, which seemingly cannot be done in an unconditionally stable way for primitive variable MHD.

**Algorithm 4.5.1 (BDF2LE for MHD in Elsässer variables)** *Let  $\mathbf{f}_1, \mathbf{f}_2$  and the initial conditions  $\mathbf{v}_0, \mathbf{w}_0$  be given. Define  $\mathbf{v}_h^{-1} = \mathbf{v}_h^0, \mathbf{w}_h^{-1} = \mathbf{w}_h^0$  to be nodal interpolants of  $\mathbf{v}_0, \mathbf{w}_0$  and choose a time step  $\Delta t > 0$ . For  $n = 0, 1, 2, 3, \dots$  find  $(\mathbf{v}_h^{n+1}, q_h^{n+1}, \mathbf{w}_h^{n+1}, r_h^{n+1}) \in (\mathbf{X}_h, Q_h, \mathbf{X}_h, Q_h)$  such that for all  $(\boldsymbol{\chi}_h, p_h, \boldsymbol{\phi}_h, l_h) \in$*

$(\mathbf{X}_h, Q_h, \mathbf{X}_h, Q_h)$

$$\begin{aligned} & \frac{1}{2\Delta t} \left( 3\mathbf{v}_h^{n+1} - 4\mathbf{v}_h^n + \mathbf{v}_h^{n-1}, \boldsymbol{\chi}_h \right) + b^*(\mathbf{w}_h^n, \mathbf{v}_h^{n+1}, \boldsymbol{\chi}_h) + b^*(\tilde{\mathbf{B}}_0, \mathbf{v}_h^{n+1}, \boldsymbol{\chi}_h) \\ & \quad + \frac{\nu + \nu_m}{2} (\nabla \mathbf{v}_h^{n+1}, \nabla \boldsymbol{\chi}_h) + \frac{\nu - \nu_m}{2} (\nabla (2\mathbf{w}_h^n - \mathbf{w}_h^{n-1}), \nabla \boldsymbol{\chi}_h) \\ & \quad - (q_h^{n+1}, \nabla \cdot \boldsymbol{\chi}_h) = (\mathbf{f}_1^{n+1}, \boldsymbol{\chi}_h), \end{aligned} \quad (4.33)$$

$$(\nabla \cdot \mathbf{v}_h^{n+1}, p_h) = 0, \quad (4.34)$$

$$\begin{aligned} & \frac{1}{2\Delta t} \left( 3\mathbf{w}_h^{n+1} - 4\mathbf{w}_h^n + \mathbf{w}_h^{n-1}, \phi_h \right) + b^*(\mathbf{v}_h^n, \mathbf{w}_h^{n+1}, \phi_h) + b^*(\tilde{\mathbf{B}}_0, \mathbf{w}_h^{n+1}, \phi_h) \\ & \quad + \frac{\nu + \nu_m}{2} (\nabla \mathbf{w}_h^{n+1}, \nabla \phi_h) + \frac{\nu - \nu_m}{2} (\nabla (2\mathbf{v}_h^n - \mathbf{v}_h^{n-1}), \nabla \phi_h) \\ & \quad - (r_h^{n+1}, \nabla \cdot \phi_h) = (\mathbf{f}_2^{n+1}, \phi_h), \end{aligned} \quad (4.35)$$

$$(\nabla \cdot \mathbf{w}_h^{n+1}, l_h) = 0. \quad (4.36)$$

**Theorem 4.5.2** *Let  $\mathbf{u}_0, \mathbf{B}_0 \in L^2(\Omega)$  and  $(\mathbf{v}_h^{n+1}, q_h^{n+1}, \mathbf{w}_h^{n+1}, r_h^{n+1})$  be the solution to the Algorithm 4.5.1, and  $\mathbf{f}_1, \mathbf{f}_2 \in L^\infty(\mathbb{R}_+; \mathbf{V}_h^*)$  be given. If*

$$\Delta t < \frac{2h^2\nu\nu_m}{C_I^2(\nu - \nu_m)^2(\nu + \nu_m)}, \quad (4.37)$$

then we have

$$\begin{aligned} & \left( \|\boldsymbol{\chi}_v^{n+1}\|_G^2 + \|\boldsymbol{\chi}_w^{n+1}\|_G^2 \right) + \frac{\nu\nu_m\Delta t}{8(\nu + \nu_m)} \left( \|\nabla \mathbf{v}_h^{n+1}\|^2 + \|\nabla \mathbf{w}_h^{n+1}\|^2 \right) \\ & \leq \left( \frac{1}{1 + \gamma} \right)^{n+1} \left( \|\boldsymbol{\chi}_v^0\|_G^2 + \|\boldsymbol{\chi}_w^0\|_G^2 + \frac{\nu\nu_m\Delta t}{8(\nu + \nu_m)} (\|\nabla \mathbf{v}_h^0\|^2 + \|\nabla \mathbf{w}_h^0\|^2) \right) \\ & \quad + \frac{2\gamma^*(\nu + \nu_m)}{\nu\nu_m} \left( \|\mathbf{f}_1\|_{L^\infty(\mathbb{R}_+; \mathbf{V}_h^*)}^2 + \|\mathbf{f}_2\|_{L^\infty(\mathbb{R}_+; \mathbf{V}_h^*)}^2 \right), \end{aligned}$$

where  $\gamma = \min\{2, \frac{C_I^2\nu\nu_m\Delta t}{8C_{PF}^2(\nu + \nu_m)}\}$ ,  $\gamma^* = \max\{\frac{1}{2}\Delta t, \frac{8C_{PF}^2(\nu + \nu_m)}{C_I^2\nu\nu_m}\}$ ,  $C_{PF}$  is the Poincaré's-Friedrichs' constant from (2.6), and  $C_I$  is given by (4.1).

**Proof:** First take  $\boldsymbol{\chi}_h = \mathbf{v}_h^{n+1}$  in (4.33),  $p_h = q_h^{n+1}$  in (4.34),  $\phi_h = \mathbf{w}_h^{n+1}$  in (4.35),  $l_h = r_h^{n+1}$  in (4.36) and use relation (4.3) to produce

$$\begin{aligned} & \frac{1}{2\Delta t} \left( \|\boldsymbol{\chi}_v^{n+1}\|_G^2 - \|\boldsymbol{\chi}_v^n\|_G^2 \right) + \frac{1}{4\Delta t} \|\mathbf{v}_h^{n+1} - 2\mathbf{v}_h^n + \mathbf{v}_h^{n-1}\|^2 + \frac{\nu + \nu_m}{2} \|\nabla \mathbf{v}_h^{n+1}\|^2 \\ & = -\frac{\nu - \nu_m}{2} (\nabla \mathbf{w}_h^{n+1}, \nabla \mathbf{v}_h^{n+1}) + \frac{\nu - \nu_m}{2} (\nabla (\mathbf{w}_h^{n+1} - 2\mathbf{w}_h^n + \mathbf{w}_h^{n-1}), \nabla \mathbf{v}_h^{n+1}) \\ & \quad + (\mathbf{f}_1^{n+1}, \mathbf{v}_h^{n+1}) \end{aligned} \quad (4.38)$$

and

$$\begin{aligned}
& \frac{1}{2\Delta t} \left( \|\boldsymbol{\chi}_w^{n+1}\|_G^2 - \|\boldsymbol{\chi}_w^n\|_G^2 \right) + \frac{1}{4\Delta t} \|\mathbf{w}_h^{n+1} - 2\mathbf{w}_h^n + \mathbf{w}_h^{n-1}\|^2 + \frac{\nu + \nu_m}{2} \|\nabla \mathbf{w}_h^{n+1}\|^2 \\
&= -\frac{\nu - \nu_m}{2} (\nabla \mathbf{v}_h^{n+1}, \nabla \mathbf{w}_h^{n+1}) + \frac{\nu - \nu_m}{2} (\nabla (\mathbf{v}_h^{n+1} - 2\mathbf{v}_h^n + \mathbf{v}_h^{n-1}), \nabla \mathbf{w}_h^{n+1}) \\
&\quad + (\mathbf{f}_2^{n+1}, \mathbf{w}_h^{n+1}). \quad (4.39)
\end{aligned}$$

To bound the left hand side of (4.38), we apply the Cauchy-Schwarz and the Young's inequalities with  $\varepsilon = \frac{\nu + \nu_m}{2}$  on the first right hand side term which gives:

$$\begin{aligned}
\frac{\nu - \nu_m}{2} (\nabla \mathbf{w}_h^{n+1}, \nabla \mathbf{v}_h^{n+1}) &\leq \frac{|\nu - \nu_m|}{2} \|\nabla \mathbf{w}_h^{n+1}\| \|\nabla \mathbf{v}_h^{n+1}\| \\
&\leq \frac{\nu + \nu_m}{4} \|\nabla \mathbf{v}_h^{n+1}\|^2 + \frac{(\nu - \nu_m)^2}{4(\nu + \nu_m)} \|\nabla \mathbf{w}_h^{n+1}\|^2,
\end{aligned}$$

Similarly, the second term on the right hand side of (4.38) can be bounded with  $\varepsilon = \frac{\nu \nu_m}{\nu + \nu_m}$  and inverse inequality as

$$\begin{aligned}
& \frac{\nu - \nu_m}{2} (\nabla (\mathbf{w}_h^{n+1} - 2\mathbf{w}_h^n + \mathbf{w}_h^{n-1}), \nabla \mathbf{v}_h^{n+1}) \\
&\leq C_I h^{-1} \frac{|\nu - \nu_m|}{2} \|\mathbf{w}_h^{n+1} - 2\mathbf{w}_h^n + \mathbf{w}_h^{n-1}\| \|\nabla \mathbf{v}_h^{n+1}\| \\
&\leq \frac{\nu \nu_m}{2(\nu + \nu_m)} \|\nabla \mathbf{v}_h^{n+1}\|^2 + \frac{C_I^2 h^{-2} (\nu - \nu_m)^2 (\nu + \nu_m)}{8\nu \nu_m} \|\mathbf{w}_h^{n+1} - 2\mathbf{w}_h^n + \mathbf{w}_h^{n-1}\|^2
\end{aligned}$$

With the choice of  $\varepsilon = \frac{\nu \nu_m}{2(\nu + \nu_m)}$ , the forcing term is estimated with

$$\begin{aligned}
(\mathbf{f}_1^{n+1}, \mathbf{v}_h^{n+1}) &\leq \|\mathbf{f}_1^{n+1}\| \|\nabla \mathbf{v}_h^{n+1}\| \\
&\leq \frac{\nu \nu_m}{4(\nu + \nu_m)} \|\nabla \mathbf{v}_h^{n+1}\|^2 + \frac{\nu + \nu_m}{\nu \nu_m} \|\mathbf{f}_1^{n+1}\|_{\mathbf{V}_h^*}^2. \quad (4.40)
\end{aligned}$$

Plug these estimates into (4.38) to produce

$$\begin{aligned}
& \frac{1}{2\Delta t} \left( \|\boldsymbol{\chi}_v^{n+1}\|_G^2 - \|\boldsymbol{\chi}_v^n\|_G^2 \right) + \frac{1}{4\Delta t} \|\mathbf{v}_h^{n+1} - 2\mathbf{v}_h^n + \mathbf{v}_h^{n-1}\|^2 + \frac{\nu + \nu_m}{4} \|\nabla \mathbf{v}_h^{n+1}\|^2 \\
&\leq \frac{3\nu \nu_m}{4(\nu + \nu_m)} \|\nabla \mathbf{v}_h^{n+1}\|^2 + \frac{(\nu - \nu_m)^2}{4(\nu + \nu_m)} \|\nabla \mathbf{w}_h^{n+1}\|^2 \\
&+ \frac{C_I^2 h^{-2} (\nu - \nu_m)^2 (\nu + \nu_m)}{8\nu \nu_m} \|\mathbf{w}_h^{n+1} - 2\mathbf{w}_h^n + \mathbf{w}_h^{n-1}\|^2 + \frac{\nu + \nu_m}{\nu \nu_m} \|\mathbf{f}_1^{n+1}\|_{\mathbf{V}_h^*}^2. \quad (4.41)
\end{aligned}$$

Using the same technique, the left hand side of (4.39) can be bounded as follows:

$$\begin{aligned}
& \frac{1}{2\Delta t} \left( \|\boldsymbol{\chi}_w^{n+1}\|_G^2 - \|\boldsymbol{\chi}_w^n\|_G^2 \right) + \frac{1}{4\Delta t} \|\mathbf{w}_h^{n+1} - 2\mathbf{w}_h^n + \mathbf{w}_h^{n-1}\|^2 + \frac{\nu \nu_m}{4(\nu + \nu_m)} \|\nabla \mathbf{w}_h^{n+1}\|^2 \\
&\leq \frac{3\nu \nu_m}{4(\nu + \nu_m)} \|\nabla \mathbf{w}_h^{n+1}\|^2 + \frac{(\nu - \nu_m)^2}{4(\nu + \nu_m)} \|\nabla \mathbf{v}_h^{n+1}\|^2 \\
&+ \frac{C_I^2 h^{-2} (\nu - \nu_m)^2 (\nu + \nu_m)}{8\nu \nu_m} \|\mathbf{v}_h^{n+1} - 2\mathbf{v}_h^n + \mathbf{v}_h^{n-1}\|^2 + \frac{\nu + \nu_m}{\nu \nu_m} \|\mathbf{f}_2^{n+1}\|_{\mathbf{V}_h^*}^2. \quad (4.42)
\end{aligned}$$



Now adding these two equations results

$$\begin{aligned}
& \frac{1}{2\Delta t} \left( \|\chi_v^{n+1}\|_G^2 + \|\chi_w^{n+1}\|_G^2 \right) + \frac{\nu\nu_m}{4(\nu + \nu_m)} \left( \|\nabla \mathbf{v}_h^{n+1}\|^2 + \|\nabla \mathbf{w}_h^{n+1}\|^2 \right) \\
& \quad + \frac{1}{2\Delta t} \left( \frac{1}{2} - \frac{C_I^2 h^{-2} (\nu - \nu_m)^2 (\nu + \nu_m)}{4\nu\nu_m} \Delta t \right) \\
& \quad \times \left( \|\mathbf{v}_h^{n+1} - 2\mathbf{v}_h^n + \mathbf{v}_h^{n-1}\|^2 + \|\mathbf{w}_h^{n+1} - 2\mathbf{w}_h^n + \mathbf{w}_h^{n-1}\|^2 \right) \\
& \leq \frac{1}{2\Delta t} \left( \|\chi_v^n\|_G^2 + \|\chi_w^n\|_G^2 \right) + \frac{\nu + \nu_m}{\nu\nu_m} \left( \|\mathbf{f}_1^{n+1}\|_{\mathbf{V}_h^*}^2 + \|\mathbf{f}_2^{n+1}\|_{\mathbf{V}_h^*}^2 \right), \quad (4.43)
\end{aligned}$$

and multiplying by  $2\Delta t$  and dropping the non-negative left hand side second term by using  $\Delta t$  restriction (4.37) gives

$$\begin{aligned}
& \left( \|\chi_v^{n+1}\|_G^2 + \|\chi_w^{n+1}\|_G^2 \right) + \frac{\nu\nu_m\Delta t}{2(\nu + \nu_m)} \left( \|\nabla \mathbf{v}_h^{n+1}\|^2 + \|\nabla \mathbf{w}_h^{n+1}\|^2 \right) \\
& \leq \left( \|\chi_v^n\|_G^2 + \|\chi_w^n\|_G^2 \right) + \frac{2(\nu + \nu_m)\Delta t}{\nu\nu_m} \left( \|\mathbf{f}_1^{n+1}\|_{\mathbf{V}_h^*}^2 + \|\mathbf{f}_2^{n+1}\|_{\mathbf{V}_h^*}^2 \right). \quad (4.44)
\end{aligned}$$

The last step follows from the application of the same technique as in Theorem 4.2.2.

□

**Remark 4.5.3** *It is proven in [82] that if  $1/2 < \nu/\nu_m < 2$ , then there is no timestep restriction for stability.*

#### 4.5.1 Numerical Experiment

We now present numerical experiments for the linearized BDF2 scheme for MHD in Elsässer variables, given by Algorithm 4.5.1. The goal of the numerical experiment is to test the stability time step restriction of [82] which states that the method is unconditionally stable when  $1/2 < \nu/\nu_m < 2$ . We test values of  $\nu/\nu_m$  inside and outside of this range, and find that this restriction is sharp. As a test problem, we select initial conditions and forcing terms as follows:

$$\begin{aligned}
\mathbf{v}_0 &= \begin{pmatrix} \cos(y) \\ \sin(x) \end{pmatrix}, & \mathbf{f}_1 &= \begin{pmatrix} \sin(x+y) \\ \cos(x-y) \end{pmatrix}, \\
\mathbf{w}_0 &= \begin{pmatrix} \sin(y) \\ \cos(x) \end{pmatrix}, & \mathbf{f}_2 &= \begin{pmatrix} \cos(x-y) \\ \sin(x+y) \end{pmatrix}.
\end{aligned}$$

We take  $(\mathbf{P}_2, P_1^{disc})$  Scott-Vogelius finite elements, and  $s = 1$ . We then calculate the approximate solutions of Algorithm 4.5.1 on  $16 \times 16$  barycenter uniform mesh of the domain  $\Omega = (0, 1)^2$ . All computations are run to  $T = 500$  for varying  $\Delta t$  and  $\nu, \nu_m$ . The results are seen below as plots of  $(\|\mathbf{v}_h^{n+1}\|^2 + \|\mathbf{w}_h^{n+1}\|^2)$ .

In Figure 4.5 and 4.6, we observe that the solutions are stable in the case  $1/2 < \nu/\nu_m < 2$ . However, the linearized BDF2 discrete solutions fail to be stable outside of this interval as in Figure 4.7 and Figure 4.8. The solutions remain stable in the limit case  $\nu/\nu_m = 2$  as in Figure 4.9 whereas remain unstable for  $\nu/\nu_m = 2.105$  (Figure 4.10).

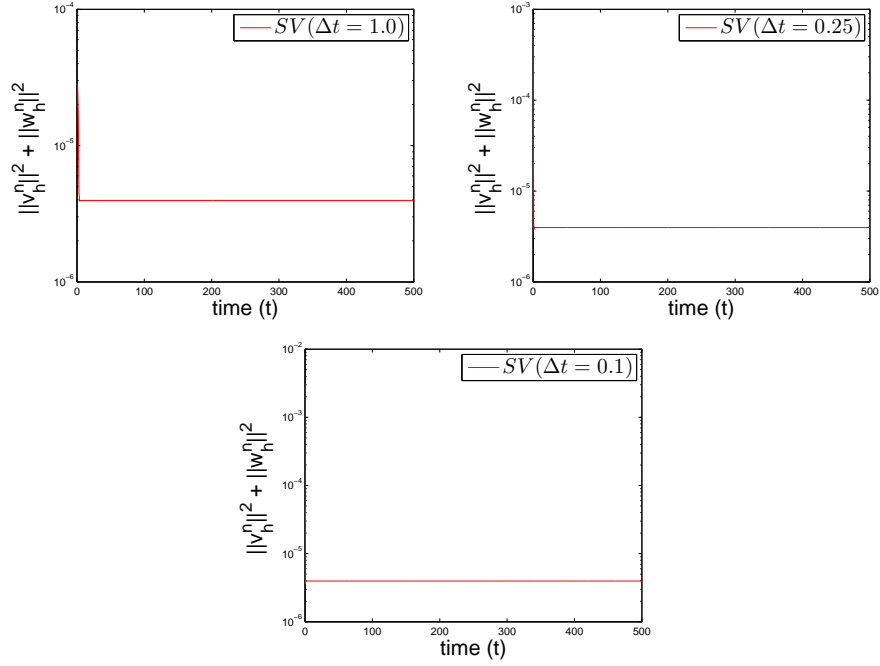


Figure 4.5: Energy vs. time for discrete velocity solutions of MHD in Elsässer variables with  $\nu = 1.0, \nu_m = 1.0$  ( $1/2 < \nu/\nu_m < 2$ ).

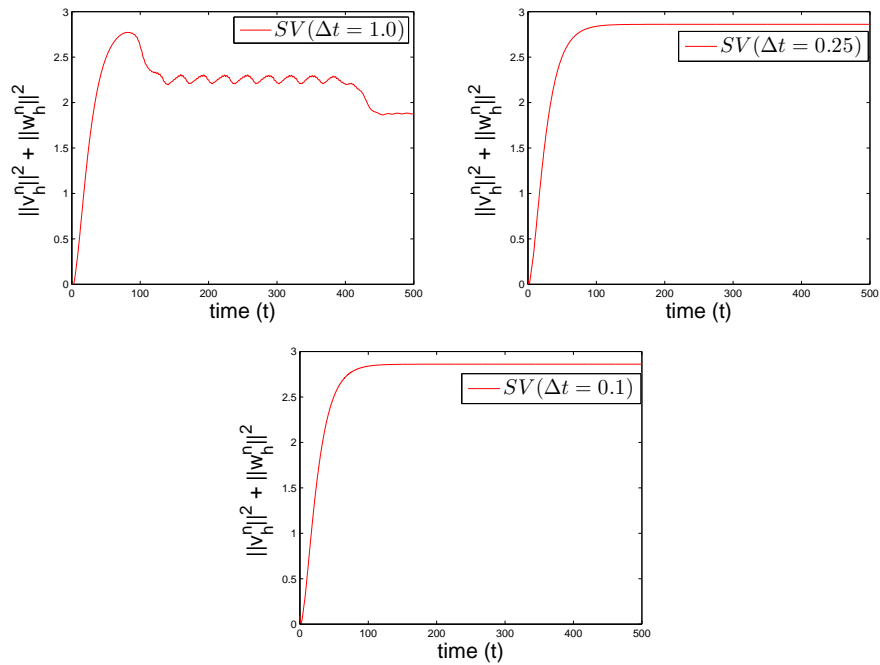


Figure 4.6: Energy vs. time for discrete velocity solutions of MHD in Elsässer variables with  $\nu = 0.0125, \nu_m = 0.01$  ( $1/2 < \nu/\nu_m < 2$ ).

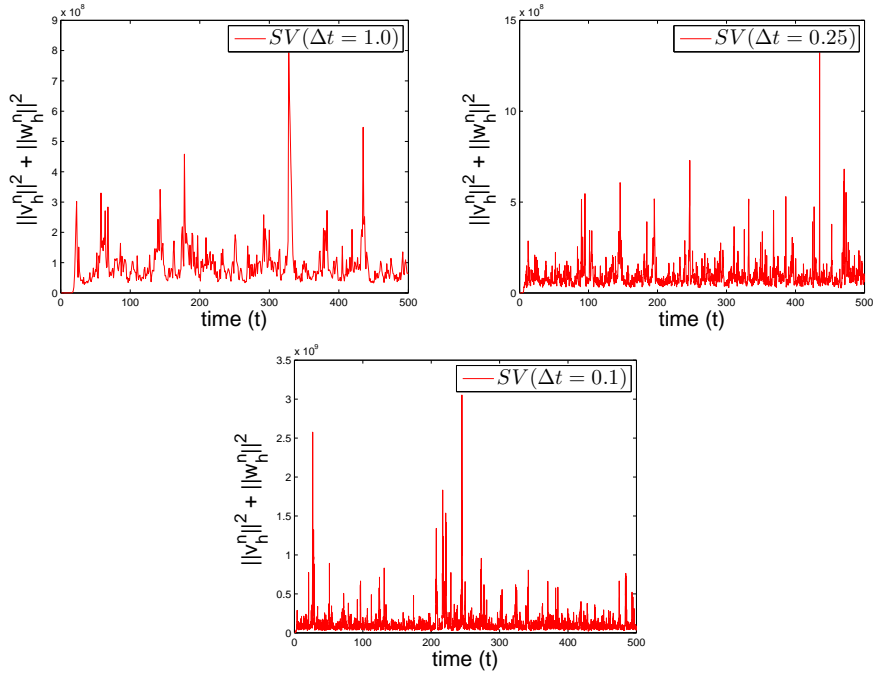


Figure 4.7: Energy vs. time for discrete velocity solutions of MHD in Elsässer variables with  $\nu = 0.01$  and  $\nu_m = 1$  ( $\nu/\nu_m < 1/2$ ).

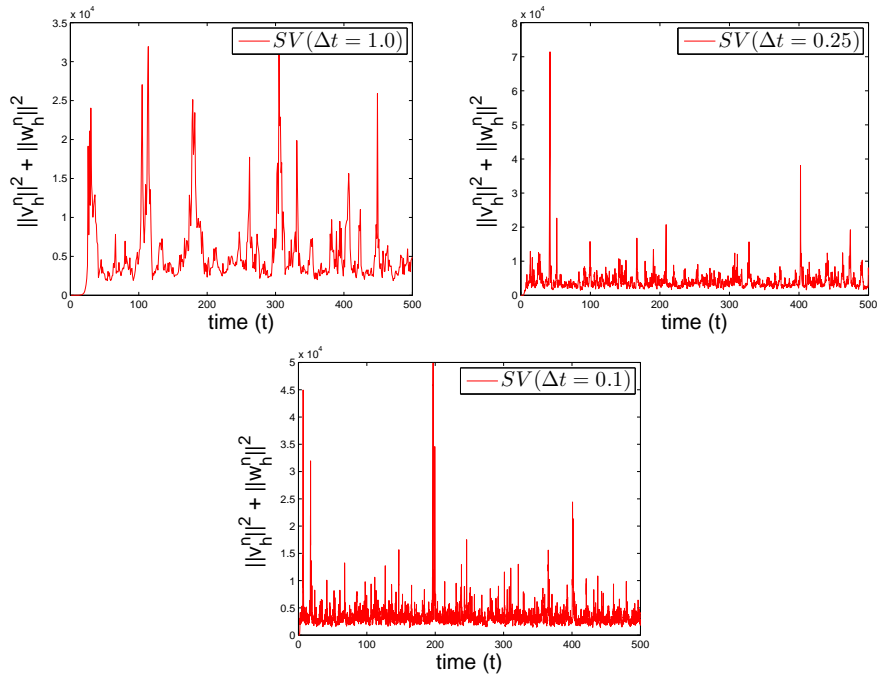


Figure 4.8: Energy vs. time for discrete velocity solutions of MHD in Elsässer variables with  $\nu = 0.01$  and  $\nu_m = 0.001$  ( $\nu/\nu_m > 2$ ).

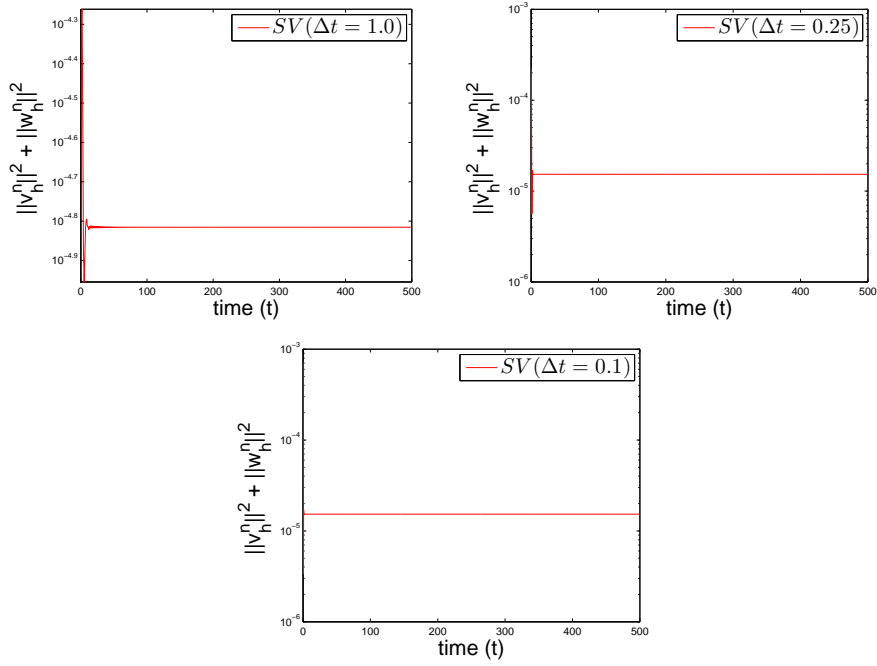


Figure 4.9: Energy vs. time for discrete velocity solutions of MHD in Elsässer variables with  $\nu = 1$  and  $\nu_m = 0.5$  ( $\nu/\nu_m = 2$ ).

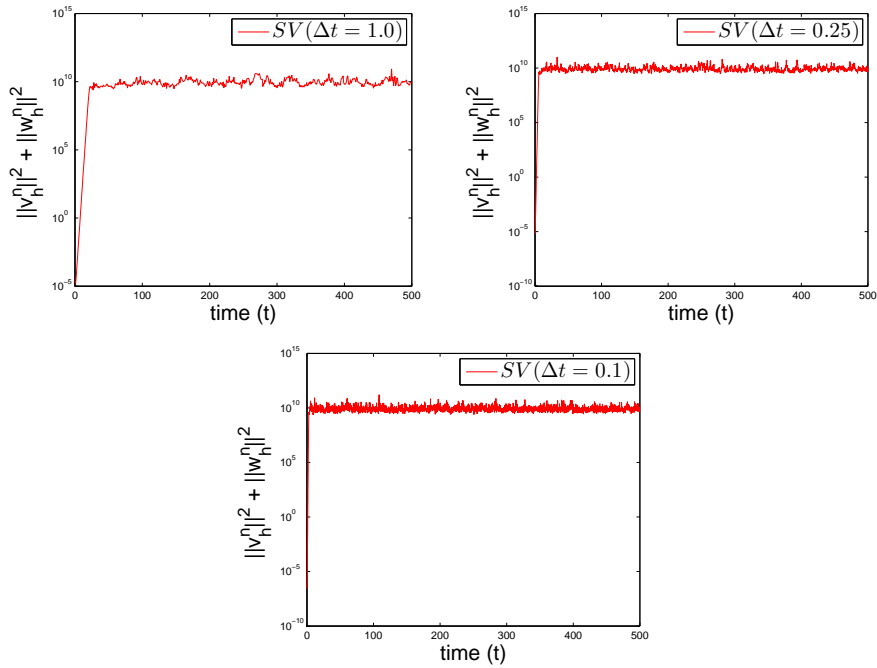


Figure 4.10: Energy vs. time for discrete velocity solutions of MHD in Elsässer variables with  $\nu = 0.2$  and  $\nu_m = .095$  ( $\nu/\nu_m = 2.105$ ).



## CHAPTER 5

### CONCLUSIONS AND FUTURE WORK

This thesis focused on the development of the numerical methods for multiphysics flow problems. In Chapter 2, an efficient fully discrete VMS method for the incompressible non-isothermal fluid flows is studied. The VMS stabilization is explicitly decoupled from the Boussinesq system, and thus it can be used with other types of flow solvers than Step 1 of the algorithm. In the proposed algorithm, the Boussinesq system is also decoupled, and the transport equation is solved separately from the fluid equations. Despite the decouplings, we proved that the algorithm is unconditionally stable with respect to timestep size, and that it converges optimally in both space and time provided the parameters  $\alpha_1 = O(h^2)$ ,  $\alpha_2 = O(h^2)$ , and the coarse mesh width satisfies  $H \leq O(h^{1/2})$ . Numerical experiments were given that verified the theory, and showed the effectiveness of the scheme.

In Chapter 3, we proposed, analyzed and tested an efficient penalty-projection method for MHD system. We proved that this method is equivalent to the fully coupled solutions for large penalty parameters. Convergence of the penalty-projection scheme to the coupled scheme was found to be first order as  $\gamma \rightarrow \infty$ , which agrees with our theory. Finally, we tested numerical scheme with MHD channel flow over a step, and observed that the changing of physical behavior as the coupling number was increasing.

In the last chapter, we studied long time behavior of the NSE and related multiphysics problems using BDF2LE timestepping together with finite element method. We proved that the approximate solutions of the proposed algorithm for the NSE, Boussinesq and MHD in primitive variables are uniformly bounded at all time without time step restriction. For MHD in Elsässer variables, we obtained conditionally long

time stability. In addition, we implemented two numerical experiment for the NSE. In the first numerical experiment, we showed the stability property of the BDF2LE scheme is better than the CNLE for smaller viscosities. In the second numerical experiment for the NSE, we observed that divergence-free elements can provide better solutions over long-time simulation than non-divergence-free elements. The key difference in the elements is the treatment of the irrotational part of the forcing; This results from divergence-free elements (correctly) do not allow the irrotational part of the forcing to affect the velocity, and this error can accumulate to reduce accuracy of the solution over long times.

## 5.1 Future Work

There are several research direction inspired from Chapter 2. One possible direction is that the modification of the scheme to the second order timestepping such as BDF2 or Crank-Nicolson can be done in a straightforward manner. However, we suspect the analysis will work in a similar manner. Modifications of the scheme to higher order timestepping would require different analysis, probably more technical, but may well be worth the effort, particularly since the explicit VMS stabilization herein would be used as a post-processing.

Another research direction is the extension of the algorithm to the nonlinear eddy viscosity type of projection-based stabilization. The error analysis requires to use monotonicity and Lipschitz continuity.

This type of post-processing can be applied for different types of fluid problems. The same analysis can be extended to MHD in primitive variables, also in Elsässer variables.

For Chapter 4, we believe that more testing of the scheme needs performed. Also, for MHD problems with higher Reynolds number, reduced order modeling with large eddy simulation, in the context of the scheme proposed herein, should be explored.



## REFERENCES

- [1] R.A. Adams. *Sobolev Spaces*. Academic Press, Newyork, 1975.
- [2] M. Akbas, S. Kaya, M. Mohebujjaman, and L. G. Rebholz. Numerical analysis and testing of a fully discrete, decoupled algorithm for MHD in Elsässer variable. *Int. J. Numer. Anal. Model.*, 13(1):90–113, 2016.
- [3] D. N. Arnold and J. Qin. Quadratic velocity/linear pressure Stokes elements. In R. Vichnevetsky, D. Knight, and G. Richter, editors, *Advances in Computer Methods for Partial Differential Equations VII*, pages 28–34. IMACS, 1992.
- [4] S. Badia, R. Codina, and J. V. Gutiérrez-Santacreu. Long-term stability estimates and existence of a global attractor in a finite element approximation of the Navier–Stokes Equations with numerical subgrid scale modeling. *SIAM J. Numer. Anal.*, 48(3):1013–1037, 2010.
- [5] G. Baker. Galerkin approximations for the Navier–Stokes equations. Harvard University, August 1976.
- [6] M. A. Belenli, L. G. Rebholz, and F. Tone. A note on the importance of mass conservation in long time stability of Navier-Stokes simulations using finite elements. *Appl. Math. Lett.*, 45:98–102, 2015.
- [7] M.A. Belenli, S. Kaya, L. Rebholz, and N. Wilson. A subgrid stabilization finite element method for incompressible magnetohydrodynamics. *Int. J. Comput. Math.*, 90(7):1506–1523, 2013.
- [8] M. Benzi, M. A. Olshanskii, L. G. Rebholz, and Z. Wang. Assessment of a vorticity based solver for the Navier-Stokes equations. *SIAM J. Numer. Anal.*, 247:216–225, 2012.
- [9] D. Biskamp. *Magnetohydrodynamic Turbulence*. Cambridge University Press, Cambridge, 2003.
- [10] P. B. Bochev, M. D. Gunzburger, and R. B. Lehoucq. On stabilized finite element methods for the Stokes problem in the small time step limit. *Int. J. Numer. Methods Fluids*, 53(4):573–597, 2007.
- [11] P. B. Bochev, M. D. Gunzburger, and J. N. Shadid. Stability of the SUPG finite element method for transient advection-diffusion problems. *Comput. Methods Appl. Mech. Engrg.*, 45:285–312, 2004.

- [12] A. Bowers, S. Le Borne, and L. G. Rebholz. Error analysis and iterative solvers for Navier-Stokes projection methods with standard and sparse grad-div stabilization. *Comput. Methods Appl. Mech. Engrg.*, 275:1–19, 2014.
- [13] E. Braack, M. Burman, V. John, and G. Lube. Stabilized finite element methods for the generalized Oseen problem. *Comput. Methods Appl. Mech. Engrg.*, 196:853–866, 2007.
- [14] S. Brenner and L.R. Scott. *The Mathematical Theory of Finite Element Methods, 3rd edition*. Springer-Verlag, 2008.
- [15] F. Brezzi and M. Fortin. *Mixed and Hybrid Finite Element Methods*. volume 15 of *Springer Series in Computational Mathematics*, Springer-Verlag, 1991.
- [16] A. N. Brooks and T. J. R. Hughes. A multi-dimensional upwind scheme with no crosswind diffusion . *Finite Element Method for Convection Dominated Flows (ed. T. J. R. Hughes) Applied Mechanics Division*, 34:19–35, 1979.
- [17] A. N. Brooks and T. J. R. Hughes. Streamline upwind/Petrov-Galerkin formulations for convection dominated flows with particular emphasis on the incompressible Navier-Stokes equations . *Comput. Methods Appl. Mech. Engrg.*, 32:199–259, 1982.
- [18] A. Buffa and S. H. Christiansen. A dual finite element complex on the barycentric refinement. *Math. Comput.*, 76(260):1743–1769, 2007.
- [19] E. Burman. Consistent SUPG-method for transient transport problems: Stability and convergence. *Comput. Methods Appl. Mech. Engrg.*, 199:1114–1123, 2010.
- [20] E. Burman and M. A. Fernández. Analysis of the PSPG method for the transient Stokes’ problem. *Comput. Methods Appl. Mech. Engrg.*, 200:2882–2890, 2011.
- [21] Y. A Cengel and A. J. Ghajar. *Heat and Mass Transfer: Fundamentals and Applications*. McGraw-Hill Education, New York, 2015.
- [22] W. Chen, M. Gunzburger, D. Sun, and X. Wang. Efficient and long time accurate second-order methods for Stokes-Darcy system. *SIAM J. Numer. Anal.*, 51(5):2563–2584, 2013.
- [23] A. J. Chorin. Numerical solution of the Navier-Stokes equations. *Math. Comput.*, 22:745–762, 1968.
- [24] A. J. Chorin. On the convergence of discrete approximations to the Navier-Stokes equations. *Math. Comput.*, 23:341–353, 1969.

- [25] A. Cibik and S. Kaya. A projection based stabilized finite element method for steady-state natural convection problems. *J. Math. Anal. Appl.*, 381:469–484, 2011.
- [26] A. Cibik and S. Kaya. Finite element analysis of a projection-based stabilization method for the Darcy–Brinkman equations in double-diffusive convection. *Appl. Math. Lett.*, 64:35–49, 2013.
- [27] R. Codina. Stability analysis of the forward Euler scheme for the convection-diffusion equation using the SUPG formulation in space. *Int. J. Numer. Method. Engrg.*, 36(9):1445–1464, 1993.
- [28] R. Codina. Comparision of the finite element methods for solving the diffusion-convection-reaction equation. *Comput. Methods Appl. Math. Engrg.*, 156:185–210, 1998.
- [29] S. S. Collis. Monitoring unresolved scales in multiscale turbulence modeling. *Phys. Fluids*, 13:1800–1806, 2001.
- [30] B. R. Cousins, L. G. Rebholz, and N. E. Wilson. Enforcing energy, helicity and strong mass conservation in finite element computations for incompressible Navier–Stokes simulations. *J. Comput. Phys.*, 218:1208–1221, 2011.
- [31] P. A. Davidson. *An Introduction to Magnetohydrodynamics*. Cambridge Texts in Applied Mathematics, Cambridge University Press, 2001.
- [32] O. Dorok, W. Grambow, and L. Tobiska. Aspects of finite element discretization for solving the Boussinesq approximation of the Navier-Stokes equation. In R. Rannacher F.-K. Hebeker and G. Wittum, editors, *Numerical Methods for the Navier-Stokes equations*, volume 47 of *Notes on Numerical Fluid Mechanics*, pages 50–61. Proceedings of the International Workshop held at Heidelberg, October 1993, 1994.
- [33] W. E and J. G. Liu. Projection method I: Convergence and numerical boundary layers. *J. Numer. Anal.*, 32:1017–1057, 1995.
- [34] W. E and J. G. Liu. Projection method III: Spatial discretization on the staggered grid. *Math. Comput.*, 71:27–47, 2001.
- [35] W. M. Elsässer. The hydrodynamic equations. *Phys. Rev.*, pages 79–183, 1950.
- [36] B. Ewald and F. Tone. Approximation of the long-term dynamics of the dynamical system generated by the two-dimensional thermohydraulics equations. *Int. J. Numer. Anal. Model.*, 10(3):509–535, 2013.
- [37] C. Foias, O. Manley, R. Rosa, and R. Temam. *Navier-Stokes Equations and Turbulence*. Cambridge University Press, 2001.

- [38] V. P. Fragos, S. P. Psychoudaki, and N. A. Malamataris. Computer-aided analysis of flow past a surface-mounted obstacle. *Internat. J. Numer. Methods Fluids*, 25:495 – 512, 1997.
- [39] L. Franca, G. Hauke, and A. Masud. Revisiting stabilized finite element methods for the advective–diffusive equation. *Comput. Methods Appl. Mech. Engrg.*, 195(13):1560–1572, 2006.
- [40] L. P. Franca, T. J. R. Hughes, and R. Stenberg. Stabilized Finite Element Methods for the Stokes Problem. In M. Gunzburger and R.A. Nicolaides, editors, *Incompressible Computational Fluid Dynamics*, Notes on Numerical Fluid Mechanics, pages 87–107. Cambridge University Press, 1993, 1993.
- [41] L. P. Franca, V. John, G. Matthies, and L. Tobiska. An inf-sup stable and Residual-Free Bubble Element for the Oseen Equations. *SIAM J. Numer. Anal.*, 45(6):2392–2407, 2007.
- [42] L. P. Franca and Hughes T. J. R. Two classes of mixed finite element methods. *Comput. Methods Appl. Mech. Engrg.*, 69(1):89–129, 1988.
- [43] J. Frutos, B. Garcia-Archilla, V. John, and J. Novo. Grad-div stabilization for the evolutionary Oseen problem with inf-sup stable finite elements. *J. Sci. Comput.*, 66(3):991–1024, 2016.
- [44] G. P. Galdi. *An Introduction to Mathematical Theory of the Navier-Stokes equations*. Volume I, Springer, Berlin, 1994.
- [45] K. Galvin, A. Linke, L. G. Rebholz, and N. E. Wilson. Stabilizing poor mass conservation in incompressible flow problems with large irrotational forcing and application to thermal convection. *Comput. Methods Appl. Mech. Engrg.*, 237/240:166–176, 2012.
- [46] V. Girault and P.-A. Raviart. *Finite element methods for Navier-Stokes equations: Theory and Algorithms*. Springer-Verlag, 1986.
- [47] S. Gottlieb, F. Tone, C. Wang, X. Wang, and D. Wirosoetisno. Long time stability of a classical efficient scheme for two dimensional Navier-Stokes equations. *SIAM J. Numer. Anal.*, 50(1):126–150, 2012.
- [48] V. Gravemeier, W. A. Wall, and E. Ramm. A three-level finite element method for the instationary incompressible Navier-Stokes equations. *Comput. Methods Appl. Mech. Engrg.*, 193:1323–1366, 2004.
- [49] V. Gravemeier, W. A. Wall, and E. Ramm. Large eddy simulation of turbulent incompressible flows by a three-level finite element method. *Internat. J. Numer. Methods Fluids*, 48(10):1067–1099, 2005.

- [50] P. M. Gresho. On the theory of semi-implicit projection methods for viscous incompressible flow and its implementation via a finite element method that also introduces a nearly consistent mass matrix. Part 1: Theory. *Internat. J. Numer. Methods Fluids*, 11(5):587–620, 1990.
- [51] P. M. Gresho and S. T. Chan. On the theory of semi-implicit projection methods for viscous incompressible flow and its implementation via a finite element method that also introduces a nearly consistent mass matrix. Part 2: Implementation. *Internat. J. Numer. Methods Fluids*, 11(5):621–659, 1990.
- [52] J. Guermond, P. Mineev, and J. Shen. An overview of projection methods for incompressible flows. *Comput. Methods Appl. Mech. Engrg.*, 195:6011–6045, 2006.
- [53] J. L. Guermond. Stabilization of Galerkin approximations of transport equations by subgrid modeling. *M2AN, Math. Model. Numer. Anal.*, 33(6):1293–1316, 1999.
- [54] M. D. Gunzburger. *Finite element methods for viscous incompressible flows: A guide to theory, practice, and algorithm*. Academic Press Inc., Boston, 1989.
- [55] E. Hairer and G. Wanner. *Solving Ordinary Differential Equations II: Stiff and Differential Algebraic Problems, second edition*. Springer-Verlag, Berlin, 2002.
- [56] F. Hecht. New development in freefem++. *J. Numer. Math.*, 20, 3-4:251–265, 2012.
- [57] T. Heister, M. A. Olshanskii, and L. G. Rebholz. Unconditional long-time stability of velocity-vorticity method for 2D Navier-Stokes equations. *Numerische Mathematik*, pages 1–25, 2016.
- [58] J. Heywood and R. Rannacher. Finite element approximation of the nonstationary Navier-Stokes problem. Part II: Stability of solutions and error estimates in time. *SIAM J. Numer. Anal.*, 19(2):750–777, 1986.
- [59] J. Heywood and R. Rannacher. Finite element approximation of the nonstationary Navier-Stokes problem. Part IV: Error analysis for the second order time discretization. *SIAM J. Numer. Anal.*, 2:353–384, 1990.
- [60] T. J. R. Hughes. Multiscale phenomena: Green’s functions, the Dirichlet-to-Neumann formulation, subgrid-scale models, bubbles and the origin of stabilized methods. *Comput. Methods Appl. Mech. Engrg.*, 127:387–401, 1995.
- [61] T. J. R. Hughes, L. P. Franca, and M. Mallet. A new finite element formulation for computational fluid dynamics: VI. Convergence analysis of the generalized SUPG formulation for linear time-dependent multi-dimensional

- advective-diffusive systems. *Comput. Methods Appl. Mech. Engrg.*, 63:97–112, 1987.
- [62] R. Ingram. Unconditional convergence of high-order extrapolations of the Crank-Nicholson, finite element method for the Navier-Stokes equations. *Int. J. Numer. Anal. Model.*, 10(2):257–297, 2013.
- [63] J. E. A. John and W. L. Haberman. *Introduction to fluid mechanics*. Prentice Hall, 1980.
- [64] V. John. Slip with friction and penetration with resistance boundary conditions for the navierstokes equations—numerical tests and aspects of the implementation. *J. Coput. Appl. Math.*, 147:287–300, 2002.
- [65] V. John and S. Kaya. A finite element variational multiscale method for the Navier-Stokes equations. *SIAM J. Sci. Comput.*, 26(5):1485–1503, 2005.
- [66] V. John and S. Kaya. Finite element error analysis of a variational multiscale method for the Navier-Stokes equations. *Adv. Comput. Math.*, 28:43–61, 2008.
- [67] V. John, S. Kaya, and W. Layton. A two-level variational multiscale method for convection- dominated convection-diffusion equations. *Comput. Methods Appl. Mech. Engrg.*, 195:4594–4603, 2006.
- [68] V. John and A. Kindl. Numerical studies of finite element variational multiscale methods for turbulent flow simulations. *Comput. Methods Appl. Mech. Engrg.*, 199:841–852, 2010.
- [69] V. John and A. Liakos. Time dependent flow across a step: the slip with friction boundary condition. *Internat. J. Numer. Methods Fluids*, 50:713–731, 2006.
- [70] V. John and J. Novo. Analysis of the PSPG Stabilization for the evolutionary Stokes equations avoiding time-step restrictions. *SIAM J. Numer. Anal.*, 53(2):1005–1031, 2015.
- [71] V. John and M. Roland. Simulations of turbulent channel flow at  $Re_\tau = 180$  with projection-based finite element variational multiscale methods. *Internat. J. Numer. Methods Fluids*, 55(5):407–429, 2007.
- [72] C. Johnson, U. Nävert, and J. Pitkäranta. Finite element methods for linear hyperbolic problems. *Comput. Methods Appl. Mech. Engrg.*, 45:285–312, 1984.
- [73] C. Johnson and Nävert U. An analysis of some finite element methods for advection-diffusion problems. *Analytical and Numerical Approaches to Asymptotic Problems in Analysis*, (O. Axelsson, L. S. Frank and A. Van der Sluis), eds. North-Holland, Amsterdam, 1981.
- [74] N. Ju. On the global stability of a temporal discretization scheme for the Navier–Stokes equations. *IMA J. Numer. Anal.*, 22:577–597, 2002.

- [75] J. Kim and P. Moin. Application of a fractional-step method to incompressible Navier-Stokes equations. *J. Comput. Phys.*, 59:308–323, 1985.
- [76] L. D. Landau and E. M. Lifshitz. *Electrodynamics of Continuous Media*. Pergamon Press, Oxford, 1960.
- [77] W. Layton. *Introduction to Finite Element Methods for Incompressible, Viscous Flow*. SIAM Publ., 2008.
- [78] W. Layton, C. C. Manica, M. Neda, M. Olshanskii, and Rebholz L. G. On the accuracy of the rotation form in simulations of the Navier–Stokes equations. *J. Comput. Phys.*, 228:3433–3447, 2009.
- [79] W. Layton, L. Roehe, and H. Tran. Explicitly uncoupled VMS stabilization of fluid flow. *Comput. Methods Appl. Mech. Engrg.*, 200:3183–3199, 2011.
- [80] W. Layton, H. Tran, and X. Xiong. Long time stability of four methods for splitting the evolutionary Stokes–Darcy problem into Stokes and Darcy sub-problems. *J. Comput. Appl. Math.*, 236(13):3198–3217, 2012.
- [81] H. K. Lee, M. A. Olshanskii, and L. G. Rebholz. On error analysis for the 3D Navier-Stokes equations in Velocity-Vorticity-Helicity form. *SIAM J. Numer. Anal.*, 49(2):711–732, 2011.
- [82] Y. Li and C. Trenchea. Partitioned second order method for magnetohydrodynamics in Elsässer variables. Technical Report TR-MATH 15-03, Pittsburgh University, Department of Mathematics, Pittsburgh, February, 2015.
- [83] A. Linke, M. Neilan, L. Rebholz, and N. Wilson. Improving efficiency of coupled schemes for Navier-Stokes equations by a connections to grad-div stabilized projection methods. *WIAS*, 2013.
- [84] J.-G. Liu, C. Wang, and H. Johnston. A fourth order scheme for incompressible Boussinesq equations. *J. Sci. Comput.*, 18(2):253–285, 2003.
- [85] J. Löwe and G. Lube. A projection based variational multiscale method for Large-Eddy simulation with application to non-isothermal free convection problems. *Math. Models Methods Appl. Sci.*, 22:1–31, 2012.
- [86] M. Olshanskii and Reusken A. Grad-div stabilization for the Stokes equations. *Math. Comput.*, 73(248):1699–1718, 2003.
- [87] M. Olshanskii, G. Lube, Heister T., and J. Löwe. Grad-div stabilization and subgrid pressure models for the incompressible the Navier-Stokes equations. *Comput. Methods Appl. Mech. Engrg.*, 198:3975–3988, 2009.
- [88] H. Ozoe. *Magnetic Convection*. Imperial College Press, 1996.

- [89] A. Prohl. On Pressure Approximation via Projection Methods for Nonstationary Incompressible Navier–Stokes Equations. *SIAM J. Numer. Anal.*, 47(1):158–180, 2008.
- [90] J. Qin. *On the convergence of some low order mixed finite elements for incompressible fluids*. PhD thesis, Pennsylvania State University, 1994.
- [91] J. Qin and S. Zhang. Stability and approximability of the P1-P0 element for Stokes equation. *Preprint University of Delaware*, 2000.
- [92] D. D. Schnack. *Lectures in Magnetohydrodynamics*. Springer-Verlag, Berlin Heidelberg, 2009.
- [93] J. Shen. Long time stability and convergence for fully discrete nonlinear Galerkin methods. *Appl. Anal.*, 38(4):201–229, 1990.
- [94] J. Shen. On error estimates of of projection methods for Navier-Stokes equations: First Order Scheme. *SIAM J. Numer. Anal.*, 29:57–77, 1992.
- [95] J. Shen. On error estimates of some higher-order projection and penalty-projection methods for the Navier-Stokes equations. *Numer. Math.*, 62:49–74, 1992.
- [96] J. Shen. On Pressure stabilization method and projection method for unsteady the Navier-Stokes equations. In D. Knight R. Vichnevetsky and G. Richter, editors, *Advances in Computer Methods for Partial Differential Equations-VII*, Notes on Numerical Fluid Mechanics, pages 658–662. IMACS, 1992, 1992.
- [97] J. Simo and F. Armero. Unconditional stability and long-term behavior of transient algorithms for the incompressible Navier–Stokes and Euler equations. *Comput. Methods Appl. Mech. Engrg.*, 111(1):111–154, 1994.
- [98] B. Soffientino and M. E. Q. Pilson. The Bosphorus Strait: A Special Place in the History of Oceanography. *Oceanography*, 18(2):1–8, June,2005.
- [99] T. Tachim Medjo and F. Tone. Long time stability of a classical efficient scheme for an incompressible two-phase flow model. *Asymptot. Anal.*, 95:101–127, 2015.
- [100] R. Temam. *Navier-Stokes Equations: Theory and Numerical Analysis*. North Holland Publishing Company, NewYork, 1977.
- [101] T. E. Tezduyar and D. K. Ganjoo. Petrov-Galerkin Formulations with weighting functions dependent upon spatial and temporal discretization: Application to transient convection-diffusion problems. *Comput. Methods Appl. Mech. Engrg.*, 59:49–71, 1986.



- [102] T. E. Tezduyar, J. Liou, and D. K. Ganjoo. Incompressible flow computations based on the vorticity-stream and velocity-pressure formulations. *Computers and Structures*, 35:445–472, 1990.
- [103] L. Tobiska and R. Verfurth. Analysis of a streamline diffusion finite element method for the Stokes and Navier-Stokes equations. *SIAM J. Numer. Anal.*, 33(1):107–127, 1996.
- [104] F. Tone. On the Long-time stability of the Crank-Nicholson scheme for the 2D Navier-Stokes equations. *Numer. Meth. Part D. E.*, 23(5):1235–1248, 2007.
- [105] F. Tone. On the long-time stability of the implicit Euler scheme for the 2D space-periodic Navier–Stokes equations. *Asympt. Anal.*, 51(3-4):231–245, 2007.
- [106] F. Tone. On the long-time  $h^2$ -stability of the implicit Euler scheme for the 2D Magnetohydrodynamics equations. *J. Sci. Comput.*, 38:331–348, 2009.
- [107] F. Tone, X. Wang, and D. Wirosoetisno. Long time dynamics of 2D double-diffusive convection: analysis and/of numerics. *Numeriche Mathematics*, 130(3):541–566, 2015.
- [108] F. Tone and D. Wirosoetisno. On the long-time stability of the implicit Euler scheme for the two-dimensional Navier-Stokes equations. *SIAM J. Numer. Anal.*, 44(1):29–40, 2006.
- [109] C. Trenchea. Unconditional stability of a partitioned IMEX method for magnetohydrodynamics flows. *Appl. Math. Lett.*, 27:97–100, 2014.
- [110] J. Van Kan. A second-order accurate pressure-correction scheme for viscous incompressible flow. *SIAM J. Sci. Stat. Comput.*, 7:870–891, 1986.
- [111] X. Wang. An efficient second order in time scheme for approximating long time statistical properties of the two dimensional Navier-Stokes equations. *Numer. Math.*, 121(4):753–779, 2012.
- [112] N. Wilson, A. Labovsky, and C. Trenchea. High Accuracy Method for Magnetohydrodynamics System in Elsässer Variables. *Comput. Methods Appl. Math.*, 15(1):97–110, 2015.
- [113] S. Zhang. A new family of stable mixed finite elements for the 3d Stokes equations. *Math. Comput.*, 74:543–554, 2005.
- [114] S. Zhang. Divergence-free finite elements on tetrahedral grids for  $k \geq 6$ . *Math. Comput.*, 80:669–695, 2011.
- [115] S. Zhang. Quadratic divergence-free finite elements on Powell-Sabin tetrahedral grids. *Calcolo*, 48:211–244, 2011.



# CURRICULUM VITAE

## PERSONAL INFORMATION

**Surname, Name:** Akbaş Belenli, Mine

**Nationality:** Turkish (TC)

**E-mail:** miakbasb@metu.edu.tr

## EDUCATION

<b>Degree</b>	<b>Institution</b>	<b>Year of Graduation</b>
M.S.	Mersin University, Mathematics	2007
B.S.	Erciyes University, Mathematics	2001
High School	Tarsus Cumhuriyet Lisesi	1996

## PROFESSIONAL EXPERIENCE

<b>Year</b>	<b>Place</b>	<b>Enrollment</b>
2001-2004	MEB	Mathematics Teacher
2004-2009 (February)	Mersin University	Research Assistant
2009/February- 2009/September	Duzce University	Research Assistant
2010-	METU	Research Assistant

## AWARDS

**2013-2014** 2214/A

The Scientific and Technical Research Council of Turkey (TUBITAK)

## PUBLICATIONS

1. M. Akbas, S. Kaya, L. Rebholz, and N. Wilson, *A subgrid stabilization finite element method for incompressible magnetohydrodynamics*, International Journal of Computer Mathematics, 90(7), 1506-1523, 2013.
2. M. Akbas, S. Kaya, and L. Rebholz, *An explicitly decoupled variational multiscale method for incompressible, non-isothermal flows*, Comput. Methods Appl. Math., 15(1), 1-20, 2015.
3. M. Akbas, L. Rebholz, and F. Tone, *A note on the importance of mass conservation in long-time stability of Navier-Stokes simulations using finite elements*, Applied Mathematics Letters, 45, 98-102, 2015.
4. M. Akbas, S. Kaya, M. Mohebujjaman and L. Rebholz, *Numerical analysis and testing of a fully discrete, decoupled penalty-projection algorithm for MHD in Elsässer variable*, International Journal of Numerical Analysis and Modeling, 13(1), 90-113, 2016.
5. M. Akbas, S. Kaya and L. Rebholz, *On the stability at all times of linearly extrapolated BDF2 timestepping for multiphysics incompressible flow problems*, accepted for publication in Numerical Methods for Partial Differential Equations, 2016.

## International Conference Publications

1. F. G. Abdullayev, M. Akbas, *Approximation Properties of Fourier Series in Domains of Complex Plane*, Mathematical Analysis, Differential Equations and Their Applications, Uzhgorod, Ukraine, September 18-23, 2006.
2. M. Akbas, F. G. Abdullayev, *On the Pointwise Convergence of the Fourier Series of Orthonormal Polynomials in the Region with Zero Angles*, Mathematical Analysis Differential Equations and Their Applications, Famagusta, North Cyprus, September 12-15, 2008.
3. M. Akbas, S. Kaya, L. G. Rebholz, *Numerical Studies on a Second Order Method Explicitly Decoupled Variational Multiscale Method*, accepted for pub-

lication ENUMATH Proceedings, Lecture Notes in Computational Science and Engineering, 2016.